UNIVERSITY OF LIVERPOOL

Developing three-dimensional co-cultures of the small intestinal epithelium with intestinal dendritic cells as a disease model for enteric infections

Thesis submitted in accordance with the requirements of the University of Liverpool for the degree of Doctor in Philosophy

Luke Johnston

September 2018

Table of Contents

Abstract

Current models for studying enteric infections fail to fully recapitulate the complexities of the small intestinal epithelium *in vivo* and are also too simplistic in that they do not contain elements of the mucosal immune system such as dendritic cells, important in intestinal homeostasis. More complex models incorporating these elements would be beneficial to study enteric infections, such as *T. gondii*, which enters the host through the small intestinal epithelium and can cause severe encephalitis and birth defects. Identification of the host and parasite pathways involved in invasion of the epithelium by *T. gondii* might lead to the generation of novel therapeutics or vaccines.

Organoid cultures have recently been developed, where intestinal stem cells divide *in vitro* to generate 3D structures recapitulating the cellular diversity and architecture of the small intestinal epithelium. This makes organoids a promising model for studying enteric infections and inflammatory diseases. However, organoids have not been fully exploited for studying enteric infections, due to an inaccessible luminal surface. Furthermore, very few studies have attempted to co-culture immune cell populations with the organoids.

The work carried out in this doctoral thesis set out to address the lack of suitable models for studying early infection events. Organoids were dissociated to expose the luminal surface to infection by *T. gondii*. Live imaging showed the expulsion of infected cells into the lumen, a possible mechanism for the spread of infection in the intestine seen *in vivo*. The injection of parasite effector proteins into host cells that were not subsequently infected was observed, suggesting an extensive manipulation of host cells. This method will allow for high throughput analyses that could be used in drug screenings for the development of novel compounds that protect against infection. However, infection events are not restricted to the luminal surface of the epithelium, the physiologically relevant route of infection. To address this, protocols were developed for the microinjection of *T. gondii* into the luminal space of organoids. This method restricts infection to the luminal surface and allows for the visualisation of parasite infection, transmigration, and host cell responses.

Dendritic cells with a small intestinal phenotype were derived from bone marrow, providing a widely accessible method for studying the function of intestinal dendritic cells. Co-culture of these dendritic cells with organoids provides a novel model that captures more elements of the intestinal environment than existing models. Co-cultures led to the unexpected finding that organoids suppressed aldehyde dehydrogenase expression in dendritic cells, while live imaging revealed characteristic behaviours such as luminal sampling, and surveillance of the organoid surface by dendritic cells.

The models developed in this study provide important tools in studying host-pathogen interactions during early infections of the small intestinal epithelium. They can be adapted to include organoids and dendritic cells derived from knockout or transgenic mice that may elucidate the molecular pathways involved in intestinal homeostasis. These can also be applied to a wider field of research including inflammatory diseases, such as Crohn's disease, whereby dendritic cells are suggested to exhibit abnormal responses to the commensal flora. Improving our understanding of the mechanisms involved in intestinal homeostasis and infection using these novel models can lead to the generation of novel therapeutics and vaccines.

List of Tables

List of Figures

List of Supplementary Movies

List of Abbreviations

3D	3-dimensional
ALDH	Aldehyde dehydrogenase
AMPs	Anti-microbial peptides
APCs	Antigen presenting cell
Batf3	Basic leucine zipper transcription factor ATF-like 3
BM	Bone marrow
BMP	Bone morphogenesis protein
CCR	Chemokine receptor
CD	Crohn's disease
cDC	Conventional dendritic cell
CDP	Common DC precursor
CRPBII	cellular retinoic-acid binding protein 2
DC	Dendritic cell
DN	Double negative
DSS	Dextran sulphate sodium
EGF	Epidermal growth factor
FAE	Follicle-associated epithelium
Flt3L	FMS-like tyrosine kinase 3
FoxP3	Forkhead box P3
GABA	γ-aminobutyric acid
GAPs	Goblet cell antigen passages
GM-CSF	Granulocyte macrophage colony stimulating factor
HSC	Haematopoietic stem cell
IBD	Inflammatory bowel disease
Id2	DNA-binding protein inhibitor
IEC	Intestinal epithelial cell

IEL	Intraepithelial lymphocytes
IFN	Interferon
IgA-IC	Immunoglobulin A immune complexes
IL	Interleukin
ILC	Innate lymphoid cells
Irf	Interferon regulatory factor
LGR5	Leucine-rich repeat-containing G-protein coupled receptor 5
MAMP	Microbe-associated molecular pattern
MHCII	Major histocompatability complex II
MIC	Micronemal proteins
MLN	Mesenteric lymph node
MUC2	Mucin-2
NLR	NOD-like receptor
pDC	Plasmacytoid dendritic cell
PP	Payer's patch
PRR	Pattern recognition receptor
PV	Parasitophorous vacuole
RA	Retinoic acid
RAR	Retinoic acid receptor
REGIII-g	Regenerating islet-derived III-γ
ROL	Retinol
RON	Rhoptry neck protein
ROP	Rhoptries
ROR-γt	Retinoic acid-receptor related orphan receptor γt
SAG	GPI-anchored surface antigens
SCFA	Short chain fatty acid
SED	Subepithelial dome

SI LP	Small intestinal lamina propria
STAT	Signal transducer and activator of transcription
TA	Transit amplifying
TED	Transepithelial dendrite
TF	Transcription factor
Th	T helper
TLR	Toll-like receptor
TNF	Tumour necrosis factor
Treg	Regulatory T cell
TSLP	Thymic stromal lymphopoietin
UC	Ulcerative colitis
VAD	Vitamin A deficient

Acknowledgements

I would like to acknowledge and thank the following important people for their support throughout my doctoral degree.

Firstly, I would like to express my gratitude to my supervisor Dr. Janine Coombes for the continuous support and patience throughout my PhD study. Without her support and encouragement this project would not have been possible.

I would like to thank both the University of Liverpool and the Biotechnology and Biological Sciences Research Council (BBSRC) for funding this research project.

I am grateful for the help provided by the technical team, especially Catherine Hartley whose knowledge in cell and parasite culture was invaluable. Thanks to the Centre for Cell Imaging in helping with the start of the microinjection study and for providing support during imaging.

I would like to thank my friends and family for their continued support throughout this doctorate. I am forever grateful for the support provided by my parents, both financially and, most importantly, emotionally. I would not be writing this thesis without them.

And finally, to my Grandfather, who couldn't be here to see me complete my doctorate. You have been my inspiration and I hope this doctoral thesis makes you proud.

Chapter 1: General introduction

1.1 Enteric pathogens

Diseases derived from foodborne pathogens are an important cause of global morbidity and mortality in addition to posing a hindrance to socioeconomic development. It is estimated that over 200 pathogens cause foodborne-illnesses, with 31 pathogens attributed to over half the cases of disease resulting in 600 million illnesses and 420 thousand deaths globally in 2010 (World Health Organization, 2015). Incidence is greatly variable throughout the global population with highest burdens associated with low-income regions such as Africa where the unimproved water and sanitation conditions, and the high prevalence of HIV/AIDS contribute to disease burden.

Infections primarily cause diarrhoeal symptoms with the major pathogens involved including norovirus, *Campylobacter*, *Salmonella*, and *Staphylococcus*. Foodborne transmission of helminths such as *Fasciola* also induce illness, and parasites, including *Toxoplasma gondii*, are attributed to 33 900 deaths globally in 2010 (World Health Organization, 2015). Difficulties in diagnosing the causative agents of foodborne-diseases are a result of the non-specific symptoms that the large numbers of pathogens share. Along with the wrongful diagnoses of chronic diseases attributed to enteric infections, the number reported by the World Health Organization are regarded as conservative estimates. Foodborne-illnesses are therefore likely to cause a much higher burden on the economy due to the costs of healthcare and loss of productivity.

1.1.1 Infections of the gastrointestinal tract

The human intestine has one of the largest surface areas exposed to the external environment and is therefore a major site of potential infection. Following ingestion of certain pathogens, the first site of infection is the gastrointestinal tract that consists of the mouth, oesophagus, stomach, small and large intestines, the colon and rectum. Foodborne pathogens differ in disease severity, clinical symptoms and their duration such that some pathogens induce secretory diarrhoea by producing exotoxins and others invade epithelial cells to initiate an inflammatory response resulting in inflammatory diarrhoea, such as some strains of *Escherichia coli* and *Salmonella enterica*, respectively. The small intestine is considered the primary area of contact between host cell and pathogen. Studying early infection events within the small intestinal epithelium may allow for the identification of novel targets that can be exploited for the development of effective therapies. In order to achieve this, we must understand the homeostatic processes of the small intestine that includes the structure and diversity of the small intestine epithelium and the functions of small intestinal epithelial cells in mucosal homeostasis.

There is an increasing abundance of antimicrobial resistance in enteric pathogens, including *Campylobacter* and *Shigella* (Sack *et al.*, 2001), requiring the development of new treatments or vaccines. The development of novel vaccines and therapeutics relies on the better understanding of early infection events within the intestinal epithelium and the host-pathogen interactions that initiate mucosal protection. With the lack of suitable models of the small intestinal epithelium, the development

of relevant models for the study of early infection by enteric pathogens is urgently required.

1.2 Small intestinal epithelium

The intestinal epithelium provides a physical barrier of defence against external products. The second layer of defence is the mucus that also provides a physical barrier but also contains antimicrobial proteins that cover the intestinal surface. The third layer of defence are the immune cells that reside within the lamina propria, the dense connective tissue underlying the intestinal epithelium. All these layers, and the muscularis mucosae, constitute the mucosal layer.

The small intestinal epithelium consists of a crypt domain and villus domain. The small intestinal epithelium has one of the highest turnover rates in the whole body. This surface is continually renewed by the supply of cells from stem cells that reside within the crypt domains residing at the base of villi. These stem cells are identified by expression of growth factor target gene leucine-rich repeat-containing G-protein coupled receptor 5 (*Lgr5*), polycomb group protein (BMI1) and atypical homeobox protein (HOPX). They divide asymmetrically to produce transit amplifying cells that differentiate into epithelial cells including enteroendocrine cells, goblet cells, Paneth cells, absorptive enterocytes, tuft cells and M cells. Paneth cells reside beside the Lgr5+ stem cells providing signals that maintain the stem cell's state. They are identified by their large eosinophilic granules that aid in host defence against pathogens by secretion of anti-microbial compounds (Wilson *et al.*, 1999). Goblet cells secrete mucins that form a major part of the mucus layer. There are at

least 10 types of enteroendocrine cells, and those within the small intestine are sensors of luminal content, secreting hormones that regulate many processes such as glucose levels and food intake. Enterocytes produce digestive enzymes and transport contents from the lumen. M cells transport luminal content across the epithelium to immune cells and are therefore important in mucosal immunity. Tuft cells (or brush cells) express chemosensory receptors and are involved in initiating Th2 immunity against infection (Howitt *et al.*, 2016). The small intestinal epithelium is polarised, differing in structure and function between apical and basal sides of the cell that is important in intestinal homeostasis.

It has been proposed that the small intestinal epithelium contains 2 stem cell populations, the LGR5+ cells within the crypt domain and BMI1+ cells 4 cells above (+4) the crypt base (Barker *et al.*, 2007). Our understanding of the relationship between the two populations is still scarce. It is believed that the LGR5+ stem cells are responsible for the regenerative capabilities of the small intestinal epithelium, whereas the +4 BMI1+ cells are quiescent and suggested to increase proliferation during epithelial damage (Yan *et al.*, 2012). In general, adult stem cells are maintained in their undifferentiated state by their niche environment. The maintenance of their stemness, defined by their self-renewal capacity in an undifferentiated state, are provided by direct cell signalling, growth factors, and the extracellular matrix they reside in. Within the crypt domains of the small intestinal epithelium, LGR5+ cells are interspersed by Paneth cells and their direct contact and secretion of signalling factors retains the stem cell's stemness. This is provided by EGF, TGF-α, Wnt3 and the Notch ligand Dll4 that induces cell proliferation in an

undifferentiated state (VanDussen *et al.*, 2012; Sato and Clevers, 2013a). Proliferation of LGR5+ stem cells within crypt domains push daughter cells upwards towards the villus tip. Within the transit amplifying region these cells differentiate into the distinct epithelial cell lineages. Through this progression up the crypt-villus axis, cells eventually undergo a form of programmed cell death at the villus tip known as anoikis. Here apoptotic cells are removed from the small intestinal epithelium into the lumen and subsequently removed with the mucus layer.

1.2.1 Small intestinal stem cell niche

Stem cell proliferation and differentiation are tightly regulated by four signalling pathways. Wnt is a key component in maintaining stemness and proliferation of stem cells and transit amplifying cells (Korinek *et al.*, 1998). Wnt signalling induces the stabilisation of β-catenin that subsequently binds and activates the transcription factor Tcf4 that maintains stemness. Epidermal growth factor (EGF) plays an intrinsic role in maintaining stem cell fate and TA proliferation (Wong *et al.*, 2012). Lastly, bone metamorphic protein (BMP) is prevalent in the villus compartment of the small intestinal epithelium, involved in supressing the expression of stemness genes through Smad1/5/8 and Smad4 signalling, and is inhibited by transgenic Noggin in the crypt domains (Haramis *et al.*, 2004). R-spondin is a ligand to Lgr5 and is a Wnt signal enhancer and is crucial *in vivo* for the survival of stem cells (De Lau *et al.*, 2011). Paneth cells are key to providing a niche environment for maintaining the stem cell's fate by Notch signalling and Wnt3 signalling. Mesenchymal cells also provide Wnt signalling, whereas BMP inhibitors (Noggin) and R-spondin are

provided by nonepithelial sources. BMP expressed from cells in the villous compartment supresses stemness genes and provides a spatial gradient of low BMP at the crypt domain and high BMP at the villus compartment, allowing for the differentiation of the small intestinal epithelium as cell move up the crypt-villus axis. Gradients of Wnts and EGF decrease up the crypt-villus axis, thereby not driving the transcription of stemness genes and allowing differentiation into four major epithelial cell types (Figure 1).

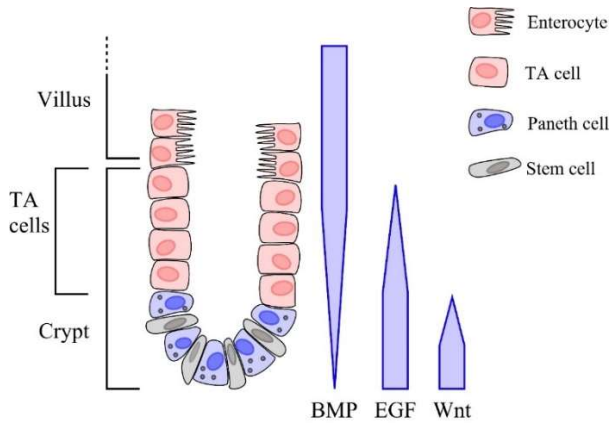

Figure 1. Schematic of signalling in the intestinal stem cell niche
Stem cells are adhered to Paneth cells and receive signalling for stem cell maintenance. Spatial gradients of BMP, Wnt, and EGF signals occur along the crypt-villus axis that affects stem cell state and cell differentiation.

1.2.2 Small intestinal epithelium plays a role in host defence against pathogens

The small intestine must provide a physical barrier to the external environment to prevent infections by pathogens and yet must maintain a balance of symbiotic microbes known as the microbiota. To achieve this, secretory cells of the small intestinal epithelium have distinct roles in intestinal homeostasis. Goblet cells of the small intestine predominantly secrete mucin 2 (MUC2) that is integral in the formation of the mucus layer. This mucus layer acts as a physical barrier between

host cells and the external environment and interacts with immune cells to alter their function (chapter 1.17.1, page 81). Paneth cells produce antimicrobial peptides (AMPs) that target pathogens that penetrate the mucus layer.

Aside from the key role Paneth cells play in maintaining stem cell fate and in differentiation of secretory cells, they produce AMPs that are vital in host defence against pathogens. Pathogens that penetrate the mucus layer interact with the small intestinal epithelium that results in Paneth secretion of AMPs to prevent infection. Paneth cells secrete α-defensins (or cryptdins) that are involved in pathogen clearance, such as α-defensins type 5 and 6 that are essential in host protection against *Salmonella* infections in humans (Salzman *et al.*, 2003). Paneth cells also secrete lysozyme and REGIII proteins, all involved in host defence to pathogens (Vaishnava *et al.*, 2011). Defects in Paneth cell function to generate AMPs results in significant disease, for example the loss of α-defensin 5 results in the development of an inflammatory bowel diseases, therefore AMPD play an important role in intestinal homeostasis (Wehkamp *et al.*, 2004).

1.2.3 Tight junctions of the intestinal epithelium provide a physical barrier against infection

Adjacent cells of the small intestinal epithelium attach through intercellular junctions to maintain barrier integrity. This is to produce another physical barrier, after the mucus layer, to prevent pathogens from entering the body. There are four types of junctions, the apical complex formed of a tight junction followed by adherens junction then a desmosome, and gap junctions (Figure 2). Tight junctions

span the intercellular space at the apical side of the intestinal epithelial cells that allows molecules of nanometres through. There are four groups of transmembrane proteins that much up tight junctions in the small intestinal epithelium; occludins, claudins, junction-adhesion-molecules (JAMs), and Coxsackievirus and Adenovirus Receptor (CAR) proteins. Occludins and claudins interact with neighbouring cells through extracellular loops whereas JAMs and CARs attachment involves IgG-like domains. Adherens junctions, desmosomes and gap junctions control intracellular signalling and cell-cell adhesion (Guttman and Finlay, 2009). These cell adhesion complexes compartmentalise the external environment from the lamina propria of the intestines, however some pathogens are known to disrupt cell junctions as a means of crossing the small intestinal epithelium.

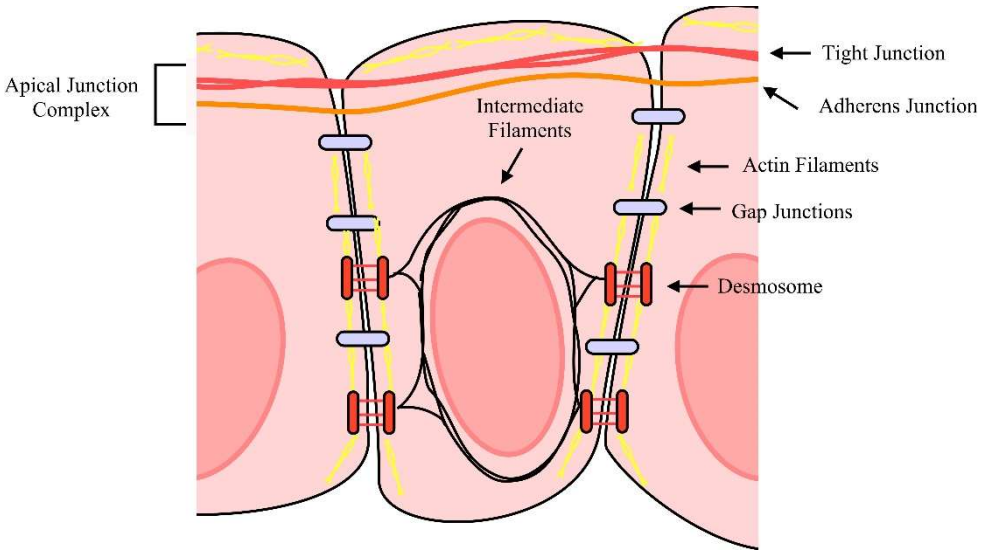

Figure 2. Schematic showing arrangement of junctions in the polarised intestinal epithelium.
The apical junction complex is formed of tight junctions and adherens junctions at the most apical side of the epithelium. Gap junctions and desmosomes are situated below the apical junction complex. Intermediate filaments attach to desmosomes, and actin filaments attach to tight junctions and adherens junctions.

Disruption of cellular tight junctions increases the permeability of the small intestinal epithelium that results in the onset of disease symptoms such as diarrhoea. *Escherichia coli* (*E. coli*) utilise a type 3 secretion system to inject effector proteins within the cytoplasm of host cells resulting in gastroenteritis symptoms such as diarrhoea. This affects the host cytoskeleton that ultimately disrupts cellular tight junctions and increases epithelial integrity (Roxas *et al.*, 2010).

Studying the events that increase permeability of the small intestinal epithelium that cause gastroenteritis is important to determine key factors that can be exploited to develop novel vaccines.

1.3 Current infection models of the small intestine

Various types of models have been utilised to study host-pathogen interactions of the small intestinal epithelium. These include *in vitro* monolayer cultures, primary epithelial cultures, *ex vivo* tissue cultures, and *in vivo* models. The ideal culture would contain the cellular diversity and structure to provide a representative tool for studying enteric infections.

1.3.1 *In vitro* immortalised cell lines

Several intestinal epithelial cell lines exist that derive from tumorigenic cells and are therefore immortalised and are highly proliferative. The benefits of using these cells lines involve their low cost running and ease of culture with their high proliferation providing high throughput screening applications. A key limitation to their use is their reduced complexity and low physiological relevance due to their tumour-like

characteristic that diverges from their *in vivo* counterpart. The colonic adenocarcinoma cell line Caco-2 provides a monolayer of polarised enterocyte-like cells and is a routinely used culture for investigations of intestinal physiology. Their use in infection modelling involved analysing basic invasion assays and have elucidated many mechanisms in pathogenic infections.

Monolayers may not be representative of the small intestinal epithelium due to their differing structure and limited cellular diversity. Moreover, culture of these cells lines over a period of time alters their physiology such that they can form multiple layers, decrease in transepithelial electrical resistance and cellular diversity, and increase in proliferation over passage (Lu *et al.*, 1996; Briske-Anderson, Finley and Newman, 1997). This means that host-pathogen interactions using *in vitro* cell lines may vary in results depending on cell passage number and can even vary between laboratories. Within cell line cultures, there is typically a dominating cell type. With Caco-2 cells these are functionally similar to enterocytes involved in nutrient absorption, however derive from a colorectal origin. The lack of secretory cells, Paneth cell and goblet cells, is an important consideration since these are involved in the secretion of antimicrobial products and cytokines/chemokines that influence the host response to infections. Without these cell types, host-pathogen interactions cannot be accurately recapitulated. These cell lines do not possess the same tight junctions and have reduced transepithelial resistance as the small intestinal epithelium. They are also known to form multiple layers, which makes it difficult to study pathogen manipulation of epithelial barrier function.

1.3.2 3D cultures of immortalised cell lines

Improvements to the Caco-2 cell model by increasing goblet cell abundance with the addition of HT29-MTX still has its limitations (Béduneau *et al.*, 2014). This is due to the culture on a 2D platform, whereby tissue architecture influences cell mechanisms and behaviour in a 3D environment. This 3D environment is established through the production of extracellular matrix within tissues and interact directly with cells to aid in their differentiation and function. Therefore, adding a 3D quality to current 2D culture may improve resemblance of *in vivo* physiology. Culturing these cells lines on to scaffold improves cellular differentiation and resembles *in vivo* functionality. This is evident in culturing of Caco-2/HT29-MTX on a synthetic scaffold poly-lactic-glycolic acid (PLGA) to produce small intestinal epithelial topography contacting both differentiated and undifferentiated IECs, just as *in vivo* (Costello *et al.*, 2014). Although an improvement on modelling the small intestinal epithelium, these cultures lack all the cell types of the epithelium such as Paneth cells that are crucial for infection studies.

1.3.3 Explant and primary adult tissue cultures

To attain an *in vitro* model of the small intestinal epithelium incorporating tissue structure and cellular diversity, explant culture of tissue can be used. This would provide a suitable model to study infections, however most studies utilising explants of the SI were designed for permeability studies. A major issue utilising explants and primary adult tissue cultures is the short-term viability. This is due to the thickness of the tissues that prevent oxygenation of the interior. These can be

improved using perfusion systems, however these are technically challenging procedures and the benefits are not yet fully understood. This limitation of culture period may make this method redundant in modelling enteric infections. However, they can prove useful in certain short term infection studies, such as the use of explant intestinal tissue maintained in an Ussing chamber to visualise the transmigration of *T. gondii* across the epithelium (Barragan and Sibley, 2002). Ultimately, this culture system relies heavily on biopsies and animals for the isolation of tissue. The repeated use of animals in experiments is unfavourable, and their short-term viability make explants and primary tissue cultures undesirable to study enteric infections.

1.3.4 *In vivo* models of enteric infections

The limitations posed by *in vitro* models for studying host-pathogen interactions in the SI means that the use of *in vivo* models is necessary to mimic enteric infections. The advent of knockout or gene silencing techniques in animal models provides a vital tool, however there are several challenges with using *in vivo* models.

Pathogens are administered through oral gavage or through intravenous or intraperitoneal injections. The limitations of oral gavage are that it does not represent a realistic exposure scenario whereby the chewing stress and potential accidental aspiration may result in different outcomes of results. It is also difficult to quantify the administration of pathogens through this method. Enteric pathogens generally develop sparse foci of infection along the surface area of the intestine during early stages of infection. This presents difficulties in analysing host-pathogen

interactions during infection since the whole tissue needs to be analysed thereby losing localised responses to infection against a background of mostly unperturbed tissue.

Using animal models to study infections related to other species may not mimic the pathophysiology of infection. An example is the bacteria *Campylobacter jejuni*. Disease pathology differs between mice and humans whereby infection in mouse models are relatively resistant to colonisation by *C. jejuni* and requires humanised gut flora for the establishment of disease or genetic manipulation to develop exaggerated inflammatory responses (Bereswill *et al.*, 2011; Haag *et al.*, 2012). The differences in disease severity within hosts therefore poses a potential species mismatch when using an animal model to study host-pathogen interactions for diseases in other species.

Larger animal over mouse models for the study of infections to improve relevance is challenging. Acquiring ethical approval is difficult due to potential animal welfare issues and costs involved in maintaining these animals in large facilities is a limiting factor. Since the introduction of the 3Rs (replacement, reduction and refinement) in using animals for research, we need to develop new strategies and methods that reduced the use of animals in infection studies (Prescott and Lidster, 2017).

1.3.5 Organ-on-a-chip models of the intestine

In the last few years, new model systems have been developed that better represent *in vivo* environment of the small intestine. Organ chips are microfluid

devices that contain chambers inhabited by cells that are subjected to continuous perfusion with medium to provide a model that closely resembles organ physiology. For the intestine, models have been developed that incorporate intestinal epithelial cells, commensal bacteria, immune cells, and pathogens. For example, a study using the cell line Caco-2 in perfusion with commensal bacteria resulted in transcriptional responses that differed from that of a simple coculture. However, this model is very complex and is limited by the separation of microbial and IECs and by the short life span of cells in these perfusion cultures (Shah *et al.*, 2016).

Microfluid 2-channel Gut Chip models have been established that recapitulates the physiology of the intestinal epithelium that undergo peristalsis-like motions (Kim *et al.*, 2016). This model incorporates the small intestinal epithelium, immune cells in the form of peripheral blood mononuclear cells, commensal bacteria, and microvascular endothelial cells. Caco-2 cells in this Chip retained stem cell-like features and differentiated into the four lineages of the small intestinal epithelium; enteroendocrine cells, enterocytes, goblet cells, and Paneth cells, in a crypt-villus morphology. Gut Chips mimic the dynamic human intestinal microenvironment to a higher degree than current 2D and ex vivo 3D cultures and can integrate pathogenic bacteria to study interactions that are more physiologically relevant.

However, the use of immortalised cells lines is still an issue with regards to this culture method and the varying differences in cultures and mechanistic set-up between laboratories leads to varying results. Therefore, a more suitable model may be derived from stem cells within the small intestinal epithelium cultured in

ECM to provide a 3D culture, termed organoids, that closely resembles the physiology of its *in vivo* counterpart.

1.4 Small intestinal organoids

An organoid is defined as a self-organising, tissue like structure that contains the various cell types of its specific organ. These *in vitro* cultures are within ECM gel and supplied with specific growth factors that allows for the efficient maintenance and expansion of their stem cell populations. Intestinal organoids derive from Lgr5+ stem cells that reside within crypt structures of the small intestinal epithelium, that proliferate and differentiate to develop bud-like crypt structures and villous cells containing the differentiated cell types of the intestinal epithelium that enclose a central lumen (Figure 3) (Sato *et al.*, 2009).

Crypt cells of the small intestine of mice are embedded in Matrigel, an ECM gel, and cultured in medium containing EGF, noggin, and R-spondin. These conditions mimic the physiological intestinal epithelial niche microenvironment that generate organoids for mice, and have since been optimised for other species including humans, cat, dog, pig, cow, horse, sheep, and chicken (Sato *et al.*, 2011; Powell and Behnke, 2017; Derricott *et al.*, 2018; Hamilton *et al.*, 2018). Due to the expansion of small intestinal epithelial stem cells and their longevity in culture, these organoid systems can expand indefinitely, allowing for the reduction of animals in research. Organoids provide a more suitable model of the intestinal epithelium due to their similar architecture and cell diversity.

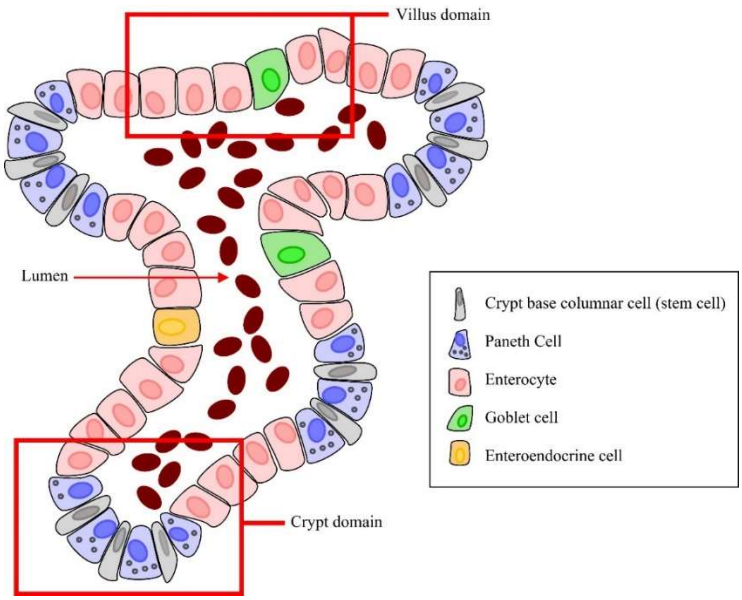

Figure 3. 2D Schematic of a small intestinal organoid
Organoids develop into crypt-villus structures containing all the multiple cell types of the small intestinal epithelium.

1.4.1 Intestinal organoids as models for infectious diseases

The use of organoids as disease models have mostly concentrated on drug development assays and cancer models with limited use in studying enteric infections. Since this study began, intestinal organoids have been developed as a suitable infection model for bacteria, such as *Salmonella* (Wilson *et al.*, 2014; Zhang *et al.*, 2014; Forbester *et al.*, 2015), *Clostridium difficile* (Leslie *et al.*, 2015), and *Escherichia coli* (Karve *et al.*, 2017), viruses such as rotavirus (Yin *et al.*, 2015; Hakim *et al.*, 2018), norovirus (Zhang *et al.*, 2017), and influenza (L. Huang *et al.*, 2017), and parasites such as *Cryptosporidium parvum* (Zhang *et al.*, 2016; Heo *et al.*, 2018).

Infections of murine organoids with *Salmonella enterica* serovars Typhimurium decrease the expression of certain tight junction proteins such as ZO-1 and some claudins resulting in the disruption of the barrier integrity. Inflammatory cytokines

also increase in expression such as IFN-γ and TNF-α, with reduction in stem cells markers, all of which are seen *in vivo* (Zhang *et al.*, 2014). Another study utilising this infection model described the importance of α-defensins expressed by Paneth cells in the prevention of bacterial growth (Wilson *et al.*, 2014). Using *Salmonella* in human organoids derived from pluripotent stem cells expressed similar results to the murine infection model, with the increased expression of inflammatory cytokines (Forbester *et al.*, 2015). *Clostridium difficile* infections of human organoids from pluripotent stem cells presented with a loss of barrier integrity, and this was determined to depend on the toxin TcdA expressed by the anaerobic bacterium (Leslie *et al.*, 2015). Human organoids infected with O157:H7 *Escherichia coli* displayed changes in cell adhesion protein expression and increased expression of inflammatory cytokines such as TNF-α and IL-1β. Polymorphonuclear cells were added to this infection and increased attraction to sites of infection was observed (Karve *et al.*, 2017). These studies reveal the relevance of using intestinal organoids to study host-pathogen interactions with bacteria.

Organoids present a suitable model for viral infections that are difficult to model using cell lines. Rotavirus is able to replicate in human organoid cultures, with the induction of IFN signalling (Yin *et al.*, 2015; Hakim *et al.*, 2018). Treatments with IFN-γ and antivirals such as ribavirin inhibited rotaviral growth, however organoids were less sensitive to these antiviral treatments than infected cells line which is representative of that seen *in vivo,* therefore supports the use of organoids rather than cell lines for testing therapeutics. There are very limited models that allow for the efficient replication of norovirus *in vitro*. Human organoids infected with

norovirus allow a limited expansion of the virus but is still a promising alternative model. Norovirus infects enterocytes, therefore the development of factors to increase enterocyte quantities within organoids may improve expansion of the virus *in vitro*. Organoids have recently been developed to model avian influenza H9N2 subtype that replicates in avian intestines and spread in faeces posing a significant zoonotic health risk (L. Huang *et al.*, 2017). Infection of murine intestinal organoids resulted in a decrease in Paneth cells and subsequently stem cell markers that affected the growth and differentiation of organoids. This is a new model for the influenza virus and is yet to be fully exploited. Organoids provide a better alternative to cell lines in modelling viral infections since organoids support the replication of viruses otherwise seen *in vivo* with similar pathology.

In vitro models for parasites with complex life cycles such as *Cryptosporidium parvum* (*C. parvum*) are inefficient for parasite propagation. However, these models consist of monolayers derived from kidney and colon cell lines, not representative of the small intestinal epithelium. Intestinal and lung organoids generated from human biopsy samples provide relevant models for *C. parvum* infection, with microinjections into the lumen of these organoids restricting infection to the luminal surface. Here, *C. parvum* propagated, developed into infectious oocysts and underwent a complete life cycle as determined by electron microscopy and transcriptomics, with a type I response initiated in host cells (Heo *et al.*, 2018). Organoid expansion was restricted upon infection, stem markers decreased in expression and Wnt signalling was reduced otherwise involved in stem cell

maintenance (Zhang *et al.*, 2016). This reveals that organoids can be used as an appropriate infection model for enteric parasites.

Enteric infections occur at the luminal surface of the small intestinal epithelium. However, organoids present technical difficulties in reflecting this physiologic route of infection due to the enclosed lumen. The small intestinal epithelium is polarised, with different receptors at either basal and apical sides. Therefore, infection from one side may incur different host responses to that of the basal side. One way to restrict infection to the luminal surface is through the use of a microinjection system that delivers pathogens directly into the luminal space of organoids (Wilson *et al.*, 2014; Forbester *et al.*, 2015; Karve *et al.*, 2017; Heo *et al.*, 2018). This technique has primarily applied to bacteria, although a very recent study has injected parasites of a relatively larger size (Heo *et al.*, 2018). These studies have allowed for the assessment of host-pathogen interactions that more closely mimics that of *in vivo* infections due to the close physiological relevance.

An alternative method of exposing the luminal surface for infection is through the culture of organoids to produce monolayer sheets (Liu *et al.*, 2018; Thorne *et al.*, 2018)(L. Luu, 2017 PhD thesis, University of Liverpool). The transfer of organoids onto collagen sheets allow for the generation of an IEC monolayer with the luminal surface exposed and have subsequently been successfully infected with *T. gondii* (L. Luu, 2017 PhD thesis, University of Liverpool).

It should be noted that the definitive host of *T. gondii* are felids, with no current culture mechanism providing a tool for assessing the sexual life cycle of this

parasite. The definitive host for the sister taxon *Isospora suis* is in pigs and this parasite can only complete its life cycle *in vitro* within epithelial cells derived from pigs. This portrays the importance of generating species-specific models to accurately model pathogen interactions with the host. Therefore, organoids from felids may provide a model for the life cycle of *T. gondii* and for the production of sporozoites in culture (Powell and Behnke, 2017).

1.5 *Toxoplasma gondii*

T. gondii is an obligate intracellular parasite belonging to the phylum Apicomplexa that also includes the parasites *Cryptosporidium* and *Neospora*. *T. gondii* is considered one of the most successful parasites in the world due to its global distribution with 25-30% of the world's population exposed or chronically infected (Montoya and Liesenfeld, 2004; Robert-Gangneux and Dardé, 2012). Seroprevalence varies between regions with low seroprevalence observed in North America, South East Asia, and Northern Europe (10-30%), and high prevalence in warm, humid areas such as Latin America and tropical African countries (>60%) (Pappas, Roussos and Falagas, 2009).

The parasite is normally asymptomatic in healthy hosts, disseminating from the intestine to the central nervous system and skeletal muscle tissues which includes brain, spinal cord, and the retina where they remain latent within cysts in the form of bradyzoites. However, reactivation of latent parasites can occur in immune compromised populations, such as those with AIDS, causing toxoplasmic encephalitis. Congenital transmission of the parasite from mother to foetus through

the placenta can cause disastrous birth defects resulting in miscarriages or blindness and mental retardation caused by abnormal neuronal development (Black and Boothroyd, 2000). Although infections with this parasite are often described as asymptomatic in immune-competent adult hosts, recent studies suggest a link to certain mental conditions such as bipolar disease, rage disorder, and schizophrenia within immune competent people (Xiao *et al.*, 2018). This shouldn't be surprising since behavioural traits are affected in rodents with *T. gondii* whereby infections override the natural impulse to avoid feline odour increasing the chances of predation, and hence transmission of the parasite (Ingram *et al.*, 2013).

T. gondii is characterised by the CDC as a "neglected parasitic infection", with many aspects of their functional biology yet to be fully established (Centers for Disease Control and Prevention, 2016). This includes the route of invasion across the intestinal epithelium and the ability of the parasites to manipulate immune cells for their dissemination throughout the body. Improvements in our understanding of biological functions of *T. gondii* infections will improve vaccine and therapeutic designs toward this globally prevalent parasite.

1.5.1 Life cycle

T. gondii has a complex lifecycle alternating between sexual and asexual replication in definitive hosts and intermediate, respectively. Their definitive hosts being members of the Felidae family whereby sexual replication takes place in the small intestine and shedding of environmentally-resistant oocysts in faeces occurs (Dubey and Frenkel, 1972). Ingestion of these oocysts, that contain the highly infectious

form of *T. gondii* known as sporozoites, from contaminated water or food results in infection of intermediate hosts of which are virtually all warm-blooded vertebrates (Dubey, 1998). *T. gondii* invades the small intestine, differentiate into the highly replicative form, tachyzoites, and spreads throughout the body forming encysted bradyzoites within muscle and the central nervous system. Bradyzoites are a latent, slow replicating form of *T. gondii* that can persist for the lifetime of the host. Infections of the host with *T. gondii* can also occur following consumption of bradyzoite cysts in undercooked meat. Following consumption of either oocysts or cysts, the first interactions between the parasite and the host is in the small intestinal epithelium.

1.5.2 Pathogenesis

T. gondii infections are usually asymptomatic or cause mild flu-like illness in immune competent hosts. However, ocular toxoplasmosis and rare outbreaks of more serious disease such as toxoplasmic encephalitis can occur in healthy individuals (Bowie *et al.*, 1997; Demar *et al.*, 2007). Reactivation of parasitic cysts can occur in newly immune deficient people that can cause clinical disease (Black and Boothroyd, 2000). This parasite also poses a risk to foetuses of previously uninfected mothers whereby congenital transmission through the placenta can occur resulting in miscarriage or abnormal neuronal developments such as blindness and mental retardation (Black and Boothroyd, 2000). The two infectious forms of *T. gondii* reside within oocysts and tissue cysts known as sporozoites and bradyzoites, respectively. Infections in humans are commonly acquired through

ingestion of oocysts shed in cat faeces, which can contaminate water or vegetation, or through ingestion of tissue cysts in undercooked meat (Jones and Dubey, 2010, 2012)

1.5.3 *Toxoplasma gondii* types

The serovars of *T. gondii* are grouped into clonal lineages I, II and III that dominate Europe and North America (Howe and Sibley, 1995). Although genetically similar, differing by only 1-2% at the nucleotide level, virulence between these types of *T. gondii* varies (Grigg *et al.*, 2001). Type I (which includes the strain RH) are known to be highly virulent, able to cross cellular barriers, and are more motile than types II (Pru and ME49 strains) and III (which includes VEG), which are less virulent and stimulate stronger immune responses in hosts hindering their dissemination and pathology (Barragan and Sibley, 2002). Whole genome sequencing between strains have shown conserved genes and variation in regions associated with proteins involved in invasion, replication, and motility (Jones, Korcsmaros and Carding, 2017). It is therefore of interest to study different strains and their virulence to identify the factors required for virulence within certain strains and provide alternative targets to develop novel vaccines.

T. gondii that do not confer to the genotypes of types I-III are referred to as atypical strains. These are mainly found in South America and differ in pathogenicity from the typical lineages (Dardé, 2008). Atypical strains possess a greater genetic diversity that typical strains providing difficulty in establishing their virulence, although virulence is observed in mice at isolation. Little is known about the

virulence of these atypical strains, however comparisons of ocular toxoplasmosis reveals the significance of atypical virulence in South America (de-la-Torre *et al.*, 2013). Here, Colombian patients had either a type I or atypical strain infection whereas French patients were infected with the type II strain, with further symptoms incurred within the Colombian patients.

1.5.4 Prevalence of *Toxoplasma gondii* in agriculture

Ingestion of undercooked meats containing bradyzoite cysts is a public health risk to humans. Changes in farming management by improving biosecurity regulations, increased rodent control, and through confined housing of farm animals has resulted in an overall drop in prevalence of *T. gondii* within livestock animals over the last three decades (Food Standards Agency, 2012). Epidemiological studies have shown that, compared to beef and poultry, there is a greater chance of pork being contaminated with *T. gondii*, which implies that this meat is a major source of zoonotic transmission (Dubey *et al.*, 2005; Guo *et al.*, 2015). Although seroprevalence in pigs is generally decreasing, parts of Europe are witnessing an increase due to outdoor rearing (Food Standards Agency, 2012). This recent change to more outdoor farming systems may have caused an increase in seroprevalence within some European countries such as Germany, where 11.7% of organic finishing pigs and 31.6% of sows are seropositive (Food Standards Agency, 2012).

Transmission of *T. gondii* to sheep is caused through grazing in pastures contaminated with oocysts. Toxoplasmosis in sheep is the second most common cause of sheep abortion with approximately 0.5 million lambs are lost each year

costing the UK farming industry £12-24 million annually (Food Standards Agency, 2012). This also poses as a zoonotic health risk to humans with a seroprevalence of 30% of sheep in Europe, highlighting the importance for the development of preventative treatments for the spread of *T. gondii* (Food Standards Agency, 2012). Vaccines are available to prevent the congenital transmission in sheep, but not for treatment or prevention of infection (Buxton and Innes, 1995). These generally target the tachyzoite form and not the latent bradyzoites. Cystic parasites within livestock pose a zoonotic threat toward humans through the ingestion of undercooked meat, thereby highlighting the importance for preventative measures against infection.

Within the last 25 years it has been stated that as much as 75% of new human pathogens have emanated from animals and is predicted to continue to rise (King *et al.*, 2006).

1.5.6 Treatments for *Toxoplasma gondii*

There are currently no human vaccines against *T. gondii*, with current medications eradicating the invasive tachyzoites but not the cystic bradyzoites (Black and Boothroyd, 2000; Valentini *et al.*, 2014). These include pyrimethamine, also used as a malaria medication, and sulfadiazine. These treatments have severe side effects and the reactivation of bradyzoite cysts can occur at any time, therefore requiring long term treatment. *T. gondii* elicits protective immunity to reinfection in most individuals, relying on cellular immunity mediated by CD4+ and CD8+ cells that secrete IFN-γ, a Th1 response. The mechanisms involved in *T. gondii* immunity have

not been fully elucidated, with the complex biological characteristic of *T. gondii* providing difficulties in generating effective vaccines.

There is only one commercially available vaccine, known as Toxovax®, provided for livestock (Buxton and Innes, 1995). This vaccine is based on a live-attenuated S48 tachyzoite strain, and has been used in New Zealand, France and the UK. However, this is only effective against congenital transmission and not as a treatment directed against the zoonotic bradyzoite cysts (Food Standards Agency, 2012). Since this is a live-attenuated vaccine, this treatment runs the risk of developing adverse effects, is very expensive, and has a short shelf life. Due to the complex life cycle of *T. gondii* that involve stage-specific antigens, and the diverse array of strains and genotypes, vaccine candidates have been largely unsuccessful. However, vaccines containing ROP8 DNA, a rhoptry protein essential for parasite invasion, induces a protective immune response in mice to infection (Parthasarathy *et al.*, 2013). DNA vaccines are relatively inexpensive and easy to produce, safe, and heat stable. They also show great promise as a vaccine candidate against *T. gondii* infection. A DNA vaccine encoding TgESA10, an excretory-secretory antigen, elicits a strong Th1 response that resulted in high IFN-γ production and protection against infection (Wang *et al.*, 2015). Providing multi-antigenic DNA vaccines improves immunity even further since these vaccines may contain antigen DNA involved during different stages of the *T. gondii* life cycle. Vaccines with DNA encoding GRA17 and GRA23 induced a much greater immune response with greater IFN-γ and IgG production that increased survival time in mice (Zhu *et al.*, 2017). Other vaccine candidates have been considered, including those that deliver pathogenic recombinant proteins to

elicit immune responses. Induction of both mucosal and cellular immune responses is also driven by DCs. Therefore, driving DCs activation to *T. gondii* infections may improve protection to infection. Vaccines targeting the delivery of SAG1 antigen protein to DCs improved both local and systemic immune responses with an increase in IFN-γ and Th1 activation (Lakhrif *et al.*, 2018). These are all potential vaccine targets for future development, however there remains a significant requirement for safer and more effective drugs and vaccines.

1.5.7 Morphology of *Toxoplasma gondii*

Apicomplexan parasites are heavily polarised within their elongated shape (Figure 4). The apical region is distinctive in its density of unique organelles, including rhoptries and micronemes. The apical complex is made up the conoid and the apical ring. The organelles secrete proteins through the apical complex that are required for parasite invasion, motility, adhesion, and development of the parasitophorous vacuole (PV). The apical ring serves as part of the microtubule-organising center. Another unique structural feature of apicomplexans is the chloroplast-like organelle termed the apicoplast. The pellicle surrounds the parasites consisting of the plasma membrane and inner membrane complex (Figure 4). The pellicle is closely associated with a number of cytoskeletal elements such as actin, myosin, and microtubules (Morrissette and Sibley, 2002).

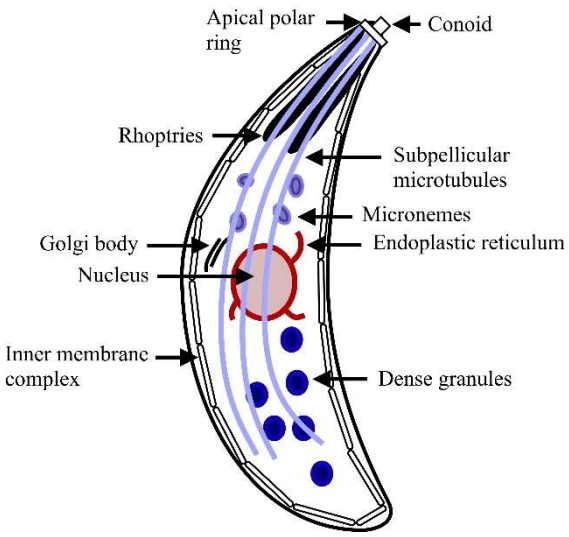

Figure 4. Schematic of the morphology of apicomplexans
Apicomplexans such as *T. gondii* are polarised with the apical polar ring and conoid at the apical side of the parasite. These structures play a role in cell invasion. Rhoptries, micronemes, and dense granules are secretory organelles involved in cell invasion and PV formation.

Host cell attachment, motility, cell invasion, and development of the PV all derive from the apical region of apicomplexans through organelle secretion. These allow them to successfully infect all warm-blooded, nucleated cells and replicate within relative safety of host cell defences within the PV. The PV is derived from the host membrane, with the secreted proteins from *T. gondii* modifying the vacuole to enable nutrient transfer and subversion to host cell defences to allow for parasite replication.

1.6 *Toxoplasma gondii* infections of the small intestinal epithelium

Consumption of bradyzoite-containing tissue cysts or sporozoite-containing oocytes leads to the rupture of cysts or oocysts and liberation of parasites that transmigrate across the small intestinal epithelium. This has been proposed to occur in two ways; active penetration of cells or through the paracellular route (Dubey, 1997; Barragan

and Sibley, 2002; Barragan, Brossier and Sibley, 2005; Weight and Carding, 2012). Invasive parasites reside within cells in parasitophorous vacuoles made up from the host cell's membrane. This allows for a particular environmental niche for their replication (Lingelbach and Joiner, 1998). The parasites subsequently convert to a highly replicative form known as tachyzoites, generally 5µm long and 2µm wide (Black and Boothroyd, 2000). These replicate asexually within cells of intermediate hosts with a generation time of between 6 to 8 hours before cell egress (Black and Boothroyd, 2000). The epithelial cells respond by producing cytokines, chemokines and anti-microbial peptides upon invasion (Ju, Chockalingam and Leifer, 2009; Morampudi, Braun and D'Souza, 2011). *T. gondii* tachyzoites has also been shown to adhere to the epithelium through interactions with cell surface proteins, such as ICAM-1, and disrupt tight junctions as they traverse this barrier (Barragan, Brossier and Sibley, 2005; Weight and Carding, 2012). *T. gondii* then effectively disseminates throughout the body by invading highly migratory nucleated cells of the host, including those of the immune system such as dendritic cells that migrate to lymph nodes and ultimately the central nervous system or muscle tissue (Courret *et al.*, 2006; Lambert *et al.*, 2006; Weidner and Barragan, 2014).

In general, we know remarkably little about how *T. gondii* interacts with the small intestinal epithelium during early infection events. Using *in vivo* disease models to study the interactions between *T. gondii* and the intestinal epithelium is limiting due to the difficulties in locating the scarce sites of invasion within a whole tissue sample. The responses to these initial invasions are relatively small and localised, making their detection challenging. *In vitro* models use monolayer cultures of

intestinal epithelial cells derived from embryonic sources, allowing for the study interactions such as the early responses to infection (Ju, Chockalingam and Leifer, 2009; Morampudi, Braun and D'Souza, 2011). However, such studies are scarce.

1.6.1 *Toxoplasma gondii* invasion of the small intestinal epithelium

Most of our knowledge of *T. gondii* interactions with the small intestinal epithelium derive from *in vitro* cultures derived from cell lines assumed to operate similarly to the small intestinal epithelium. Glycosylphosphatidylinositol (GPI)-anchored surface antigens (SAGs) and SAG-related sequence (SRS) proteins are expressed on the surface of *T. gondii*. In tachyzoites, six of these are the most abundant on the parasite surface: SAG1-3 and SRS1-3. These allow for the initial attachment to the surface of a host cell. *T. gondii* lack cilia or flagella that otherwise aid pathogens to move, and therefore contain a unique form of motility known as gliding motility. Here, adhesive proteins of the parasite attached to the surface of cells allows for translocation governed by actin-dependent myosin motors, where this process is also involved in cell invasion. This gliding motility allows the parasite to move along the surface of the host cell to position itself at an optimal site for invasion. Adhesion to cell surfaces is mediated by micronemal proteins (MICs) at the apical end of the parasite (Figure 5). These are expressed by secretory organelles known as micronemes. There are approximately 15 MICs that are secreted during parasite adhesion of host cells (Carruthers, Giddings and Sibley, 1999) and genetic ablation of certain MICs attenuates invasion, such as MIC1 and MIC3 whereby deletion of both genes results in non-virulent forms of the parasite (Cérède *et al.*, 2005). The

expression of such a large array of protein ligands increases the chances of *T. gondii* infecting a wide range of hosts and for a stronger binding interaction.

The commitment to invasion is usually dependent on the expression of another MIC protein, apical membrane antigen (AMA1). This interacts with proteins originating from the "neck" region of another secretory organelle termed rhoptries (ROPs). These rhoptry neck (RON) proteins form a complex with AMA1 on the surface to form a moving junction (Alexander *et al.*, 2005), namely RON2. The moving junction closely resembles that of tight junctions, and as invasion continues the moving junction migrates up the parasite away from the apical side, causing the parasite to move into the host cell. ROPs are secreted into the host cell that begin the formation of the parasitophorous vacuole (PV). As the parasite moves into the host cell with the moving junction migrating toward the posterior, the structure acts as a sieve removing proteins from the host and parasite plasma membrane such as MIC proteins (Charron and Sibley, 2004). This may be a cause as to the lack of fusion between lysosomes and the PV membrane within host cells. As the parasite invades the cells, it remains surrounded by the PV created by invagination of the host cell plasma membrane. The PV creates a niche environment for parasite replication and survival as it provides physical separation from the host cell cytoplasm.

ROPs and dense granules secreted by the intracellular *T. gondii* modify the PV membrane (PVM) to allow access of nutrients within the cytosol and combating host cell defences. The dense granules GRA17 and GRA23 allow for the diffusion of small molecules such as tryptophan and cholesterol across the PVM to the parasite

(Gold *et al.*, 2015). GRAs 2, 4 and 6 form the intravacuolar membrane, providing support for the PVM and nutrient trafficking (Mercier and Cesbron-Delauw, 2015). Other GRAs have been identified although their functions are not yet defined, with suggestions that some of these proteins translocate to the host cell nucleus from the PV to increase host cell metabolism and the p53 suppressor pathway, such as GRA16 and GRA24 (Hakimi and Bougdour, 2015).

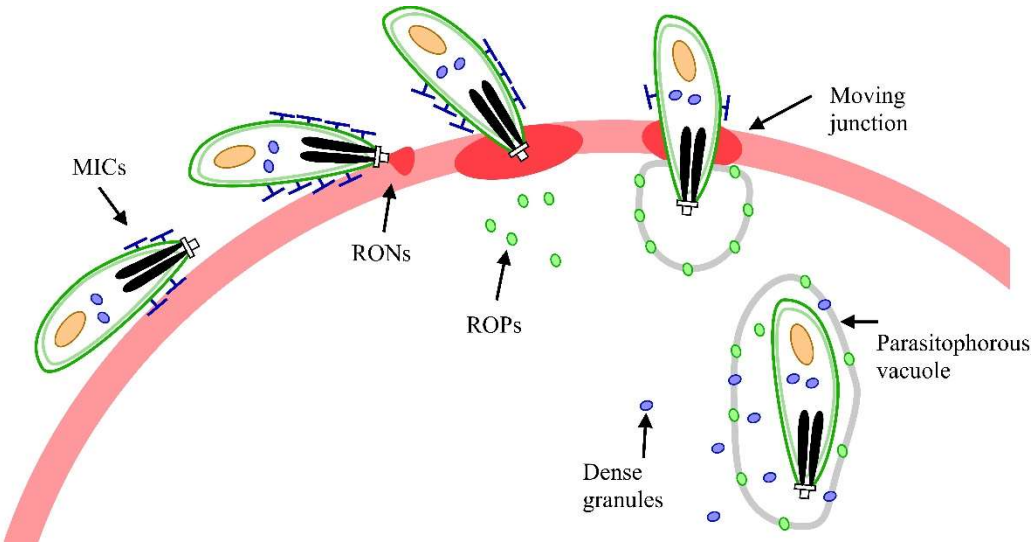

Figure 5. Schematic of the invasion events of *T. gondii* into host cells and subsequent formation of the PV. Initial attachment to the cell surface involves SAG1 and subsequent expression of MICs that also attach to the surface. The release of RONs interact with parasite-derived AMA1 that intimately binds the cell surface and forms the moving junction. ROPs are subsequently injected into the host cell cytoplasm with some ROPs aiding in parasitophorous vacuole development. Active penetration of the host cell occurs by pulling on the surrounding moving junction complex. This invaginates the host cell membrane to form the PV. Dense granules are secreted to fully form the PV.

Within the protective environment of the PV, *T. gondii* is able to undergo replication by internal budding to produce two daughter cells. Repeated cycles of replication form clusters or 'rosettes' within host cells. Parasites egress from host cells causing destruction of the cells and release of parasites into the intestinal lumen for further infection (Gregg *et al.*, 2013).

1.6.2 Host cell manipulation by *Toxoplasma gondii*

Host cells contain natural defences against pathogenic invasion. In order for *T. gondii* to successfully replicate within host cells the parasite must manipulate the host cell machinery in order to evade immunity. These processes are still being elucidated, however resistance to *T. gondii* is dependent on IFN-γ for the innate and adaptive immune responses. This inflammatory cytokine induces a number of antimicrobial defences including the induction of nitric oxide synthase, upregulation of reactive oxygen species, and through upregulating the expression of antiparasitic genes including IFN-γ-regulated GTPases (IRGs) that degrade the PVM. *T. gondii* can evade this host defence by the expression of ROP1 and ROP17 that inactivate IRGs. The binding of IFN-γ to its receptor results in the phosphorylation of the signal transducer and activator of transcription 1 (STAT1) protein that bind to the gamma-activated sequence (GAS) in the host cell, resulting in the transcription of genes necessary for driving immunity. Infections with *T. gondii* block STAT1-mediated transcription with no functional affects to the STAT1 protein since they still bind to GASs in the host cell nucleus. The blocking of this immune pathway is through the expression of *T. gondii* inhibitor of STAT1-dependent transcription (TgIST) by the parasite that binds activated STAT1 dimers associated with GASs and blocks their transcription, and also causes the recruitment of a chromatin-modifying complex, Mi-2/NuRD, to activated STAT1 complexes in the nucleus (Olias *et al.*, 2016). There are differences in host cell manipulation between *T. gondii* strains. For example, type II strains do not activate STAT3 activation in fibroblasts whereas types I and II did through the expression of GRA15 (Rosowski *et al.*, 2011).

Another host defence mechanism towards *T. gondii* is through the CD40-dependent autophagy of the PVM within macrophages. However, *T. gondii* activates EGF receptor signalling through the expression of MICs, specifically MIC3 and MIC6, that prevents the expression of the autophagy protein LC3 and hence the formation of autophagosomes in host cells (Muniz-Feliciano *et al.*, 2013).

Mice that lack myeloid differentiation primary-response protein 88 (MyD88) show defective production of IFN-γ (Scanga *et al.*, 2002). MyD88 induction is through Toll-like receptor (TLR) stimulation that drive immune responses to infection. *T. gondii* profilin activates TLR11/12, responsible for immune activation to *T. gondii*, however it has also been suggested that *T. gondii* interacts with TLR9 on host cells that results in type I interferon secretion and α-defensin 5 production from Paneth cells (Foureau *et al.*, 2010; Santamaria, Perez Cabarello and Corral, 2016). These are involved in reducing parasite viability and infection. Certain strains of *T. gondii* have been shown to downregulate the production of β-defensins, although the precise mechanisms and effector molecules involved remain unclear (Morampudi, Braun and D'Souza, 2011). Each strain differ in their activation of host cell response, such as NF-κB signalling in IECs (Rosowski *et al.*, 2011), and their ability to transmigrate across the intestinal epithelium whereby type I strains have long-distance migration that results in a greater efficiency in transmigration than type II and type III strains (Barragan and Sibley, 2002). Elucidating the mechanisms in which *T. gondii* affects host cell defences to infection could provide novel therapeutics against parasitic infection.

1.6.3 *Toxoplasma gondii* transepithelial migration across the small intestinal epithelium

Ingestion of bradyzoite or sporozoite cysts causes the cysts to rupture due to the acid pH and digestive enzymes. The parasites infect the small intestinal epithelium and convert to tachyzoites that replicate and disseminate throughout the body (Dubey, 1997). However, it remains unclear how the parasite crosses the epithelial barrier with evidence of both an intracellular and paracellular route.

Migration across polarised SI cells is strain dependent with type I tachyzoites showing superior migratory ability (Barragan and Sibley, 2002). Transmigration may be important to the parasite for dissemination to prevent early activation of immune responses by the infection of cells. Intercellular adhesion molecule 1 (ICAM-1) is upregulated during *T. gondii* infection with binding of MIC2 on the parasite surface aiding in transepithelial migration through the paracellular route (Barragan, Brossier and Sibley, 2005). Transmigration does not alter barrier integrity during early stages of infection *in vitro* (Barragan, Brossier and Sibley, 2005), however after 24h barrier integrity is disrupted through the redistribution of tight junctions from the surface of host cells to the cytoplasm (Weight *et al.*, 2015; Briceno *et al.*, 2016). Parasites colocalise with the tight junction protein occludin, pointing to its importance in migration. Interestingly, bradyzoite infections of IECs *in vitro* caused a greater disruption of the epithelial barrier and greater loss of tight junction integrity suggesting that the different factors expressed by this life stage may have a greater transmigration ability (Weight *et al.*, 2015).

It is suggested that invasion of the epithelial barrier *T. gondii* can occur through both direct invasion or through the paracellular route and the preference may be subject to parasite strain. Since transepithelial migration occurs during early stage of infection, monolayer cultures and ex vivo tissues have been utilised to image this occurrence. These techniques have limitations in that monolayer cultures are not representative of the small intestinal epithelial cell diversity and the short-term viability of ex vivo tissues. Therefore, a more suitable model is required to more accurately characterise the transmigration process of *T. gondii* across the small intestinal epithelium.

1.7 *Toxoplasma gondii* utilises immune cells for dissemination

After crossing the epithelial barrier, *T. gondii* is thought to invade immune cells and utilise their migratory pathways to disseminate through the host. Early after infection (2 days), the predominant immune cell population harbouring parasites in the small intestine were $CD11c^+$, likely to be resident DC populations very early in infection. $CD11c^+$ cells were also heavily parasitized in the draining mesenteric lymph node from days 3-7 post infection. This suggested that CD11c+ DCs, which migrate constitutively from intestine to MLN, were carrying the parasite with them. Indeed, CD11c high cells are almost completely absent from foci of infection later in infection (days 7-8), suggesting an early and intense migration of the DCs to the MLN, carrying the parasites with them (Coombes *et al.*, 2013). Direct invasion of DCs prevents detection of the parasite by other immune cells, known as a "Trojan horse" mechanism (Courret *et al.*, 2006; Bierly *et al.*, 2008; Cohen and Denkers,

2015). *In vitro* studies of parasite-infected intestinal DCs show evidence for an increased DC motility that might be involved in the spread of the parasite (Lambert *et al.*, 2006; Weidner *et al.*, 2013; Kanatani, Uhlén and Barragan, 2015). Moreover, infected DCs have decreased RA and IL-12 production that are otherwise involved in driving a T helper 1 (Th1) response. (Cohen and Denkers, 2015). There is still much to be understood about the interaction between DCs and *T. gondii* that may aid in developing therapies targeting spread of infection. Elucidating these interactions may divulge new factors that can be utilised for the production of vaccines or therapeutics to prevent infections.

At later time-points after infection, neutrophils and monocytes were preferentially invaded, with only a low percentage of infected DCs (Coombes *et al.*, 2013; Gregg *et al.*, 2013). Infected neutrophils increased spread of the parasite within the small intestine by retrograde migration into the lumen, so may not be key cells in the dissemination throughout the body.

1.8 Conventional dendritic cells

Dendritic cells (DCs) are professional antigen presenting cells (APCs) present in virtually every tissue throughout the body and play an important role in bridging the innate and adaptive immune systems. All DCs derive from a common bone marrow progenitor from which DCs can be divided into three main groups, specifically monocyte-derived DCs, plasmacytoid DCs, and conventional DCs (cDCs). Of interest are cDCs that sample antigens within particular tissue environments with subsequent migration to draining lymph nodes and antigen presentation to T cells,

driving their maturation and proliferation into effector T cells or regulatory T cells. These T lymphocytes then produce an immune response in the tissue of cDC source. The developmental pathways of cDCs are still a topic of uncertainty. It is currently thought that haematopoietic stem cells within the bone marrow differentiate into common myeloid progenitors that develop into common DC precursors (CDP). The CDP generates pre-cDCs that migrate from the bone marrow to populate lymphoid and non-lymphoid tissues where they further differentiate into cDCs.

Development of cDCs is partly regulated by cytokines expressed in their local environment. It was originally thought that granulocyte macrophage colony stimulating factor (GM-CSF) was the main cytokine in cDC development and was originally used to produce DCs *in vitro*, sometimes including interleukin 4 (IL-4) (Yokota *et al.*, 2009; Zhu *et al.*, 2013). However, mice lacking GM-CSF or its receptor showed limited reduction in DC populations within lymphoid organs, with only significant decreases in non-lymphoid tissue suggesting that GM-CSF is dispensable for cDC development (Vremec *et al.*, 1997). DC precursors all express the FMS-like tyrosine kinase 3 (Flt3) receptor and expression of Flt3 ligand (Flt3L) by stromal, endothelial and T cells is the main cytokine regulating DC development (D'Amico and Wu, 2003; Naik *et al.*, 2007). Evidence for the importance of this cytokine on cDC development is shown in mice lacking Flt3L or its receptor with a significant scarcity of all DC populations (McKenna *et al.*, 2000). Injections of Flt3L *in vivo* caused a tenfold expansion of cDCs, showing the importance of Flt3L in cDC development (Maraskovsky *et al.*, 1996).

1.9 Dendritic cells of the small intestine

The difficulty in dendritic cell isolation from the intestine and the imprecise identification criteria used have resulted in many aspects of their functions yet to be elucidated. DCs from lymphoid and non-lymphoid tissues were originally isolated by their surface expression of CD11c and MHCII. However, it is now known that macrophages within this tissue also express these characteristics, therefore a more definitive phenotype was needed to distinguish the two cell types. More recently proposed classification systems use CD64 or F4/80 to distinguish macrophages, leaving cDCs to be classified on the basis of CD11b and/or CD103 expression (Mowat, 2018). Flt3L is specifically expressed in cDCs and is required for their development from bone marrow precursors (McKenna *et al.*, 2000). These cDCs are seen migrating in lymph nodes where they can prime T cells and only have a lifespan of a few days. However, macrophages are not Flt3L-dependent, have a lifespan of many weeks and are not seen migrating in lymph nodes or seen conditioning T cells (Persson, Scott, *et al.*, 2013). Therefore, these functional differences provide an additional means to discriminate between the two cell types.

Since the improvements in flow cytometric discrimination of DCs and macrophages, it has been established that there are two main subsets of cDCs known as cDC1s and cDC2s, based on their ontogeny through their differing reliance on transcription factors (TFs) and their cell surface expression profiles. The cDC subsets are described based on CD103 and CD11b expression (**Table 1**). The cDC1 subset comprise $CD103^{+}CD11b^{+}$ cDCs, and the cDC2 subset comprise $CD103^{+}CD11b^{-}$,

$CD103^{-}CD11b^{+}$, and $CD103^{-}CD11b^{-}$ cDCs. The two subsets are also distinguished between the specific cross-species markers such as the X-C motif chemokine receptor 1 (XCR1) associated with cDC1s or signal regulatory protein α (SIRPα/CD172a) in cDC2s (Bachem *et al.*, 2012; Becker *et al.*, 2014).The generation and survival of cDC1s is dependent on the TFs basic leucine zipper transcription factor ATF-like 3 (Batf3), interferon regulatory factor 8 (Irf8) and DNA-binding protein inhibitor (Id2), and cDC2s on interferon regulatory factor 4 (Irf4) (Persson, Uronen-Hansson, *et al.*, 2013; Guilliams *et al.*, 2016) (reviewed in (Sichien *et al.*, 2017)). Intestinal cDCs can also be divided by function since cDC1 is the main driver of Treg development and cross-present antigens to CD8+ T-cells and present soluble antigens to CD4+ T cells via MHCII, whereas cDC2s also promote oral tolerance through soluble antigen presentation, but also drive Th2 and Th17 responses to infection. Most research on identifying the cDC subsets within the intestine have been carried out using mouse models, however these subsets LP of mice can be identified in Human SI LP (Watchmaker *et al.*, 2014).

1.9.1 Peyer's patches

Within the small intestine of mammals lie lymphoid follicles known as Peyer's patches (PPs). These are characterised by the presence of specialised epithelial cells known as M cells with underlying follicles of clustered B cells with T cells zones forming a dome shape known as the subepithelial dome (SED). These PPs structures are specialised for sampling of foreign material within the lumen of the small intestine and the subsequent induction of immune responses. The epithelial cells

surrounding M cells, or the follicle-associated epithelium (FAE), lack goblet cells that otherwise create the mucus layer that establishes a physical layer of protection between the external environment and the small intestinal epithelium. Their absence in the FAE therefore increases interactions between pathogens and the FAE. Following adherence of antigens from the lumen to M cells, rapid transportation into the SED allows for the uptake of the antigens by mononuclear phagocytes, namely macrophages and DCs which induce an immune response. Both cDC1 and cDC2 cells have been found within PPs, with the double-negative (DN) $CD103^{-}CD11b^{-}$ cDC2 being the most prominent cDC population. DN cDCs are considered to be immature cDC2 cells due to their similarity in transcriptional programming but lack in maturation marker genes (Iwasaki and Kelsall, 2001; Bonnardel *et al.*, 2017). Upon *in vitro* culture DN cDC2s upregulate the expression of MHCII and CD11b, thereby further suggesting that DN cDC2s are an immature homeostatic stage of cDC2s (Bonnardel *et al.*, 2017). In mouse models deficient in retinoic acid-receptor related orphan receptor γt (RORγt), involved in lymphoid tissue development and therefore devoid of isolated lymphoid follicles and PPs, show only cDC1 and $CD103^{+}CD11b^{+}$ and $CD103^{-}CD11b^{+}$ cDC2s in their intestinal-draining lymph nodes suggesting DN cDC2s derive only from PPs in the small intestine (Cerovic *et al.*, 2012). However, this minor population is heterogenous and its functions remain unclear, and since infections of the small intestine can occur anywhere within the epithelium and PPs are specialised regions for luminal sampling, PPs and DN cDC2s will not be considered further in this report.

1.9.2 Intestinal lamina propria

DCs also reside throughout the lamina propria (LP) of the intestine, a thin layer of connective tissue beneath the epithelium that along with the epithelium makes up the mucosa, that drive immune tolerance towards commensal bacteria or pathogen clearance during infections. All subsets have been seen migrating within the lymphatic system signifying each has the ability to initiate adaptive immune responses, with the predominant subset within the small intestine being $CD103^{+}CD11b^{+}$ cDCs (Denning *et al.*, 2011; Scott *et al.*, 2015). The proportions of these populations differ markedly along the length of the intestine such that the SI is mostly made up of $CD103^{+}CD11b^{+}$ cDC2s, with $CD103^{+}CD11b^{-}$ cDC1s predominating in the colon (Houston *et al.*, 2016). This may reflect the varying physiological necessities of these tissues, differences in the conditioning of cDCs by the tissue environment, and by the distinct microbiota in those regions, yet the functional significances are yet to be determined.

Table 1. Overview of DC subsets in the intestine.
Bold text within 'surface markers' column indicates defining cell surface characteristics. Bold text within location column highlights predominant location of cDC subsets. Abbreviations, CO LP: colonic lamina propria; SI LP: small intestinal lamina propria; PPs: Payer's patches; TFs: transcription factors

Subset	Surface markers	Location	TFs	Functions	Refs
cDC1/ CD8α$^+$/ XCR1$^+$	CD11c$^+$ **CD103$^+$** **CD11b$^-$** CCR7$^+$ **XCR1$^+$**	**CO LP**, SI LP	Batf3, Irf8, Id2	• Prime Th1 cells • Major source of RA in MLN for CCR9/$\alpha_2\beta_4$ induction in T cells • Prime CD4$^+$ and CD8$^+$ T cells • Induction of IELs and FOXP3$^+$ T_{REG} cells	(Coombes *et al.*, 2007; Edelson *et al.*, 2010; Becker *et al.*, 2014; Luda *et al.*, 2016)
cDC2/ CD8α$^-$/ SIRPα$^+$	CD11c$^+$ **CD103$^+$** **CD11b$^+$** CCR7$^+$ **SIRPα$^+$** CX3CR1^{lo}	**SI LP**, CO LP	Irf4, Klf4, Notch2	• Prime Th17 and Th2 cells • Regulate ILC function through production of IL-23 • Presentation of soluble antigens • Induces FOXP3$^+$ T_{REG} cells development	(Lewis *et al.*, 2011; Becker *et al.*, 2014; Scott *et al.*, 2015, 2016; Mayer *et al.*, 2017)
	CD11c$^+$ **CD103$^-$** **CD11b$^+$** CCR7$^+$ **SIRPα$^+$** CX3CR1^{int}	**CO LP**, SI LP	Zeb2 Irf4 Notch2 (?)		
	CD11c$^+$ **CD103$^-$** **CD11b$^-$** **SIRPα$^+$**	PPs	Irf4	• May mature into CD11b+ cDC2s and acquire their functional characteristics • Presentation of soluble antigens	(Bonnardel *et al.*, 2017)

				• Induces FOXP3$^+$ T_{REG} cells development	
pDC	CD11c^{int} CCR9$^+$	SI LP from blood	E2-2, Id2, Zeb2	• Produce type I and III interferons • Critical in antiviral immune response • Prime Treg and Th17 cells	(Bonnefoy *et al.*, 2011; Scott *et al.*, 2016)
moDC	CD11c$^+$ CD103$^-$ CD11b$^+$ CD64+ CCR2$^+$	CO LP, SI LP, from blood	Zbtb46, Irf4	• Recruited to sites of infection to promote inflammation	(Zigmond *et al.*, 2012; Segura and Amigorena, 2013)

1.10 Development of conventional dendritic cells

Conventional DCs develop within the bone marrow from haematopoietic stem cells (HSC) in a process called haematopoiesis. These asymmetrically divide to produce an HSC and multipotent progenitors where the latter further differentiates to produce progenitor cells of myeloid and lymphoid lineages. From here, the myeloid progenitor cells further differentiate into macrophage and DC precursors (Naik *et al.*, 2007). The common DC precursors develop into pre-cDCs and pre-pDCs that migrate to several lymphoid and non-lymphoid tissues where pre-cDCs differentiate into the cDC subsets of that tissue. For intestinal cDCs, exposure to RA in the BM imprints these cells with the gut homing receptor $\alpha_4\beta_7$, termed pre-mucosal DCs (pre-μDCs) (Zeng *et al.*, 2013). The factors involved in determining cDC differentiation from common bone marrow progenitor cells are still unclear.

Culturing BM with Flt3L generates cDC1s, cDC2s and pDCs and, as previously stated, is indispensable for the generation of cDCs. Although Flt3L plays a continuous role in cDC development, GM-CSF is important for the generation of $CD103^+$ cDCs in the intestine from pre-cDCs (Bogunovic *et al.*, 2009). A suggested source of GM-CSF is from innate lymphoid cells (ILCs) dependent on crosstalk with activated macrophages (Mortha *et al.*, 2014). Other cytokine signalling within the LP of the SI is necessary for the differentiation of the cDC subsets and depends on communication between other immune cells such as macrophages, ILCs, IELs, and the intestinal epithelium during intestinal homeostasis and infections.

1.11 Functions of cDC1s in the small intestine

The BATF3 and IRF8-dependent subset of cDCs (cDC1) characteristically express XCR1, CD103 and CD8α, lack expression of CD11b and represent approximately 5% of murine intestinal DCs (Edelson *et al.*, 2010; Bachem *et al.*, 2012). The elucidation of their physiological functions have relied on mouse models that lack transcription factors required for their development. These include *Itgax-cre.Irf8* $^{fl/fl}$ mice that resulted in a reduction of $CD4^+$ and $CD8^+$ T cells and $CD8\alpha\beta^+TCR\alpha\beta^+$, $CD8\alpha\alpha^+TCR\alpha\beta^+$ and $CD8\alpha\alpha^+TCR\gamma\delta$ IELs within the SI (Luda *et al.*, 2016; Ohta *et al.*, 2016). The cDC1 subset are known to be the major subtype involved in antigen cross-presentation to T cells in MLNs, therefore the reduction in intestinal $CD8\alpha\beta^+$ T cells may be consequence to the depletion of this cDC subset in this mouse model.

$CD103^+$ DCs express Cadm1 that interacts with Crtam on lymphocytes in the MLNs. This keeps T cells adhered to DCs that sustains exposure to TGF-β and RA to induce

gut homing receptor expression on the T cells and promote the conversion of $CD4^+$ T cells into $CD4^+CD8^+$ T cells (Cortez *et al.*, 2014). Depletion of cDC1s using *Batf3*$^{-/-}$ mouse models resulted in reduced numbers of $CD4^+CD8\alpha\alpha^+$ IELS, known to be cytotoxic and restricted to MHCII interactions with their development relying on $CD4^+$ T cell exposure to RA and TGF-β. Infections of this mouse model with the enteric parasite *Trichuris muris* (*T. muris*) and *Leishmania major* (*L. major*) failed to generate a Th1 response (Martínez-López *et al.*, 2015; Demiri *et al.*, 2017). During low-dose infection with *T. muris*, induction of Th1 cells failed with an increase in Th2 cytokines and clearance of the parasite. This suggests possible interplay between cDC1 and cDC2 subsets during helminthic infections since cDC2s are involved in Th2 responses. IL-12 production is mostly expressed by cDC1s in MLN during enteric infections as evidenced in *T. gondii* and *L. major* infections in mice (Cohen and Denkers, 2015; Martínez-López *et al.*, 2015). Therefore, a reduction in IL-12 production due to the depletion of cDC1s may be a reason for the loss of Th1 response during infections since IL-12 is required for directing IFN-γ production in T cells and Natural Killer cells (Mashayekhi *et al.*, 2011).

Cross-presentation of exogenous antigens is limited to cDC1s of the SI. Cross-priming occurs during inflammatory responses where cDC1s induce the differentiation of naïve CD8+ T cells into IFN-γ-expressing cytotoxic T-cells involved in eliminating tumours or virally infected cells (Cerovic *et al.*, 2015; Sun *et al.*, 2017). This cross presentation leads to the influx of effector T cells into the LP. Ablation of cDC1s in a diphtheria toxin A subunit (DTA) expression of XCR1 (XCR1-DTA) mouse model resulted in decreased populations of intraepithelial and LP T cells (Ohta *et al.*,

2016). Reductions in the LP included TCRαβ$^+$ T cells, CD4$^+$ and CD8$^+$ subpopulations, and all IEL subsets. XCL1 and XCL2 are ligands for XCR1 in humans (only XCL1 in mice) and are produced primarily by natural killer cells and activated CD8$^+$ T cells. In these XCR1 and XCL1 deficient mice, XCR1 cDCs accumulated in the LP with reduced numbers in the MLN providing a possible crosstalk model whereby XCL1-expressing T cells attract nearby XCR1 cDCs that promote their survival and maintenance of IELs and T cells and in turn aids in the maturation of XCR1 cDCs that promote their migration to MLNs in a CCR7-dependent manner (Ohta *et al.*, 2016). The XCR1-DTA mouse model highlights the importance of XCR1-XCl1 cross-talk between T cells and XCR1 cDCs in T cell homeostasis and survival.

The generation of FOXP3$^+$ Tregs in the MLN relies on production of RA, and expression of TGF-β by cDCs. TGF-β activation from the latent to active form that can engage TGF-β receptor is established through the action of integrin αvβ8 (Worthington *et al.*, 2011). The integrin αvβ8 is restricted to cDC1s in the LP and is regulated by cues from the microenvironment, specifically TGF-β, RA, and Toll-like receptor (TLR) agonists that are present in high concentrations in the SI (Iliev, Mileti, *et al.*, 2009; Boucard-Jourdin *et al.*, 2016). The source of intestinal RA and TGF-β can potentially derive from stromal cells and epithelial cells for conditioning of cDCs (Iliev, Mileti, *et al.*, 2009). The close association of cDCs with the intestinal epithelium places them for contact with intestinal microbial products that interact with TLRs, promoting αvβ8 expression preferentially in cDC1s as well as CCR7 and MHCII upregulation. Differential expression of αvβ8 in intestinal DCs may therefore result from their exposure to different intestinal microbes. However, mice deficient

in cDC1s display normal proportions of FoxP3$^+$ Treg cells within the intestine, indicating that other immune cells may play roles in inducing tolerance such as macrophages (Denning *et al.*, 2007; Luda *et al.*, 2016).

1.12 Functions of cDC2s in the small intestine

The expression of SIRPα (CD172a) distinguishes the cDC2 subsets in the small intestine. SIRPα is a transmembrane receptor to the ligand CD47 that is ubiquitously expressed, with this interaction inhibiting phagocytosis. The binding of CD47 with SIRPα causes the phosphorylation of the immunoreceptor tyrosine-based inhibitory motif in the cytoplasmic tail of SIRPα. This causes the recruitment of src homology-1-domain containing protein tyrosine phosphatases (SHP-1) and SHP-2 which is involved in phagocytosis and cell migration (Xu *et al.*, 2017).

The cDC2 subset includes cDCs expressing CD103$^+$CD11b$^+$, CD103$^-$CD11b$^+$, and a small proportion of DN cDCs. The CD103$^+$CD11b$^+$ subtype is closely related to CD103$^-$CD11b$^+$ cells determined by their transcriptional similarities (differing by 100-200 genes), with the deletion of TGFβRI in mouse models showing a marked reduction in CD103$^+$CD11b$^+$ cDCs and a greater proportion of CD103$^-$CD11b$^+$ cDCs (Bain *et al.*, 2017). This suggest TGFβR signalling differentiates a proportion of CD103$^-$CD11b$^+$ cells to CD103$^+$CD11b$^+$. The *IRF4*, *Notch2* and *Klf4* dependent cDCs are the major migratory population of DCs from the SI LP to surrounding MLNs. *CD11c-cre.Irf4$^{fl/fl}$* mice that lacked Irf4-dependent DCs and *CD11c-cre.Notch2$^{fl/fl}$* mice that lacked Notch2-dependent DCs had significant reductions in mucosal Th17 cells . Th17 cell priming in surrounding MLNs is IL-6 dependent, with the absence of

migratory $CD103^{+}CD11b^{+}$ cDCs from the small intestinal mucosa in MLNs resulting in reduced levels of IL-6 and hence Th17 differentiation (Lewis *et al.*, 2011; Persson, Uronen-Hansson, *et al.*, 2013). However, it is unclear whether Notch2 is necessary for the development of $CD103^{-}CD11b^{+}$ cDCs since Notch2 knockout mice only have a partial reduction of this subset (Lewis *et al.*, 2011; Satpathy *et al.*, 2013). The $CD103^{-}CD11b^{+}$ cDC subset have been shown to induce Th17 differentiation *in vitro* which may suggest its importance in driving colonic Th17 responses (Scott *et al.*, 2015). Although the depletion of cDC2s reduces the number of Th17 cells, there is still a remaining population suggesting the involvement of other mononuclear phagocyte subsets contributing to the priming of Th17 responses. Nonetheless, these models highlight the importance of cDC2s in the generation and maintenance of mucosal Th17 responses.

Mouse models are an important tool for assessing DC functions *in vivo*. However, results obtained from these mouse models cannot be attributed to one sole subset. This is because other DC subsets are also affected, for instance in $Flt3^{-/-}$ mice the $CD103^{+}CD11b^{+}$ cDC subset is greatly reduced, however so are approximately 40% of $CD103^{+}CD11b^{-}$ DCs and a large proportion of $CD103^{-}CD11b^{+}$ DCs (Bogunovic *et al.*, 2009). Notch2 knockout mice lack $CD103^{+}CD11b^{+}$ DCs but have an increase in $CD103^{+}CD11b^{-}$ DCs in the LP (Lewis *et al.*, 2011). Deletion of cDC2-dependent TFs through the use of Cd11c-Cre mouse models may not necessarily result in deletion of the cDCs subset themselves, rather it may involve impaired function. Therefore, results from these models should be carefully interpreted.

The cDC2 subsets are also known to be important for the development of Th2 responses to helminth infections, such as in mouse models infected with the parasitic worm *N. brasiliensis* (Gao *et al.*, 2013), *Schistosoma mansoni* (Everts *et al.*, 2016; Mayer *et al.*, 2017), *Trichuris muris* (Demiri *et al.*, 2017), and *Heligmosomoides polygyrus* (Everts *et al.*, 2016; Redpath *et al.*, 2018). Injections with *Schistosoma mansoni* eggs into the subserosa of the intestine of mice caused the migration of cDCs into MLNs, with both $CD103^{-}CD11b^{+}$ and $CD103^{+}CD11b^{+}$ cDCs responsible for priming antigen-specific Th2 and inducing IFN-γ responses (Mayer *et al.*, 2017). The *S. mansoni* infection model showed regional specific heterogeneity amongst the cDC2 subsets whereby $CD103^{+}CD11b^{+}$ cDCs induce Th2 response within the small intestine and $CD103^{-}CD11b^{+}$ cDCs performing the same task within the colon. Mouse models lacking IRF4 and therefore cDC2s, *Cd11c-cre.Irf4*$^{fl/f}$, showed that the infections with *S. mansoni* do not induce a Th2 response, as also shown in *Trichuris muris* infections (Demiri *et al.*, 2017). Deletion of the cDC1s subset through *Batf3*$^{-/-}$ and *Cd11c-cre.Irf8*$^{fl/fl}$ mice enhanced Th2 response during infections with *S. mansoni* (Everts *et al.*, 2016) and *T. muris* (Demiri *et al.*, 2017), respectively, suggesting suppressive effects of the cDC1 subset on cDC2s through the constitutive expression of IL-12.

In tissues other than the small intestine, DCs detect microbial structures to confer an inflammatory response through pattern recognition receptors (PRR). However, transfer of microbial components from the lumen of the SI through mechanisms described below causes constitutive PRR stimulation in cDCs associated with the induction of immune tolerance. Therefore, initiation of an inflammatory response to

enteric pathogens does not solely rely on conservative stimulation of PRRs, rather the added presence of immunoglobulin A (IgA) immune complexes (IC) with invading pathogens that enter the LP stimulate proinflammatory responses in $CD103^+$ cDCs (Hansen *et al.*, 2018). The IgA-IC complexes interact with the Fc alpha receptor I (FcαRI, or CD89) and PRRs on $CD103^+$ intestinal cDCs which cross-talk to induce an amplified expression of TNF, IL-1β, and IL-23, all proinflammatory cytokines that promote both IL-17 production by Th17 cells and IL-22 by intestinal innate lymphoid cells type 3 (ILC3) (Hansen *et al.*, 2018). The specific subset of $CD103^+$ cDCs that respond to IgA-IC is not clear, but the promotion of Th17 and ILC3 cells is characteristic of $CD103^+CD11b^+$ cDCs (Persson, Uronen-Hansson, *et al.*, 2013; Satpathy *et al.*, 2013).

ILCs share similarities in phenotype and functions to T lymphocytes but lack antigen-specific receptors. They play roles in innate and adaptive immunity by communicating with a range of immune cells involved in intestinal homeostasis. IL-22 production by ILCs promotes barrier integrity of the small intestinal epithelium by inducing antimicrobial peptide production in epithelial cells, namely the bactericidal C-type lectin RegIIIγ (Zheng, 2008, Nat. Med 14). Notch2 knockout mice infected with *Citrobacter rodentium* showed IL-22 production in ILC3s were dependent on exposure to IL-23 derived from $CD103^+CD11b^+$ cDC2s (Satpathy *et al.*, 2013). However, these DCs may not be the sole source of IL-23 as $CD103^-CD11b^+$ cDCs and macrophages are known to express IL-23 that can induce ILC3 production of IL-22 (Aychek *et al.*, 2015). In this study it was also shown that IL-23 expression in $CD103^-CD11b^+$ DCs and macrophages prevented the production of IL-12 in cDC1s,

providing protection against a fatal Th1 cell response. This displays a further occasion where these intestinal cDC subsets cooperate during infections.

1.13 T cell functions in intestinal homeostasis

The largest population of T cells in the body reside throughout the intestinal LP and epithelium, of which a large proportion are $CD4^+$ T cells. These are conditioned in secondary lymphoid organs where their activation results in their migration to the LP. Here they can remain as tissue-resident memory T cells over a prolonged period. $CD4^+$ T cells comprise a heterogenous population of T helper 17 (Th17) cells that produce interleukin 17 (IL-17), T helper 1 cells (Th1) that are known to produce IFN-γ, and diverse subsets of Tregs. IELs express CCR9, a gut homing receptor to CCL20 expressed by the intestinal epithelium, and the integrin CD103 that interacts with E-cadherin on the intestinal epithelium. Approximately 90% of IELs express T cell receptors (TCRs) and can be divided into conventional or unconventional subsets. Conventional IELs are derived from antigen-primed T cells that migrate to the intestinal epithelium and are characterised as $CD4^+TCR\alpha\beta^+$ and $CD8\alpha\beta^+TCR\alpha\beta^+$ IELs. However, unconditional IELs migrate directly to the intestinal epithelium and are characterised as $CD8\alpha\alpha^+TCR\alpha\beta^+$ and $CD8\alpha\alpha^+TCR\gamma\delta^+$ IELs. These IELs help maintain intestinal homeostasis through expression of T helper properties during resting state and infections (reviewed in (Van Kaer and Olivares-Villagómez, 2018)).

1.14 Antigen uptake by dendritic cells in the intestine

As a major antigen-presenting cell, intestinal cDCs are exposed to foreign antigens such as food proteins, the microbiota and to self-antigens. Delivery of these antigens to MLNs is crucial for the development of tolerance to commensal bacteria and for initiation of the adaptive immunity towards enteric pathogens. Upon antigen uptake in the intestine, cDCs migrate to surrounding MLN via a chemokine receptor 7 (CCR7) -dependent manner. Here they present antigen to resident T cells for their induction into effector T cells (Jang *et al.*, 2006). In the steady state, cDCs of the intestine are deemed tolerogenic, and presentation of antigens from commensal microbiota or dietary proteins in this state promotes the generation of forkhead box P3 (FoxP3+) regulatory T cells (Treg) that maintain tolerance towards these products (Coombes *et al.*, 2007). $CD103^+$ cDCs in the MLN imprint Treg cells with the gut-homing receptors CCR9 and $\alpha_4\beta_7$ through the expression of retinoic acid (RA) (Iwata *et al.*, 2004; Coombes *et al.*, 2007).

Exposure to luminal content is achieved through several mechanisms including goblet cell antigen passages (GAPs) (McDole *et al.*, 2012), extension of dendrites through the epithelium into the lumen (Niess *et al.*, 2005; Chieppa *et al.*, 2006; Farache *et al.*, 2013), M cells in PPs (Jang *et al.*, 2004), macrophage transfer (Mazzini *et al.*, 2014), or in antigen-antibody complexes transported across IECs (Yoshida *et al.*, 2004).

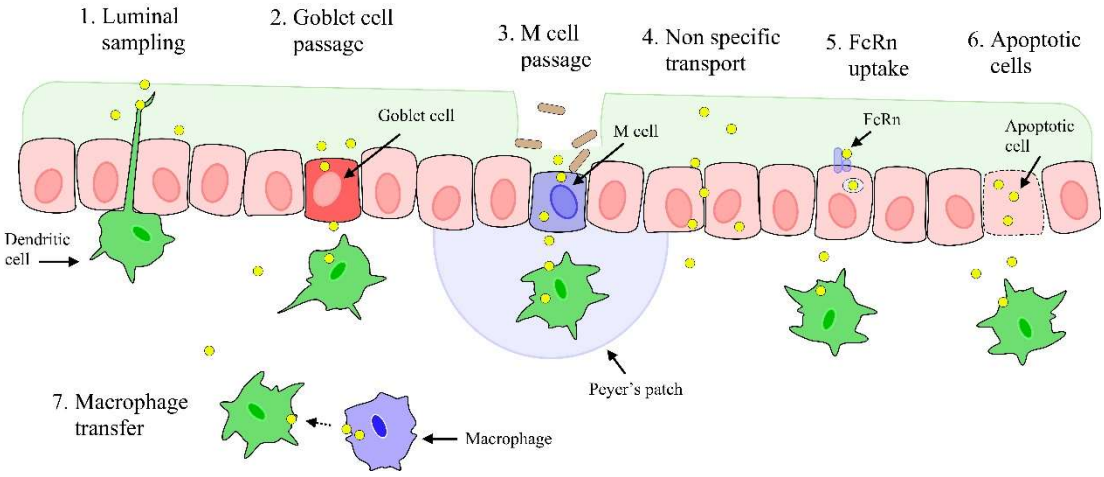

Figure 6. Schematic of antigen delivery mechanisms for the induction of intestinal homeostasis
Antigens in the intestinal lumen can come into contact with DCs through various methods. **1**, DCs can extend intraepithelial dendrites to sample the luminal space. **2**, Goblet cells can transport antigen to closely associated DCs. **3**, M cells within Peyer's Patches can transport antigen to DCs. **4**, Antigen can pass between epithelial cells or directly across the epithelium by enterocytes. **5**, Enterocytes can internalise antigen for transport by transcytosis using FcRn on their cell surface. **6**, Cells that undergo apoptosis due to senescence of infection are phagocytosed by DCs. **7**, Antigen transfer between macrophages and DCs can also occur.

1.14.1 Goblet cell associated antigen transfer

The *in vivo* imaging of CD11c-YFP mice revealed the uptake of dextran into goblet cells, with subsequent transfer to $CD11c^{+}CX3CR1^{-}$ cells (McDole *et al.*, 2012). It was noted that extensions of transepithelial dendrites into the luminal space for sampling was not seen during the 50 experiments taken. However, infections with *Salmonella typhimurium* increased this luminal sampling to 2% of $CD11c^{+}CX3CR1^{-}$ cells. This study used a macrophage marker CX3CR1 to distinguish between $CD103^{+}$ and CD103- cells, since cDC2s have been shown to express low to intermediate levels of this receptor (Aychek *et al.*, 2015; Scott *et al.*, 2015). Using a dual reporter mouse of CD11c-YFP and CX3CR1-GFP, the assumption stood that $CX3CR1^{-}$ cells are $CD103^{+}$ DCs and $CX3CR1^{+}$ cells are CD103- DCs. This criteria for distinguishing DC subsets is optimistic since $CD11c^{+}CX3CR1^{+}$ cells could be macrophages as identified by another study (Farache *et al.*, 2013), however this study nicely presents antigen

transfer from goblet cells to $CD11c^{+}CX3CR1^{-}$ cells, suggesting that this process occurs mostly in the cDC1 subset in the intestine. Infection with *S. typhimurium* inhibits goblet cell transfer of dietary antigens through exposure to IL-1β by stromal cells, this then prevents T cell proliferation to luminal antigen and restricted the dissemination of the pathogen (Kulkarni *et al.*, 2018).

1.14.2 Luminal sampling through transepithelial dendrites

Imaging within small intestine of live mice *in vivo* has shown $CD11c^{+}CX3CR1^{-}$ cells from within the epithelium extending transepithelial dendrites (TED) into the luminal space (Farache *et al.*, 2013). Farache *et al* use the same dual reporter mouse as the study assessing goblet antigen transfer (McDole *et al.*, 2012), but suggest that double positive cells ($CD11^{+}CX3CR1^{+}$) are macrophages, not $CD103^{-}$ DCs. Here, $CD103^{+}$ cells inhabit the LP with only few cells patrolling the epithelium. Upon infection with *S. typhimurium* more CD103 cells are recruited to the epithelium where expression of tight junction proteins allows the DCs to penetrate tight junctions between epithelial cells with dendrites extending into the luminal space. The cells engulf bacteria and upregulate CCR7 for migration to MLNs for antigen presentation to T cells. Although it was shown that *Salmonella* antigen is delivered to MLNs primarily by $CD103^{+}CD11b^{+}$ DCs in other studies (Bogunovic *et al.*, 2009), the lack of CX3CR1 expression in this study suggests that luminal sampling is restricted to $CD103^{+}CD11b^{-}$ cells. This suggests that $CD103^{+}CD11b^{+}$ DCs attain antigen by alternative methods. The presence of $CD103^{+}$ DCs in the epithelium makes sense since CD103 binds E-cadherin present on the basolateral

side of epithelial cells. Since epithelial cells condition DCs to express RA, the close contact between IECs and $CD103^+$ DCs explains the ability of $CD103^+$ DCs to express RA for T cell conditioning after antigen uptake and migration to MLNs.

1.14.3 Transfer of antigens from Macrophages to dendritic cells

Mice depleted of $CX3CR1^+$ cells were incapable of extending protrusions into the intestinal lumen (Niess *et al.*, 2005) and CD103 DCs sampling the lumen is a rare event (Farache *et al.*, 2013), it is therefore suggested that this action is limited to $CX3CR1^+$ macrophages. Since intestinal macrophages do not migrate to the MLNs where T cells are conditioned towards oral tolerance, luminal antigen acquired by TEDs in macrophages can be transferred to DCs in the LP via the gap junction connexin 43 with subsequent migration of DCs to the MLNs (Mazzini *et al.*, 2014). However, this study shows that CX3CR1 intermediate cells managed to uptake the antigen, which does not rule out the $CD103^-CD11b^+$ cDC subtype that has intermediate levels of CX3CR1 expression (Table 1).

Current intravital microscopy models are unable to sufficiently distinguish macrophages and DCs subpopulations in situ precisely. Improvements in these models or development of new models may elucidate many of the remaining questions concerning role of each cell type during antigen acquisition, oral tolerance and adaptive immune conditioning. In this sense, a co-culture model of intestinal organoids and dendritic cells would be a useful step forward.

1.15 Environmental conditioning determines dendritic cell function

Intestinal cDCs are characteristically different to cDCs in other tissues, suggesting factors within their local environment may drive their development and functional specialisations. Even within the intestine, differing characteristics of cDC subsets are determined by their regional location along intestine. This may be in part due to the microbial components, nutrient uptake, and functional differences along the length of the intestine. The addition of conditioned supernatant from an Caco-2 epithelial cell line culture to human monocyte-derived DCs induced expression of IL-10, a characteristic of colonic DCs (Rimoldi *et al.*, 2005). This was thought to be caused by expression of thymic stromal lymphopoietin (TSLP) by the colonic cell line, the first indication that the local environment can condition DCs into an intestinal phenotype.

Other metabolites that modulate intestinal cDC function includes short chained fatty acids (SCFA) that interact with the aryl hydrocarbon receptor (AhR). Metabolites mainly derived from the diet or microbial by-products can activate AhR, a ligand induced transcription factor shown to be involved IL-22 production in lymphocytes (Zelante *et al.*, 2013). Cre-mediated deletion of AhR in CD11c+ cells within mice resulted in a decrease in CD103+ cDCs in the MLN and aberrant Wnt signalling in all APC subsets (Chng *et al.*, 2016). Here, SI LP cDCs expressed lower levels of the Treg inducers TGFβ1 and ALDH1a2, although Treg numbers remained unaffected suggesting compensatory mechanisms for their development. The ablation of AhR in CD11c+ cells reduced Paneth cell numbers and increased goblet

cell populations within the small intestinal epithelium, possibly due to aberrant Wnt signalling from $CD11c^+$ cells. To prove whether this alteration in small intestinal epithelium make-up was directly due to $CD11c^+$ cells, these were isolated from the MLN of AhR depleted mice and co-cultured with intestinal organoids. Paneth cell numbers were likewise reduced, suggesting AhR signalling in $CD11c^+$ cells could participate in modulating the epithelial lineages of the small intestinal epithelium. Interestingly, the increased goblet cell population in AhR depleted mice resembles the phenotypes in patients suffering from Crohn's Disease, with reported reductions in AhR proteins in inflamed portions (Gersemann *et al.*, 2009; Monteleone *et al.*, 2011).

Metabolism of dietary fibre into SCFAs by members of the microbiota is known to be involved in mediating anti-inflammatory effects in the intestine. Butyrate has been given most attention for its beneficial effects on colonic health. Deletion of the G-protein-coupled receptor (GPR109A) for butyrate in mice resulted in colitis and decrease of Treg development, with butyrate implementing a tolerogenic phenotype in splenic $CD11c^+$ DCs and $CD11b^+$ macrophages from wild-type mice determined by the expression of *Aldh1a1* and *IL-10* mRNA (Singh *et al.*, 2014).

As previously mentioned, TGFβ in the intestine can drive differentiation of $CD103^-$ $CD11b^+$ cDCs into a $CD103^+CD11b^+$ cDC phenotype (Bain *et al.*, 2017). This immunosuppressive cytokine is abundant in the intestine, with IECs the most likely source. Increased expression of TGFβ is determined by gut inflammation, cell injury, and even interactions with the microbiota whereby SCFAs and ATP result in

exacerbated TGFβ production by colonic IECs (Atarashi *et al.*, 2011). In the absence of TGFβR1 in $CD11c^+$ cells within mice, the $CD103^+CD11b^+$ subset is greatly reduced, and cDCs are less able to prime Treg cells (Bain *et al.*, 2017). This represents the key role TGFβ plays in intestinal homeostasis and cDC development.

Another apparent key immunomodulator of intestinal homeostasis is the cytokine granulocyte-macrophage colony-stimulating factor (GM-CSF). Interactions between the microbiota and macrophages causes the release of IL-1β that drive the expression of GM-CSF from ILC3s, which in turn act on DCs to maintain Treg homeostasis through RA and IL-10 production (Mortha *et al.*, 2014). Lamina propria stromal cells of the SI also produce GM-CSF shown to increase RA production in cDCs that is known to induce Treg development (Vicente-Suarez *et al.*, 2015). Patients with Crohn's Disease usually have neutralising antibodies to GM-CSF within the intestine possibly contributing to the onset of disease. However, treatment with recombinant GM-CSF only alleviates symptoms in some of these patients, indicating the intricate and variable mechanisms involved in conserving intestinal homeostasis. The metabolite most accredited to conditioning cDCs in the intestine is RA involved in key roles during steady state and in inflammation.

1.16 Retinoic acid

1.16.1 Sources of retinoic acid

RA is an important mediator in intestinal immune homeostasis since it is known to induce Treg cells and tolerance towards commensal bacteria, but RA can also

promote an inflammatory environment during disease and pathogenesis. RA is a metabolite derived from vitamin A (or retinol), an essential nutrient obtained from the ingestion of meat and plants that contain carotenoids and retinyl esters, respectively. Retinol can be processed by intestinal epithelial cells into retinal, then RA that can be subsequently released into the intestinal microenvironment, or into retinyl esters that are packaged into chylomicrons to be stored in the liver. Retinol stores from the liver are released into circulation bound by retinol-binding protein to be taken up by cells of the body.

The uptake of retinol by intestinal epithelial cells into the cytosol is converted to retinaldehyde (or retinal) by alcohol dehydrogenases that is further metabolised by aldehyde dehydrogenase enzymes (ALDH) into RA (Figure 7). There are many isoforms of ALDH, of which the most studied are ALDH1a1, ALDH1a2, ALDH1a3. The most abundant isoform of RA is *all-trans*-RA, and within the cytosol bind to either cellular retinoic-acid binding protein 1 for degradation through cytochrome P450 family 26 (CYP26) or bind to cellular retinoic-acid binding protein 2 (CRPBII) for translocation to the cell nucleus. Here, RA activates retinoic acid receptors (RARs) and retinoid X receptors (RXR) resulting in their dimerization that induces gene expression by allowing the binding to retinoic acid response elements (Figure 7).

Tissue retinol levels are greatest within the small intestinal microenvironment, derived from diet uptake or bile from where retinol is stored in the liver. Intestinal epithelial cells metabolise retinol into RA since they have been shown to express ALDH1a1 (Bhattacharya *et al.*, 2016) and the expression of CRPBII in IECs is crucial

for inducing ALDH1a2 expression in intestinal DCs (McDonald *et al.*, 2012). IEC-conditioned medium contained RA that ultimately induced a tolerogenic phenotype in DCs (Iliev, Spadoni, *et al.*, 2009). Therefore, IEC-derived RA is important for conditioning DCs. However, stromal cells of the lamina propria are also a source of RA in the small intestine known to affect DC conditioning (Vicente-Suarez *et al.*, 2015).

Within MLNs RA acts on DCs and T cells to induce gut homing receptor expression in T cells. Sources of RA in MLNs are derived from DCs and stromal cells. The importance of stromal cells in MLNs has been shown in mice transplanted with peripheral lymph nodes (pLN), that do not express RA-synthesising enzymes, into the mesentery. Gut homing T cells are not generate in the transplanted pLNs even in the presence of intestinal DCs (Hammerschmidt *et al.*, 2008). However, bone marrow-derived DCs that do not express RA-synthesis enzymes injected into MLNs of CCR7 knockout mice did not induce the gut homing receptors on T cells, namely α4β7 and CCR9. This suggests that RA or other factors from MLN stromal cells and cDCs are both required to induce gut tropism.

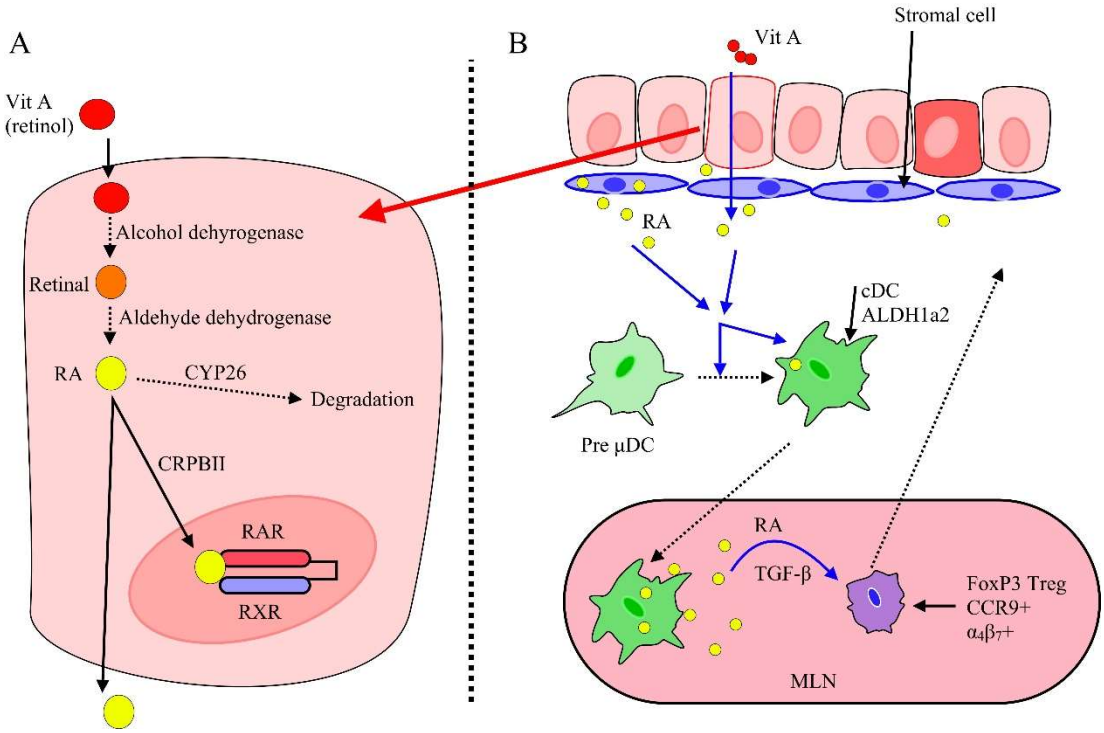

Figure 7. Schematic showing vitamin A metabolism into RA and the effects of RA on DC development and function.
A, intestinal epithelial cells convert vitamin A into RA that is released into the lamina propria. **B**, RA from stromal cells and intestinal epithelial cells condition pre-µDCs into cDCs with upregulated ALDH1a2. These cDCs migrate to MLNs and express RA and TGF-β that imprints T cells with gut homing α4β7 and CCR9 and condition them into FoxP3 Tregs.

1.16.2 Retinoic acid in intestinal homeostasis

IECs not only forms a physical barrier of protection against the external environment, but their sensing of luminal contents aids in shaping immune responses. Aside from the direct effects RA imparts on immune cell development and function, RA is also known to influence IEC differentiation. Deletion of RARα in mice resulted in an increased abundance of goblet cells and Paneth cells and a decrease in enteroendocrine cells (Jijon *et al.*, 2018). The reduction in mononuclear phagocytes also observed here could be in part due to the increased mucus produced by the more abundant goblet cells, impeding the direct contact between

IECs and the microbiota that would otherwise shape the immune system. IEC-derived RA drives a tolerogenic phenotype in DCs, an important factor during the induction of oral tolerance towards commensal bacteria (Iliev, Mileti, *et al.*, 2009; Villablanca *et al.*, 2011).

As previously mentioned, RA imprints T cell with gut homing receptors $\alpha_4\beta_7$ and CCR9 within MLNs (Figure 7) (Iwata *et al.*, 2004). Vitamin A deficient (VAD) mice had a significantly reduced number of T cells within the LP of the SI, proving the importance of diet-derived RA. RA plays a role in the generation of IgA secreting intestinal B cells, whereby VAD mice lack IgA secreting cells due to the impaired induction of gut homing receptors on B cells and an inability to synergise with IL-5 or IL-6 produced by DCs (Mora *et al.*, 2006). These results demonstrate the important role of RA in the regulation of adaptive immunity. A major source of RA that is important in directing an effective adaptive immunity is provided by DCs in response to the intestinal microenvironment.

1.16.3 Retinoic acid in DCs

RA is thought to induce RA production in cDCs through the upregulation of ALDH1A2. Intestinal DCs derive from precursors in bone marrow where RA is thought to aid in their differentiation along a cDC lineage to a gut-like phenotype and imprinting with the gut-homing integrin receptor, $\alpha_4\beta_7$. VAD mice are deficient in $CD103^+CD11b^+$ cDCs in the intestine and lymphoid tissues, highlighting the importance of RA in intestinal DC development (Klebanoff *et al.*, 2013). RA also has a direct effect on DCs through the upregulation of a retinaldehyde dehydrogenase

1a1 (ALDH1a2) enzyme that induces further production of RA (Molenaar *et al.*, 2011), however these pre-cDCs do no produce RA (Zeng *et al.*, 2013)(data not shown), rather this must occur upon entry to the small intestinal LP where RA levels are high (Zeng *et al.*, 2016). Exposure to RA here has a role in the differentiation of cDCs into the intestinal cDC subsets and expression of *Aldh1a2* resulting in RA production, most prominent in cDC1 subset (Jaensson-Gyllenbäck *et al.*, 2011). There are different levels of ALDH expression in cDCs along the length of the small intestine, possibly in part due to increased vitamin A absorption in the proximal small intestine (Villablanca *et al.*, 2011).

RA plays a role in both anti-inflammatory and pro-inflammatory responses. In the steady state, RA from DCs inhibits IL-6, IL-21 and IL-23 signalling in naïve T cells preventing differentiation to Th17 cells (Xiao *et al.*, 2008). RA produced by $CD103^+$ DCs in humans can condition Treg cells to release IL-10, an anti-inflammatory cytokine that is pivotal in maintaining immune homeostasis, since deficiency in IL-10 is linked to IBD (Bakdash *et al.*, 2015). In combination with TGF-β, RA induces the development of Treg cells, whereas TGFβ alone drives Th17 differentiation (Coombes *et al.*, 2007; Bain *et al.*, 2017). Induction of Ig class switching to IgA in B cells involves RA from DCs exposed to commensal antigens (Mora *et al.*, 2006). These studies show the importance of RA in suppressing inflammatory T helper responses and establishing tolerance with Treg cell development. During infection inflammatory cytokines counteract or work in conjunction with RA to induce Th1, Th2 and Th17 responses. IL-1 can counteract RA-mediated inhibition of Th17 development by enhancing IL-6 signalling and overriding FOXP3 expression by RA

(Basu *et al.*, 2015). A Th1 response is generated by RA during infections in combination with IL-15, an inflammatory cytokine that is also present in patients with coeliac disease (DePaolo *et al.*, 2011). Here, the expression of IL-12 and IL-23 from DCs generates a Th1 response. In combination with IL-4, RA increases Th2 development (Iwata, Eshima and Kagechika, 2003). Therefore, RA is fundamental in developing Treg cells and supressing Th17 cell differentiation but is also indispensable for the initiation of Th1 and Th2 responses. Suppression of RA production in DCs during certain infections allows for the upregulation of inflammatory response to enhance the clearance of particular pathogens (Hurst and Else, 2013). The milieu of cytokines involved in each process is finely tuned for the effector outcome of T helper response and is still not fully understood.

1.17 The intestinal microbiota

1.17.1 Establishment of tolerance in intestinal epithelial interactions with the microbiota

The gut of mammals is colonised by an abundance of microorganisms collectively termed the microbiota. These provide essential nutrients that the host is otherwise unable to generate from dietary products. Balancing tolerance towards commensal microbes and driving pathogen clearance relies on many aspects of intestinal biology including the intestinal epithelium, and innate and adaptive immune cells. Luminal contents are prevented from interaction with the intestinal epithelium due to a thick mucus layer and IgA. Goblet cells secrete MUC2, the hyperglycosylated mucin that forms a physical barrier between the epithelium and microbiota. In the

small and large intestines of mice the lower levels of mucus closest to the epithelium are devoid of bacteria. In germ free mice this mucus layer is more penetrable by bacteria than conventional mice suggesting an influence on mucus production by commensal bacteria (Johansson *et al.*, 2015). Further verification is provided by the normalisation of the mucus layer by administration of microbiota from conventional mice. Mucus also affects adaptive immunity by imprinting DCs with anti-inflammatory properties through the construction of galectin-3-Dectin-1-FcγRII-β receptor complexes that drive β-catenin activation (Shan *et al.*, 2013). Here, β-catenin inhibits the expression of pro-inflammatory cytokines through the NF-κB pathway and increases transcription of TGF-β1 and RA involved in Treg development.

Besides from providing a physical barrier between commensals and pathogens IECs also express antimicrobial products to prevent attachment to their surface. Interactions between microbe-associated molecular patterns (MAMPs) and PRRs on the epithelial cell surface, such as toll-like receptors (TLRs), results in the expression of antimicrobial products. The regenerating islet-derived III-γ (REGIII-γ) protein is expressed by Paneth cells into the mucus layer and binds peptidoglycan moieties of bacteria to break down the cell wall. The production of REGIII-γ is stimulated through TLR-MyD88 signalling and aids in maintaining intestinal homeostasis through spatial segregation of bacteria from the epithelial surface (Vaishnava *et al.*, 2011).

Distinguishing between harmful pathogens and commensal bacteria is based partly on mode of infection whereby pathogenic bacteria possess virulence factors that allow them to directly invade IECs thereby introducing their MAMPs into the cytosol where they interact with NOD-like receptors (NLRs). Commensal bacteria are non-invasive and therefore less potent activators of NLRs. The microbiota is restricted to interactions with IECs through binding of MAMPs to apical TLRs. However, interactions with TLRs on the basolateral side of IECs signals a barrier breach and initiates inflammatory responses. Certain commensal bacteria possess the ability to further reduce immune response towards them through the dampening of the classical NF-κB pathway, otherwise responsible for immune activation within cells through expression of pro-inflammatory genes. *Bacteroides* and *Lactobacillus* spp. are examples of commensal bacteria that behave in this way. Naturally, NF-κB dimers are sequestered by IκB complexes within the cytosol and PRR signalling causes the phosphorylation of IκB resulting in its degradation and the release of NF-κB for their nuclear transport. Both species of commensal bacteria block the phosphorylation of IκB thereby preventing nuclear transport of NF-κB (Neish *et al.*, 2000). *Bacteroides* spp. further dampen this signalling by inducing expression of peroxisome-proliferation-activated receptor-γ that is responsible for exporting NF-κB from the nucleus (Kelly *et al.*, 2004). These are mechanisms by which both the small intestinal epithelium and commensal bacteria restrict inflammatory immune responses and maintain tolerance.

1.17.2 Establishment of tolerogenic dendritic cells by the microbiota

The symbiotic relationship between the host and commensal bacteria is essential for nutrient processing, production of essential vitamins, and protection against pathogens for the host. One mechanism in developing tolerance towards commensal bacteria relies of the spatial segregation of bacteria from the epithelial surface as mentioned above. This is achieved by a mucus layer, REGIII-γ secretion, and by IgA antibodies. Secretory IgA antibodies, described above, coat commensal bacteria to prevent access to immune cells and IECs, known as immune exclusion. A fine balance is achieved in IgA expression to obtain tolerance towards commensals and inflammation towards pathogens. Low affinity, polyspecific IgA bind commensal bacteria to prevent attachment to epithelial cells, whereas high affinity, monospecific IgA binds pathogens for their neutralisation. IgA is produced by plasma cells, with Peyer's patches harbouring the majority of IgA-producing cells. M cells within PPs transport commensal bacteria across the epithelium where DCs interact with and induce B cell Ig switching to IgA secretion. Another possible source of IgA production is through the induction of Treg cells, driven by the exposure to TGFB, to produce IgA against commensal bacteria that further prevents their interaction with the immune system and the intestinal epithelium (Macpherson and Uhr, 2004; Cong *et al.*, 2009). Upon infection by luminal microbes, IgA-IC complexes interact with DCs to induce an inflammatory response against the invasive pathogen, ensuring luminal residents and pathogens are excluded from the LP (Hansen *et al.*, 2018).

It is within the interest of the microbiota to aid the host in clearing pathogens via non-inflammatory means. This is to reduce collateral damage of commensal bacteria loss otherwise resulting from inflammation. Indirect stimulation of TLRs by commensal bacteria on DCs initiate MyD88-dependent Th1 responses against *T. gondii* infections to prevent systemic infection (Benson *et al.*, 2009). This is one of many ways in which the microbiota plays a role in protection against systemic infection, including priming of neutrophils, macrophages and natural killer cells.

The studies examining the processes of initiating oral tolerance towards the microbiota have seen several advances in recent years that have expanded our knowledge. Transfer of microbiota antigen to the MLNs by DCs induce Treg development through the expression of RA, IL-10 and TGFB. Treg cells migrate to the intestinal LP to express IL-10 and TGFB that inhibits the production of inflammatory cytokines within effector cells. Macrophage secretion of IL-10 with the LP supports the local expansion of these Treg cells involved in tolerance to proteins. It is still unclear as to which DC subset is responsible for establishing and maintaining tolerance towards commensal bacteria due to imprecise APC identification criteria in early studies. Likewise, how DCs can discriminate between pathogenic and commensal bacteria is unknown since both share components responsible for innate and adaptive immune responses.

1.18 Dendritic cells in inflammatory bowel diseases

The fine balance in maintaining homeostasis of the intestine can be altered to produce an inflammatory environment by abnormal immune responses towards the

commensal flora. Although the pathogenesis of IBD is largely unknown, impaired sensing and killing of commensal bacteria contribute to IBD, with mutations in susceptibility genes for host-microbe interactions leading to the onset of IBD such as Crohn's disease. Mutations in *NOD2*, the gene encoding an intracellular PRR, is associated with CD and is also associated with diminished α-defensin production in Paneth cells, allowing for the accumulation of bacteria that may lead to inflammation (Hugot *et al.*, 2001; Wehkamp *et al.*, 2004). Induction of NOD2 induces autophagy within cells, a process of degrading intracellular contents by the release of granules containing antimicrobial peptides. Mutations in autophagy regulatory genes are also linked to CD, such as the autophagy related gene 16-like 1 (*ATG16L1*) whereby their mutant form causes abnormal granule formation within Paneth cells of mice, a pathology also observed in CD patients (Cadwell *et al.*, 2008). This defective gene also affects DC autophagy in CD patients with impairment in bacterial elimination (Cooney *et al.*, 2010).

Although cytokines and metabolites are important in intestinal homeostasis, irregular levels are present within patients with IBD. Patients with CD express lower levels of TSLP in the intestine, a cytokine expressed by intestinal epithelial cells that imposes a tolerogenic phenotype on cDCs allowing for an inflammatory environment (Rimoldi *et al.*, 2005). Increased expression of inflammatory cytokines IL-6 and IL-12 in DCs from CD patients has been observed, with increased levels of TLR2 and TLR4 (Hart *et al.*, 2005). This means that DCs within CD patients are activated and are likely key initiators of inflammatory responses in IBD.

RA is known for its tolerogenic effects in intestinal homeostasis, therefore impairment in RA production may increase susceptibility to inflammation. In Patients with ulcerative colitis (UC), a form of IBD concentrated to colonic tissue, have reduced ALDH1a1 expression from cells in the colon with an increase in cytochrome P450 family 26 subfamily A member 1 (CYP26A1) enzyme that metabolises the breakdown of RA (Bhattacharya *et al.*, 2016). This is likely due to the inflammatory environment causing $CD103^+$ DCs to adapt their function from a TGF-β and RA expressing phenotype to an IL-6 inflammatory phenotype in a colitis mouse model (Laffont, Siddiqui and Powrie, 2010). Another colitis model in mice is achieved through the administration of dextran sulphate sodium (DSS) that impairs intestinal epithelial barrier integrity allowing for the influx of bacteria and hence the onset of inflammation. During the early stages of this acute colitis model, RA production increased to induce IL-22 production in ILC3s that stimulate the repair of the small intestinal epithelium. However, repeated dosage of DSS, a model for chronic colitis, caused a reduction in ALDH1a1 expression in the intestinal epithelium suggesting chronic inflammation causes the reduction of available RA (Bhattacharya *et al.*, 2016). Reductions in RA is symptomatic of UC, however RA levels are increased in CD patients with *CYP26B1* polymorphisms with an inability to break down RA (Fransen *et al.*, 2013). This is the only reported reduction of RA in CD patients, otherwise ALDH expression in intestinal $CD103^+$ DCs in CD is the same as those of healthy individuals (Magnusson *et al.*, 2016). The main models used for studying IBD pathogenesis relies on mouse models of colitis. Due to the intricacy of

IBD and the variability of disease, it remains unclear which animal model best represents that of human IBD with more suitable models needed to be generated.

1.19 Coculture models of immune cells with organoids

Organoids provide a model that is representative of the intestinal epithelium, suitable for studying infection and disease. However, this model still lacks other aspects that contribute to pathology, in particular immune cells. The addition of immune cells to organoid cultures would enhance the physiological relevance of 3D models that would more closely resemble the microenvironment that enteric infections would encounter *in vivo*. Due to the recent developments in organoid technology, cocultures with immune cells have been limited. Splenic T cells have been cultured with organoids that resulted in morphological changes to those resembling intraepithelial lymphocytes (IELs) such as dendrites and movement between organoid cells (Rogoz *et al.*, 2015). Expanding on this study, organoids have been cultured with αβT and γδT IELs isolated from the small intestine (Nozaki *et al.*, 2016). IELs are difficult to culture and suggesting that this is due to a lack of IEC-derived factors. Coculture of IELs with organoids provided an expansion in IEL number over a period of 2 weeks when cultured in the presence of IL-2, IL-7 and IL-15 in organoid cultures. This study also used 3D imaging to show the multidirectional movements along the basolateral surface of organoids, a characteristic seen *in vivo*.

Organoids can form a monolayer by culturing on collagen, exposing the luminal surface. Macrophages have been applied to the basolateral side of organoid

monolayers derived from human biopsies (Noel *et al.*, 2017). The addition of macrophages increased barrier integrity in organoids and upon their infection with *E. coli* macrophages were conditioned to extend intraepithelial projections and phagocytosis of the bacteria. Another study microinjected *E. coli* into the lumen of organoids derived from human pluripotent stem cells, resulting in an increase in IL-18 expression (Karve *et al.*, 2017). IL-18 is a chemoattractant for neutrophils, therefore this research group added polymorphonuclear neutrophils to infected organoid samples and observed increased migration to sites of infection.

DCs isolated from the MLN of mice have been cultured with organoids (Chng *et al.*, 2016). In this study, the effects of the receptor AhR in DCs on organoid cell configuration were analysed. The loss of AhR signalling in DCs resulted in the upregulation of Mucin 2 and goblet cell differentiation, similar to *in vivo* experiments. However, these DCs were added to intestinal crypts that do not provide all the differentiated cell types of the small intestinal epithelium during the early stages of these cultures.

These coculture models of immune cells with organoids resemble many of the features seen *in vivo*, therefore these will prove valuable in assessing the crosstalk behaviour between immune cells and the intestinal epithelium. However, there remains to be a developed model of DC/organoid cocultures whereby the DCs required need to resemble the phenotype of mucosal DCs and in culture with fully formed organoids.

1.20 Intestinal dendritic cells and *Toxoplasma gondii* infections

1.20.1 Recruitment of DCs to the infected small intestinal epithelium

Infection of IECs with *T. gondii* result in the expression of chemokines and cytokines for the recruitment of immune cells (chapter 1.6, page 44). This milieu of inflammatory signals leads to the influx of DCs to the sites of infection. Egress of parasites from IECs results in cell death which provides further inflammatory signalling for immune activation.

Tissue damage or necrotic cell death releases cytosolic or nuclear components that initiates an inflammatory response. Adenosine 5'- trisphosphate (ATP) is a cytosolic molecule that is sensed by ATP-gate purinergic P2x receptors (P2XRs) outside of the cells. Activation of P2X7R by ATP can activate inflammasome formation through NLR family, pyrin domain containing 3 (NLRP3) to secrete IL-1β. This inflammatory cytokine is important in intestinal immunity as it attracts neutrophils to the site of infection that produce IFN-γ. Infections of intestinal epithelial cell lines by *T. gondii* caused the induction of TNF-α, IL-6, CCL5, and IL-1β production through the P2X7R-NLRP3 pathway (S.-W. Huang *et al.*, 2017; Quan *et al.*, 2018). This inflammatory pathway recruits CD103+ DCs to the epithelium of the intestine in mice after *T. gondii* infection, but not in P2X7R knockout mice (S.-W. Huang *et al.*, 2017). IECs also contain TLRs that recognise microbial components. For example, the intracellular TLR9 recognises CpG motifs of *T. gondii* DNA to stimulate galactin-9 production (Hayen *et al.*, 2018). Intestinal DCs are influenced by galactin-9 to induce an increase in ALDH expression in DCs (De Kivit *et al.*, 2017).

Many of the studies used to assess early infection events of *T. gondii* on the small intestinal epithelium rely on monolayer cultures and cell lines. These have provided much information on the production of cytokines during infections that would attract immune cells to the small intestinal epithelium. However, these may not be representative of natural pathophysiology due to the lack of cellular diversity otherwise seen *in vivo*.

1.20.2 *Toxoplasma gondii* infections of DCs

DCs are known to be key for resistance to *T. gondii* as a critical source of IL-12 since this cytokine induces the expression of IFN-γ in NK cells and T cells. $Flt3L^{-/-}$ mice showed high susceptibility to toxoplasmosis, with decreased IL-12 and IFN-γ expression, impaired NK cell response, and a reduction in T cells (Dupont *et al.*, 2015). Ablation of the cDC1 subset in infected $Batf3^{-/-}$ mice showed increased susceptibility to infection with decreased IL-12 and subsequent IFN-γ, with administration of IL-12 restoring resistance to infection (Mashayekhi *et al.*, 2011). Invasion of DCs can cause the stimulation of intracellular TLRs. In particular, profilin expressed by *T. gondii* necessary for invasion serves as a ligand to TLR11 for IL-12 production (Pifer *et al.*, 2011). Other intracellular TLRs also provide resistance to infection by sensing of parasitic nucleic acids such as TLRs 3, 7, and 9 (Santamaria, Perez Cabarello and Corral, 2016).

Isolation of cDC subsets from the SI LP of orally infected mice showed an increase in IL-12 production only in those cells not directly infected with *T. gondii* (Cohen and Denkers, 2015). A possible explanation for the increased expression of IL-12 in non-

infected cDCs may be due to response to soluble parasite factors or debris. However, IL-12 expression in MLNs by DCs is greater than those from SI LP, suggesting a delayed response of IL-12 production after infection. RA expression, the metabolite involved in Treg induction, is also repressed in all cDC subsets in the LP following infection (Cohen and Denkers, 2015). This reduction may prevent T cell recruitment to the LP since RA expressed by DCs in the MLN imprint the gut homing receptor CCR9 and $\alpha_4\beta_7$. However, to confirm this cDCs from the MLNs would need to isolated and analysed following *T. gondii* infections. These studies show that the increased IL-12 levels in mice infected with *T. gondii* mostly derive from non-infected DCs in response to TLR signalling, suggesting possible immunosuppressive roles of the parasite.

1.20.3 Intestinal dendritic cells in *Toxoplasma gondii* dissemination

Infected DCs undergo morphological changes that coincide with increased migratory capacity. Changes include cytoskeletal actin redistribution, loss of podosomes, and redistribution of the surface integrins CD18 and CD11c, all of which impact cell adhesion (Weidner *et al.*, 2013). This could be in part due to secreted factors from the parasite, in such that inhibition of rhoptry proteins nullifies the onset of morphological changes. Podosomes are actin-rich structures that strongly interact with the extracellular matrix, and during DC maturation these structures are dissolved to increase migration towards lymph nodes. The change in shape of DCs, termed “amoeboid”, loss of podosomes, and expression of chemokine receptor CCR7 are all hallmarks of DC maturation that occurs during infection. Although DCs also express TLRs on their cell surface, activation of these are not

responsible for the increased motility of DCs, hence are MyD88-independent and only occurs through direct invasion of parasites (Lambert *et al.*, 2006; Weidner *et al.*, 2013).

The effects of *T. gondii* on DC motility are strain specific. In particular, type II *T. gondii* increased migration and dissemination of infected DCs in mice (Lambert *et al.*, 2009). However, type I *T. gondii* only slightly increased DC motility and are mostly seen as extracellular parasites in the spleen. This provides a suggestion that type I *T. gondii* enter the circulation as extracellular parasites, with this hypothesis further verified by their increased capacity for transepithelial migration (Barragan and Sibley, 2002). Types II and III *T. gondii* increase DC motility and also exhibit a reduced capacity for transepithelial migration, suggesting that their dissemination is dependent on hijacking of immune cells. This hypermigratory phenotype in DCs is a cause of γ-aminobutyric acid (GABA) expression, a neurotransmitter known to be involved in cell migration. Upon infection with *T. gondii*, DCs increase their expression of GABA that initiates hypermotility through $GABA_A$ receptor signalling and the influx of Ca^{2+} (Fuks *et al.*, 2012; Kanatani *et al.*, 2017). However, although GABAergic inhibition affects motility, it does not affect podosome frequency or cell cytoskeleton morphology (Weidner *et al.*, 2013). This suggests a downstream mechanism of GABA on DC motility following initial signalling form *T. gondii* infections. So, *T. gondii* infections of intestinal DCs alters the immune cell's morphology to increase migration for subsequent parasite dissemination. This is proposed to occur through podosome dissolution, cytoskeletal remodelling, and

increase in GABA production and CCR7 expression. All these processes increase the capacity of DCs to increase speed and directional motility.

1.21 Aims and objectives

Due to the novelty of intestinal organoids, limited research has been carried out on methods to infect them with enteric pathogens (Wilson *et al.*, 2014; Forbester *et al.*, 2015; Leslie *et al.*, 2015; Saxena *et al.*, 2016; Zhang *et al.*, 2016). This is due to the luminal surface of the epithelial cells where infections occur being obstructed by the enclosed shape of the organoids. In particular, organoids have yet to be used to model *T. gondii* infections to assess the defence responses from host cells during early stages of infection and to establish uncertain characteristics such as the primary route of infection across the epithelium. Improving our understanding of the key role of DCs in *T. gondii* dissemination may generate novel therapies and vaccines against infection. However, most studies rely on live animal models that do not provide information on the earliest infection events. Therefore, using organoids cocultured with intestinal DCs as models for *T. gondii* infection, may provide a valuable tool in assessing host-pathogen responses to *T. gondii* infections, and may even be further developed for other enteric infections.

Aim 1: Develop intestinal organoids as an infection model for *T. gondii* through generating protocols that provide large samples at high infection rates for high throughput analyses.

Aim 2: Optimise methods for the microinjection of *T. gondii* into the luminal space of organoids for live image analysis of infection and transepithelial migration at the physiologically relevant route.

Aim 3: Develop an *in vitro* culture of cDCs with an intestinal phenotype for coculture with organoids. Assess the conditioning effects of cDCs in culture with organoids, and the interactions using live imaging techniques. Assess interactions between cDCs and organoids infected with *T. gondii*.

Chapter 2: Materials and methods

2.1 Mice

Female, germ-free, C57Bl/6J mice between 7-8 weeks of age were purchased from Charles River. ROSA$^{mT/mG}$ mice were previously described (Muzumdar *et al.*, 2007) and provided by the Biological Specimens Unit of the University of Liverpool. All mice were culled by cervical dislocation schedule 1 procedure and tissue transported on ice to IC2 (Liverpool Science Park) where experiments were carried out. All mice were maintained in accordance to the Animals Scientific Procedures Act 1986 (ASPA).

2.2 Murine small intestinal organoid cultures

2.2.1 Crypt isolation and culture

Small intestinal organoids were developed as previously described with some alterations (Sato and Clevers, 2013b). The jejunum of the small intestine of C57B1/6 or ROSA$^{mT/mG}$ mice were removed and flushed with phosphate buffered saline solution without Ca^{++} or Mg^{++}, pH7.2 (PBS) (Sigma Aldrich). The intestines were cut open longitudinally and further washed to remove debris and mucus before cutting into approximately 0.5cm sections. Tissues were washed in PBS through agitation again and incubated in ice-cold 30mM EDTA for 5 minutes. The tissues were removed from the EDTA, transferred to PBS and shaken for 15 seconds to remove epithelial cells before incubating in EDTA again. PBS fractions were analysed for crypts under a light microscope. This incubation/shaking process was repeated for a

total of 5 fractions and the fraction with the most crypts was filtered through a 70µm strainer and centrifuged at 1200rpm for 5 minutes. Crypt quantity was assessed by counting crypt structures in 30µl of solution and centrifuged at 300g for 5mins at 4C. Matrigel (Corning) was diluted to 70% with IntestiCult OGM mouse basal medium (catalogue number 06005; StemCell Technologies) and used to resuspend crypts. These were plated onto 9mm coverslips in a 48 well plate at 300 crypts/30µl aliquots or onto tissue culture-treated 24 well plates at 500 crypts/50µl aliquot. The Matrigel was allowed to polymerise for 20-30 minutes at 37°C before the addition of IntestiCult mouse basal medium with 1% penicillin/streptomycin (P/S) (10,000 U penicillin, 100 mg/ml streptomycin, Sigma) and incubated at 37°C, 5% CO_2.

2.2.2 Organoid passage

Every 7 days the organoids were passaged by mechanical disruption and to remove luminal content. PBS was added to each organoid sample to disrupt the Matrigel and passed through a 27G needle. This was transferred to a 15mL tube with added PBS, centrifuged at 300g for 5 minutes and cultured in Matrigel as described above. Organoids were passaged at a 1:3 or 1:4 ratio.

2.3 Bovine small intestinal organoid cultures

Bovine organoids were generated by Dr. Hayley Derricott by the isolation of crypts from the small intestine of cows taken from abattoir (Derricott *et al.*, 2018). Organoids were frozen and stored in liquid nitrogen.

Organoids were thawed from liquid nitrogen stores in a water bath until liquid. Organoids were added to PBS and centrifuged at 50g for 3mins. Matrigel diluted to 70% in bovine organoid medium was used to resuspend the organoid pellet and plated onto well plates as with murine organoids. Bovine organoid medium consisted of 50% IntestiCult mouse basal medium, 50% Wnt3a-conditioned media (gifted from Dr Carrie Duckworth, University of Liverpool) with added 1ug/mL R-spondin 1 (Peprotech), 100ng/mL noggin (Peprotech), 100ng/mL EGF (Peprotech), 1.5um CHIR99021 (Tocris), 5um Y27632 (Tocris), 5um SB202190 (Tocris), 250nM A8301 (Tocirs) and 100ug/mL Primocin (InvivoGen). This was added to bovine organoid cultures after Matrigel had polymerised for 20-30 mins at 37C. Medium was changed every 2-3 days and passaged after 7-10 days. Passages involved resuspending organoid cultures in PBS and fragmenting using the pipette. Organoids were centrifuged at 50g for 3 mins and cultured in Matrigel as above.

2.4 *Toxoplasma gondii* culture

Two clonal strains of *T. gondii* were used in this study: type I, RH virulent strains and type II, Pru strain with two genetically modified types of Pru strain used. Pru-GFP strain was kindly donated by Dr Eva Frickel, Francis Crick Institute, and Pru-tdTomato-Cre kindly gifted by Anita Koshy, Stanford University. All *T. gondii* types were maintained in the immortalised Vero cell line that are derived from African green monkey kidney epithelial cells (ATCC).

Vero cultures and those with *T. gondii* were cultured in T25 vent-lidded flasks with high-glucose Dulbecco's Modified Eagle's Medium supplemented with 10% foetal bovine serum (FBS) and 1% P/S. Cultures were incubated at 37°C, 5% CO_2.

2.4.1 Vero cell culture

Vero cultures were passaged every 7 days or when confluent. Culture medium was removed, and cells rinsed with PBS before the addition of Trypsin-EDTA (Gibco) and incubated for 5 min at 37°C, 5% CO_2. Cell detachment was analysed using a light microscope and the flask agitated to suspend cells. Trypsin action was inhibited with the addition of DMEM with 10% FBS and cell counts performed with equal volume of trypan blue. New cultures were seeded at 4 x 10^5 cells per T25 flask and incubated at 37°C, 5% CO_2.

2.4.2 *Toxoplasma gondii* culture

Newly passaged Vero cells were cultured overnight before the addition of parasites from thawed cryovials or from culture. Cells from parasite cultures were removed using a cell scraper and passed through a blunt end needle three times to break up the cells and release intracellular tachyzoites. The suspension was centrifuged at 2000rpm for 10 mins and resuspended in medium with a cell count performed. The RH strain and Pru strain were seeded at 1x10^4 and 1x10^6 parasites per 24h Vero culture, respectively. Cultures were assessed every day using a light microscope and passaged when egress of parasites from Vero cells were observed, approximately every 7 days.

2.4.3 *Toxoplasma gondii* purification

Purification of *T. gondii* was necessary for infections of organoids. Vero cells were removed from parasite cultures using a cell scraper and passed through a blunt end needle three times. PBS was added and the suspension centrifuged at 2000rpm for 10 mins and resuspended in 5mL PBS. PD-10 desalting columns (GE HealthCare Life Sciences) were used to purify the parasites. Storage liquid in the columns were discarded and columns washed twice with 5mL PBS. The cell suspension was added to the column and the flow through collected. The column was washed with a further 5mL PBS and collected. A parasite count was performed with desired numbers isolated before centrifuging at 2000rpm for 10 mins.

2.5 Organoid infections with *Toxoplasma gondii*

Organoids were removed from Matrigel as per passage protocol by disruption with PBS. Organoids were centrifuged at 300g for 5 mins and resuspended in a low volume of 10^6 or 10^7 *T. gondii* (in approximately 50µL). These were incubated at 37°C for 1 hour before washing with organoid media and culture in Matrigel as described above.

2.6 Fixing and staining of infected organoid samples

All organoid samples for staining were cultured on 9mm coverslips in 48 well plates. Medium was removed from organoid samples and gently washed with PBS. Samples were fixed for 30 mins in 4% paraformaldehyde (PFA) at room temperature before gently washing again with PBS.

To stain fixed organoid samples, washes every 20 mins for 2 hours with washing buffer (PBS, 1% serum, 0.1% Triton X-100) were performed. Samples were incubated at room temperature for 4 hours in blocking solution (PBS, 10% serum, 1% Triton X-100) (Table 2). Primary antibodies were diluted in blocking solution, added to samples and incubated overnight at 4°C. Samples were washed three times with washing buffer and secondary antibodies diluted in washing buffer were added for 2 hours at room temperature. Organoid samples were then washed every 20 mins with PBS for 2 hours before coverslips were extracted. All washing, blocking and staining steps were carried out on a plate rocker.

To prevent the compression of organoid samples against glass slides, 7mm diameter 1mm thick O-rings were glued to glass slides and Hydromount (Scientific Laboratory Supplies) pipetted into the O-rings. Organoid samples were inverted onto the Hydromount and allowed to dry at room temperature. Samples were stored at 4°C before imaging.

2.6.1 Immunofluorescence staining and confocal imaging

For the characterisation of organoid cells, organoids were stained with phalloidin in combination with lysozyme, chromogranin A, mucin-2, or E-cadherin (Table 2).

For staining of infected organoids from C57Bl/6J mice, Rhodamine-Phalloidin stain was used to stain for F-actin in organoids, or e-cadherin for basolateral staining of epithelial cells and SAG-1 for *T. gondii* with anti-mouse AF488 secondary antibody (Table 2). When staining these infected organoids for GRA7, phalloidin AF-647 was

used for organoid staining, SAG-1 and AF488 for *T. gondii,* and anti-rabbit TRITC secondary antibody for GRA7.

Table 2. Antibodies and stains used for confocal imaging of organoids and those infected with T. gondii. BSA: bovine serum albumin

Stain	**Host**	**Target**	**Blocking serum**	**Manufacturer**
Rhodamine-phalloidin		F-actin	BSA/ donkey/ goat	Life Technologies
Phalloidin-AF647		F-actin	BSA/ donkey/ goat	Life Technologies
DAPI		Nucleus		Life Technologies
SAG-1 (TP3)	Mouse	Surface protein of *T. gondii*		Abcam
GRA7	Rabbit	Dense granule 7 from *T. gondii*		Gift from David Sibley, University of Washington
Chromogranin A	Rabbit	Enteroendocrine cells		Insight Biotechnology

Mucin-2 (H-300)	Rabbit	Goblet cells		Insight Biotechnology
Lysozyme (BGN/06/961)	Mouse	Paneth cells		Abcam
Villin (C-19)	Mouse	Microvilli/brush border		Abcam
E-cadherin (24E10)	Rabbit	Tight junctions		BD Transduction Laboratories
Anti-rabbit TRITC	Donkey	Rabbit primary antibodies	Donkey serum	Stratech Scientific Ltd
Anti-rabbit FITC	Donkey	Rabbit primary antibodies	Donkey serum	Stratech Scientific Ltd
Anti-mouse AF488	Donkey/Goat	Mouse primary antibodies	Donkey /Goat serum	Stratech Scientific Ltd
Anti-mouse AF647	Rat	Mouse primary antibodies	BSA/Rat serum	Biolegend

All images were acquired at the Centre for Cell Imaging in the Institute of Integrative Biology, University of Liverpool using Zen Black software (Zeiss) on a Zeiss LSM880 multiphoton upright confocal microscope with the laser lines Diode (405nm), Argon (488nm), DPSS-5610 (561nm) and HeNe633 (633nm). Objectives used were W-Plan Apochromat 40x/1.0 Dic water immersion (Zeiss) and Pan-Apochromat 63x/1.0 oil DIC M27 oil immersion (Zeiss).

2.7 Imaris image analysis of infected organoids

Infected organoid samples were quantified for *T. gondii* using Imaris x64 v8.2.1 image analysis software (BitPlane). Automated parasite counts were manually checked for accuracy.

The “spots” function was used to determine parasite numbers. Here, Imaris software allocates spots onto fluorescent signals of certain channels so to be quantified. For *T. gondii* quantification, GFP fluorescence of the parasite was carried out by 2 steps: first, “surfaces” function was used to generate an iso-surface of the organoid using the F-actin stain that allows for the quantification of its volume; second, the “masking” application of this “surface” was used to assess overlapping signals from the GFP parasites. This allows for a channel ascribed to intracellular parasites. The “spots” function was used on this new intracellular parasite channel to determine parasite number. A manual count was then carried out to ascertain the precision of the automated count using the “section” tab that allows viewing of sections from all planes: XY, XZ, YZ.

2.8 Microinjections of *Toxoplasma gondii* into the luminal space of organoids

2.8.1 Optimisation of microneedle production

Due to the relatively large size of *T. gondii* (3-6µm) compared to pathogens previously microinjected into the luminal space of organoids (*S. typhimurium*, *H. pylori*, Noro virus), the microneedle bore size needed to be significantly larger to prevent blockage of the microneedle tip. Therefore, a bore size of approximately 10µm was determined to be sufficient.

Consistency of microneedle production was required, therefore using the P-2000 micropipette puller (Sutter Instruments) allowed for the control of many variables such a weight, temperature, velocity, and delay when pulling thin-walled, 0.75µm internal diameter glass capillaries (TW100-4; World Precision Instruments). Some microneedles were bevelled (EG-400; Narishige) since pulling of these needles may cause the tips to seal closed.

This method proved inconsistent in microneedle production of a suitable bore size. It helped determine that a bore size of 10µm is optimal to prevent needle blockage but any larger then pressure compensation problems occurred, and the needle tip length should be short to decrease the chances of blockage. Therefore, microneedles were pulled using the simpler pulling machine (PC-10; Narishige) at different weights and temperature to provide a short microneedle tip. These were then loaded onto the microinjector system and the tips broken in a dish until an

approximate bore size of 10µm was achieved. Optimal pulling conditions were 355g at 50°C.

2.8.2 Organoid culture for microinjections

Organoids were resuspended from Matrigel using PBS and centrifuges at 300g for 5 mins. Supernatant was removed and 1mL of medium (IntestiCult mouse basal medium) added and centrifuged again. The supernatant was removed and 70% Matrigel diluted in organoid medium was added on ice. Organoids were plated onto low-wall, glass bottom, 3.5cm culture dishes as a thin layer, incubated for 20-30 mins at 37°C for Matrigel polymerisation, and organoid medium added. These were cultured overnight at 37°C, 5% CO_2. Organoids to be injected with live *T. gondii* for live imaging were cultured onto 3.5cm, glass bottom grid, low-wall, culture dish (80156, ibidi).

2.8.3 Microinjections of fluorescent microspheres and *Toxoplasma gondii* into the lumen of organoids

Proof of principle experiments were carried out by loading either 2µm (L4530; Sigma Aldrich) or 6µm (17156-2; Polysciences Europe) fluorescent microspheres into microneedles for microinjections into organoids. Both murine and bovine organoids were used. Microneedles were loaded onto a microinjector system with an Eppendorf FemtoJet Microinjector. Injections were carried out using an Epifluorescence Microscope (Zeiss) and acquired using ImageJ software.

T. gondii were purified using PD-10 columns as described above. Purified parasites were centrifuged at 2000rpm for 10 mins, supernatant removed, and centrifuged again to remove residual PBS with PBS added to attain a density of 3-4x10^8/ml. These were loaded into previously made micropipettes (as above) using 3-5µL of parasite suspension and Eppendorf Microloader tips (Scientific Laboratory Supplies). The medium was removed from the organoid sample and placed under an Epifluorescnet microscope (Zeiss). The microneedles were loaded onto the microinjector system and lowered onto organoids. The needle was then moved laterally to pierce into the organoid and parasite were injected using 0.1 sec injection rate with increasing injection pressure from 100hPa to 300hPa until parasites enter the lumen. The microneedle was removed from the organoid and brought out of the Matrigel to position the sample to another organoid for the process to be repeated.

Live imaging of organoids microinjected with live *T. gondii* were carried out using ROSA$^{mT/mG}$ organoids and *T. gondii* Pru-GFP. Time-lapse images of z-stacks were acquired using the LSM 880 MP confocal microscope with Airyscan (Zeiss) and the 2-photon Chameleon laser was set to 920 nm. Emission light was separated with 490 or 555 dichroics. Bandpass filters 525/25 and 590/20 M were used to minimise spectral overlap. All images were analysed using the Zen Black software as described above.

2.8.4 Microinjections of CpG ODN into organoid samples

Organoids were cultured onto 9mm coverslips in a 48 well plate overnight as described above. Coverslips were removed and placed onto a glass bottom, 3.5cm culture dish for microinjections. Microneedles were produced using a lower weight (225g) and higher temperature (60°C) to produce a thinner bore size of approximately 3µm to allow for greater control of compensation pressures. Compensation pressure was determined by placing the microneedle onto the glass bottom dish away from the organoid sample and assessing the movement of fluid and adjusting to prevent movement in or out of the needle. The organoids were injected with 5µM CpG ODN (M362, Invivogen) or PBS (control) as described above.

2.9 Bone marrow culture to produce dendritic cells with a gut-like phenotype

2.9.1 Bone marrow isolation

Femurs and tibias of C57B1/6 mice were removed and tissue scraped off in PBS using a scalpel. The bones were soaked in 70% ethanol for 5 minutes. The epiphyses of the long bones were cut using the scalpel and the bone marrows were flushed out with RPMI 1640 medium supplemented with 2mM L-glutamine and 1% P/S using a syringe and 27G needle. Cells were centrifuged at 1500rpm for 5 minutes and suspended in ACK lysis buffer for 3 minutes at room temperature before filtering through a 70µm filter, centrifuging and resuspending in culture medium.

2.9.2 Bone marrow culture method 1

BM cells were cultured at $1x10^6$ cells/mL in a 6 well plate in complete RPMI 1640 medium containing 10% (vol/vol) FBS, 2mM L-glutamine, 1% (vol/vol) P/S and 50µM 2-mercaptoethanol. Combinations of recombinant GM-CSF (576304, Biolegend), recombinant Flt3L (550702, Biolegend) and recombinant IL-4 (574302, Biolegend) were added to the cultures as described in chapter 5 (page 118).

2.9.3 Bone marrow culture method 2

BM cells were cultured at $1.5x10^6$ cells/ml in a 6 well plate in complete RPMI 1640 medium containing 10% (vol/vol) FBS, 2mM L-glutamine, 1% (vol/vol) P/S, 50µM 2-mercaptoethanol, and 200ng/ml Flt3L (550702, Biolegend), with 20ng/ml GM-CSF (576304, Biolegend) added from day 6 of culture. A proportion of the BM culture was treated with 1µM of retinoic acid (R2625, Sigma) from day 6. Medium was added on day 5 (100ng/ml Flt3L) and cells harvested on day 8 by gentle pipetting to collect non-adherent and loosely adherent cells.

2.9.4 Dendritic cell enrichment

BM-derived DCs were enriched using positive selection MACS for CD11c (Miltenyi) as per manufacturer's instructions with some slight alterations. BMDCs were harvested on day 8 by pipetting and centrifuged at 1500rpm for 5 mins and resuspending in buffer (PBS with 2% FBS), blocked with CD16/32 antibody on ice for 20 mins. MACS buffer (PBS with 2% FBS and 2mM EDTA) was added and centrifuged. Cells were resuspended in MACS buffer at $400µl/10^8$ cells and CD11c

microbeads added at 50µl/10^8 cells. These were incubated in the fridge for 20 mins before more MACS buffer was added and the samples centrifuged at 200g for 10 mins. LS columns (Miltenyi) were placed in a magnetic stand and rinsed with MACS buffer. Cells were resuspended in 500µl of MACS buffer and added to the column, discarding the flow through. Columns were rinsed three times and placed in a 15mL falcon tube. 5mL of MACS buffer was added to the column and cells were flushed out using the plunger. A cell count was performed and required amounts were separated and centrifuged at 200g for 10 mins.

2.10 Co-culture of bone marrow-derived gut-like dendritic cells with organoids

2.10.1 Organoid/DC cocultures to assess dendritic cell conditioning

DCs derived from bone marrow were isolated and enriched for CD11c as above. Organoids were removed from Matrigel through disruption with PBS and centrifuged at 300g for 5 mins. DCs were resuspended in Matrigel and added to organoid samples at 2x10^6/mL and aliquoted at 100µl onto 9mm coverslips in a 48 well plate. These samples were incubated at 37°C for 20-30 mins and organoid medium added and incubated at 37°C, 5% CO_2. After 24 hours if incubation the organoid/DC samples were resuspended in PBS and centrifuged at 1500rpm for 5 mins for staining (chapter 2.12, page 114).

2.10.2 Time-lapse imaging of DC/organoid cocultures

The DCs cultured from bone marrow were isolated and enriched as described above. They were resuspended in DMEM without FBS at 1x10^6/mL and 2µM

carboxyfluorescein succinimidyl ester (CFSE) added and incubated for 7 mins at room temperature. Cells were washed with DMEM containing 10% FBS at 1500rpm for 5 mins, resuspended in Matrigel and left on ice to prevent polymerisation. Organoids generated from ROSA$^{mT/mG}$ mice were removed from Matrigel using PBS and centrifuged at 300g for 5 mins. The supernatant was removed, and organoids centrifuged again to remove residual PBS. Isolated DCs in Matrigel were added to the organoids at 1.1x10^5/mL of DCs, plated onto glass bottom 3.5cm culture dishes and incubated at 37°C for 20-30 mins. Samples were transported to the CCI for live imaging where phenol-red-free DMEM/F12 (ThermoFisher Scientific, 11039021) was added to the samples.

Time-lapse images of z-stacks were acquired over a 50-minute period at 2-minute intervals using the LSM 880 MP confocal microscope with Airyscan (Zeiss) and the 2-photon Chameleon laser was set to 920 nm. Emission light was separated with 490 or 555 dichroics. Bandpass filters 525/25 and 590/20 M were used to minimise spectral overlap.

2.10.3 Motility and morphology analysis of dendritic cells in culture with organoids using Imaris imaging software

Once the time-lapse images of DC/organoid cocultures were obtained, Imaris software was used to analyse DC morphology and motility (Figure 8). Selecting only the CFSE channel (Figure 8B), the 'surfaces' function was used to cover the CFSE fluorescence of the DCs (Figure 8C). In organoid samples, infected cells express eGFP that were manually removed from the 'surface' selection. The 'surfaces'

function allows the tracking of each individual DC over the time-lapse period (Figure 8D) as well as providing data on their morphology.

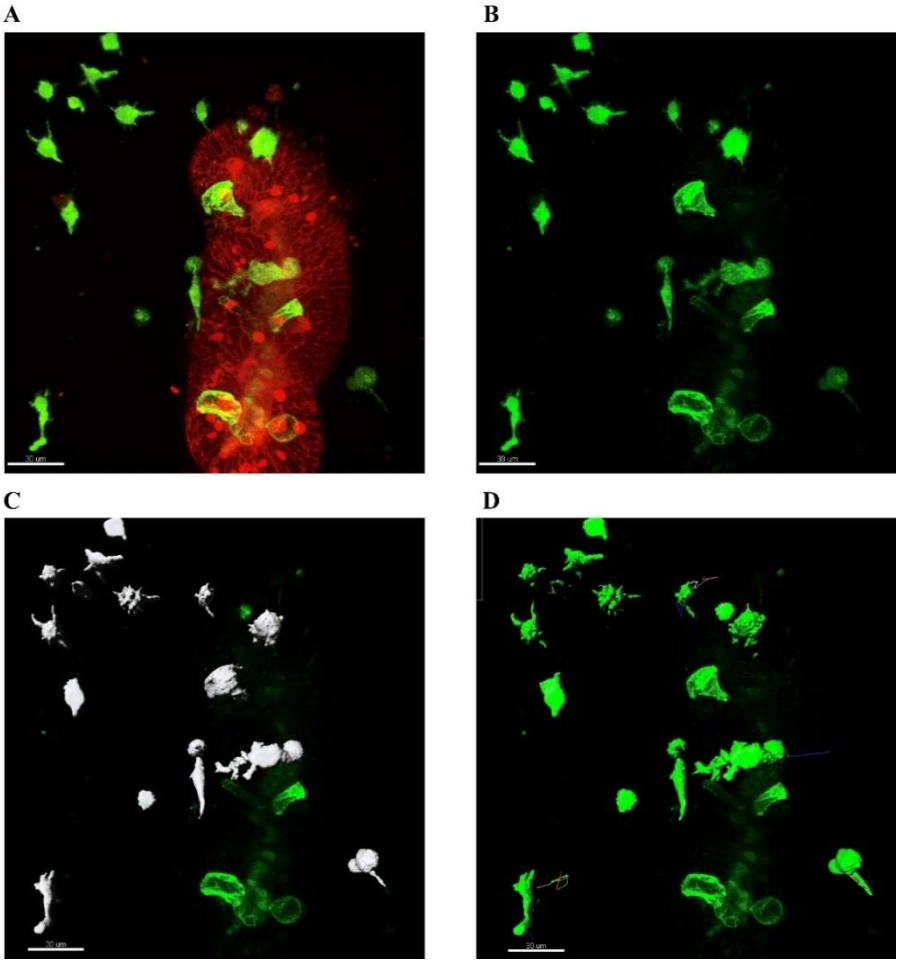

Figure 8. Imaris analysis of DC motility and morphology
DCs were labelled with CFSE and cocultured with ROSA$^{mT/mG}$ organoids and imaged using 2-photon microscopy and analysed using Imaris software. **A**, is a representative sample of a DC and infected organoid coculture. DCs are CFSE labelled (green) and organoids express tdTomato (red) with infected cells expressing eGFP (green). **B**, the channel for eGFP and CFSE was selected for the 'surfaces' function. **C**, using the 'surfaces' function, gDCs were selected and eGFP cells were removed from selection. **D**, the surfaces function also allows the tracking of individual DCs over the time-lapse period with tracks marked as multicoloured lines. Scale bar 30µm

2.10.4 Coculture of dendritic cells with TLR9-activated organoids

Organoid samples on 9mm coverslips were microinjected with 5µM CpG ODN (M362, Invivogen) as described above (chapter 2.8.4, page 108). These organoid

samples were placed back into a 48 well plate and incubated overnight at 37°C, 5% CO_2. PBS was used to gently wash the samples and purified BM-derived DCs were added to the organoids at $2x10^5$ cells per sample ($1x10^6$/ml). These were incubated overnight and resuspended in PBS for flow cytometric analysis.

2.11 Isolation of dendritic cells from the lamina propria of the small intestine

DCs were isolated from the LP of the small intestine of mice as previously described with some alterations (Cohen and Denkers, 2015). Small intestines were harvested from C57Bl/6J mice and PPs removed. The tissue was cut longitudinally to butterfly the small intestine and washed three times in PBS. The small intestine was cut into approximately 0.5cm lengths, washed in PBS and incubated in Hanks' Balanced Salt solution (HBSS) supplemented with 5% FBS, 5mM EDTA and 10mM HEPES in an orbital shaker for 20 minutes at 250rpm at 37°C. This was repeated for a total of three times with shaking for 20 secs in PBS between each incubation to remove all epithelial cells. The tissues were minced with scissors and incubated in HBSS with 1.5mg/ml collagenase VIII (C2139, Sigma Aldrich) and 40µg/mL DNAse I (DN25, Sigma Aldrich) for 20 minutes in an orbital shaker at 200rpm, 37°C and vortexed for 20 seconds to allow for thorough dissociation. The suspensions were passed through 100µm and 30µm filters and centrifuged at 1500rpm for 5 minutes. In some instances, Percoll density separation was then performed whereby the cell pellet was resuspended in 40% Percoll, layered onto 80% Percoll and centrifuged at 1,000g for 20 minutes with no brake. Cells at the interphase were collected. Cells were enriched for $CD11c^+$ cells by positive selection with CD11c microbeads

(Miltenyi) through two LS columns (Miltenyi) as described above (chapter 2.9.4, page 109). Enriched cells were then analysed using flow cytometry (chapter 2.12, page 114) and added to organoid cultures for live imaging as in chapter 2.10.2, page 110. Time-lapse images of z-stacks were acquired over a 50-minute period at 2-minute intervals using the LSM 880 MP confocal microscope with Airyscan (Zeiss) and the 2-photon Chameleon laser was set to 920 nm. Emission light was separated with 490 or 555 dichroics. Bandpass filters 525/25 and 590/20 M were used to minimise spectral overlap. Motility of DCs were analysed using the Imaris imaging software (chapter 2.10.3, page 111).

2.12 Flow cytometric analysis of dendritic cells and DC/organoid cocultures

Samples were suspended in buffer (PBS with 2% FBS) with CD16/32 blocking antibody (1/1000 dilution) on ice for 20 mins. Fluorescent conjugated antibodies were added to samples as in Table 3 for 30 mins on ice and washed twice with buffer at 1500rpm for 5 mins. Samples were processed using MACSQuant Analyzer (Miltenyi Biotec) and analysed with FlowJo (Tristar). Live cells were gated using FSC/SSC plot and aggregates excluded by SSC pulse width.

Table 3. Antibodies used for flow cytometry analysis of DCs

Antibody	**Fluorescent conjugate**	**Dilution**	**Clone**	**Manufacturer**
Fixable Viability Dye ef450		1/400	N/A	eBioscience
CD11b	APC-efluor 780	1/500	M1/70	
CD11c	APC-efluor 780	1/500	N418	
I-A/I-E (MHCII)	BV421	1/1000	M5/114.15.2	Biolegend
CD11c	FITC	1/200	N418	
CCR9	PE	1/200	9B1	
CD103	PE	1/200	2E7	
Armenian Hamster IgG isotype	PE	1/200	HTK888	
CD45	PE/Cy7	1/1000	30-F11	
CD103	PE/Cy7	1/800	2E7	
F4/80	APC	1/200	BM8	

CCR7	APC	1/200	4B12	
Rat IgG2a κ isotype	APC	1/200	RTK2758	
CD11c	APC	1/200	N418	
CD11b	APC/Fire 750	1/800	M1/70	

2.12.1 ALDEFLUOR assay optimisation

Before staining for cell surface markers, DCs were stained for intracellular aldehyde dehydrogenase enzyme using ALDEFLUOR kit (StemCell Technologies) as per manufacturer's instructions with alterations. Cells were resuspended in ALDEFLUOR buffer with half the volume of each sample added to the DEAB inhibitor (90µM) as the control. ALDEFLUOR reagent (365nM) was added to each sample and control, mixed, and incubated at 37°C for 30 mins. Samples were centrifuged at 1500rpm for 5 mins and resuspended in ALDEFLUOR buffer for further staining.

BMDCs derived from culture with GM-CSF, Flt3L, and RA were used to determine the concentrations of ALDEFLUOR reagent, Diethylaminobenzaldehyde (DEAB) reagent as the control, and cell density for the optimal detection of ALDH activity (Figure 9).

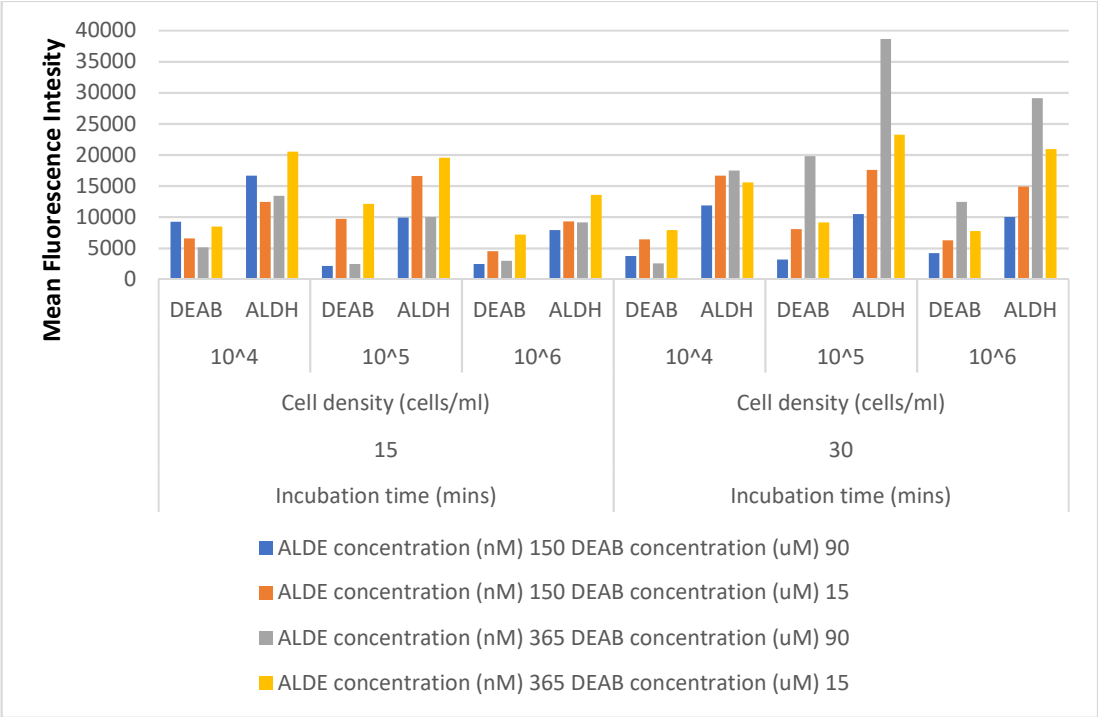

Figure 9. Optimisation of ALDEFLUOR assay kit for optimal detection of ALDH in DCs
BM cells cultured in Flt3L, GM-CSF and RA were used to optimise aldefluor staining. Differing concentrations of ALDEFLUOR reagent and the blocking control were used to determine the greatest intensity of ALDH compared to the control. Results derived from a single experiment.

Chapter 3: Development of intestinal organoid cultures as a disease model for Toxoplasma gondii

3.1 Introduction

Current models of the intestinal epithelium for studying enteric infections are unsuitable due to the lack of cellular diversity in monolayer cultures and the difficulty in detecting early infection events in live animal models. Intestinal organoids have been developed that recapitulate the cellular diversity and architecture of the small intestinal epithelium, making them a far superior model for enteric infections. However, organoids have been established as an infection model for only a limited number of pathogens and not yet optimised for *T. gondii* infection. Such a model would contribute vital understanding of early infection events in the small intestinal epithelium.

3.1.5 Current models for *Toxoplasma gondii* infection of the small intestinal epithelium

Assessing the interactions and responses of intestinal epithelial cells during early infections with *T. gondii* mostly relies on monolayer cultures (Barragan and Sibley, 2002; Barragan, Brossier and Sibley, 2005; Ju, Chockalingam and Leifer, 2009; Gopal, Birdsell and Monroy, 2011; Morampudi, Braun and D'Souza, 2011; Weight *et al.*, 2015; Briceno *et al.*, 2016). Epithelial cell lines have been shown to respond to *T. gondii* infection through the expression of soluble factors that allow them to communicate with immune cells to aid in pathogen clearance (Ju, Chockalingam and

Leifer, 2009; Morampudi, Braun and D'Souza, 2011). *T. gondii* disrupts cell-cell contacts between epithelial cells to improve their transmigration across the intestinal barrier between host cells (Dubey, 1997; Weight *et al.*, 2015). They also directly invade epithelial cells where they replicate and egress to spread infection (Dubey, 1998; Barragan and Sibley, 2002; Gregg *et al.*, 2013). Little is known about the host defence mechanisms in infections with an established PV. It is also uncertain whether the paracellular or intracellular route contributes more to establishing infection, and whether this differs with parasite strain. The studies that proposed these mechanisms involved monolayer cultures that are poorly representative of the structure or diversity of the intestinal epithelium and may therefore not provide physiologically relevant results. *In vivo* mouse models have been used to assess later stages of infection. However, locating rare foci of infection and analysing small, local physiological changes against a large background of normal tissue is very difficult, especially when analysing early stages of infection (Gregg *et al.*, 2013). The use of organoids as a model for *T. gondii* infections provides a more suitable tool for assessing host-pathogen interactions during early infection events.

3.1.2 Small intestinal organoids

An *in vitro*, 3D, intestinal epithelial model has been established, otherwise known as intestinal organoids, that provide the structure and cellular diversity seen *in vivo* (Sato *et al.*, 2009). Here, the crypt structures that contain both stem cells and Paneth cells are isolated from the intestinal epithelium and cultured in a 3D

extracellular matrix with growth factors R-spondin-1, epidermal growth factor, and Noggin. The crypt structures proliferate to produce further crypts in the form of buds and a villus-like, polarised epithelium surrounding a central lumen that fills with apoptotic cells resulting from normal cell turnover of intestinal epithelial cells. Organoids can be cultured and expanded for many months, even lasting over 1.5 years without any genetic alterations, minimising the requirement for experimental animals (Sato *et al.*, 2009). Due to the cell diversity and architecture of organoids recapitulating that of the small intestinal epithelium, responses to infection would be of physiological relevance. One study briefly mentions infected organoids with *T. gondii*, however no methodology was provided, nor any measurements (Klotz, Aebischer and Seeber, 2012). Therefore, establishing protocols for the infection of organoids would provide a valuable tool to elucidate events during early infections that could lead to the development of novel vaccines or therapies against *T. gondii* infection.3.1.3 Organoids as a disease model for enteric infections

Although intestinal organoids provide a more suitable disease model of the intestinal epithelium, not many infection studies have been carried out. This may be due to the difficulties in infecting organoids through the apical surface since they retain an enclosed lumen. Nevertheless, infections have been carried out with bacteria, viruses, and more recently parasites with methods of infection including microinjections into the luminal space, and incubation of pathogen with organoids in solution before culture. The relevance of organoids as an infection model was established in early studies with *Salmonella enterica* serovar Typhimurium in murine organoids (Zhang *et al.*, 2014). Infected organoids had disrupted tight

junctions, initiation of inflammatory responses through NF-κB signalling, and a reduction in stem cell markers that also occurs during *in vivo* infections. This model has since been translated into human organoids, whereby the microinjections of *Salmonella* induced increased organoid expression of *IL-8*, *IL1B*, *IL23A*, and *TNF* (Forbester *et al.*, 2015). Microinjections of *Clostridium difficile* into the lumen of human organoids also resulted in the loss of barrier integrity (Leslie *et al.*, 2015). Organoids have been important in modelling rotavirus infections that have otherwise relied on inappropriate monolayer systems that provide inconsistent results and difficulties in replicating human rotaviruses. Organoids support human rotavirus infection and replication, and resemble the reduced sensitivity to antivirals and increased fluid secretion observed *in vivo* (Yin *et al.*, 2015; Saxena *et al.*, 2016). To date, the only parasite used in organoid infection models is *Cryptosporidium parvum* (*C. parvum*) that were added to murine crypts in solution for 30 minutes at 37°C before culture (Zhang *et al.*, 2016), and microinjected into the lumen of organoids (Heo *et al.*, 2018). *C. parvum* completed its life cycle within organoids and resulted in the decrease in organoid propagation through the downregulation of stem cell markers, adding further insight into Cryptosporidiosis. Organoids have been used for *T. gondii* infections, however this was only briefly mentioned with no results acquired (Klotz, Aebischer and Seeber, 2012). These studies have established the suitability of organoids as an infectious disease model.

Organoids would be a suitable model to characterise the virulence of *T. gondii* types. Type I *T. gondii* are known to be highly virulent, able to cross cellular barriers, and are more motile than types II and III which are less virulent and stimulate

stronger immune responses in hosts hindering their dissemination and pathology (Barragan and Sibley, 2002). Due to their increased virulence, the type I RH strain of *T. gondii* was used to prove infection of organoids, with type II Pru strain subsequently used to optimise infection rates since they do not express a long distance migratory phenotype unlike Type I RH. Therefore, rather than migrate between epithelial cells, type II Pru are more likely to invade cells. Since organoids are the most relevant model of the small intestinal epithelium for studying early infection events and their use to model *T. gondii* may elucidate the important features of host-pathogen interactions at early stages of infection. The aim of this study was to develop intestinal organoids as a high throughput model of infection for *T. gondii*. Using this model, interactions between host cells and parasites can be assessed using fluorescence microscopy and in real time. This may reveal previously unknown features of the host-parasite dialogue.

Aims: Generate a high throughput infection protocol of intestinal organoids with *T. gondii*

Objectives:

a) Generate a protocol that maximises infection of organoids with *T. gondii*
b) Validate that organoids contain intracellular parasites
c) Assess infection rates and organoid cell exposure to *T. gondii* over a period of time

3.2 Methods

3.2.1 Small intestinal organoid culture

Small intestinal organoids were developed as previously from C57B1/6 mice and ROSA$^{mT/mG}$ mice (Chapter 2.2, page 96). Crypts were cultured in Matrigel diluted to 70% with IntestiCult. These were plated onto coverslips in a 48 well plate at 300 crypts/30µl aliquots or a 24 well plate at 500 crypts/50µl. The Matrigel was allowed to set for 20-30 minutes at 37°C before the addition of IntestiCult mouse basal medium with 1% P/S and incubated at 37°C, 5% CO_2.

Every 7 days the organoids were passaged by resuspending in PBS, passing through a 27G needle and centrifuging at 200g for 5 minutes. Matrigel with IntestiCult mouse basal medium was added and plated as above.

3.2.2 Staining of organoid cultures

Organoid cultures were fixed at days 5-7 in 4% PFA solution for 30 minutes at room temperature. Organoids were stained as described above (Chapter 2.6, page 100) with the following primary antibodies: mouse anti-villin, rabbit anti-Chromogranin A, mouse anti-Mucin-2, rabbit anti-E-cadherin, and mouse anti-lysozyme (Abcam). Secondary antibodies included anti-rabbit FITC and anti-mouse AF488. Phalloidin-AF647 was used to label F-actin. Stained samples were mounted in Hydromount solution onto rubber O-rings with 1mm depth to prevent compression.

3.2.3 *Toxoplasma gondii* culture and purification

Three strains of *T. gondii* were cultured in Vero cells: RH, Pru-GFP, and Pru-tdTomato-Cre, as described above (chapter 2.4, page 98). Parasites were passaged upon egress of cells by scraping the culture and passing through a blunt end needle. Parasites were added onto $4x10^5$ Vero cells cultured for 24h in a $25cm^2$ culture flask in DMEM supplemented with 10% FCS, 1% P/S. *T. gondii* were purified before infecting organoids, using PD-10 desalting column. Briefly, parasite cultures were scraped and passed through a blunt end needle to break open cells and release the parasite. The solution was added to a PD-10 column and rinsed with PBS.

3.2.4 Organoid infection with *Toxoplasma gondii* through passage

Organoids were removed from Matrigel by disruption with PBS. After centrifuging at 300xg for 5 minutes, purified *T. gondii* were added to organoids in a low volume of media. The organoids were pipetted to break them open and expose the luminal surface for infection, then incubated at 37°C for the times specified. For optimisation of infection protocols, differing parasite densities per infection sample were used, and a short centrifugation step of 2000rpm for 1 minute added before incubation and culture in Matrigel, as previously described.

3.2.5 Infected organoid fixing and staining

Infected organoid samples were fixed in 4% PFA for 30 minutes at room temperature. Samples were stained as described above (Chapter 2.6, page 100). Primary antibodies included rabbit anti-E-cadherin, rabbit anti-GRA7 and mouse

anti-SAG1 (TP3). Secondary antibodies were anti-rabbit TRITC, anti-mouse AF488. F-actin was stained using Phalloidin AF647, and Phalloidin-rhodamine. Confocal z-stack images were acquired using an 880 confocal microscope (Zeiss) with a 40x water immersion objective. All samples were analysed using Imaris software (Bitplane) as described above for quantification of infected parasites (Chapter 2.7, page 104).

All fixed images were acquired at the CCI using Zen Black software (Zeiss) on a Zeiss LSM880 multiphoton upright confocal microscope with Airyscan and laser lines Diode (405nm), Argon (488nm), DPSS-5610 (561nm) and HeNe633 (633nm)

3.2.6 Live imaging of infected organoids

Organoids from ROSA$^{mT/mG}$ mice were infected with *T. gondii* Pru-tdTomato-Cre and cocultured with BM-derived gut-like DCs in Matrigel (Chapter 2.10, page 110). Time-lapse images of z-stacks were acquired over a 1-hour period at 2-minute 40-second intervals using the LSM 880 MP confocal microscope with Airyscan (Zeiss) and the 2-photon Chameleon laser was set to 920 nm. Emission light was separated with 490 or 555 dichroics. Bandpass filters 525/25 and 590/20 M were used to minimise spectral overlap. Images were analysed using Imaris (Bitplane) software (chapter 2.10.3, page 111).

3.3 Results

3.3.1 Crypts from the small intestine of mice give rise to 3D organoid cultures of the small intestinal epithelium

Intestinal organoids have been previously developed through the isolation and culture of crypt structures from the small intestinal epithelium (Sato *et al.*, 2009). The generation of organoids was to be established in our laboratory, followed by validation of their suitability for infection models based on cell composition, polarisation and susceptibility to infection with *T. gondii*. The jejunum of C57Bl/6 mice were isolated and washed in EDTA to remove epithelial cells. The fraction with the greatest density of crypt structures was used. Crypts were evident by their finger-like projections with dark granules at the tip, representing Paneth cells (Figure 10, Day 0). Crypts were cultured in Matrigel with IntestiCult medium that contained the growth factors R-spondin, Noggin, and EGF, and over the course of 7 days can be seen expanding and proliferating to produce bud-like structures (Figure 10, white arrows) around a central enclosed lumen (Figure 10, black arrows). After 7 days in culture, organoids were passaged by passing through a needle to break up the organoids and resuspended in Matrigel with growth medium.

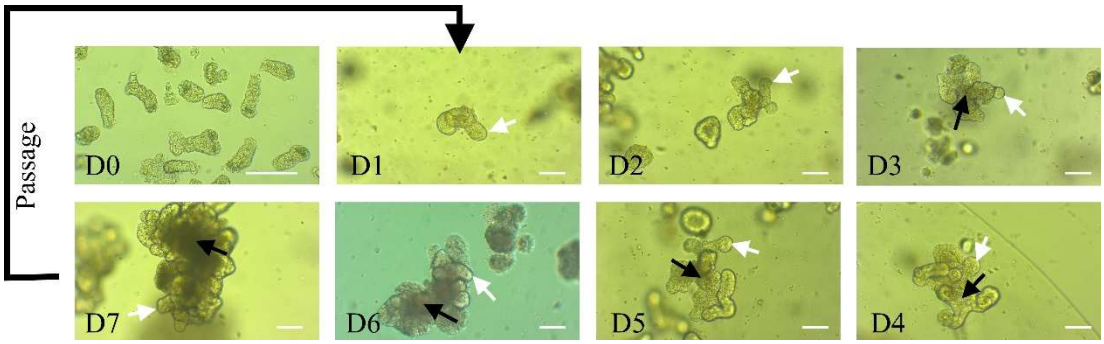

Figure 10. Crypts from the small intestine of mice give rise to 3D organoid cultures of the small intestinal epithelium
Crypts were isolated from the jejunum of C57Bl/6 mice and cultured in Matrigel with growth medium for 7 days before passage. Images show development of organoids over a 7-day culture period. Crypts are seen to round up (D1) and proliferate to produce bud-like structures (white arrows) around an enclosed central lumen (black arrows). On day 7, organoids are passaged to produce cultures with similar morphology to day 1 organoids. Scale bar: 200µm

3.3.2 Organoids contain differentiated cells of the small intestinal epithelium

In order to be a useful model of infection, organoids should be appropriately polarised, and possess an array of major epithelial cell types involved in host defence. To verify the development of suitable intestinal organoid cultures, organoids from C57Bl/6 mice were assessed for all the differentiated cell types of the small intestinal epithelium, and markers of polarisation. Organoids were stained with antibodies to Lysozyme (Paneth Cells), Chromogranin A (enteroendocrine cells) and Muc2 (Goblet cells). F-actin and DAPI staining were used to identify epithelial cell membranes and nuclei, respectively (Figure 11). Enteroendocrine cells, goblet cells and Paneth cells were all observed in organoid cultures (Figure 11). Goblet cells appeared along both bud-like structures of organoids and amongst cells surrounding the lumen. Enteroendocrine cells were observed within bud-like structures along with Paneth cells. The localisation of Paneth cells to bud-like

structures indicates that these are similar to the crypt structures present in the intestinal epithelium where Lgr5+ stem cells and Paneth cells reside.

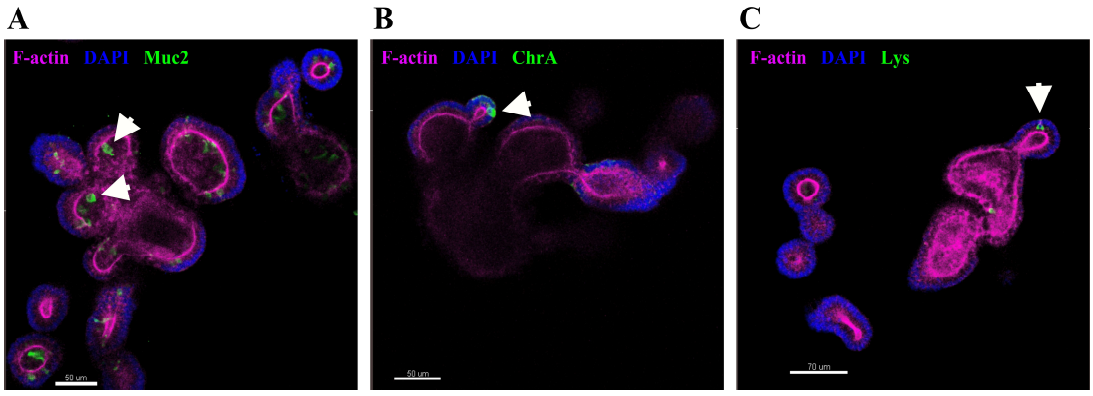

Figure 11. Small intestinal organoids contain differentiated cell types of the small intestinal epithelium. Organoids were cultured for 7 days, fixed with 4% PFA and stained with antibodies to markers of various differentiated cell types of the small intestinal epithelium. Confocal images of small intestinal organoids stained with Phalloidin-AF647 (F-actin, magenta), DAPI (nuclei, blue) and (**A**) anti-Mucin2 (Goblet cells, green) (**B**) anti-Chromogranin A (enteroendocrine cells, green) or (**C**) anti-Lysozyme (Paneth cells, green). Scale bar: 50µm

3.3.3 Organoids are composed of a polarised epithelium

The small intestinal epithelium is polarised containing different receptors at different densities between the apical and basal surfaces, therefore differing in function. To assess polarisation of the organoid epithelium, organoids were stained for E-Cadherin, F-actin, and villin. Villin is present on brush border of the small intestinal epithelium only on the apical side, facing the lumen. The brush border was observed by villin staining within organoids, although very weak, that indicate the apical surface of enterocytes (Figure 12A). E-cadherin is involved in the formation of adherens junctions that is prevalent along the basolateral surface of the small intestinal epithelium, while F-actin is concentrated at the apical surface. Staining of organoids with these markers clearly shows polarisation with E-cadherin

strongly associated with the basolateral surface and F-actin at the apical surface (Figure 12B).

These results show that organoids containing polarised, differentiated intestinal epithelial cells were successfully cultured in our laboratory and therefore provide a suitable model of the small intestinal epithelium for enteric infections.

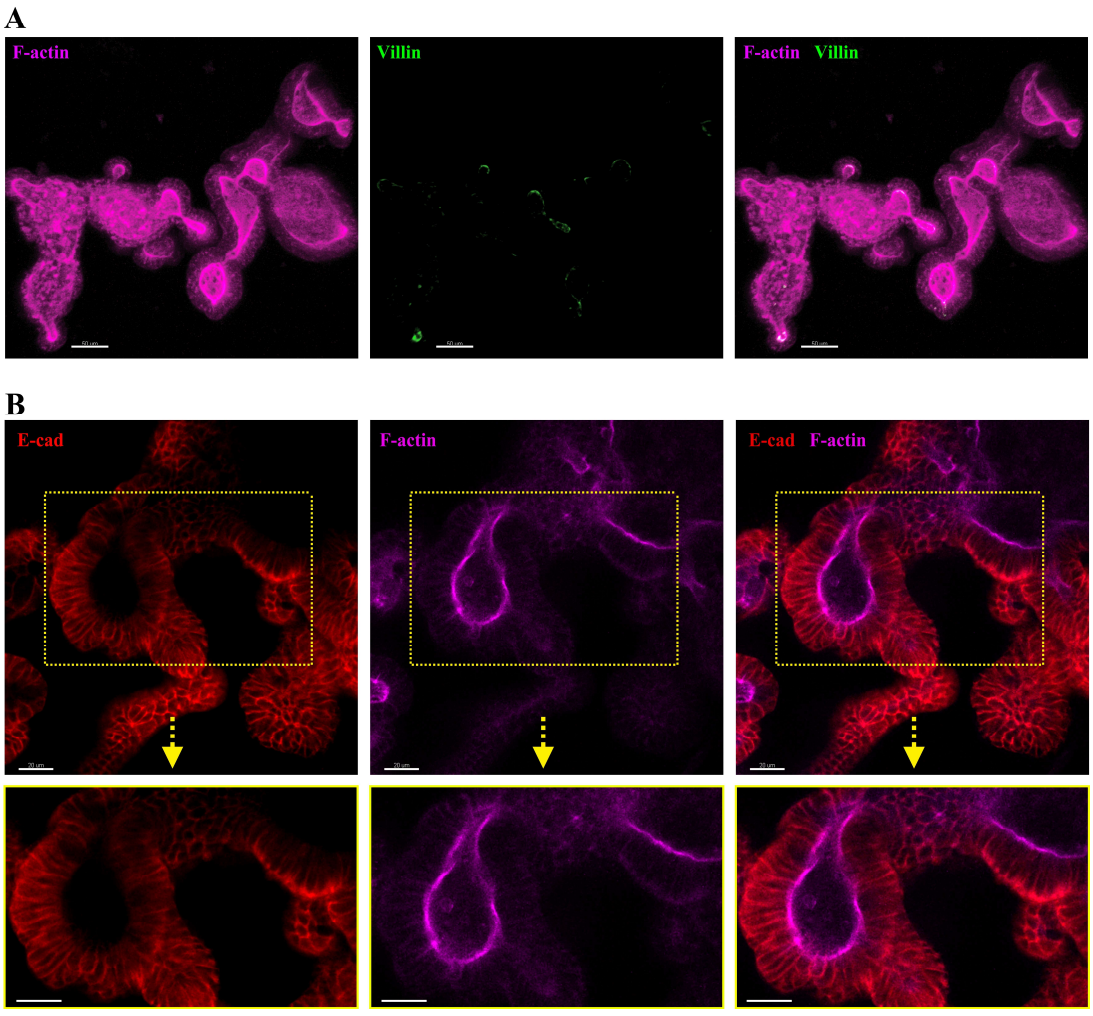

Figure 12. Organoids are composed of polarised cells.
Organoids were fixed in 4% PFA and labelled for Phalloidin-AF647 (F-actin, magenta) and antibodies to determine polarity of organoid cells. **A**, Organoids were stained with Phalloidin-AF647 (F-actin, magenta) and anti-villin (brush border, green). Scale bar 50µm. **B**, Organoids were stained with anti-E-Cadherin (red) and Phalloidin-AF647 (F-actin, magenta) to determine polarisation and images were acquired by confocal microscopy. Images show cross-section of a z-stack image. Scale bar: 20µm

3.3.4 Incubating organoids with *T. gondii* in suspension prior to culture in Matrigel improves the infection rate

In preliminary experiments that aimed to infect organoids with *T. gondii,* parasites were added to the Matrigel of organoid cultures, but no productive infection was observed. This may have been due to the parasite being unable to migrate through the Matrigel, or due to a preference for invasion at the inaccessible luminal surface of the organoid. Therefore, organoids were removed from Matrigel using PBS, disrupted by pipetting to expose the luminal surface, and incubated with *T. gondii* at 37°C for 1 hour before re-embedding in Matrigel. In preliminary experiments using the RH strain successful invasion was observed, but only for a very small proportion of the parasites added to the culture (data not shown). This would make it challenging to detect host responses to the parasite in organoid cultures. Therefore, optimisation of infection rates of organoids with *T. gondii* was carried out.

An infection assay was carried out to optimise a method to provide high infection rates of organoids with *T. gondii*. For these experiments we employed a GFP-expressing strain of *T. gondii* Pru since they do not express a long-distance migratory phenotype unlike Type I RH. Therefore, rather than migrate between epithelial cells, type II Pru are more likely to invade cells. Two densities of parasites were used, as well as an optional short centrifuge step before incubating at 37°C for either 30 minutes or 1 hour. Samples were then cultured for 4 hours to allow full invasion of parasites and organoid restoration before fixing, staining, and imaging by confocal microscopy (Figure 13). Images were analysed as cross-sections using

Imaris software whereby successful invasion of the organoid epithelium was considered to have taken place when a parasite was completely surrounded by F-actin staining of the host cell.

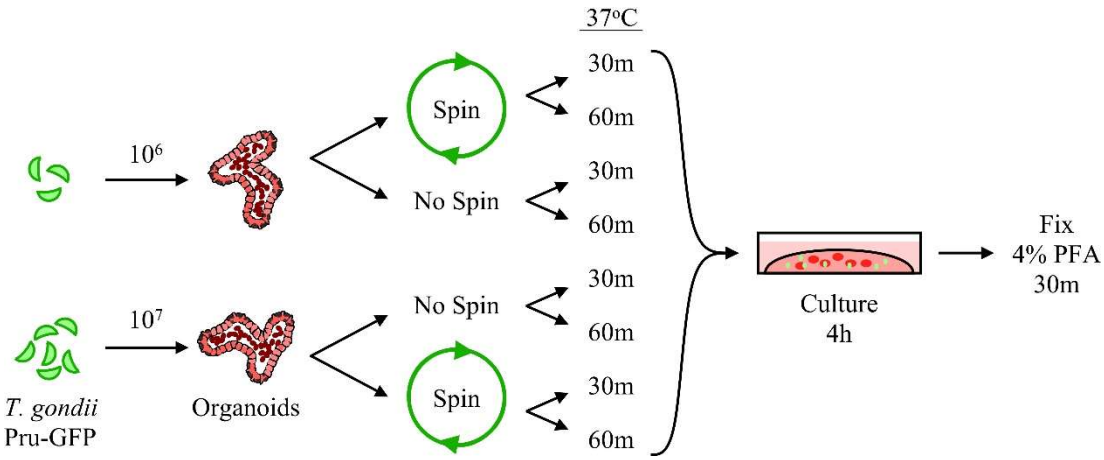

Figure 13. Schematic of the optimisation protocol for increasing the infection rate of *T. gondii* in organoids. Organoids were infected with either 10^6 or 10^7 *T. gondii* Pru-GFP, with or without a short spin at 2000rpm for 1 minute. Samples were incubated for either 30m or 1h before culture in Matrigel and growth medium for 4h. Samples were fixed with 4% PFA for 30m, stained and imaged by confocal microscopy.

Keeping the suspension volumes of organoids and *T. gondii* low for incubations during infection was important in improving infection rates, as this ensured close contact between the parasite and organoid. After some preliminary attempts at infection, parasite densities of 10^6 and 10^7 *T. gondii* were suspended in a total volume of 50µl with organoids ($2x10^7$/ml and $2x10^8$/ml, respectively). During these preliminary experiments, the longest incubation time was 2 hours. However, organoid viability was compromised after 2 hours in solution, therefore incubation time was reduced to a maximum of 1 hour. The organoid and *T. gondii* suspensions were pipetted vigorously to open the organoids to expose the luminal surface to infection. In general, 10^7 parasites incubated for 1 hour with organoids provided a

greater infection rate compared to 10^6 parasites that were consistently low over all conditions (Figure 14A). The short spin prior to incubations could have aided in increasing contact between parasite and organoid, however no difference was seen in infection rates between the two conditions (Figure 14). Increasing the incubation time from 30m to 1h increased the infection rate of organoids only in samples with 10^7 parasites, although this was not statistically significant (Figure 14A). The parasite density of 10^7 per sample at 1h incubation provided the optimum infection rate, with following experiments using this condition without a short spin since this provided less variability.

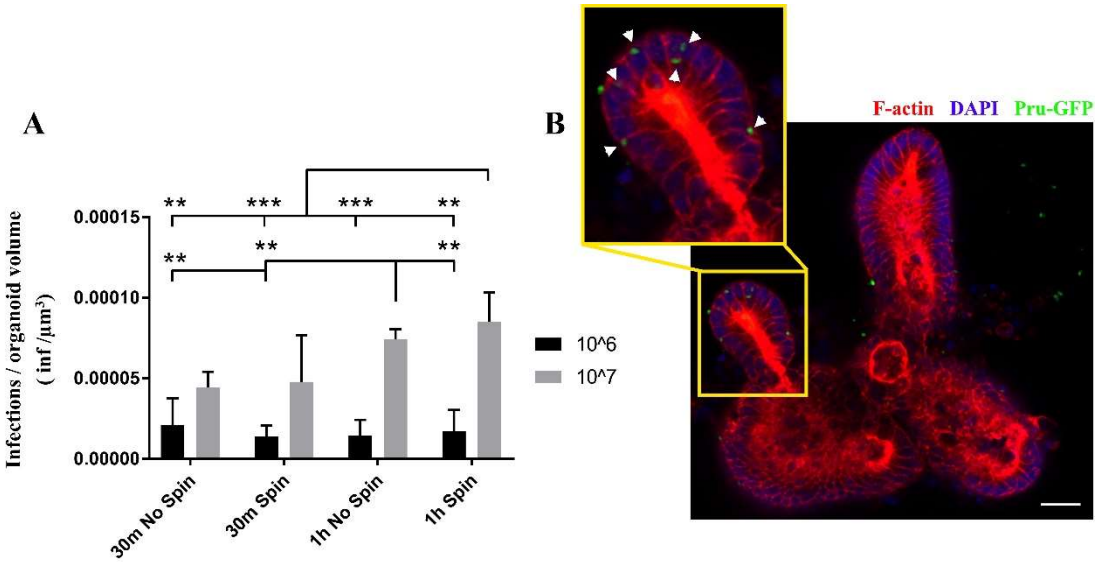

Figure 14. Organoids incubated with 10^7 *T. gondii* for one hour provides the best infection rate
Organoids were removed from Matrigel by disruption with PBS. *T. gondii* Pru-GFP were added to organoid samples at a density of 10^6 or 10^7 parasites per 50µl. Some samples were centrifuged for 1m at 2000rpm, and all samples were incubated for 30m or 1h at 37°C. After incubation, samples were cultured in Matrigel and growth medium for 4h before fixing and staining for confocal imaging. **A**, organoids were assessed for infections using Imaris software and quantified. Graph depicts the number of infection events per μm^3 of organoid as defined by the presence of a parasite enclosed within host cell f-actin staining. **B**, a cross-section of a z-stack image of an infected organoid with 10^7 parasites incubated for 1h. Enlarged section clearly shows parasites within organoid cells (white arrows). Scale bar 30µm. Graph represents pooled data from of 3 independent experiments, 2 samples per condition with triplicate measurements in each sample, showing mean +/- SEM. **P <0.005, ***P <0.0005. Two-way ANOVA with Tukey's mean comparisons test.

3.3.5 Disrupting organoids through pipetting successfully opens the luminal surface to infection

This method of infection utilises a vigorous pipetting action to break open the organoids and expose the luminal surface for infection. Live imaging of infected organoids verified the presence of live and motile *T. gondii* within organoid lumen (Figure 15). Although not limiting infection to the luminal surface, this method does allow for infection through this route.

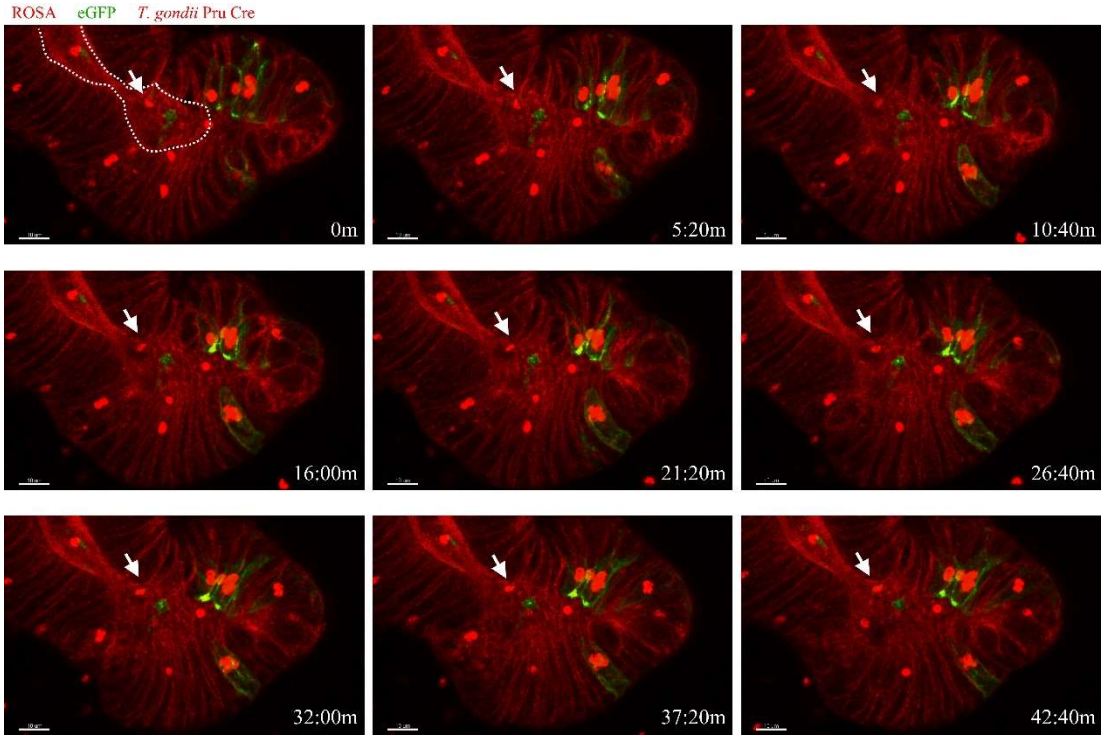

Figure 15. Infection protocol introduces live *T. gondii* to the luminal surface of organoids.
Organoids from ROSA $^{mT/mG}$ mice were infected with *T. gondii* Pru-tdTom-Cre for 24h and time-lapse imaging by 2-photon microscopy. Live and motile *T. gondii* were present within the organoid lumen (white arrows). Dotted line represents luminal surface. Scale bar 10µm

3.3.6 Use of *Toxoplasma* gondii-cre confirms productive infection of epithelial cells

After invasion of a cell *T. gondii* establishes a parasitophorous vacuole (PV) in which it resides and replicate. Formation of the PV is influenced by the secretion of

parasite proteins from micronemes and rhoptries upon invasion, some of which enter the host cell cytosol. Therefore, the detection of rhoptry proteins (for example, toxofilin) within organoid cells would verify successful infection by *T. gondii*. ROSA$^{mT/mG}$ mice constitutively express membrane tdTomato in all cells, but when exposed to Cre recombinase the tdTomato gene is cleaved and eGFP is expressed in its place (Figure 17A). Organoids derived from these mice were infected with a genetically modified *T. gondii* line*,* which expresses a toxofilin-cre fusion protein, that is released into host cells upon invasion. Infected cells of ROSA$^{mT/mG}$ organoids should therefore express eGFP. This would confirm productive infection, rather than paracellular migration or attachment to the organoid surface. Previous studies using this reporter strain of *T. gondii* revealed possible communication between infected cells and neighbouring cells, as well as sites of Cre exposure without *T. gondii* infection (Koshy *et al.*, 2012). Using this reporter strain of *T. gondii* with ROSA$^{mT/mG}$ organoids would add further support to these studies within a relevant model of the intestinal epithelium.

ROSA$^{mT/mG}$ organoids were infected with *T. gondii* Pru-tdTom-Cre as described in the optimised protocol and cultured for 24, 48, and 72 hours. Confocal microscopy was used to obtain z-stack images of infected samples and analysed using Imaris software. Since both parasite and epithelium fluorescence were in the same channel, in initial experiments parasites were labelled with an antibody, TP3, to validate that the bright tdTomato expression was derived from *T. gondii* (Figure 16). Culture of infections over 72h showed sites of *T. gondii* replication as determined by large clusters of parasites and as rosettes characteristic of *T. gondii* replication

(Figure 16). Replication of *T. gondii* in organoids represents the formation of a functioning PV which displays evidence that organoids provide a suitable environment for natural *T. gondii* behaviour. Many extracellular parasites stained for the surface antigen TP3 but did not fluoresce suggesting that extracellular parasites perished over this timecourse (Figure 16).

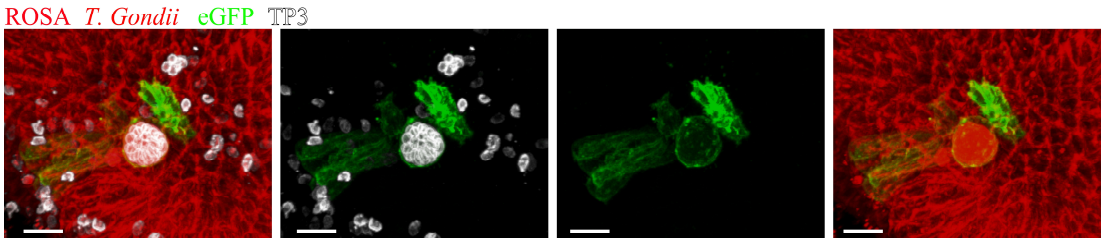

Figure 16. *T. gondii* replicate within organoid cells
ROSA$^{mT/mG}$ organoids were infected with *T. gondii* Pru-tdTom-Cre and incubated for 72h before fixing and staining for TP3. Z-stack images were acquired by confocal microscopy and analysed using Imaris. Sites of replication were observed as large clusters of parasites expressing TP3 and within eGFP^{+} cells. Scale bar: 10µm

Infected organoids showed eGFP^{+} cells (Figure 17C and D). Infections were quantified by identifying parasites using the "spots" function in Imaris, and manual deletion of *T. gondii* spots outside of the area covered by organoid fluorescence. Intracellular parasites were then manually assessed using cross-sections to confirm "spot" counts. Organoid volumes were calculated using the "surfaces" function, with eGFP^{+} cell expression counted manually, and eGFP volume quantified also using the "surfaces" function. With these values infection rates were determined as intracellular parasites per organoid volume (µm^3), eGFP^{+} cells per organoid volume (µm^3), and proportion of infected eGFP^{+} cells per total eGFP^{+} cells were calculated (Figure 17E). The infection rate of organoids increased over the 72h, however no increase was seen between 24h and 48h.

The proportion of eGFP$^+$ cell volume per organoid volume increased between 24 and 48 hours, suggesting some lag time for the effects of Cre recombinase to take effect since infected cells that did not express eGFP were observed at 24h. The proportion of infected eGFP$^+$ cells to total eGFP$^+$ cells dropped between 24 and 48h, signifying that eGFP expression increased in cells that were not infected. There are 2 possible reasons for an increase in uninfected eGFP$^+$ cells. Firstly, the division of infected eGFP-switched cells would result in both cells expressing eGFP with one daughter cell inheriting the PV. This is likely for clusters of uninfected eGFP$^+$ cells surrounding an infected eGFP$^+$ cell (Figure 18). Secondly, the secretion of Cre and other effectors into cells that the parasite did not subsequently invade would induce eGFP expression. This may explain the occurrence of eGFP$^+$ cells that are not closely associated with sites of infection (Figure 20). The migration of divided eGFP$^+$ cells from infections sites is an unlikely explanation of the occurrence of uninfected, isolated (U-I) eGFP$^+$ cells since lineage tracing experiments of the small intestinal epithelium *in vivo* show clonal expansion of epithelial cells up the crypt-villus axis (Snippert *et al.*, 2010). Also, these U-I eGFP$^+$ cells were observed in studies using a reporter line of fibroblasts which are immotile, indicating that the occurrence of these eGFP$^+$ cells is likely derived from aborted invasion of *T. gondii* that secrete effectors into the cells (Koshy *et al.*, 2012). This reporter model provides an interesting initial insight into the possible effects of *T. gondii* on intestinal epithelial cells that should be explored further.

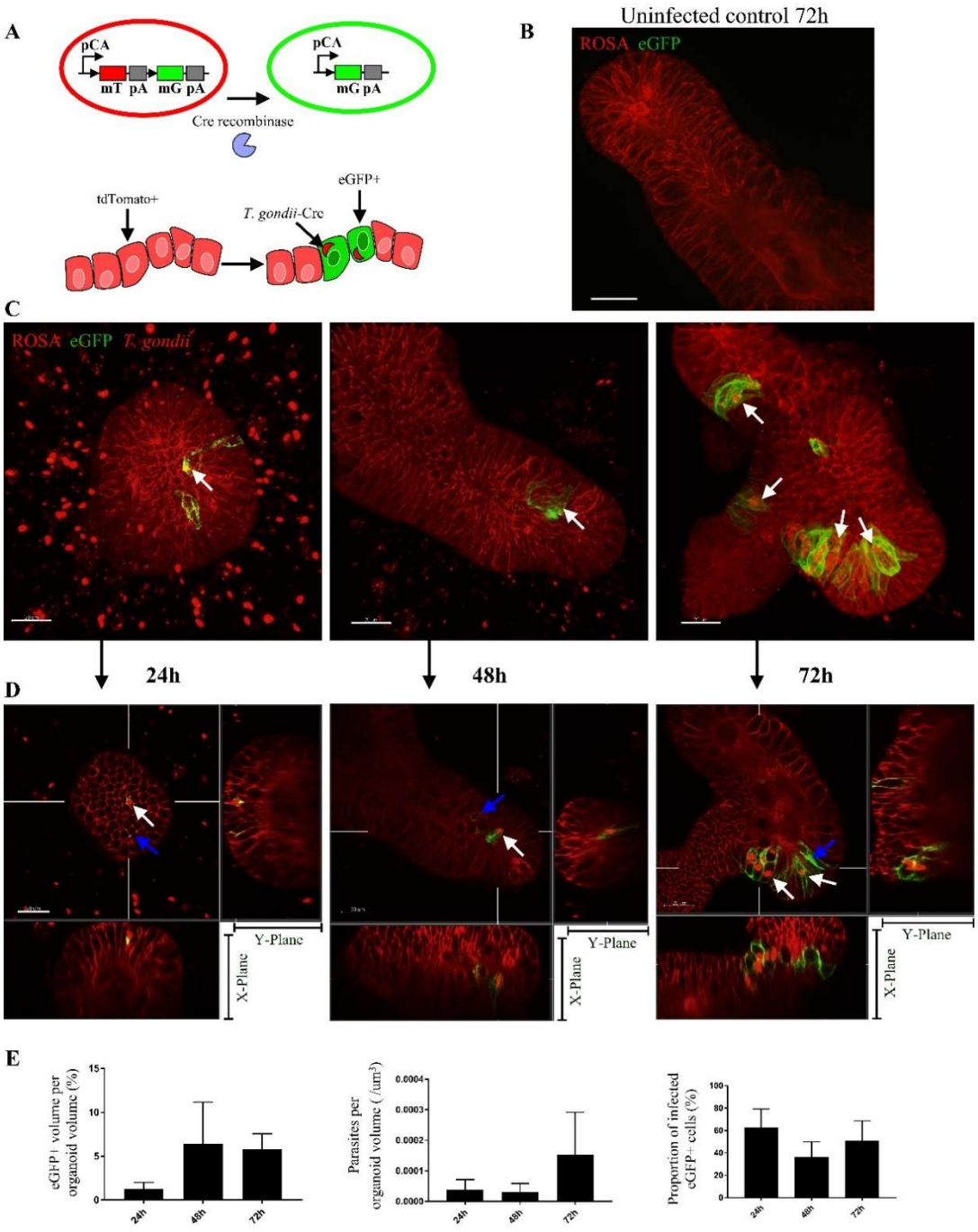

Figure 17. *T. gondii* successfully infects organoids.
ROSA$^{mT/mG}$ organoids were infected with *T. gondii* Pru-tdTom-Cre and incubated for 24, 48, and 72h before fixing and imaged using fluorescence confocal microscopy. **A**, cells from ROSA$^{mT/mG}$ mice express tdTomato fluorescence and upon exposure to Cre recombinase enzyme the tdTomato gene is cleaved allowing for the expression of eGFP. Schematic of organoids from ROSA$^{mT/mG}$ mice that fluoresce under tdTomato and upon infection with Cre-expressing *T. gondii*, infected cells should express eGFP. **B,** uninfected organoid show no eGFP expression after 72h. **C**, z-stack images taken using confocal microscopy shows organoids infected with *T. gondii* Pru-tdTom-Cre, with infected cells expressing eGFP. **D**, optical sections of infected organoids showing *T. gondii* within organoid cells (white arrow) and uninfected Cre-exposed eGFP$^+$ cells (blue arrow). **E**, bar charts showing volume of eGFP-expressing cells per organoid volume, intracellular parasites per organoid volume, and proportion of infected eGFP$^+$ cells per total eGFP$^+$ cells. Bar char represents pooled data from 2 independent experiments, 2 samples per condition with 3 replicate measurements from each sample. Mean +/- SEM. Single samples per time point, 3 images acquired from each sample. Scale bar: 20µm.

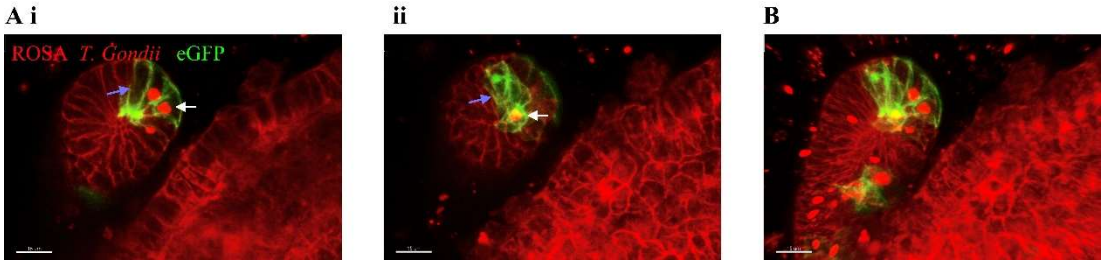

Figure 18. Uninfected organoids neighbouring infected eGFP⁺ cells also express eGFP.
ROSA$^{mT/mG}$ organoids were infected with *T. gondii* Pru-tdTom-Cre and incubated for 48h before fixing and imaged using fluorescence confocal microscopy. **Ai** and **ii,** show cross sections of infected cells (white arrows) surrounded by neighbouring uninfected eGFP⁺ cells (blue arrow). **B**, z-stack image of **A.** Scale bar 15µm

It was evident that not all infected cells expressed eGFP. This is more apparent at early timepoints after infection that may suggest a time lag for the effects of Cre on the cells' genes (Figure 17B). However, infected cells that do not express eGFP are also evident at the later timepoints even within cells containing replicating parasites (Figure 19).

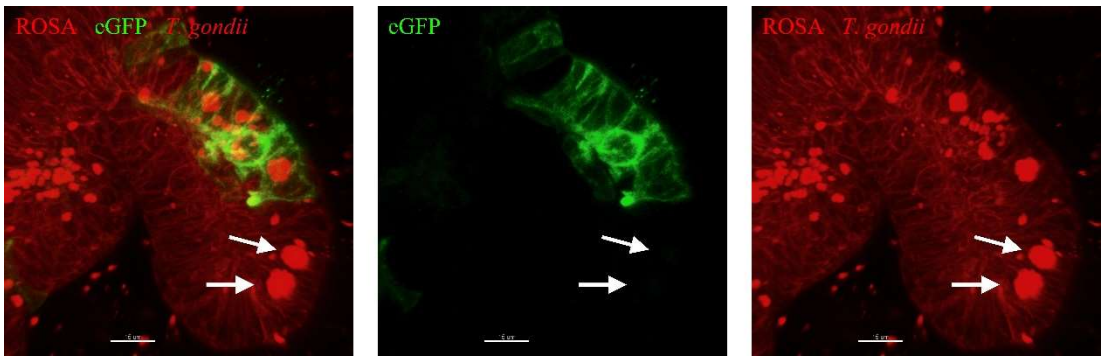

Figure 19. Some epithelial cells containing replicating *T. gondii* do not express eGFP
ROSA$^{mT/mG}$ organoids were infected with *T. gondii* Pru-tdTom-Cre and incubated for 48h before fixing and imaged using fluorescence confocal microscopy. Z-stack images were obtained, and images analysed using Imaris. Clusters of *T. gondii* represent parasite replication. Organoid cells containing clusters of *T. gondii* failed to express eGFP (white arrows). Scale bar: 15µm

3.3.7 Organoid cells express eGFP distant to sites of infection

It has been suggested that *T. gondii* performs aborted attempts of invasion whereby effector proteins are secreted into the cytosol of cells that the parasite does not

successfully invade (Koshy *et al.*, 2012). The organoid reporter model here also indicates that failed attempts of invasion occurs as evidenced in eGFP^{+} cells that are uninfected and do not neighbour infected cells, rather they are located a distance from any site of infection (Figure 20). This may suggest secretion of toxofilin-cre into the host cell cytosol during an aborted invasion attempt, causing the host cell to switch to eGFP expression.

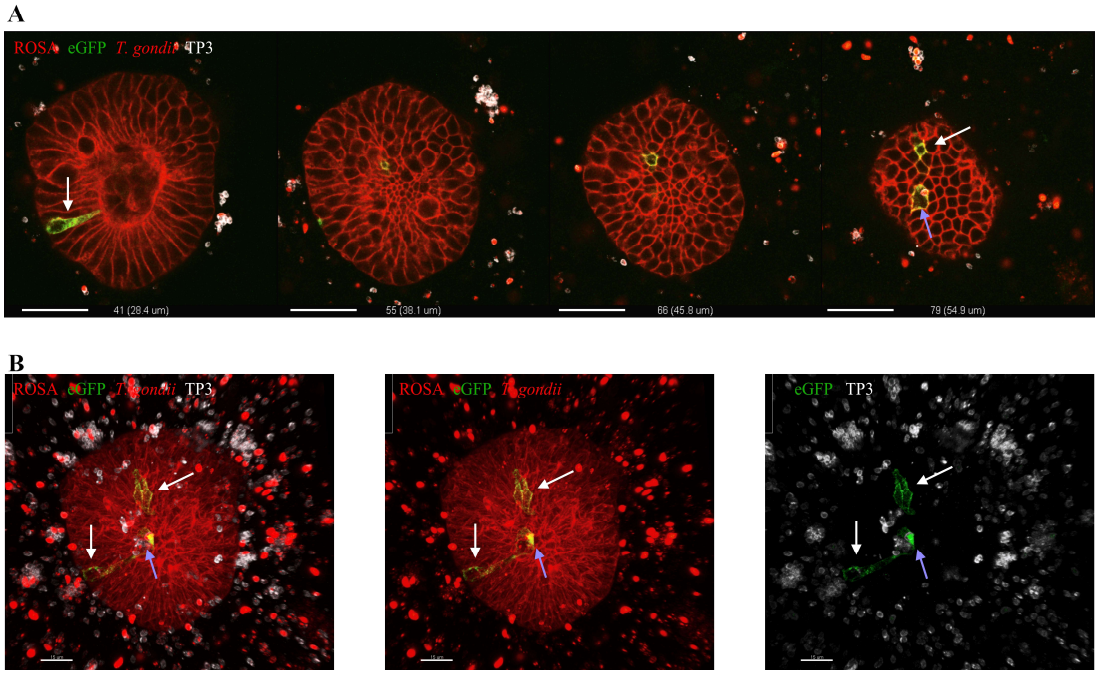

Figure 20. Uninfected organoid cells expressing eGFP were distantly located from sites of *T. gondii* infection. ROSA$^{mT/mG}$ organoids were infected with *T. gondii* Pru-tdTom-Cre and incubated for 24 before fixing and imaged using fluorescence confocal microscopy. **A,** shows cross sections of infected organoid with uninfected eGFP^{+} cells (white arrows) distantly located from sites of infection (blue arrow). Scale bar 30µm. **B**, z-stack image of infected organoid showing uninfected eGFP^{+} cells (white arrows) that were not closely associated with sites of infection (blue arrows). Scale bar 15µm

3.3.8 Infected epithelial cells are expelled into the lumen of organoids

ROSA$^{mT/mG}$ organoids infected with *T. gondii* Pru-tdTom-Cre for 24 hours were imaged using 2-photon microscopy over a period of 1h. Within a certain time-lapse image, an infected eGFP^{+} cell was observed being expelled into the lumen of the

organoid still containing the parasite (Figure 21, Movie S1). This could represent a possible reason why viable tachyzoites are seen within the lumen of orally infected mice up to 6 days post infection, which ultimately leads to the spread of *T. gondii* in the small intestine and increased infection rates over time (Coombes *et al.*, 2013; Gregg *et al.*, 2013). This may also represent normal epithelial shedding, or a specific host defence mechanism against infection, however this has not been documented or visualised in *T. gondii* infections.

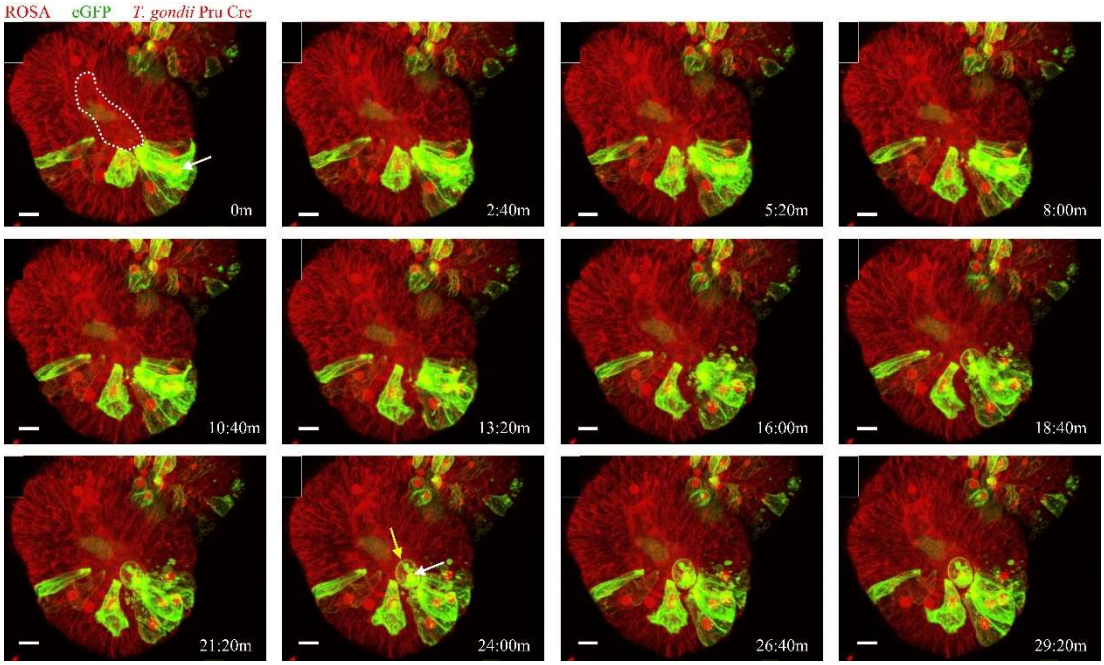

Figure 21. Organoid cells infected with *T. gondii* are expelled into the lumen
Organoids from ROSA $^{mT/mG}$ mice were infected with *T. gondii* Pru-tdTom-Cre for 24h and time-lapse imaging by 2-photon microscopy. Infected cells that are also eGFP^{+} (white arrow) were observed being expelled into the lumen of organoids (dotted line). Corresponding live image in Movie S1. Scale bar: 10µm

An eGFP^{+} cell was also expelled into the lumen of an organoid shortly after the parasite was observed exiting the cell (Figure 22, Movie S2). The egressed parasite remained within the epithelium with the expelled eGFP^{+} cell observed within the lumen. This process may contribute to the spread of *T. gondii* within the small intestinal epithelium.

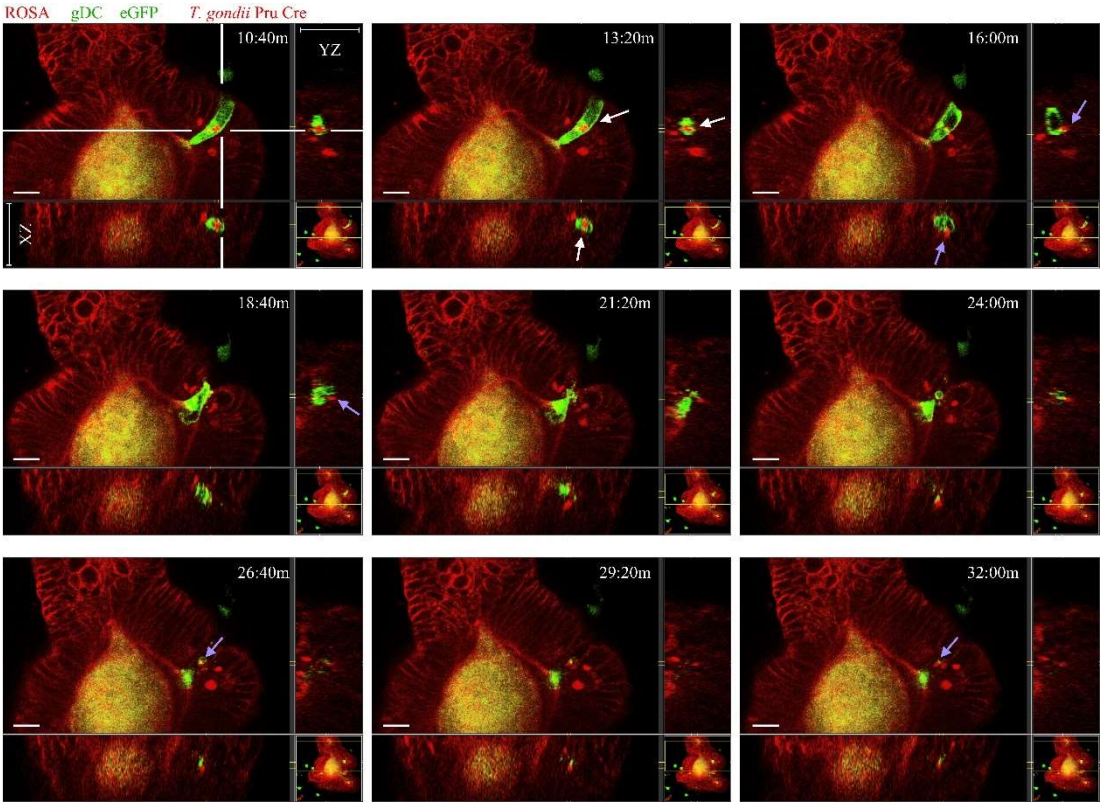

Figure 22. Organoid cells infected with *T. gondii* are expelled into the lumen, with the parasite remaining within the epithelium
Organoids from ROSA $^{mT/mG}$ mice were infected with *T. gondii* Pru-tdTom-Cre for 24h before adding gut-like DCs and time-lapse imaging by 2-photon microscopy. Images represent cross-sections of an infected sample with corresponding XZ and YZ planes as indicated. An infected cell expressing eGFP is marked with white arrows. Over time, the parasite leaves the eGFP^{+} cell (blue arrows) that is subsequently expelled into the lumen. The parasite remains within the organoid epithelium as seen at 24m (blue arrow). Scale bar 15µm. Whole image viewed in Movie S2

3.3.9 *T. gondii* travel along the paracellular route in organoid infections

The route of transepithelial migration of *T. gondii* has been proposed to involve both paracellular and intracellular routes (Barragan and Sibley, 2002; Barragan, Brossier and Sibley, 2005; Weight and Carding, 2012). It is uncertain which is primarily involved in parasite dissemination, and with the new ability to infect organoids with *T. gondii* this model may resolve these uncertainties. *T. gondii* Pru-tdTom-Cre were used to infect ROSA$^{mT/mG}$ organoids and live images acquired after 24h of infection. Extracellular *T. gondii* were seen on the surface of organoids with

low motility, whereas other parasites were observed within the epithelial layer between cells (Figure 23). ROSA$^{mT/mG}$ organoids express tdTomato at their cell membrane, therefore *T. gondii* located at these fluorescent lines are likely between cells. The parasite can be observed migrating along lines of epithelial fluorescence, moving towards the lumen. This is the first indication of *T. gondii* migration in intestinal organoids, however this was seen from the basolateral surface which is not physiologically relevant. Ideally, techniques would be developed to restrict infections to the luminal surface with live imaging providing very useful information on early interactions between *T. gondii* and the small intestinal epithelium.

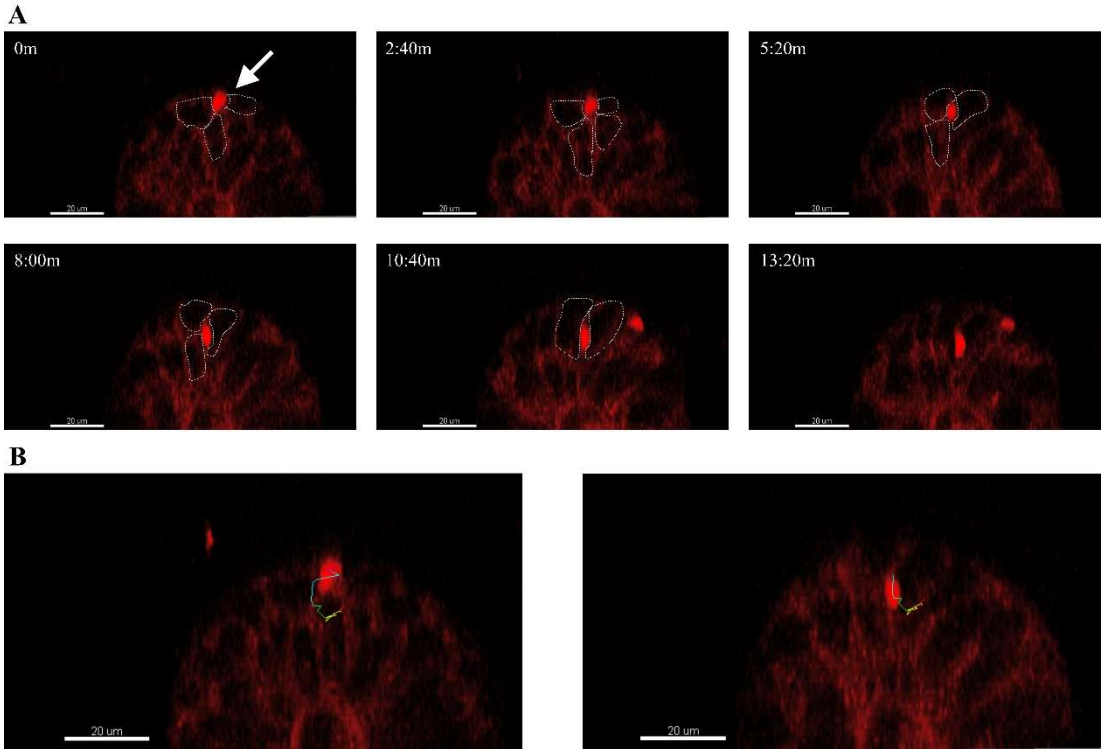

Figure 23. *T. gondii* migrate along epithelial surfaces between organoid cells
ROSA$^{mT/mG}$ organoids infected with *T. gondii* Pru-tdTom-Cre were cultured for 24h. 2-photon microscopy provided z-stack images over a time-period of 1h. **A**, T. gondii was observed migrating along lines of epithelial cell surface fluorescence with dotted lines representing individual cells. **B**, Images show the tracks of the parasite moving towards the lumen. Scale bar 20µm

3.4 Discussion

Until now, infection models of the small intestinal epithelium for *T. gondii* have mostly relied on monolayer cultures or animal models. These models are unsuitable for analysing early infection events due to the lack of cellular diversity of monolayer cultures and difficulties in locating rare foci of infections within animal models. Organoids recapitulate the cellular diversity of the small intestinal epithelium in a similar architecture therefore represent a suitable model. In this study, organoids have been successfully infected with *T. gondii*, revealing characteristic features of parasite biology, such as paracellular migration and the ability to alter the biology of host cells that they do not productively invade. This model will be a useful tool for studying host-pathogen interactions during early stages of *T. gondii* infections that would closely resemble *in vivo* infections.

Small intestinal organoids have been developed from isolated intestinal epithelial stem cells cultured in a basement membrane ECM and a cocktail of growth factors. These provide a polarised epithelium consisting of multiple differentiated cell types in a 3D conformation resembling the architecture of its *in vivo* counterpart (Sato and Clevers, 2013b). Organoids are a more suitable model for infections than monolayer cultures and animal models but have only been used as such in a limited number of studies. These have mostly focused on bacteria such as *Salmonella* and viruses such as rotavirus but have not been fully developed for *T. gondii*. One study has confirmed infection of organoids with *T. gondii* but did not expand any further (Klotz, Aebischer and Seeber, 2012). Little is known about host-pathogen

interactions during early stages of infection between *T. gondii* and the small intestinal epithelium, with current knowledge acquired using intestinal cell line cultures (Ju, Chockalingam and Leifer, 2009; Morampudi, Braun and D'Souza, 2011). Therefore, developing organoids as a model for early infections of the small intestinal epithelium may elucidate further host-pathogen interactions that may be exploited to generate novel vaccines against *T. gondii* infections. In this study, organoids were successfully infected with *T. gondii* through passage and incubation before culture in Matrigel. Successful invasion was verified by the observation of parasite replication within organoid cells and Cre-switched cells in the $Rosa^{mT/mG}$ model. Therefore, organoids can be used to model infections of the intestinal epithelium with *T. gondii*.

Genetically engineered mice that express fluorescent proteins have been an important development for the advancement of imaging *in vivo* processes. Conditional gene targeting using the recombinase system that target specific sites such as the *Cre/loxP* system is a powerful tool for studying gene function through the inversion, deletion, and translocation of genes. $ROSA^{mT/mG}$ mice are dual fluorescent reporters that constitutively express tdTomato at cell surfaces that, upon Cre recombinase exposure, is cleaved from the cell's transgene to allow expression of eGFP (Muzumdar *et al.*, 2007). Organoids were generated from the $ROSA^{mT/mG}$ reporter mouse for use with a Cre-secreting strain of *T. gondii* Pru. This strain of parasite secretes Cre recombinase under the toxofilin promoter, a rhoptry protein expressed into the host cell cytosol during cell invasion (Koshy *et al.*, 2010). $ROSA^{mT/mG}$ organoids were infected with *T. gondii* Pru-tdTom-Cre as per optimised

infection protocol and infected organoid cells expressed eGFP which confirms that *T. gondii* actively invaded cells. Interestingly, some neighbouring uninfected cells also expressed eGFP. The presence of uninfected $eGFP^+$ cells may derive from the division of $eGFP^+$ cells or the release of effector proteins from an infected cell that acts locally on neighbouring cells. Since Cre-recombinase causes a permanent switch to eGFP, daughter cells will also express eGFP, with one daughter cell inheriting the PV. This cell division of infected $eGFP^+$ cells was suggested in a similar model using fibroblast reporter cell line whereby an infected $eGFP^+$ cell was observed to be dividing (Koshy *et al.*, 2012). This could explain the presence of $eGFP^+$ cells that surround infected cells. However, *T. gondii* can inhibit the proliferation of infected cells (Wang and Gao, 2016), therefore uninfected $eGFP^+$ cells that surround an infected $eGFP^+$ cell may result from the transfer of parasite secreted factors from an infected cell. The transfer of *T. gondii* effector proteins to neighbouring cells have been proven in studies whereby cells also modulate the cell cycle of surrounding uninfected neighbouring cells, leaving them more susceptible to invasion (Lavine and Arrizabalaga, 2009). However, according to a study using the Cre secreting strain of *T. gondii*, this transfer of effector proteins is not expected to turn on eGFP expression (Koshy *et al.*, 2012). Therefore, the presence of uninfected $eGFP^+$ cells next to infected $eGFP^+$ cells likely result from the division of infected cells producing daughter cells with eGFP expression. Throughout the time-lapse imaging in this study, no proliferation of $eGFP^+$ cells were observed, although the period of imaging was relatively short. However, this organoid infection model may elucidate these confounding ideas by using multiphoton imaging over a prolonged

period, allowing for live imaging of the induction of eGFP expression in neighbouring cells, independently of cell division.

Studies using the Cre-expressing strain of *T. gondii* have revealed the injection of parasite factors into uninfected cells since eGFP expression was observed in uninfected cells that did not neighbour any sites of infection (Koshy *et al.*, 2012). It was hypothesised that these uninfected isolated (U-I) eGFP cells were invasion attempts by *T. gondii*, whereby rhoptry proteins were injected before the parasite moved on to another cell for invasion. Within our study, U-I eGFP$^+$ cells that did not neighbour infected cells in organoids were also observed. The U-I eGFP$^+$ cells may indicate a probing mechanism by *T. gondii* to evaluate suitability of host cell for invasion, suggesting possible cell selection. A rhoptry protein, ROP16, secreted by *T. gondii* activates STAT3 and STAT6 and decreases IL-12 production in immune cells, which is required for optimal protection against *T. gondii* infection (Saeij *et al.*, 2007). Therefore, the injection of multiple cells with effector proteins known to affect host cell behaviour may aid in decreasing the host defence against infection. Another suggestion for the appearance of U-I eGFP$^+$ cells could be the autophagy of *T. gondii* in infected cells. However, initiation of autophagy relies on key inducers such as IFN-γ, thought to be indispensable in the resistance to *T. gondii* infections (Burger *et al.*, 2018). Also, autophagy was not observed during the live images of infected organoids, however the imaging period were relatively short and would need to be extended to verify the source of uninfected eGFP$^+$ cells. Deciphering whether *T. gondii* have a preference for the type of cell they infect, organoids can

be used to determine this by staining infected organoids for differentiated cell types.

With the reporter model for *T. gondii* infections in organoids, infections were quantified over a 72-hour period determined by parasite number per organoid volume. Infections maintained similar levels between 24 and 48 hours. *T. gondii* exhibit an exponential growth rate in culture which suggests a reason for a higher infection rate at 72 hours (Kaufman and Maloney, 1962). Egress of parasites into the lumen was evident in studies in animal models as single tachyzoites after 3 and 6 days infection (Gregg *et al.*, 2013). Egress and reinfection may be a cause for the increased number of infected cells at 72 hours in infected organoids. Live imaging of organoids infected with *T. gondii* after 24 hours have demonstrated the expulsion of an infected $eGFP^+$ cell into the lumen of the organoid which could allow for reinfection, presenting a possible mode for the intraluminal spread of the parasite. This may also present a host defence mechanism against infection since the parasites did not egress rather the cell was expelled. *T. gondii* can suppress many apoptotic signalling pathways in the cells they infect (Graumann *et al.*, 2015), however not all infected cells are prevented from activating programmed cell death and the intestinal epithelium is known to increase cell shedding during certain infections. During *Trichuris muris* infections in mice epithelial proliferation and cell expulsion increases within the large intestine, indicating a potential mechanism of protection against infection (Cliffe *et al.*, 2005). However, the small intestinal epithelium has a naturally very high turnover rate, with many cells being shed into the lumen at any one time. Uninfected organoids were also seen to expel cells

during the period of imaging, therefore the expulsion of infected eGFP$^+$ cells may be a normal cell shedding event. To verify whether the expulsion of infected cells is a result of infection or normal cell turnover, longer time-lapse images are required to quantify the expelled cells. On a different occasion, an infected eGFP$^+$ cell was expelled into the lumen shortly after the parasite exited the cell and remained within the epithelium. Although parasite numbers did not increase between 24 and 48 hours, the proportion of eGFP$^+$ cells to the total number of infected cells decreased. Therefore, the egress of *T. gondii* from infected eGFP$^+$ cells to within the epithelium may be an explanation for the decreased proportion of eGFP$^+$ cells to total infected cells.

The route of transepithelial migration of *T. gondii* across the small intestinal epithelium occurs via the paracellular or intracellular route and it is uncertain which is responsible for the dissemination of the parasite and the relative importance of motility characteristics between different strains (Barragan and Sibley, 2002; Weight and Carding, 2012; Gregg *et al.*, 2013). Although multiphoton imaging is a powerful tool this has not been fully exploited for *T. gondii* infections. *T. gondii* have been imaged residing at tight junctions between epithelial cells of a monolayer culture using confocal microscopy of fixed samples (Barragan, Brossier and Sibley, 2005; Weight *et al.*, 2015). Live imaging of *T. gondii* migration has been reported in a cell line culture whereby the parasite travels the paracellular route (Weight *et al.*, 2015). Therefore, organoids derived from ROSA$^{mT/mG}$ mice provide a valuable tool for determining the primary route of epithelial barrier invasion by *T. gondii*. Infected organoids cultured for 24 hours and imaged using 2-photon microscopy already had

established infections, therefore the observation of new infection events or transepithelial migration would have been rare. However, on occasion parasites were observed on the basolateral surface of an organoid that proceeded to migrate toward the lumen between cells. Cells derived from this reporter mouse model express tdTomato at their cell surface, therefore parasite migration along these fluorescent lines indicate paracellular migration. Running this infection model and imaging using a multiphoton microscope at earlier infection timepoints will increase the observation of infection events and transmigration and should be a consideration for future experiments.

The aim of this chapter was to develop organoids as an infection model for *T. gondii*. Organoids can be infected with the parasite with expression of PV proteins and replication indicating natural infective behaviour. Organoids from the ROSA$^{mT/mG}$ mouse model and Cre-secreting strain of *T. gondii* provides a valuable model in visualising *T. gondii* influences on host cells and dynamics of host cell responses through cellular shedding and communication with uninfected neighbouring cells. Imaging this infection model at earlier time points may provide further details on the route of infection and transepithelial migration of *T. gondii*. However, although organoids were disrupted to expose the luminal surface for infection this method does not limit infection to the luminal surface, the physiological route of infection. Restricting infections to the apical surface may render different responses and would more accurately represent *T. gondii* infections in the small intestinal epithelium. Nonetheless, this infection model provides a high throughput method of infection that can be utilised for useful

functional analyses and live imaging for early infection events of *T. gondii* to determine factors involved in infection and host cell defence that can be exploited to develop novel drugs and vaccines against infection.

Chapter 4: Optimising protocols for microinjection of T. gondii into the lumen of intestinal organoids

4.1 Introduction

The methods established in chapter 3 for infecting organoids with *T. gondii* involve disruption of organoid integrity by vigorous pipetting to expose the luminal surface to infection. This does not restrict infection to the luminal surface but does offer a high throughput method of infection for functional analyses. The small intestinal epithelium is polarised containing different TLRs at different densities between the apical and basal surfaces. Therefore, infection from one surface may incur differing responses than those from the other. A recent technique to develop a semi-monolayer culture of organoid cells onto collagen sheets have been established that exposes the luminal surface for infection (Luu L., 2017 PhD thesis, University of Liverpool) (Thorne *et al.*, 2018). Microinjection techniques have already been established to inject bacteria and viruses into the lumen of organoids. Only during the writing of this PhD dissertation have methods been introduced to inject parasites into the organoid lumen (Heo *et al.*, 2018). In our study, a microinjection technique was optimised to inject *T. gondii* into the lumen of murine organoids for use as a relevant infection model.

4.1.1 Organoid models of infection through the luminal surface

The use of intestinal organoids as infection models have also relied on microinjections to insert pathogens into the otherwise enclosed lumen. These have

used bacteria and viruses and only very recently have parasites been injected (Wilson *et al.*, 2014; Forbester *et al.*, 2015; Leslie *et al.*, 2015; Karve *et al.*, 2017; Heo *et al.*, 2018). These studies have elucidated functional roles in host-pathogen interactions such as host cell defence against pathogens through the production of α-defensins by Paneth cells to prohibit bacterial growth (Wilson *et al.*, 2014), disruption of the epithelial barrier (Leslie *et al.*, 2015), and production of cytokines and chemokines for the recruitment of immune cells (Karve *et al.*, 2017). However, organoids used for microinjections mostly derive from human primary cells or those developed from induced pluripotent stem cell lines. Therefore, microinjections have been well established in organoids derived from humans that have a much larger and more circular morphology to murine organoids, providing greater ease in microinjection techniques due to their relatively large lumen. Although a recent publication described microinjections of *C. parvum*, an apicomplexan parasite of similar size to *T. gondii*, into human organoids, parasites have not been microinjected into murine organoids. In fact, murine organoids have been rarely used in this type of infection technique. The morphology of organoids from other species such as mouse, porcine, and bovine would provide greater challenges in microinjections due to their relatively smaller size, non-spherical shape, and small lumen, but would be useful given all the genetic tools available in the murine system.

Infections of organoids through the luminal surface with *T. gondii* would provide a model that is relevant in small intestinal epithelial cell diversification with infection through the physiological route. Microinjections of organoids with bacteria and

viruses have resembled natural infection within the host, therefore microinjections of *T. gondii* may be more representative of that *in vivo* than current monolayer systems. Due to the relatively small sizes of bacteria and viruses to parasites, the microneedles involved required a small bore size. Since *T. gondii* are relatively large, approximately 3-6µm, the bore size would need to be substantially larger for microinjections. As of conducting these experiments, no studies had been published on injecting parasites into organoids therefore optimisations needed to be carried out to perform this technique using *T. gondii*.

The aims of this chapter included the optimisation of the production of microneedles for effective injection of *T. gondii* into the lumen of organoids and to improve injection techniques to increase efficiency and proficiency in reliably injecting numerous organoids in a sample. Following optimisation of these parameters, imaging of organoids microinjected with *T. gondii* were to be carried out to prove that infection occurs through this surface and to visualise infection and transepithelial migration of the parasite.

Aim: Generate a method for microinjecting *T. gondii* into the luminal space of organoids

Objectives:

a) Produce microneedles of appropriate size for microinjecting *T. gondii*
b) Validate microinjected *T. gondii* invade organoid cells

c) Use live imaging approaches to confirm viability of injected parasites, and mechanism of invasion of the small intestinal epithelium

4.2 Methods

4.2.1 Small intestinal organoid culture

Small intestinal organoids were developed as previously described from C57B1/6 mice and ROSA$^{mT/mG}$ mice (Chapter 2.2, page 96). Crypts were cultured in Matrigel diluted to 70% with IntestiCult OGM mouse basal medium. These were plated onto 24 well plates at 500 crypts/50µl. The Matrigel was allowed to set for 20-30 minutes at 37°C before the addition of IntestiCult with 1% P/S and incubated at 37°C, 5% CO_2.

Every 7 days the organoids were passaged by resuspending in PBS, passing through a 27G needle and centrifuging at 200g for 5 minutes. Matrigel with IntestiCult was added and plated as above. For microinjections, organoids were passaged on day 5 without a needle onto a 3cm glass bottom culture dish or a low-wall, 3cm, gridded culture dish (80156, ibidi) and incubated for 1 or 2 days before microinjections.

4.2.2 *Toxoplasma gondii* culture and purification

T. gondii were maintained and purified as previously described (chapter 2.4, page 98). The Pru-GFP and Pru-tdTom-Cre strains of *T. gondii* were used for organoid microinjections. They were maintained by serial passage in monolayers of Vero cells in Dulbecco's Modified Eagle's Medium (DMEM) supplemented with 10% FBS and

1% P/S at 37°C, 5% CO_2. Parasites were purified by passing through a blunt end needle and syringe followed by filtration through a PD10 desalting column and centrifuged at 2000rpm for 10 minutes.

4.2.3 Optimised microneedle production

The optimisation of microneedle production is described above (Chapter 2.8.1, page 105) and in more detail in the results section (Chapter 4.3, page 158). Thin-wall glass capillaries (TW100-4; World Precision Instruments) were pulled using a micropipette puller (PC-10; Narishige) at 50°C with 355g of weight. Microneedle tips were broken in glass-bottom culture dishes to provide a bore size of 10µm.

4.2.4 Microinjection of organoids with *T. gondii*

Organoids were microinjected as described above (chapter 2.8, page 105). Organoids were removed from Matrigel using PBS and centrifuged at 200xg for 10 minutes. Organoids were resuspended in 70% Matrigel (diluted with IntestiCult mouse basal medium) on ice. These were plated as 40µl flat aliquots onto a 3cm glass bottom dish or plastic, gridded culture dish and incubated at 37°C for 20 minutes. IntestiCult mouse basal medium was added and the culture incubated at 37°, 5% CO_2. Microneedles were loaded with either 2µm (L4530; Sigma Aldrich) or 6µm (17156-2; Polysciences Europe) fluorescent microspheres, or with purified *T.gondii* Pru-GFP or *T. gondii* Pru-tdTom-Cre at 3-4x10^9/ml . The microneedles were loaded onto a microinjector system with an Eppendorf FemtoJet Microinjector used for injections into organoids. Microneedles were lowered onto organoids and

moved laterally to pierce the organoid. Injection pressures for *T. gondii* started at 100hPa for 0.1s and pressure increased until organoid was successfully injected. Injections were analysed using an Epifluorescent microscope (Zeiss) and images acquired using ImageJ.

4.2.6 Live imaging of infected organoids

Organoids from ROSA$^{mT/mG}$ mice were microinjected with *T. gondii* Pru-tdTom-Cre under an epifluorescence microscope (chapter 2.8.3, page 106) and transported to a 2-photon microscope (Zeiss) for time-lapse imaging and analysed using Imaris (Bitplane) software. The 'spots' function was used to track the GFP fluorescence of *T. gondii* over the time-lapse period. This provided measurements of track length, displacement and track speed.

4.2.5 Fixing and confocal imaging of microinjected organoids

Microinjections of ROSA$^{mT/mG}$ organoids with *T. gondii* Pru-tdTom-Cre were carried out on 9mm coverslips and subsequently cultured in a 48 well plate for 48h. Medium was removed from organoid samples and gently washed with PBS. Samples were fixed for 30 mins in 4% paraformaldehyde (PFA) at room temperature before gently washing again with PBS.

A 7mm diameter 1mm thick O-ring glued to a glass slide with Hydromount (Scientific Laboratory Supplies) pipetted into the O-ring was prepared. The organoid sample was inverted onto the Hydromount and allowed to dry at room temperature. Samples were stored at 4°C before imaging.

All fixed and live images were acquired at the CCI using Zen Black software (Zeiss) on a Zeiss LSM880 multiphoton upright confocal microscope with the laser lines Diode (405nm), Argon (488nm), DPSS-5610 (561nm) and HeNe633 (633nm).

4.3 Results

4.3.1 Microneedles must consist of a bore size of approximately 10µm for successful injections of 6µm microspheres

The main aim of this chapter was to develop a method of injecting *T. gondii* into the lumen of organoids. However, the relatively large size of the parasite required optimisations in many aspects of this technique, including the production of microneedles of sufficient bore size to allow the parasite to pass through undamaged. We initially produced microneedles using a pipette puller at 60°C filament temperature and 225g of weight. These produced needles of inconsistent size that needed to be broken on the bottom of a culture dish to increase bore size. If bore size was less than approximately 8µm, blockages were frequent (Figure 24A). However, increasing bore sizes to greater than 10µm increased the difficulties in controlling compensation pressure within the needles. Compensation pressure is used to prevent outflow and backflow of microneedle contents and media when not injecting. Larger bore sizes also provided difficulties in piercing the organoid cell layer to enter the lumen (Figure 24B). Here, the needle pushes the organoid rather than pierces. On other occasions the large bore size can also cause more damage to the organoid whereby the organoid does not seal itself after injection.

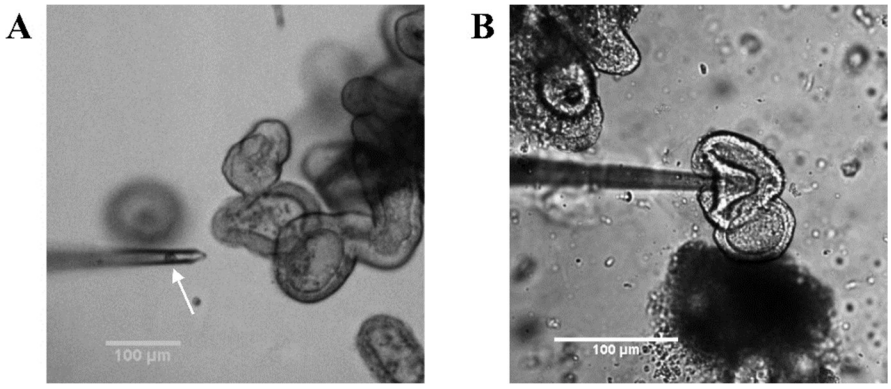

Figure 24. Microneedles must have a bore size relevant to prevent blockages and to pierce the epithelial layer of organoids
Glass capillaries were pulled using PC-10 Narishige machine with 60°C and 225g of weight. Microneedles were loaded with fluorescent microspheres and tips were broken in the culture dish. **A**, tips with a small bore size were prone to blockages (white arrow) and, **B**, tips with too large a bore size were unable to pierce organoids. Scale bar: 100µm

After more attempts and improving proficiency in technique, microspheres of 6µm diameter were successfully injected into the lumen of bovine organoids grown by Dr Hayley Derricott (Institute of Infection and Global Health, University of Liverpool) (Figure 25). Here, microneedles were produced using a higher weight of 355g and 6µm microspheres were diluted 1/10 (2.1 x 10^7/ml). The needle was lowered into the Matrigel adjacent to the organoid. The needle was then inserted into the organoid through lateral movement until the organoid was pierced and the needle tip was in the lumen. The fluorescent microspheres were seen at the tip of the needle (Figure 25A) and upon injection at 50 hPa were seen within the organoid (Figure 25B and C). After removal of the needle tip from the organoid lumen, the organoid sealed and the microspheres remained within the lumen (Figure 25D). This was the first evidence that an object of similar size to *T. gondii* can be successfully injected into the lumen of organoids. However, following experiments were mostly unsuccessful, largely playing to the inconsistent microneedle production and need

for accurate bore size. At this point, it was decided to optimise needle production to develop consistent microneedles of approximately 10µm bore size.

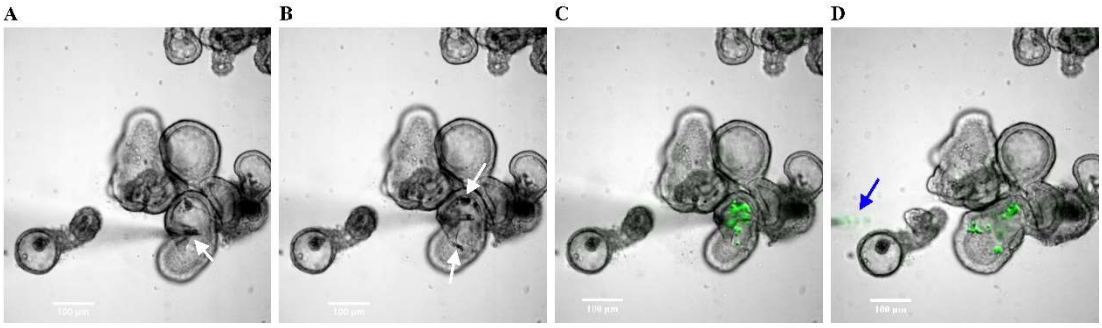

Figure 25. Microspheres of 6µm diameter can be microinjected into the lumen of organoids
Glass capillaries were pulled using PC-10 Narishige machine with 60°C and 355g of weight. Microneedles were loaded with 6µm fluorescent microspheres and tips were broken in the culture dish. **A**, the needle tip pierced the bovine organoid to enter the lumen. Microspheres can be observed at the needle tip (white arrow). **B**, microspheres (white arrows) enter the lumen after injection at 50hPa. **C**, fluorescence validates microsphere entry into the lumen and, **D**, after removal of the microneedle from the organoid, microspheres remain within the lumen. Scale bar: 100µm

4.3.2 Using an intricate microneedle pulling system does not improve microneedle production

Breaking microneedle tips on the bottom of culture dishes was undesirable as this did not produce consistent needle bore sizes and introduced foreign objects into culture. The optimisation of a method to reliably produce microneedles with a bore size of 10µm was needed. The P2000 glass capillary pulling system (Sutter Instruments) allows the control of a variety of features when producing microneedles. This instrument utilised a CO_2 laser to produce heat with a scanning pattern of the laser beam to supply heat to the glass, termed the “filament”. The “filament” function defines the distribution of heat within a scanning length and rate of scan along the glass capillary. The “velocity” function specifies the velocity that the pull occurs at. The “delay” function controls the timing of a hard pull once

the laser becomes deactivated. The “pull” function controls the force of the hard pull. Manufacturer’s suggestions for pulling borosilicate glass capillaries is set at 250-500 Watts heat, 150-250 units of pull, and a delay of 200ms. Variations in these functions were attempted to produce needle bore sizes of approximately 10µm (Table 4). The microneedle bore sizes were either approximately 2-3µm or far larger at 50-200µm in size. Therefore, some of the finer needles were bevelled on a spinning graphite disc. Here, the microneedle is manually lowered at 25-30° angles onto the disc with speeds of 20-35rpm with water applied. The distance the microneedle is lowered onto the disc could not be standardised and was carried out visually, which led to variations in microneedle production as evidenced by the differing bore sizes (Table 4). Also, the graphite disc left residue on the microneedles which is undesirable for use in cultures at it would leave graphite residue within organoid cultures after use. Therefore, using a more intricate pulling system for producing microneedles of relevant size for *T. gondii* injections was not adequate and this process required further optimisation.

Table 4. P2000 glass capillary pulling system to produce microneedles resulted in inconsistent bore sizes. The P2000 glass capillary pulling system was used to produce microneedles by varying program parameters. Microneedles were visualised using a brightfield microscope. Some microneedles were bevelled using a graphite spinning disc. H= heat (W), F=filament (mm), V=velocity, D=delay (ms), P=pull, Bore (µm)

H	F	V	D	P	Bore		Bevell	
250	3	25	150	150	1	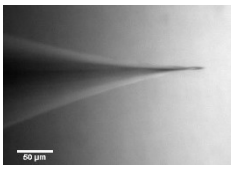	30° Speed 20	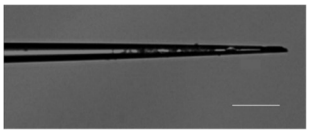
250	3	25	150	120	2	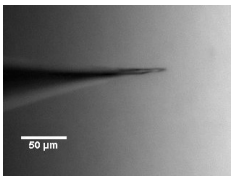	30° speed 35	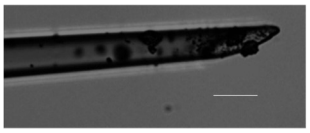
250	3	25	170	120	75	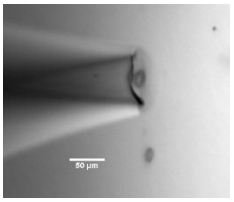		
250	3	25	160	120	2	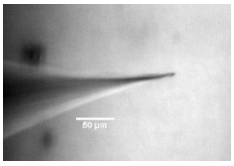	25° speed 35	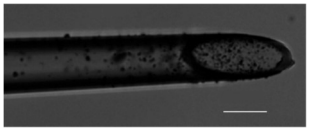
250	3	25	170	110	50	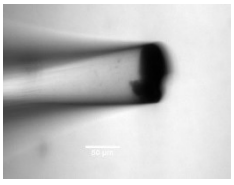		
250	2	25	170	120	2	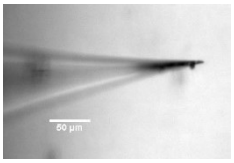		

240	3	25	170	120	2	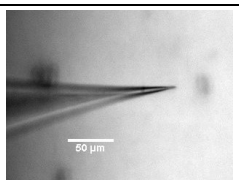		
240	3	25	170	110	50	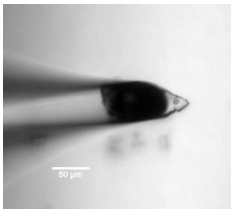		
240	3	25	170	110	60	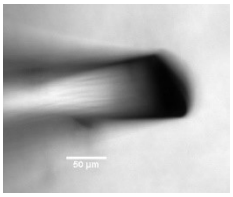		
240	3	25	170	120	60	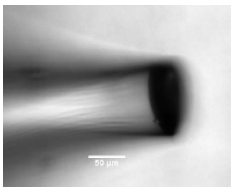		
240	3	25	160	120	2	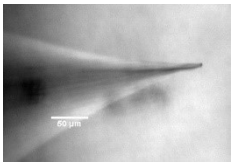		
240	3	25	160	110	3	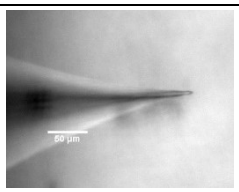		
250	3	25	160	110	200	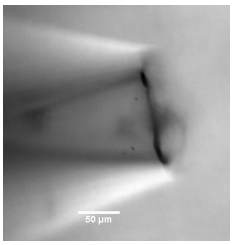		

250	3	25	150	110	3	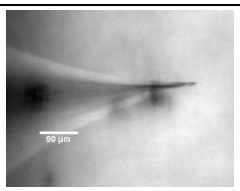		

4.3.3 Suitable microneedles can be produced using a simple pulling method

Using the P2000 micropipette pulling system did not provide suitable microneedles for further use. The intricacy also made it less favourable over the simpler PC-10 pulling system. Therefore, optimisations were carried out on this system. The aim was to produce microneedles with a shorter tip length since this is where blockages usually occurred, therefore reducing the length would reduce the risk of blockages. Lower temperatures and higher weights applied during micropipette pulling would accomplish this. Therefore, varying low temperatures and high weights were tested on the PC-10 pulling system to produce short needle tips. The lowest temperature that could be used to pull these glass capillaries was determined to be 50°C. Microneedles were then loaded onto the microinjection system and lowered into PBS in a glass-bottom culture dish. These plastic dishes have glass glued to their base which allows a certain amount of dried glue to be exposed. The microneedle tip was broken in the dish by inserting the tip into the glue, moving the tip back or forth to bend the tip, then moving the tip into the glue further until breakage (Figure 26A and B). This was repeated until a bore size of approximately 10µm was achieved. The differing heating temperatures and weights showed variations in needle tip length (Figure 26C), with the tip breakage technique allowing for the

consistent generation of 10µm bore sizes. A low temperature of 50°C and high weight of 355g produced microneedles that were suitable for microinjections based on their shorter tip lengths and relevant bore size.

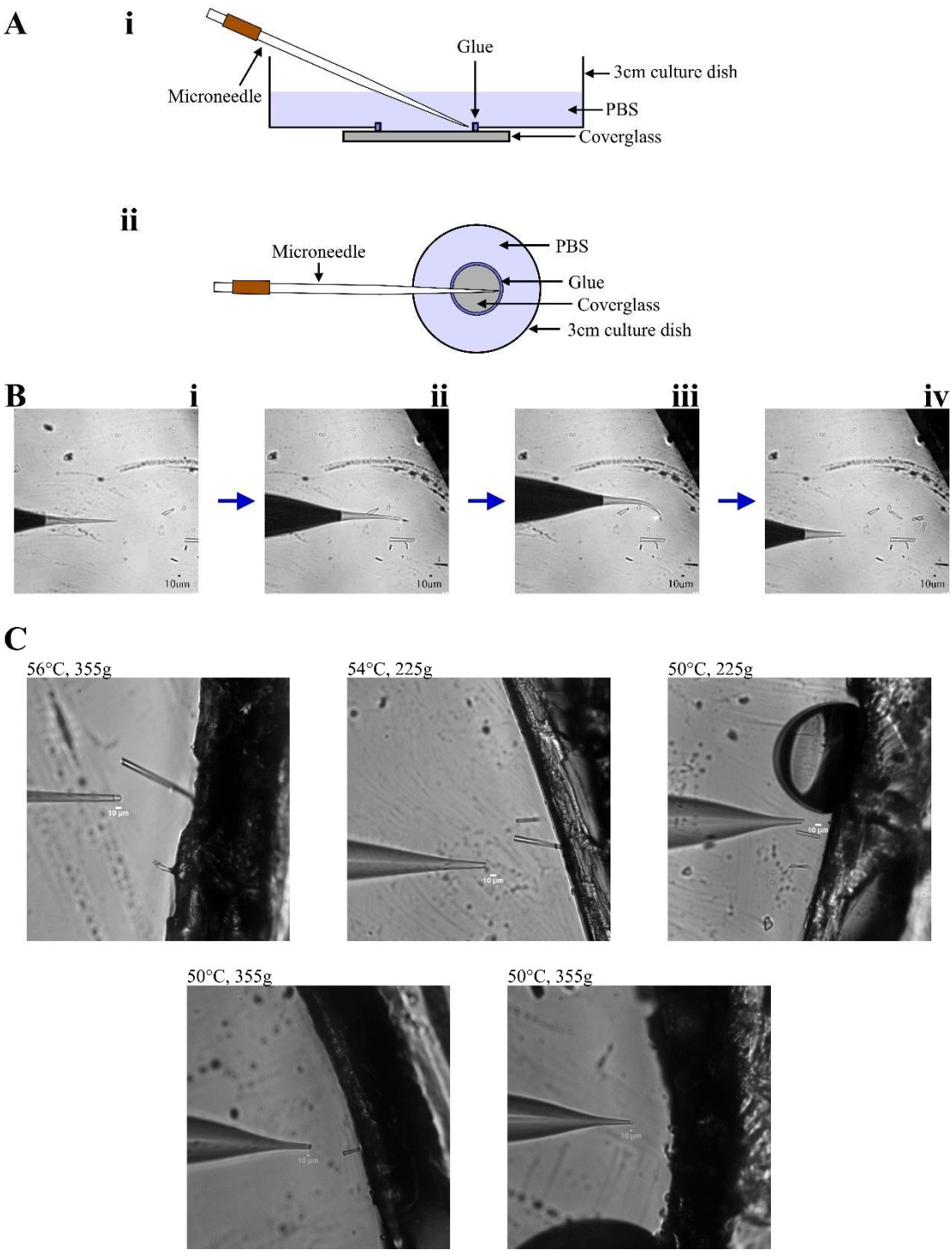

Figure 26. Producing microneedles of approximately 10um bore size is achieved through breaking pulled glass capillaries within a culture dish.
Ai, sideways schematic of a glass bottom culture dish used to break microneedles, **Aii**, above view of culture dish. Here, the cover glass is glued to the bottom of a 3cm plastic culture dish. The microneedle (produced by pulling glass capillaries) is lowered into the dish filled with PBS and is moved into the glue horizontally as shown in **B**. Once the tip is in the glue (**Bii**) the microneedle is moved up or down, making the tip bend (**Biii**). The microneedle is then moved towards the glue until the tip breaks (**Biv**). This is repeated until an approximately 10um bore length is achieved. **C**, Microneedle tip length can be altered by adjusting the heat and weight during the pulling of glass capillaries. Images show needles produced from pulled glass capillaries using differing heat and weight and broken in a culture dish to produce an approximate bore size of 10um. Scale bars: 10um

4.3.4 Optimisation of injection pressure and injection technique

With the optimisation of microneedle production, blockages were much less frequent. To gain further experience in microinjection techniques, Miss Emily Lees at the Wellcome Sanger Institute, Cambridge (as part of Professor Gordon Dougan's group) aided in improving the microinjection technique of microspheres into murine organoids. A key difference noted between our methods were the injection pressures used by this research group whereby 500-700hPa were used for their studies, a much greater quantity than injection pressures of around 50hPa used here. With this in mind, subsequent experiments microinjecting *T. gondii* into murine organoids utilised increased injection pressures.

Through further attempts, an improved technique for piercing organoids was developed. Much more success was achieved through lowering the microneedle onto the organoid as opposed to lowering the needle adjacent to the organoid. This allowed for a much clearer visualisation of depth. Then the microneedle was inserted into the lumen of the organoid through lateral movement. After injection, the microneedle was raised out of the organoid (Figure 27). This technique improved consistency in injecting organoids.

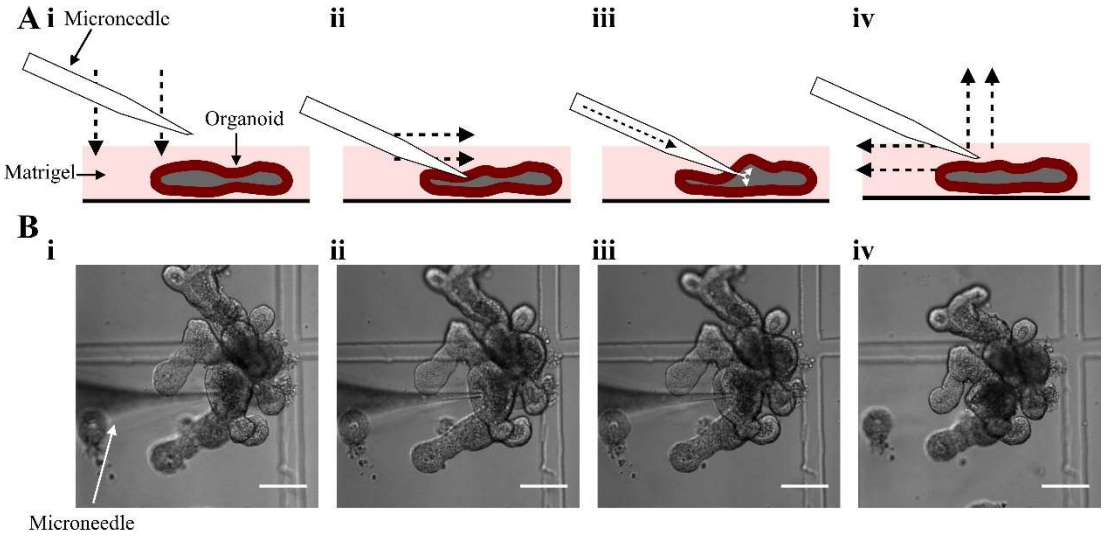

Figure 27. Optimising the piercing techniques of microneedles into organoid lumen increased efficiency
An improved efficiency in inserting microneedles into the lumen of organoids was developed. **A**, schematic of the improved technique. **Ai**, the microneedle is lowered onto the organoid to, **Aii**, press down on the organoid surface. The microneedle is moved laterally to pierce the organoid. **Aiii**, the loaded microneedle is injected into the organoid lumen. **Aiv**, the microneedle is removed from the organoid lumen by moving up and laterally away. **Bi-iv** are corresponding bright field images to the schematic. Scale bar: 100µm

4.3.5 Optimising *Toxoplasma gondii* density for microinjections

Parasite densities loaded into microneedles needed to be optimised since low densities meant few or no parasites could be injected, and high densities meant increased frequency of needle blockages. *T. gondii* Pru-GFP were loaded into microneedles at $1x10^8$/ml, however this resulted in inconsistent injections mostly resulting in mostly PBS being injected. Higher densities of 3 and $4x10^9$/ml resulted in much greater success (Figure 28). These densities required minimal compensation pressures (5-10hPa) with injection pressures of 100hPa. Upon piercing organoids, greater injection pressures were required on occasion to release blockages (approximately 300hPa) with subsequent decrease in injection pressures within the same organoid. All injections were set to 0.1s duration to prevent over-expanding the organoids. This technique provided a much greater consistency in

injecting *T. gondii* into the lumen of organoids such that successful injections occurred far more frequently than failed ones.

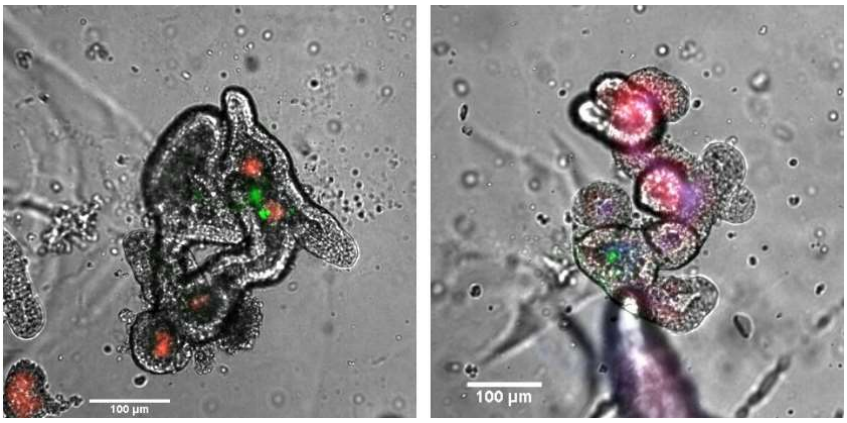

Figure 28. *T. gondii* can be injected into the lumen of organoids
T. gondii Pru-GFP were loaded into microneedles at $3x10^9$/ml and $4x10^9$/ml and used to inject murine organoids. Autofluorescence was detected using DAPI and dsRed and GFP fluorescent channels all overlapping, with individual GFP expression representing T. gondii.

An optimised technique of producing suitable microneedles has been accomplished, along with improved techniques in injecting *T. gondii* into the lumen of organoids for further experimental analyses.

4.3.6 Microinjected *Toxoplasma gondii* within the organoid lumen show limited motility

The microinjection model provides a suitable approach to image transepithelial migration and infection of *T. gondii* in the small intestinal epithelium. To achieve this, *T. gondii* Pru-GFP were injected into the lumen of $ROSA^{mT/mG}$ organoids and imaged using 2-photon microscopy to provide time-lapse images. Initial attempts showed many injected organoids perishing over the time-lapse period (Figure 29).

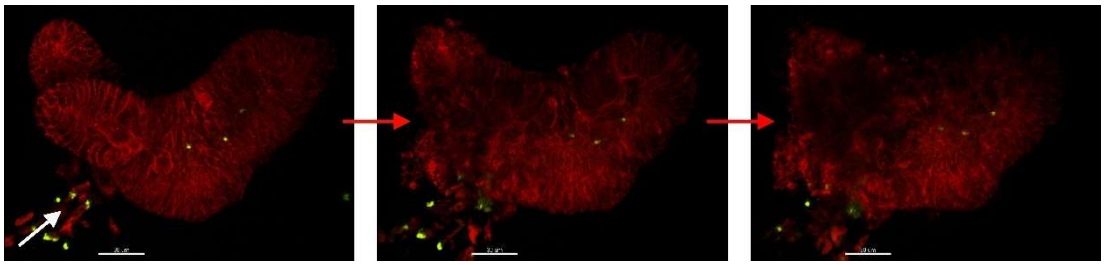

Figure 29. Microinjection of organoids with *T. gondii* can cause their demise
ROSA$^{mG/mT}$ organoids were microinjected with *T. gondii* Pru-GFP (injection site, white arrow) and time-lapse, z-stack images obtained by 2-photon microscopy. Over a period of 1.5h, organoids can be observed perishing. Scale bar 30µm

Upon replacing the media used for live imaging from phenol-red free DMEM to phenol-red free advanced DMEM/F12 or IntestiCult mouse basal medium, injected organoids became more viable. Culture dishes containing grids marked by numbers and letters allowed microinjected organoids to be located quickly between microscopes. With all conditions now optimised, 2-photon imaging of injected samples showed *T. gondii* within the lumen of organoids, with some samples showing high densities of the parasite (Figure 30).

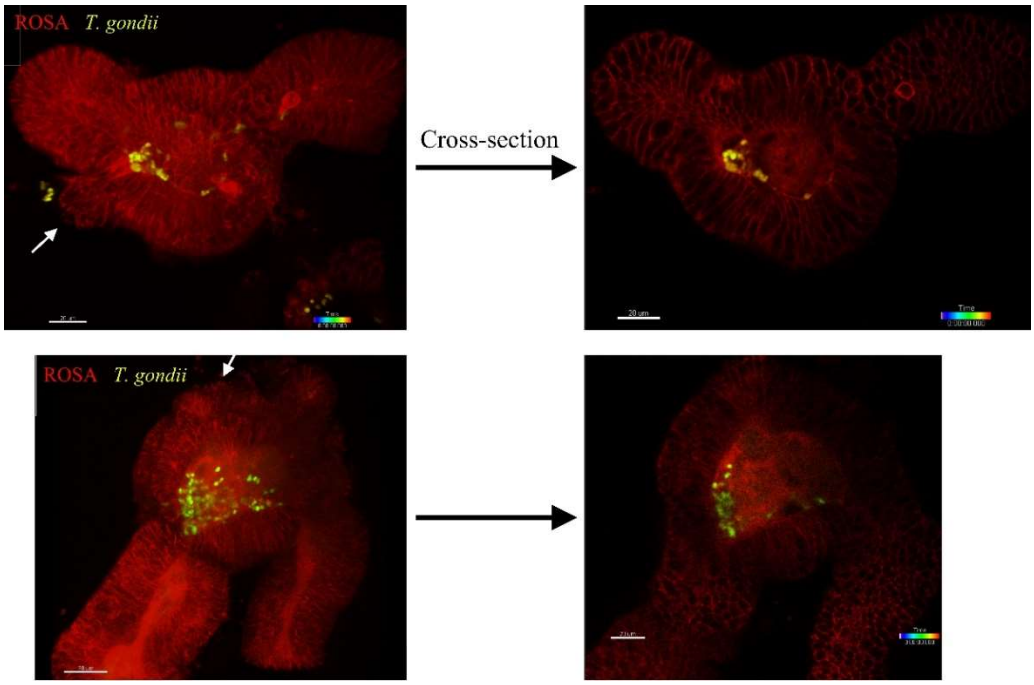

Figure 30. Large quantities of *T. gondii* can be microinjected into the lumen of organoids
ROSA$^{mG/mT}$ organoids were microinjected with *T. gondii* Pru-GFP (injection site, white arrows) and time-lapse, z-stack images obtained by 2-photon microscopy. Left images show z-stack of samples, the right show cross-sections. Scale bar 20µm.

Three successful microinjections of *T. gondii* Pru-GFP into ROSA$^{mT/mG}$ organoids were imaged over a period of 2 hours. However, parasites were observed to be immotile within the lumen with no migration across the epithelial barrier observed and parasites remaining attached to the luminal surface (Figure 31A). Parasites exhibited low speeds with low distances and track length (Figure 31B), with the higher values likely due to the movement of the organoid and not the parasites. Within the organoid lumen some parasites were seen to perish as determined by their rapid loss in fluorescence (Figure 32). No infection events were observed, however helical movement that is characteristic of *T. gondii* motility was seen with

subsequent attachment to what appears to be an extruded cell within the lumen (Movie S3).

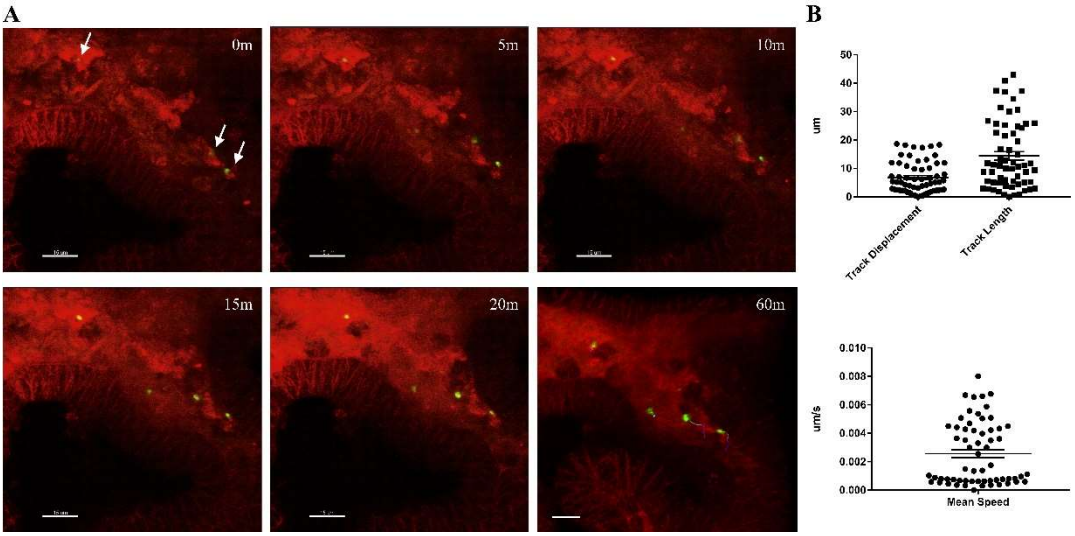

Figure 31. *T. gondii* microinjected into organoid lumen exhibit very low motility and no migration.
ROSA$^{mG/mT}$ organoids were microinjected with *T. gondii* Pru-GFP (injection site, white arrows) and time-lapse, z-stack images obtained by 2-photon microscopy over a 2h period. **A**, time-lapse imaging of a section of a microinjected organoid. White arrows indicate T. gondii with tracks visible at the 1h time point. **B**, tracking measurements of each individual parasite within the lumen of organoids during three independent experiments. Track displacement, length and mean speed were calculated. Scale bar: 15µm

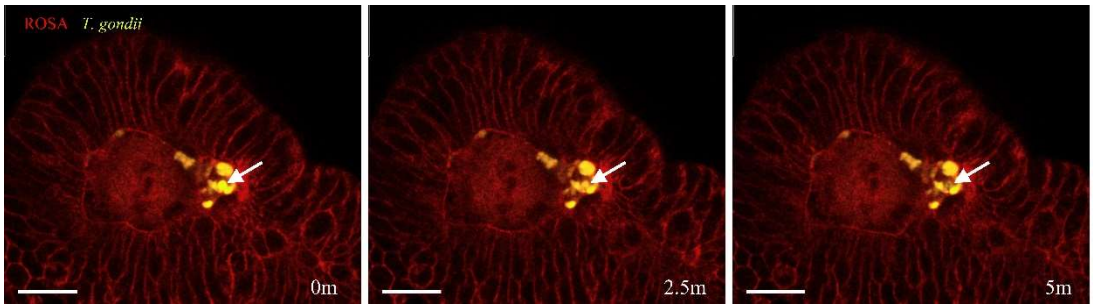

Figure 32. Microinjected *T. gondii* perish within the lumen of organoids
ROSA$^{mG/mT}$ organoids were microinjected with *T. gondii* Pru-GFP and time-lapse, z-stack images obtained by 2-photon microscopy. Some parasites perish as observed by the disappearance of parasite fluorescence (white arrows). Scale bar 20µm

4.3.7 Microinjected *Toxoplasma gondii* successfully infect organoids

To verify that *T. gondii* microinjected into the lumen of organoids successfully invade organoid cells, *T. gondii* Pru-tdTomato-Cre were microinjected into ROSA$^{mG/mT}$ organoids and incubated for 48h. Samples were fixed and z-stack images obtained by confocal microscopy (Figure 33). Using Imaris to pseudo-colour the parasites, infected cells were observed expressing eGFP indicating successful invasion of the parasite (Figure 33B), and parasites were also seen remaining in the lumen (Figure 33C). Therefore, the microinjection technique is a suitable method of infecting organoids from the luminal surface with *T. gondii*.

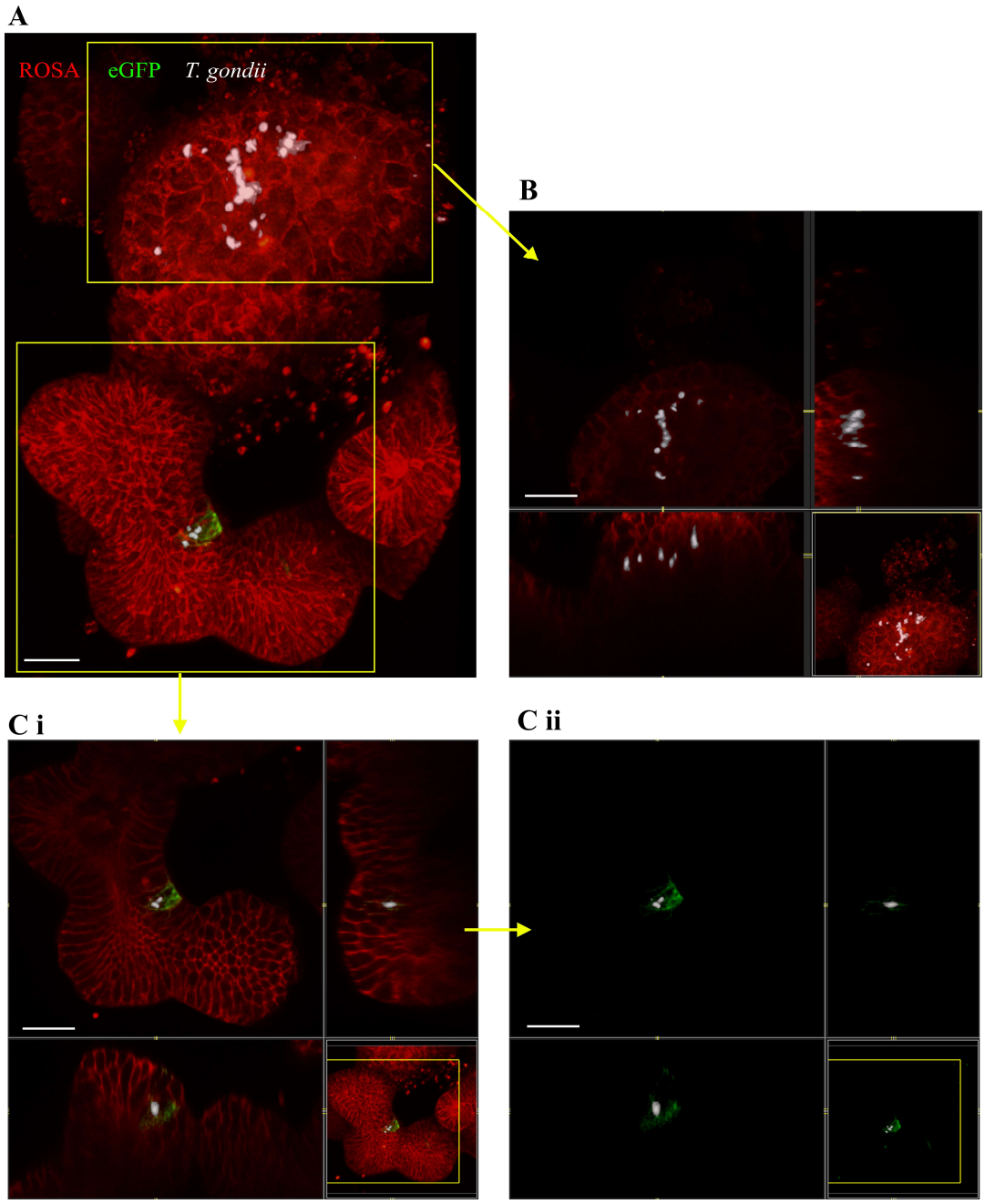

Figure 33. *T. gondii* microinjected into the lumen of organoids successfully invade organoid cells.
T. gondii Pru-tdTom-Cre were loaded into microneedles at 4x10^9/ml, microinjected into ROSA$^{mG/mT}$ organoids and incubated for 48h. Samples were fixed and z-stack images obtained by confocal microscopy. Images were analysed by Imaris with *T. gondii* pseudo-coloured for clarity. **A**, z-stack image of microinjected organoid. **B**, shows enlarged cross-section of microinjected organoid in **A** with intraluminal parasites (white arrows). **Ci**, an enlarged section of the infected site of the organoid showing eGFP$^+$ cells. **Cii**, cross-section of **Ci** showing intracellular parasites within eGFP expression. Scale bar 20µm. 63x objective.

4.4 Discussion

Organoids of the small intestinal epithelium provide a suitable model for enteric infections. However, infection studies utilising organoids have been limited. This is partially due to the architecture of organoids leading to an enclosed luminal surface, blocking the natural route of infection. Microinjections of pathogens into the luminal space of organoids is an established method of infection. During the period of this study, these pathogens involved bacteria and viruses only with no publications of parasite injections. Only during the last few months of this study have parasites been injected into human organoids (Heo *et al.*, 2018). Therefore, methods had to be established for the microinjection of *T. gondii* into organoids at the beginning of this study. The relatively small sizes of *Salmonella*, *C. difficile*, and *E. coli* that have been injected into organoids meant that microneedle production was not an issue (Wilson *et al.*, 2014; Forbester *et al.*, 2015; Leslie *et al.*, 2015; Karve *et al.*, 2017). These papers did not expand on their production of microneedles, simply stating that the tips of pulled needles were cut with sharp blades. The microneedle tips appeared to be very small in size, although never actually specified (Wilson *et al.*, 2014). Microinjections of the relatively larger *T. gondii* require a much larger needle bore size. Preliminary attempts to microinject microspheres of a similar size to *T. gondii* (6µm) resulted in many blockages of the microneedle tips. Resolving these blockages by breaking the needle tips on the culture dish aided in some successful microinjections of the microspheres, however

this method lacked consistency and required further optimisation to produce suitable microneedles. The use of a horizontal micropipette puller with many controllable aspects in order to standardise microneedle production was used. However, microneedles produced from this were either too thin or the bore sizes were too large. The thin-tipped microneedles were bevelled to increase bore size, but this method was not reproducible and created graphite residue around the needle tip. Therefore, a simpler method was optimised to generate microneedles with a tip bore size of approximately 10µm. Glass capillaries were pulled at a lower temperature of 50°C with a higher weight of 355g to generate microneedles with a short tip. This short tip length would reduce the chances of blockages since these occur in the microneedle tips. Tips were broken in a culture dish prior to use for microinjections to produce a bore size of approximately 10µm. This method of producing suitable microneedles for *T. gondii* infections is relatively quick, easy, and reproducible.

Attempts at microinjections with larger bore sizes presented problems with controlling compensation pressures. This was also determined by parasite density whereby the higher densities resulted in more control of compensation pressures. *T. gondii* at densities of 3-4x10^9/ml in PBS provided greatest control of compensation pressures, ranging from 5hPa to 15hPa, that prevented any flow from the microneedle when not injecting. This also allows for a smaller volume to be injected into the lumen that limits the expansion of organoids that could otherwise induce a stress response. Initial injection pressures were kept low at approximately 50hPa, but that did not result in many successful injections. After some training at

the Wellcome Sanger Institute, Cambridge, where this research group used higher injection pressures for *Salmonella*, injection pressures of 100hPa and over were subsequently trialled. This improved the success rate of injections of *T. gondii* into murine organoids. This was further improved by adapting the technique of piercing organoids with microneedles by lowering onto the organoid for increased depth perception. This may have also aided in pinning the organoid to prevent movement away from the approaching microneedle. With optimised parasite densities, injection pressures, and injection techniques the microinjection of *T. gondii* into the luminal space of organoids became much more consistent. Injection pressures varied between each microneedle used and usually incrementally increased from 100hPa for 0.1s until successful injection occurred, to which pressures declined back to 100hPa and this process was repeated for subsequent injections. Microinjections of *T. gondii* into the luminal space of murine organoids has now been established, with optimised protocols for the development of suitable microneedles and microinjection techniques. This will provide a valuable tool for assessing host-pathogen interactions at the physiologically relevant route of infection.

Using organoids from ROSA$^{mT/mG}$ mice, microinjections of *T. gondii* Pru-tdTom-Cre showed successful invasion of organoid cells after 48h by the expression of eGFP^{+} cells. However, considering the large amount of *T. gondii* injected into the organoid lumen, very few were successful in infection with many still seen remaining within the lumen. Attempts at time-lapse imaging of microinjections using 2-photon microscopy proved challenging, with optimisations eventually providing successful results. With this model, the observation of transepithelial migration and direct

invasion events of organoid cells by *T. gondii* was anticipated. However, *T. gondii* were deemed immotile within the lumen of organoids, remaining attached to the luminal surface with no invasion of organoid cells or migration observed. Extending imaging periods to 2 or 3h did not elucidate any further motility. This corresponds with the low rate of infection witnessed with the 48h microinjected culture. There may be a few reasons for this low rate of infection. Unlike monolayer cultures, organoids contain goblet cells that produce mucins forming a mucus layer. The mucus acts as a physical barrier between the small intestinal epithelium and microbes *in vivo*, therefore may be preventing attachment of *T. gondii* to the luminal surface of organoids. The degradation of mucus within organoids may aid in increasing contact between *T. gondii* and the epithelial surface and may be achieved through the injection of *T. gondii* along with N-acetyl cysteine. Secondly, antimicrobial expression from Paneth cells may also be preventing *T. gondii* infection. Paneth cells are known to produce defensins that have microbicidal and parasiticidal effects that kill pathogens (Wilson *et al.*, 2014) with human α-defensin 5 known to have detrimental effects on *T. gondii* (Tanaka *et al.*, 2010). Current *in vivo* models of *T. gondii* infection are analysed many days after infection, since foci are very difficult to locate early on in the intestinal epithelium (Coombes *et al.*, 2013; Gregg *et al.*, 2013). The sparsity of infections *in vivo* may result from host defence mechanisms against infection that may also be at play here in intestinal organoids. *T. gondii* strains differ in virulence and motility, with type I RH strain 3 times more likely to be observed transmigrating across epithelial cells than types II or III (Barragan and Sibley, 2002). Microinjections of *T. gondii* RH may increase the

likelihood of observing transepithelial migration. The high microinjection pressures used to inject *T. gondii* into the lumen of organoids may be detrimental to parasite viability and could suggest a reason for poor rates of invasion. However, invasion of *T. gondii* is also low within the infection protocol for organoids and parasites incubated in suspension (Chapter 3, page 118) and in cultures of organoids on collagen sheets to provide a semi-monolayer for infection (Luu L, 2017 PhD thesis, University of Liverpool). Therefore, this suggests possible defensive mechanisms applied by organoids against *T. gondii* infections that results in the low rate of infections observed in this study.

In this study, a protocol for the infection of *T. gondii* at the luminal surface of organoids has been established. This is the first incidence of microinjections using *T. gondii* and provides a valuable tool in assessing host-pathogen interactions at the physiological route of infection. Time-lapse imaging using 2-photon microscopy did not reveal any infection events or transmigration across organoids. However, co-injections with mucus degrading enzymes should be considered for future studies to potentially improve contact between *T. gondii* and the luminal surface. Although this method is technical and currently cannot be used as a high throughput method, techniques are being developed to produce automated injections within organoids that would otherwise increase samples sizes (Williamson *et al.*, 2018). This development of the microinjection system in our study will improve our understanding in host-pathogen interactions during early *T. gondii* infections.

Chapter 5: Developing a co-culture method of organoids with dendritic cells of the small intestine

5.1 Introduction

Homeostasis within the intestine relies on the cooperation between the small intestinal epithelium, immune cells of the LP, and the microbiota. Upon infection of the small intestinal epithelium, chemokines and cytokines are expressed by IECs to recruit immune cells and to activate responses to clear the pathogens. DCs play a key role in driving tolerance towards commensal bacteria and pathogen clearance during infections. However, very little is known about how DCs interact with the small intestinal epithelium during the steady state and responses to infection with no suitable models encompassing the small intestinal epithelium and intestinal DCs alone. The development of an *in vitro* culture of gut-like DCs and subsequent coculture with organoids would provide a valuable tool in assessing interactions between DCs and the small intestinal epithelium and interactions during early stages of infection.

DCs of the SI LP play a key role in intestinal homeostasis, bridging the innate and adaptive immune responses and driving tolerance towards commensal bacteria. Earlier studies into the functions of these DCs relied on CD11c and MHCII for their identification. It has since been established that intestinal macrophages also express these markers at similar levels, and therefore these markers are insufficient to distinguish bona fide cDCs. Instead, F4/80 and CD64 can be used to exclude macrophages, allowing four subsets of cDCs to be identified based on differential

expression of CD103 and CD11b (Table 1, page 59) (Figure 34). The cDC1 subset are $CD103^{+}CD11b^{-}$ and express the chemokine receptor, XCR1. They are known to cross-present antigen to $CD8^{+}$ T cells, and to induce Treg or Th1 cell differentiation. The cDC2 subset comprise of cells that are $CD103^{+}CD11b^{+}$, $CD103^{-}CD11b^{+}$, and $CD103^{-}CD11b^{-}$, and all express SIRPα. The $CD11b^{+}$ populations drive development of Th17 and Th2 responses, with the double negative $CD103^{-}CD11b^{-}$ cDCs (henceforth referred to as DN cDC2) suggested to be an immature phase to the $CD11b^{+}$ subsets (Bonnardel *et al.*, 2017). All subsets of cDCs express Aldh1a2 that allows them to produce RA that induces expression of gut homing receptors in T cells and induce expression of FoxP3 to generate T regs. The relative proportions of cDC1 and double positive $CD103^{+}CD11b^{+}$ (DP cDC2) and single positive $CD103^{-}CD11b^{+}$ (SP cDC2) in the small intestine vary between labs, but there tends to be an enrichment towards the DP cDC2 subset (Denning *et al.*, 2011; Cohen and Denkers, 2015; Scott *et al.*, 2015; Takemura and Uematsu, 2016). The composition of DC subsets in PPs remains uncertain with studies suggesting the cDC1 subset are enriched in the PPs compared to the SI LP and to be the most populous cDC in the PP (Bogunovic *et al.*, 2009), and others suggesting that the DN cDC2s are the most populous cDCs in PPs (Bonnardel *et al.*, 2017). Nonetheless, DP cDC2s are considered the most abundant population in the SI LP, with cDC1s and SP cDC2s more abundant in the colon LP. Ideally, both cDC1 and cDC2 subsets would be represented in a co-culture model, with the majority of cells deriving from cDC2. This could be achieved by isolating cDCs directly from the SI LP, or by generating gut-like cDCs from bone marrow progenitors *in vitro*.

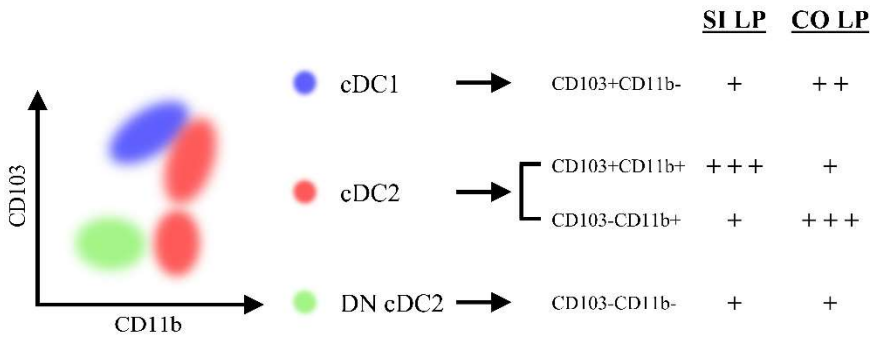

Figure 34. Schematic of the flow cytometry analysis of intestinal cDCs based on CD103 and CD11b expression and their abundance within the LP of the small intestine and colon.
Left schematic represents gating strategy for cDC1 and cDC2 subsets by flow cytometry. The cDC1 subset (blue) is CD103 +CD11b- and is most prominent in the colon lamina propria (CO LP). The cDC2 subset is divided into 3 populations that are CD11b+ (red) and CD103+ that are in greatest quantities in the small intestinal lamina propria (LP), or CD103- most prominent in the CO LP, or double negative (DN) for CD103 and CD11b (green).

5.1.1 Bone marrow culture to develop dendritic cells with a gut-like phenotype

Intestinal DCs derive from a common progenitor within the bone marrow, termed pre-mucosal DCs (pre-µDCs). Therefore, under correct conditions, *in vitro* culture of BM cells could produce cDCs with a phenotype of those from the SI LP. Early studies on the generation of DCs from BM used a culture system that included GM-CSF and, in some instances, IL-4 to produce a population of $CD11c^{+}MHCII^{+}$ cells. However, improvements in our ability to distinguish DCs and macrophages have since proven that GM-CSF cultures are greatly heterogenous with populations of cells that include macrophages and DCs resembling monocyte-derived DCs (Helft *et al.*, 2015). An alternative culture method uses Flt3L, but this generates a heterogeneous population of pDCs and cDCs (Brasel *et al.*, 2000; Mayer *et al.*, 2014). Both Flt3L and GM-CSF are implicated in the development of intestinal cDC with all four subsets dependent on Flt3L early in development. GM-CSF has also been shown to be an important factor in cDC differentiation, whereby mice lacking GM-CSFR have fewer DP cDC2s in the SI LP (Bogunovic *et al.*, 2009). A source of GM-CSF is suggested to

derive from ILCs within the intestinal LP (Mortha *et al.*, 2014), therefore exposure of developing cDCs to GM-CSF may occur at later timepoints within the LP. Exposure of bone marrow progenitors to a combination of Flt3L and GMCSF at appropriate time-points along the developmental pathway may therefore generate a cDC population with gut-like features. DP cDC2s are the most prominent subset in the intestinal LP, therefore a culture primarily consisting of this subset is most desirable.

BMDCs generated in GMCSF contain only a very minor $CD103^+$ subset, while the $CD103^+$ subset in BMDCs generated in Flt3L alone is only slightly more numerous (Mayer *et al.*, 2014; Zeng *et al.*, 2016). The cDC2 subset development and survival upon reaching the small intestine is reliant on the continued presence of GM-CSF (Bogunovic *et al.*, 2009). In line with this, the $CD103^+$ subset can be proportionally increased by addition of GM-CSF for the last 48h of Flt3L-treated BM cultures (Yokota *et al.*, 2009; Jackson *et al.*, 2011; Sathe *et al.*, 2011). However, this generates $CD103^+$ DCs that are uniformly $Id2^+$, with Id2 being implicated in cDC1, but not cDC2, development (Jackson *et al.*, 2011). DCs generated in the presence of both Flt3L and GM-CSF are also functionally different to their *in vivo* counterparts, such as the lack of TLR3 in cDC1s and lack of CD101 in DP cDC2s, a phenotype similar to that present in vitamin-A deficient mice (Zeng *et al.*, 2016). This suggests that BMDC cultures may be reliant on RA for their full development towards a gut-like phenotype. Therefore, existing methods generate either predominantly cDC1-like cells, or a mixed population of cDC1/cDC2-like cells that are not fully representative of their *in vivo* counterparts.

In addition to the definition of subsets based on CD103 and CD11b expression, generation of DCs with a gut-like phenotype can be assessed based on expression of ALDH1A2. Culture of BM in FLt3L does not induce expression of *aldh1a2* in cDCs (Yokota *et al.*, 2009), while inclusion of RA in GM-CSF cultures results in high levels of CCR9 expression, a marker for pDCs, and the absence of a prominent population of $CD103^+$ DCs. Therefore, these cannot be termed as bona fide mucosal DCs. However, when pre-cDCs are sorted from BM of Flt3L-injected mice and cultured in Flt3L and GM-CSF, the addition of RA generates DCs that emulate the transcriptomic profile of intestinal cDC1 and DP cDC2 subsets, including the induction of TLR3 expression in cDC1 and CD101 in cDC2s. How similar these are to their *in vivo* counterparts is yet to be determined (Zeng *et al.*, 2016). Studies have also demonstrated that the conditioning of cDCs with RA suppresses the pro-inflammatory gene programs, that may result in a more tolerogenic phenotype (Zeng *et al.*, 2016).

Altogether, this data suggests that gut-like cDCs can be generated with a temporally restricted cocktail of Flt3L, GMCSF and RA. However, so far studies have not successfully cultured DCs with a gut-like phenotype from BM of untreated mice. Pre-cDCs have been sorted from the bone marrow of Flt3L-treated mice and cultured with Flt3L, GMCSF and RA to generate gut-like DCs, however this technique is more technically demanding and may not necessarily be available to many laboratories (Zeng *et al.*, 2016). The ability to culture gut-like DCs directly from unsorted BM of untreated mice would provide a straightforward means of

generating DCs of relevant intestinal phenotype for high throughput studies of infections and chronic inflammatory diseases.

Table 5. Previous research on developing intestinal-like DCs from bone marrow cultures.
Previous studies utilising BM cells to induce expression of CD103 and Aldh1a2 to generate gut-like DCs have used GM-CSF, Flt3L, RA, and IL-4. Listed below are these studies, the duration of each factor the culture was exposed to, and their results. Abbreviations: Concs; concentrations, Cond. media; conditioned media

Key		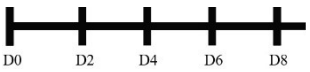		
Growth factors	**Concs**	**Culture conditions**	**Results**	**Reference**
GM-CSF Flt3L RA	100ng/ml 10ng/ml 100nM	 4-day culture in Flt3L, GM-CSF and RA.	• BM from Flt3L-treated mice sorted for pre-µDCs • Increased cDC2 population • Increased similarity in genetic profiles to *in vivo* subsets • RA supressed proinflammatory gene programs.	(Zeng *et al.*, 2016)
Flt3L RA	100ng/ml 1nM	 6-day culture in Flt3L and RA	• BM from Flt3L-treated mice sorted for pre-µDcs • RA increased $\alpha_4\beta_7$ expression on pre-µDCs • RA suppressed CCR9 expression	(Zeng *et al.*, 2013)
GM-CSF Flt3L IL-4	20ng/ml 10ng/ml 10ng/ml	 8-day culture in Flt3L. Last 48h in GM-CSF and IL-4.	• Flt3L BMDCs did not express *Aldh1a2.* • Addition of GM-CSF and IL-4 for 48h induced *Aldh1a2.*	(Yokota *et al.*, 2009)

GM-CSF RA	20ng/ml 1µM	 8-day culture in GM-CSF. RA added from D3.	• RA increased CCR9 expression, decreased CD103 and CD11c expression • 48h with RA only moderately increased CCR9	(Feng *et al.*, 2010)
GM-CSF RA IL-4	20ng/ml 1µM 20ng/ml	 4-day culture in GM-CSF. MACS enrichment and culture on collagen for 2 days with RA, last day with added IL-4.	• Increased ALDH, CD11c, and CD103 expression. • Promotes Treg differentiation through RA production in DCs	(Zhu *et al.*, 2013)
GM-CSF Flt3L	~1.8ng/ml ~65ng/ml (Cond. media)	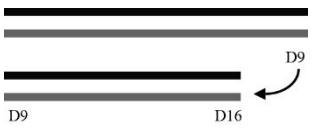 16-day culture in GM-CSF and Flt3L. Re-plated after D9.	• High CD103 and CD11b expression • Batf3-dependent associated with $CD103^{+}CD11b^{-}$ subset	(Mayer *et al.*, 2014)

5.1.2 Interactions between intestinal DCs and the small intestinal epithelium

The intestinal microenvironment conditions DCs to exhibit a tolerogenic or inflammatory phenotype depending on the steady state of the intestinal environment or initiation of inflammation through infection or disease of the epithelium, respectively. In the steady state, IECs express TGF-β, TSLP, and RA that condition DCs to become tolerogenic, endowing them with the ability to drive differentiation of $Foxp3^{+}$ regulatory T cells. IECs use ALDH1A1 to produce RA from

dietary vitamin A (retinol) that can condition DCs to increase expression of CD103 and ALDH1A2, allowing them to also contribute to the production of RA (McDonald *et al.*, 2012; Zeng *et al.*, 2016).

In the steady state cDCs patrol the SI LP, making contact with the epithelium and crawling along the surface and between epithelial cells and also extending projections between cells into the luminal space (Farache *et al.*, 2013). Although still unclear, it is thought that this process is limited to $CD11c^{+}CX3CR1^{-}$ cells, assumed to be the cDC1 subset since cDC2s express low to intermediate levels of CX3CR1 (Niess *et al.*, 2005; Farache *et al.*, 2013). Upon infection, the small intestinal epithelium express inflammatory factors and chemokines, such as CCL20, that recruit additional $CD103^{+}$ cDCs where they efficiently capture antigen (Cruickshank *et al.*, 2009; Farache *et al.*, 2013). Antigen is also transported across the small intestinal epithelium through goblet cell associated antigen passages (GAPS), then transferred to $CD103^{+}$ DCs in close contact with the epithelium (McDole *et al.*, 2012). Upon acquisition of antigen, $CD103^{+}$ cDCs then transport antigen to MLNs where presentation to T cells in the context of RA induces expression of gut-homing receptors and conditioning to effector T cells. The crosstalk between the intestinal epithelium and DCs is generally not well understood, with very little known about the direct role DCs play in intestinal epithelial defence against infections (independently of the adaptive immune system). DCs of the intestine modulate local immune cells during enteric infections such as the DP cDC2 subset expressing IL-23 following intestinal epithelial infection, and this induces IL-22 expression in ILCs that increase Paneth cell secretion of defensins against bacterial infection

(Kinnebrew *et al.*, 2012). Direct effects on the small intestinal epithelium by DCs have rarely been studied. Conditioning experiments of IECs on DCs caused an increase in IL-6 expression in DCs (Rimoldi *et al.*, 2005), with this cytokine known to be involved in in IEC proliferation and epithelial repair, therefore IL-6 expression in DCs may be involved in maintaining intestinal epithelial integrity. The cDC1 subset may control anti-inflammatory protein expression in IECs through IFN-γ since only the ablation of the cDC1 subset in DSS-colitis mouse model exacerbated inflammation (Muzaki *et al.*, 2016). However, these results do conflict with other studies using genetically engineered *Batf3*$^{-/-}$ mice whereby the loss of cDC1 did not increase intestinal inflammation, owing to the differences in the mouse models used (Edelson *et al.*, 2010). This highlights the disparity in results between studies when using mouse models to analyse the role of DCs in the intestine.

Studies analysing the DC-epithelium interactions have mostly relied on monolayer cultures which are not representative of the small intestinal epithelium. Others have used *in vivo* imaging that contain difficulties in DC subset discrimination with mouse models providing great difficulties in dissecting the involvement of particular molecular pathways in DC subsets. Therefore, a coculture method of gut-like DCs with organoids may provide a model that would recapitulate natural interactions between intestinal DCs and the small intestinal epithelium.

5.1.3 Interactions between the small intestinal epithelium and DCs during *T. gondii* infections

T. gondii invades its host through the small intestinal epithelium. Little is understood about this initial infection event, due to the difficulty detecting the parasite early after infection in *in vivo* models. *In vitro* cell line cultures suggest that a proportion of parasites invade via a paracellular route, possibly through disruption of tight junctions (Weight and Carding, 2012; Briceno *et al.*, 2016). At the same time, infection of the small intestinal epithelium results in the release of inflammatory cytokines and defensins (Ju, Chockalingam and Leifer, 2009; Morampudi, Braun and D'Souza, 2011). *In vivo* data has shown that the parasite subsequently invades DCs in the LP, which migrate away from the intestine contributing to parasite dissemination. However, due to the disparate models used, we currently understand little about the role of interactions between DCs and the small intestinal epithelium in the control or spread of infection. There are many aspects of early infection events of *T. gondii* in the small intestinal epithelium that remains uncertain such as the influence of DCs on the barrier integrity of the small intestinal epithelium, how DCs become infected with the parasite, and how DCs respond to the infection-induced release of inflammatory mediators by epithelial cells. Organoids provide a suitable model of the small intestinal epithelium to assess early invasion of epithelial cells and monitoring transmigration of *T. gondii* and may determine the relative importance of the paracellular route of the different parasite strains.

The aims of this chapter were to generate gut-like DCs from BM to develop a novel coculture model with intestinal organoids. The generation of DCs with a gut-like phenotype from BM would provide a straightforward means of developing a relevant population of DCs for co-culture and infection experiments. Live imaging experiments may reveal new DC/epithelial interactions and host-pathogen interactions during early stages of infection. From this model, future research may provide further information that could lead to novel vaccines or therapeutics being developed to improve protection again *T. gondii* infections.

Aim: Generate a DC/organoid co-culture model that can be used to model early events in enteric infection.

Objectives:

a) Produce a culture method to generate DCs with a gut-like phenotype from murine BM.
b) Develop a protocol for the coculture of DCs and organoids for live imaging and conditioning assays
c) Assess conditioning of DCs in culture with organoids
d) Use live imaging approaches to assess the dynamics of DCs in culture with organoids
e) Assess interactions between DCs and organoids infected with *T. gondii*

5.2 Methods

5.2.1 Bone marrow-derived dendritic cell culture

Bone marrow-derived dendritic cells (BMDCs) were cultured as previously described with some alterations (Jackson *et al.*, 2011; Mayer *et al.*, 2014; Zeng *et al.*, 2016). BM cells were isolated as described in chapter 2.9, page 108. Cells were cultured at $1.5x10^6$ cells/ml in a 6-well plate in complete RPMI 1640 medium containing 10% FBS, 2mM L-glutamine, 1% P/S, 50µM 2-mercaptoethanol, and 200ng/ml Flt3L, with 20ng/ml GM-CSF added from day 6 of culture (termed BMDCs). A proportion of the BM culture was treated with 1µM of retinoic acid from day 6 (termed gDCs). Medium was added on day 5 (100ng/ml Flt3L) and cells harvested on day 8 by gentle pipetting.

5.2.2 Dendritic cell isolation from the lamina propria of the small intestine

DCs were isolated from the LP of small intestines as previously described with some alterations (Cohen and Denkers, 2015). Small intestines were harvested from C57Bl/6 mice, Peyer's Patches removed, and the intestine cut open longitudinally to wash in PBS. The tissue was incubated three times in HBSS supplemented with 5% FBS, 5mM EDTA and 10mM HEPES in an orbital shaker for 20 minutes at 250rpm, 37°C. This was repeated for a total of three times with shaking in PBS for 15 seconds between incubations to remove epithelial cells. The intestines were minced and incubated in HBSS with 1mg/ml collagenase VIII (Sigma, C2139) for 20 minutes in an orbital shaker at 200rpm, 37°C, and then vortexed for 20 seconds to allow for

thorough dissociation. The suspension was passed through 100µm and 30µm filter and centrifuged at 2000rpm for 5 minutes. Cells were enriched for CD11c by positive selection with CD11c microbeads (Miltenyi, 130-108-338) through two LS columns (Miltenyi, 130-042-401). Enriched cells were then analysed using flow cytometry and added to organoid cultures in the same manner as the conditioning assays.

5.2.3 Organoid co-culture with gut-like bone marrow-derived dendritic cells for conditioning assays

Organoids were generated by isolating and culturing crypt structures from C57Bl/6 and ROSA$^{mT/mG}$ mice as described previously (chapter 2.2, page 96).

BMDCs were harvested on day 8 by collection of non-adherent and loosely adherent cells and enriched for CD11c using MACS (Miltenyi, 130-108-338). Cells were centrifuged at 1500rpm for 5 minutes and resuspended at 2x10^{6}cells/ml in 70% Matrigel diluted in IntestiCult mouse basal medium and placed on ice to prevent gel polymerisation. Organoids from C57Bl/6 mice that had been cultured for at least 5 days were extracted from Matrigel using PBS and centrifuged at 300xg for 5 minutes and supernatant removed by pipette. Matrigel/DC suspension were added to the organoids and plated in 100µl aliquots onto coverslips in a 48 well culture plate. The Matrigel was allowed to polymerise by incubating at 37°C, 5% CO_2 for 20 minutes before IntestiCult medium was added. The co-cultures were incubated at 37°C, 5% CO_2 for 24 hours.

5.2.4 Aldefluor staining

Measuring for aldehyde dehydrogenase (ALDH) expression was carried out using an ALDEFLUOR assay kit according to manufacturer's instructions (01700, StemCell Tech.) and optimised as in chapter 2.12, page 114. Cells were resuspended in ALDEFLUOR buffer (01701, StemCell Tech.) and half of each sample was added to a DEAB inhibitor (final concentration of 90µM) as a control. ALDEFLUOR reagent (final concentration of 365nM) was added to each sample and respective control and incubated for 30 minutes at 37°C before centrifuging at 1500rpm for 5 minutes. ALDEFLUOR buffer was used for the remaining cell staining.

5.2.5 Flow cytometry of organoid/BMDC cocultures

Cocultures were resuspended from Matrigel using ice-cold running buffer (PBS, 2% FCS) and dissociated by pipetting. Samples were centrifuged at 1500rpm for 5 minutes and suspended in running buffer or Aldefluor assay buffer. Measuring ALDH expression was carried out using an Aldefluor assay kit according to manufacturer's instructions with alterations as mentioned above. After labelling for ALDH, samples were suspended in ice-cold aldefluor buffer.

Cells were Fc blocked with CD16/32 antibody (16-0161-81, eBioscience) for 30 minutes on ice. Antibodies (Table 3, page 115) were added to samples for 30 minutes on ice and washed twice with buffer. Cells were analysed using MACSQuant Analyzer (Miltenyi Biotec) and data analysed with FlowJo (Tristar). Live cells were gated using FSC/SSC plots and aggregates excluded by SSC pulse width.

5.2.6 Live imaging of organoid/DC cocultures

Harvested DCs and DCs isolated from SI LP were resuspended in DMEM at $1x10^6$/ml with 2µM CFSE and incubated for 7 minutes at room temperature, protected from light. Cells were washed twice with DMEM containing 10% FCS at 1500rpm for 5 minutes and a third time with PBS, and cocultured with organoids from $ROSA^{mT/mG}$ mice in 50µl aliquots of Matrigel on glass bottom, 3cm culture dishes. Phenol-red-free DMEM/F12 (ThermoFisher Scientific, 11039021) was added and the samples imaged over a period of 50 minutes at 2-minute intervals using 2-photon microscopy on a Zeiss LSM 880 multiphoton microscope with a 40x objective.

5.2.7 Co-culture of dendritic cells and organoids infected with *T. gondii*

$ROSA^{mT/mG}$ organoids were infected with *T. gondii* Pru-tdTom-Cre as described above (chapter 2.5, page 100) and incubated for 24h at 37°C, 5% CO_2. Infected organoids were washed twice in PBS at 200g, 5 minutes. DCs that were cultured with RA (gDCs) were harvested at day 8, enriched for CD11c using positive-selection MACS, and labelled with CFSE as described above. These were added to infected organoids and control samples in 70% Matrigel diluted in IntestiCult medium and plated onto 3cm glass bottom culture dishes and incubated at 37°C, 5% CO_2 for 20 minutes. Samples were transported to the Centre for Cell Imaging (CCI) within the Institute of Integrative Biology, University of Liverpool for 2-photon microscopy. Phenol-red-free DMEM/F12 medium were added to each sample and time-lapse images with z-stacks were obtained using a Zeiss LSM880 multiphoton microscope and a 2-photon laser line.

5.2.8 Analysis of time-lapse images using Imaris software

All images were analysed using Imaris image analysis software (BitPlane), with automated quantifications analysed manually for accuracy (chapter 2.10.3, page 111). Motility parameters and morphology analysis of DCs were carried out using the "surfaces" function on Imaris, detecting the CFSE fluorescence signal for quantification by the software. These were manually checked to ensure accuracy of marked DCs and their tracking over the time-lapse periods.

5.2.9 Co-cultures of DCs and organoids microinjected with TLR9 agonists

Organoids from C57Bl/6 mice were cultured for 5-7 days before microinjecting with CpG ODN M362 or LPS. Microneedles were produced by pulling glass microcapillaries in a pipette puller with 225g of weight at 60°C and breaking the tips in a culture dish as described above (chapter 4.2.3, page 155). Microneedles were loaded with 5µM CpG ODN and microinjected into the luminal space of organoids (chapter 2.8.4, page 108). Medium was replaced, and samples cultured overnight before $2x10^5$ BMDCs and gDCs were added to microinjected organoid samples. Samples were cultured for 24 hours at 37°C, 5% CO_2, and then analysed using flow cytometry as described above.

5.2.10 Statistical analyses

Statistical significance between groups was assessed using one-way ANOVA with Tukey's post-test, two-way ANOVA with Sidaki's post-test, or Student *t* test, as stated.

5.3 Results

5.3.1 Dendritic cell isolation from the lamina propria of the small intestine

The first objective of this chapter was to isolate DCs from the SI LP to determine DC subset composition and phenotype. Cells were isolated from the SI LP by removal of SI from mice with subsequent washes in EDTA to remove epithelial cells. Collagenase was used to digest the ECM and release LP cells. Cells were enriched by positive selection CD11c MACS from Miltenyi and characterised by flow cytometry.

Since $CD11c^+$ cells of the SI LP consist of both DCs and macrophages, enrichment for $CD11c^+$ cells is likely to provide a heterogenous population. Therefore, after gating on $CD45^+CD11c^+$ cells, $F4/80^+$ macrophages were excluded from the analysis (Figure 35C). The remaining DCs were analysed for expression of CD103, aldehyde dehydrogenase (ALDH), and MHCII (Figure 35A and B). 49% of $F4/80^-$ cells expressed CD103, while 9% expressed ALDH (Figure 35Di). However, of the $F4/80^+$ cells, 23% also expressed CD103 (Figure 35Dii).

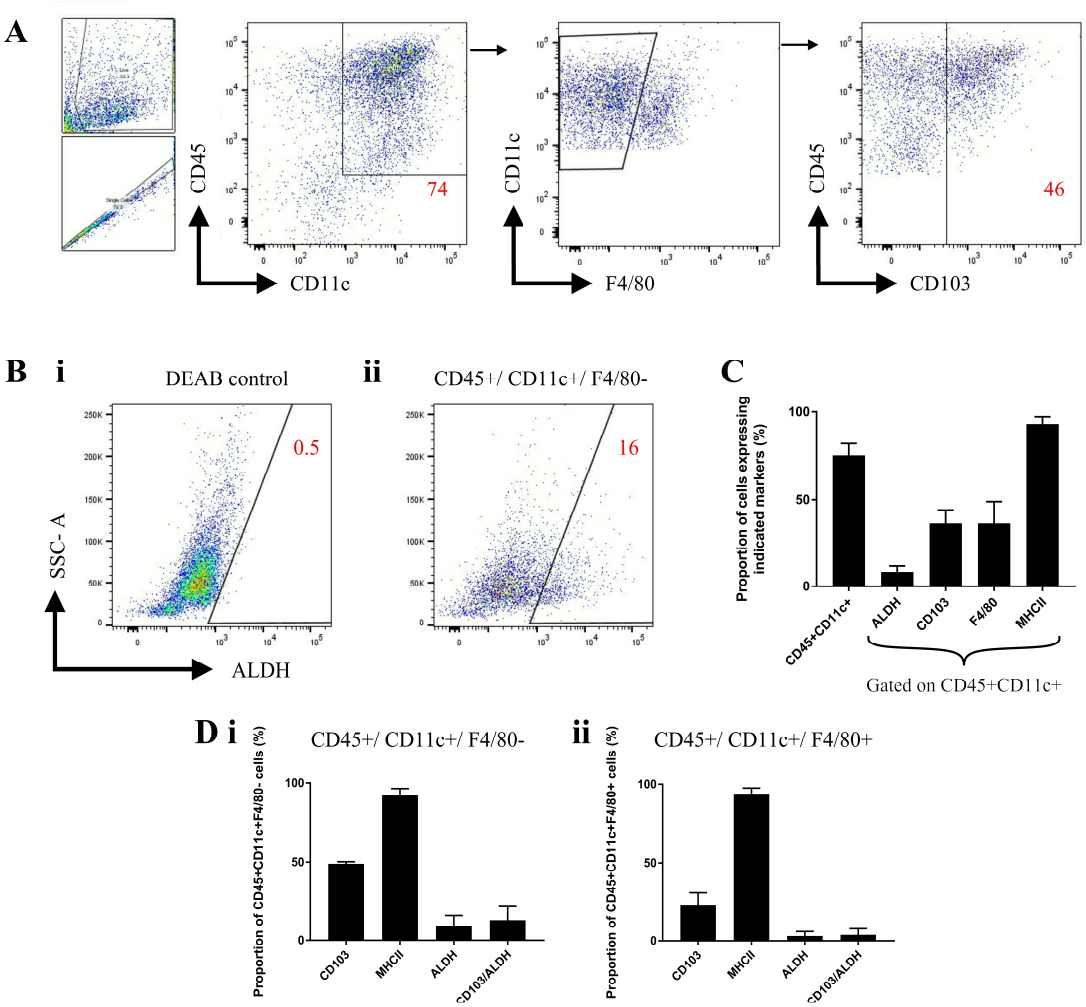

Figure 35. Isolation of dendritic cells from the lamina propria of the small intestine provide a heterogenous population of cells mostly comprising of DCs.
Cells from the LP of SI of mice were isolated, enriched for CD11c and analysed by flow cytometry. **A,** cells were gated on $CD45^+/CD11c^+/F4/80^-$ to show CD103 expression of DCs. **B,** the gated cells were analysed for ALDH expression using DEAB as the control (**i**) for the ALDH stain (**ii**). Flow data is representative of 3 independent experiments. **C**, Proportion of $CD45^+/CD11c^+$ cells expressing ALDH, CD103, F4/80, and MHCII. **D,** Proportion of $CD45^+/CD11c^+$ cells gated on (**i**) $F4/80^-$ and (**ii**) $F4/80^+$ cells expressing CD103, MHCII, and ALDH. Graphs show pooled data from of 3 independent experiments showing mean +/- SEM.

DCs of the intestine are divided into subsets based on CD103 and CD11b expression. The quantities of each subsets differ depending on their location along the small intestine, with DP cDC2s predominating in the SI LP (Denning *et al.*, 2011; Scott *et al.*, 2015). Therefore, DCs isolated from the SI LP were assessed for subset expression profiles based on CD103, CD11b, and ALDH (Figure 36). $CD45^+CD11c^+$

cells were gated for CD103 and CD11b expression (Figure 36A) and subsets were analysed for ALDH (Figure 36B) using DEAB as the negative control for gating of $ALDH^+$ cells (Figure 36A). These were quantified to show that the $CD103^+CD11b^+$ subset was the most populous, with $CD103^+CD11b^-$ and $CD103^-CD11b^+$ subsets being of lower prominence, with $CD103^-CD11b^-$ subset being lower still (Figure 36Ci). Subsets were analysed for ALDH expression with greater ALDH in the $CD103^+CD11b^-$ subset and lower proportions in $CD103^+CD11b^+$ and $CD103^-CD11b^+$ subsets. ALDH expression was almost absent in the $CD103^-CD11b^-$ subset (Figure 36Cii).

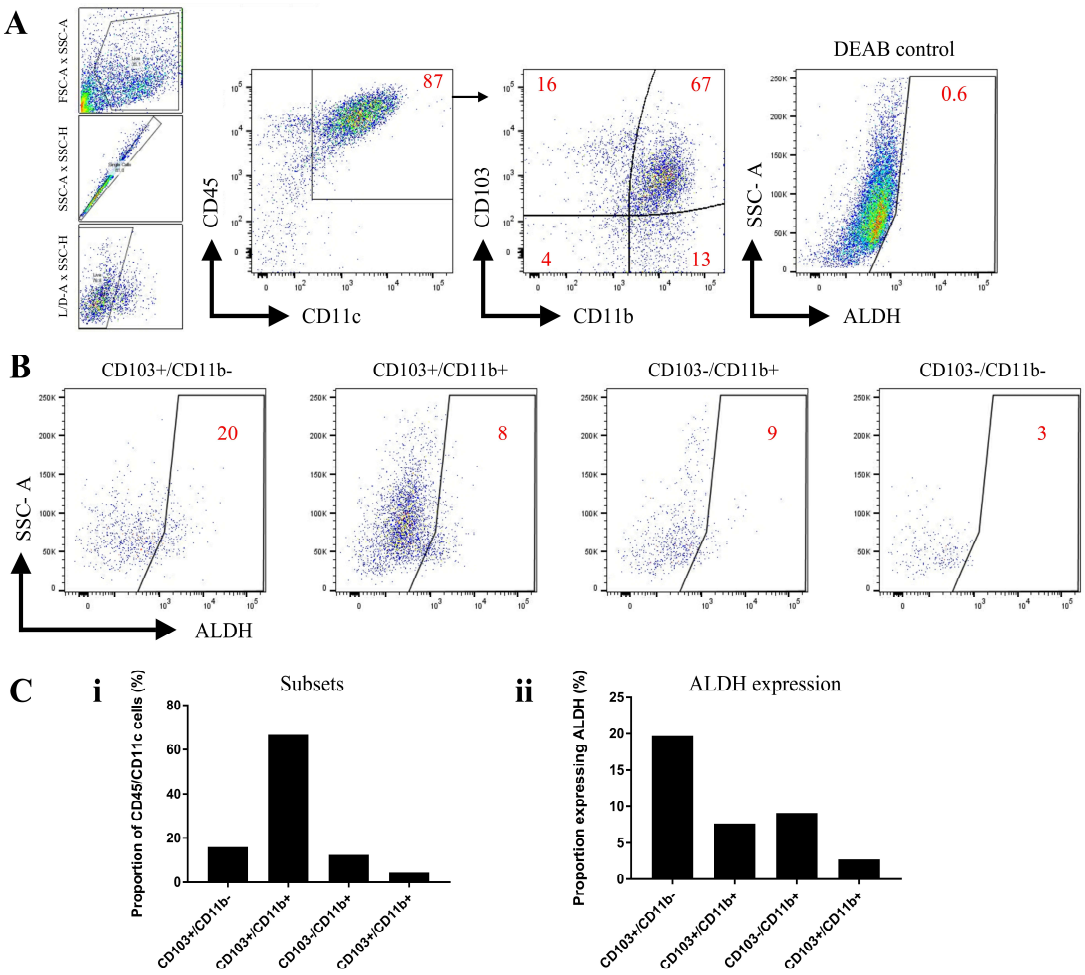

Figure 36. The cDC2 subset is the prominent population of DCs in the SI LP.
Cells from the SI LP were isolated, enriched for CD11c using MACS and characterised by flow cytometry. **A**, Cells were gated for $CD45^{+}/CD11c^{+}$ cells and analysed for subsets based on CD103 and CD11b. **B**, Subsets were analysed for ALDH expression using DEAB as the negative control. **Ci,** Subsets were quantified and, **Cii**, as too were their ALDH expression. Data from a single preliminary experiment.

5.3.2 Optimising bone marrow culture conditions to produce dendritic cells with a gut-like phenotype

The next objective of this chapter was to optimise a culture protocol for the generation of DCs with a gut-like phenotype from BM. This approach was favoured over the isolation of DCs from the LP of the SI since cell yields are too low to provide sufficient material for experiments. Previously published methods to establish a

culture of gut-like DCs from BM (Table 5) were tested and modified, as shown in Table 6. BM cells were cultured in GM-CSF, FLt3L and combinations of the two. RA was added to cultures for the last 5 days as this was shown to increase the similarity between the transcriptomic profiles of BMDCs and small intestinal cDCs in a previous study (Feng *et al.*, 2010; Zeng *et al.*, 2016). IL-4 was added to cultures for the last 24h since this had previously been shown to increase expression of CD103, CD11c, and ALDH in cultures treated with GM-CSF and RA (Zhu *et al.*, 2013). Since these cultures derive from BM it would be expected that these DCs will not be fully matured, and this can be determined by MHCII expression present on otherwise mature DCs. All culture conditions in Table 6 were analysed by flow cytometry for cell surface markers of intestinal DCs. These markers are CD103 and CD11b that are also used to determine the cDC subsets, ALDH, MHCII, and the macrophage marker F4/80.

Table 6. Culture conditions used for the optimisation of BM-derived gut-like DCs.
BM cells were cultured in GM-CSF, Flt3L, or a combination of both. RA and IL-4 were added at certain timepoints.

Key	GM-CSF	Flt3L	RA	IL-4	D0	D3	D7	D8

Culture	Growth factors	Growth factor duration in culture
1	GM-CSF	
2	GM-CSF + RA	
3	GM-CSF + RA + IL-4	
4	Flt3L	
5	Flt3L + RA	
6	Flt3L + RA + IL-4	
7	GM-CSF + Flt3L	
8	GM-CSF + Flt3L + RA	
9	GM-CSF + Flt3L + RA + IL-4	

GM-CSF cultures produced the highest proportion of $CD11c^+$ cells, however CD103 expression was very low, with intermediate ALDH expression and low MHCII (Figure 37, Culture 1). Adding RA to this culture reduced CD11c and MHCII populations, with minimal increase in CD103 and ALDH subsets, and the addition of IL-4 provided no further improvement in CD103, ALDH, or MHCII expression, while introducing a substantial contaminating $CD45^-$ population (Figure 37, Cultures 2-3). BM cells cultured in Flt3L had a larger population of $CD103^+$ cells than those cultured in GM-CSF but displayed a striking absence of ALDH expression, even in the presence of RA (Figure 37, Cultures 4-5). The addition of RA here improved $CD45^+CD11c^+$ purity and MHCII expression. IL-4 increased the quantity of $ALDH^+$ cells in Flt3L cultures with RA, but this was still lower compared to GM-CSF cultures (Figure 37 Culture 6, Figure 38). Cultures supplemented with both GM-CSF and FLt3L produced relatively small populations expressing CD103 and ALDH, whereas the addition of RA increased $CD103^+$ and $ALDH^+$ populations (Figure 37 and Figure 38). The addition of IL-4 decreased $CD103^+$ and $ALDH^+$ cells but improved $CD45^+CD11c^+$ purity (Figure 37, Culture 9). The Flt3L and GM-CSF cultures with RA provided the greatest quantity of $CD103^+$ and $ALDH^+$ populations compared to the other culture conditions (Figure 37 and Figure 38). Flt3L cultures generated cells with a more mature phenotype as demonstrated by an increased proportion of MHCII expression in comparison to GM-CSF and both GM-CSF and Flt3L cultures (Figure 38). All BM culture conditions produced lower proportions of $CD103^+$ cell populations in $CD45^+CD11c^+$ cells compared to those isolated from the LP, and RA cultures except that treated with Flt3L alone all contained higher proportions of $ALDH^+$ cells than SI LP DCs (Figure

38). Flt3L cultures have similar MHCII expression to LP DCs suggesting a more mature phenotype. Due to the relatively higher levels of $ALDH^+$ and $CD103^+$ populations, the Flt3L, GM-CSF and RA culture was further assessed for suitability for production of *in vitro*-derived gut-like DCs.

Flt3L, GM-CSF and RA derived cells were enriched for CD11c using positive-selection (MACS) and analysed by flow cytometry. Staining for F4/80 was used to identify macrophages. Two populations of $CD45^+CD11c^+$ cells were observed (Figure 39). The $CD45^{hi}CD11c^{hi}$ population had a low proportion of $CD103^+$ cells (17%) and a high quantity expressed F4/80 (65%), suggesting a primarily macrophage population. The $CD45^{int}CD11c^{lo}$ population had low $CD103^+$ (8%), lower $F4/80^+$ (21%) populations with just over half expressing MHCII (61%). This suggests a heterogenous population consisting of macrophages and DCs. Although this culture increased $CD103^+$ and $ALDH^+$ populations in BM cells, it does not produce a culture of predominantly gut-like cDCs (Figure 37).

While we achieved levels of ALDH that met or exceeded that observed *in vivo*, no culture condition produced a prominent population of $CD103^+CD11b^+$ (DP) cDC2s (as observed *in vivo*), and significant contamination with $F4/80^+$ macrophages was observed. Since the DP cDC2 subset is the most prominent in the small intestine, a culture mostly composed of these cells is desirable. Therefore, optimising BM cultures further with GM-CSF, Flt3L and RA was carried out to generate a culture of predominantly DP cDCs.

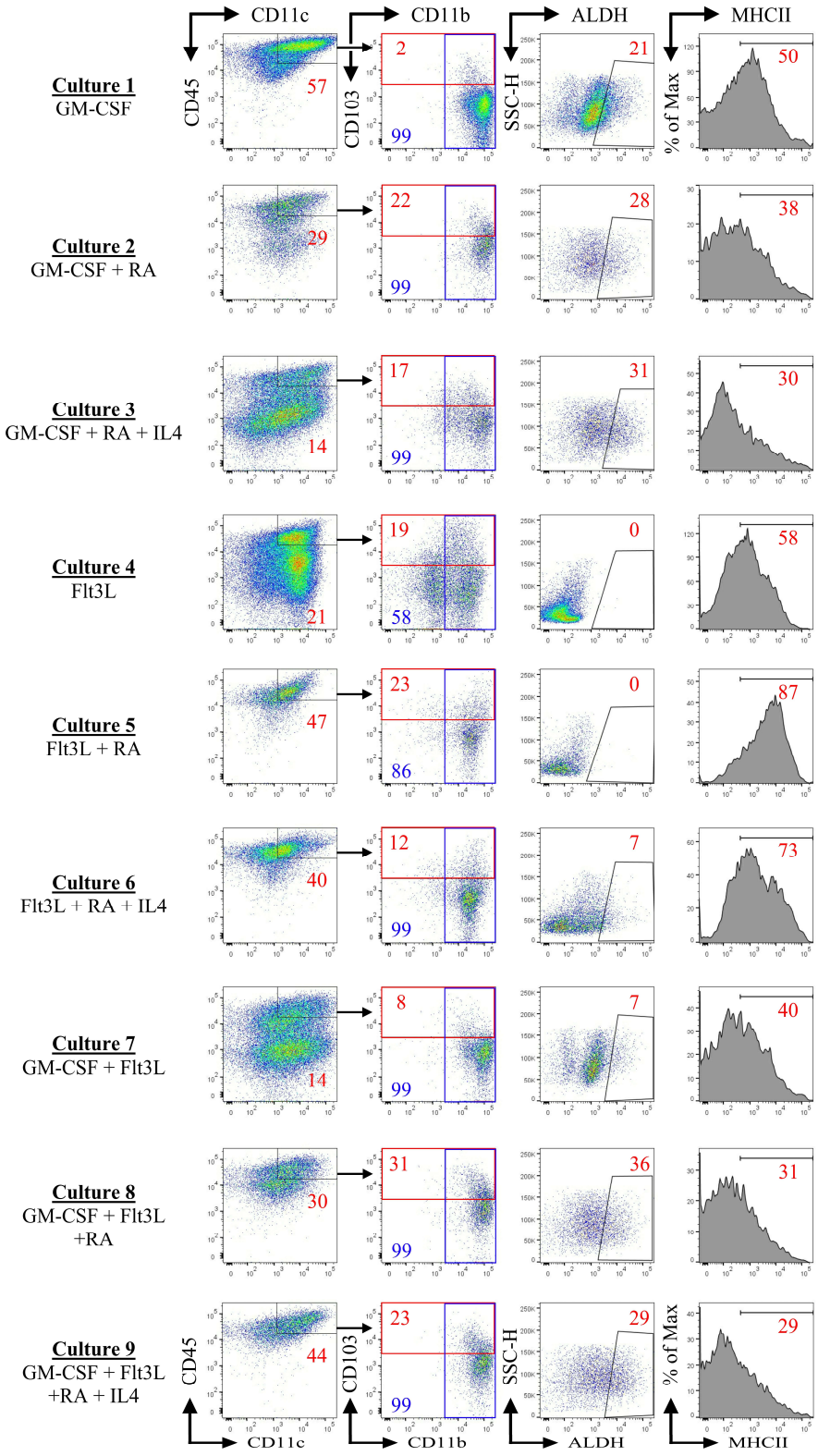

Figure 37. Expression of CD103 and ALDH on bone marrow DCs varies depending on the combination of growth factors and cytokines provided.

BM were cultured with GM-CSF, Flt3L or in combination, with or without RA and/orIL-4. RA was added on D3 and IL-4 for the last 24h (Table 6). Cells were labelled with fluorescent antibodies to the indicated surface markers, or a fluorescent marker of ALDH expression, and assessed by flow cytometry. Gating for $CD45^{+}CD11c^{+}$ cells was performed as indicated. Representative of 3 independent experiments.

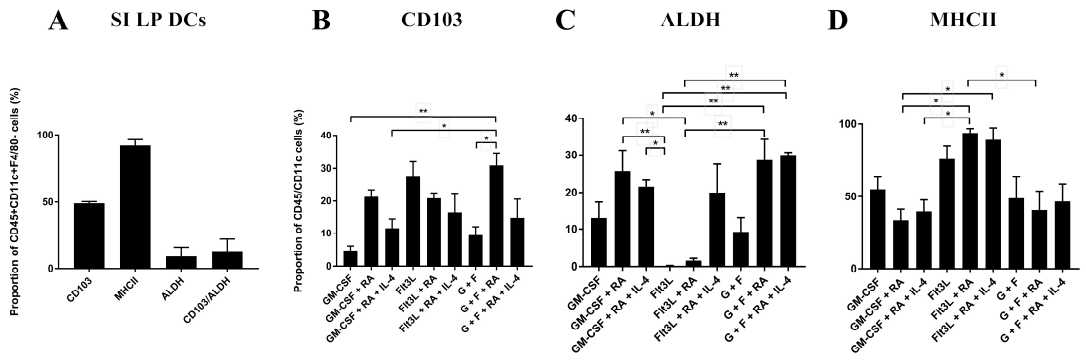

Figure 38. Bone marrow cells cultured in a combination of GM-CSF, Flt3L and RA increases both CD103 and ALDH expression.
BM cells were cultured as described in Table 6 and expression of the indicated markers analysed using flow cytometry. Analysis of SI LP DCs is provided for comparison. **A,** Graph shows proportion of SI LP expressing the indicated marker. **B-D,** Graphs depict the proportion of BMDCs expressing (**B**) CD103, (**C**) ALDH or (**D**) MHCII under the indicated culture conditions. Cells were first gated as $CD45^{+}CD11c^{+}$. Means +/- SEM is shown. Results are pooled data from 3 independent experiments. *P < 0.05, **P < 0.005; One-way ANOVA with Tukey's multiple comparisons test.

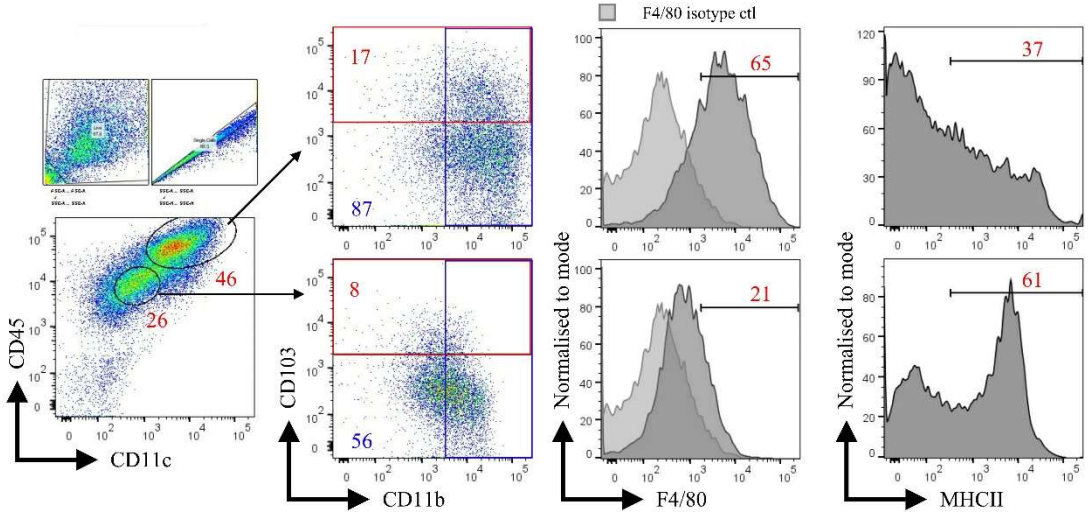

Figure 39. Culture of bone marrow cells with Flt3L, GM-CSF, and RA generates a population with high expression of macrophage marker F4/80.
BM cells were cultured in GM-CSF, Flt3L and 5 days with RA, harvested on day 8 and enriched for CD11c using MACS. Cells were analysed by flow cytometry and gated for $CD45^{hi}/CD11c^{hi}$ and $CD45^{int}/CD11c^{int}$. F4/80 isotype control represented as the light grey overlay. Data from a single preliminary experiment.

5.3.3 Sequential exposure to Flt3L, GM-CSF and RA induces a population of cDC with gut-like characteristics.

Culture of BM cells with GM-CSF, Flt3L and RA (Figure 37, culture 8, and Figure 39) produced a substantial contamination with F4/80^{+} cells, and did not generate a prominent DP cDC2 population (Figure 39). Mice devoid of GM-CSF expression still have a high number of intestinal cDCs. However this cytokine has been proven to be important for development of DP cDC2s in the small intestine, with the absence of GM-CSFR greatly reducing the proportion of this subset (Bogunovic *et al.*, 2009). ILCs and stromal cells within the intestinal LP are suggested to be an important source of GMCSF, suggesting that it acts late in cDC development (Mortha *et al.*, 2014; Vicente-Suarez *et al.*, 2015). Therefore, the ability of GM-CSF to induce cDC development in bone marrow cultures may be dependent on timing. This was demonstrated in studies where the addition of GM-CSF to Flt3L cultures for the last 48h induced an increase in CD103 and *Aldh1a2* expression (Yokota *et al.*, 2009; Jackson *et al.*, 2011). This effect was also evident in our study, whereby the addition of GM-CSF to Flt3L BM cultures for the last 48h led to a proportional increase in the cDC1 and DP cDC2 populations, and also reduced contamination with F4/80^{+} macrophages (Figure 40C).

Addition of GM-CSF to Flt3L BM cultures for the last 48h resulted in a purer DC population. However, previous studies employing GM-CSF with Flt3L cultures showed that the resulting DCs lacked many prototypical characteristics of SI cDCs, such as TLR expression and subset-specific surface expression such as TLR3 and

Clec9a in cDC1s, and TLR11 and CD101 in cDC2s (Zeng *et al.*, 2016). RA is vital for the expression of specific markers associated with intestinal cDC1 and cDC2 subsets *in vivo*, acting from both within the bone marrow and in the SI LP itself (Zeng *et al.*, 2013, 2016). Levels of RA are highest in the SI due to dietary vitamin A, therefore the conditioning effects are likely to occur further along the developmental timeline for cDCs. Therefore, the effects of adding RA for the last 48 of culture were tested. When both GM-CSF and RA were applied to Flt3L cultures for the last 48h, there was an increase in the DP cDC2s population, and a decrease in the cDC1 population, compared to Flt3L cultures that only received GMCSF for the last 48 hours (Figure 40D). Therefore, applying both GM-CSF and RA to Flt3L cultures for the last 48h generates a high density of predominantly DP cDC2s, the subset that is most prominent in the SI LP. To confirm that these DP cDC2s were phenotypically similar to their *in vivo* counterparts, the expression of ALDH was analysed. Applying both GM-CSF and RA to Flt3L cultures for the last 48h led to a dramatic increase in expression of ALDH compared to cultures with no addition of RA ($P<0.0005$, 2-way ANOVA, Sidaki's comparison) (Figure 41D). Furthermore, expression of the pDC marker CCR9 was absent (Figure 41B-D). The DP cDC2 subset is the most abundant in these BM cultures, with a further prominence in those with RA present ($P<0.0001$, 2-way ANOVA, Sidaki's comparison) (Figure 41E). Therefore, application of both GM-CSF and RA to Flt3L cultures for the last 48h leads to a gut-like population of predominantly DP cDC2s. For the rest of the dissertation, these cultures will be referred to as gDCs. Comparable cultures without RA will be referred to as BMDCs.

This is an improved method over existing protocols that require pre-treatment of mice and subsequent cell sorting for pre-cDCs in BM (Zeng *et al.*, 2016).

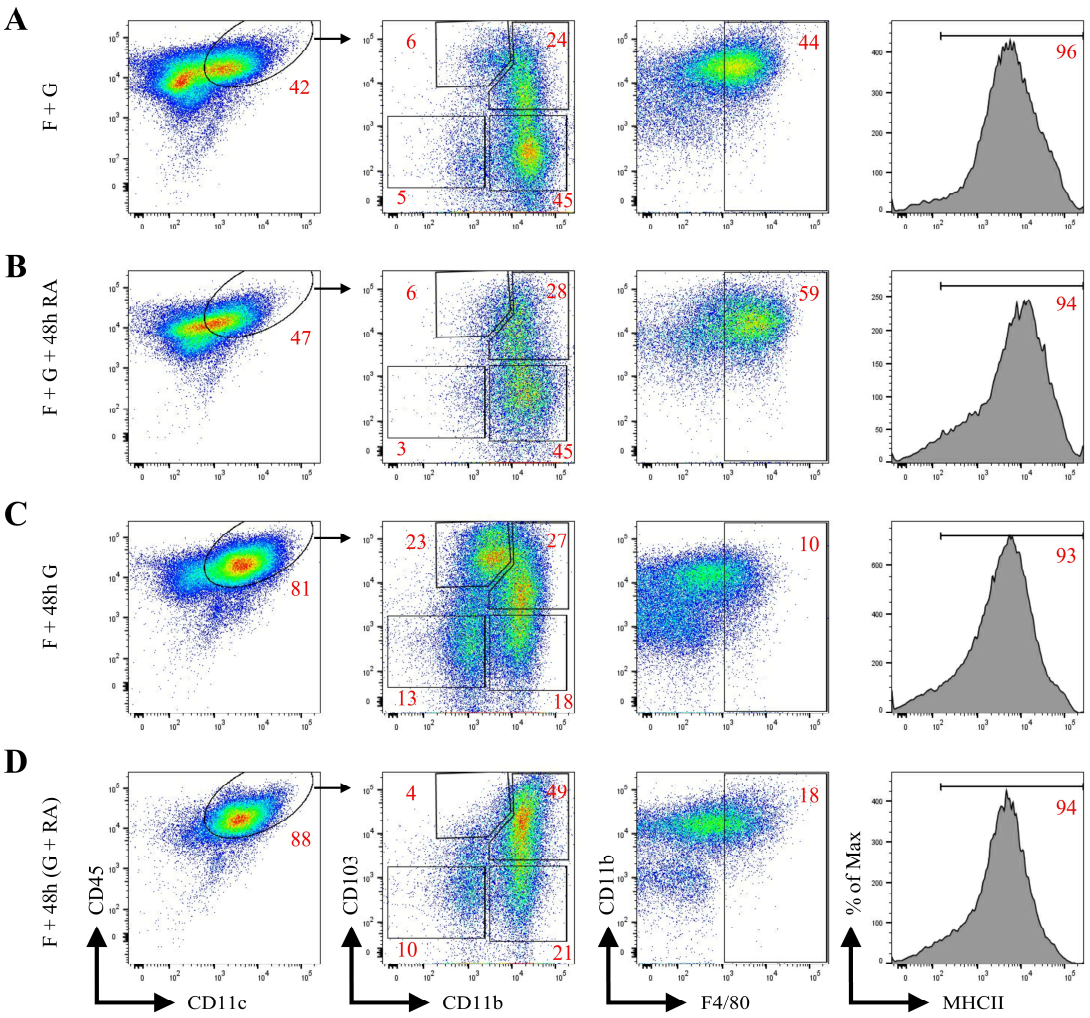

Figure 40. Adding both GM-CSF and RA for the last 48 hours of Flt3L-BM cultures increases DC purity, improves CD103 and CD11b expression, and lowers F4/80 expression.
BM cells were cultured in (**A**) Flt3L with GM-CSF and (**B**) with the addition of RA for the last 48 hours of the 8-day culture. (**C**) GM-CSF was added to Flt3L cultures for the last 48h and with (**D**) the addition of RA. Cells were gated for $CD45^{+}/CD11c^{+}$ expression to analyse CD103, CD11b, F4/80 and MHCII expression. Data representative of one experiment.

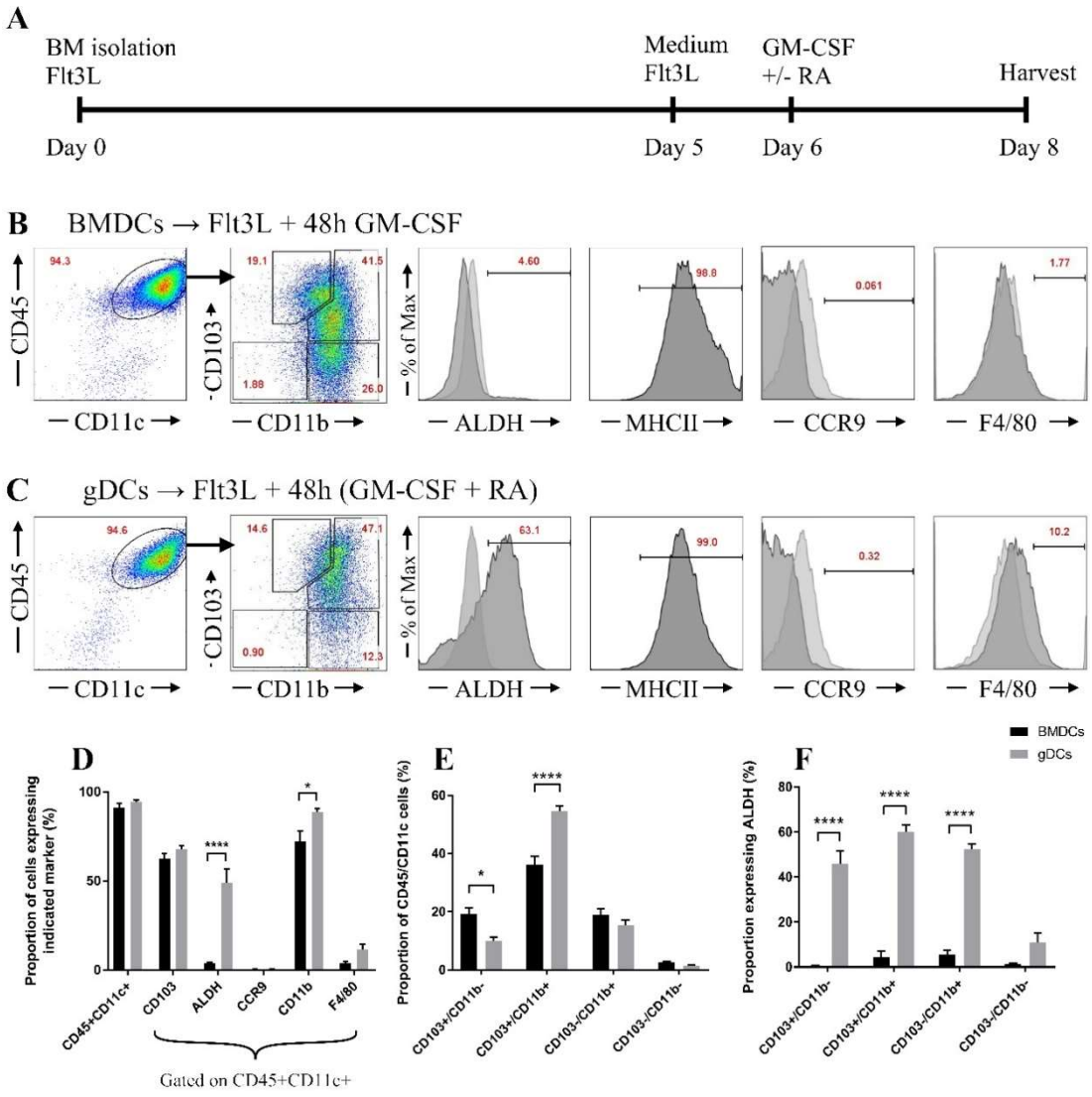

Figure 41. Optimised culture conditions of BM cells produce a high purity of DCs with gut-like characteristics. **A**, BM cells were cultured for 8 days in 200ng/ml Flt3L with 20ng/ml GM-CSF (BMDCs) and 1µM RA (gDCs) added for the last 48h. Cultures were enriched for CD11c+ cells using MACS. **B-C**, cells were analysed by flow cytometry and gated for CD45+/CD11c+ cells, with ALDEFLUOR control (DEAB), CCR9 and F4/80 isotype controls shown as light grey overlays in histograms. **D**, relative expression of cell surface markers for BMDCs and gDCs. Purity represents proportion of CD45+/CD11c+ cells in live gating. Results are pooled data from 4 independent experiments. **E-F**, CD45+/CD11c+ cells were analysed for cDC subsets based on CD103 and CD11b expression. **G**, ALDH expression in cDC subsets. Flow plots are representative of 5 independent experiments, with graphs showing pooled data from the 5 independent experiments. Graphs plotted as means with SEM. Abbreviations; ALDH: ALDEFLUOR. *P < 0.05, ***P < 0.0005, ****P < 0.0001. Two-way ANOVA with Sidaki's multiple comparisons test.

5.3.4 Coculture of dendritic cells with organoids can cause an increase in circularity

The objective for this part of the study was to provide a co-culture model of the intestinal epithelium with gut-like DCs. After establishing an *in vitro* culture of gut-like DCs, it had to be determined whether culture of these DCs with organoids would cause any morphological changes to the organoids. Organoids take on a rounded, cystic appearance when cultured with LP leukocytes from inflamed, but not control, mice (Ihara *et al.*, 2018). This appearance likely results from the production of cytokines by inflammatory DCs, which increase cellular shedding in the intestinal epithelium (Kiesslich *et al.*, 2012). Since gut-like DCs are being generated from BM in this study, they would not have been exposed to inflammatory signals and should therefore be non-inflammatory. Therefore, addition of these DCs to organoids should establish whether they drive increased cellular shedding that would be indicative of an inflammatory phenotype. BMDCs and gDCs were added to organoid wells at a density of $1x10^6$/ml and incubated for 24h (Figure 42A). Brightfield images of organoids were obtained at the time of DC addition (0h) and after 24h (Figure 42B-D). These images were used to obtain circularity results since this would be representative of the increased cellular shedding incurred during inflammation. During cellular shedding cells are released into the lumen of organoids, therefore increased cellular shedding would increase the volume of the lumen, expanding the organoid as a whole. Circularity was assessed by tracing organoids using ImageJ software and obtaining values of perimeter (P) and area (A) to calculate the circularity ($4\pi A/P^2$) (Figure 42E). At this cell density of BMDCs and gDCs, organoids did not increase their circularity over 24h

as compared to organoids cultured alone, indicating a non-inflammatory DC phenotype. Although no positive control was used in these experiments, previous experiments conducted as part of my MRes (Johnston, 2015 MRes project, University of Liverpool) revealed the addition of IFN-γ to BMDCs cultured in GM-CSF and IL-4 increased cellular shedding and circularity after 24h of co-culture (L. Johnston, 2015 MRes Project, unpublished data).

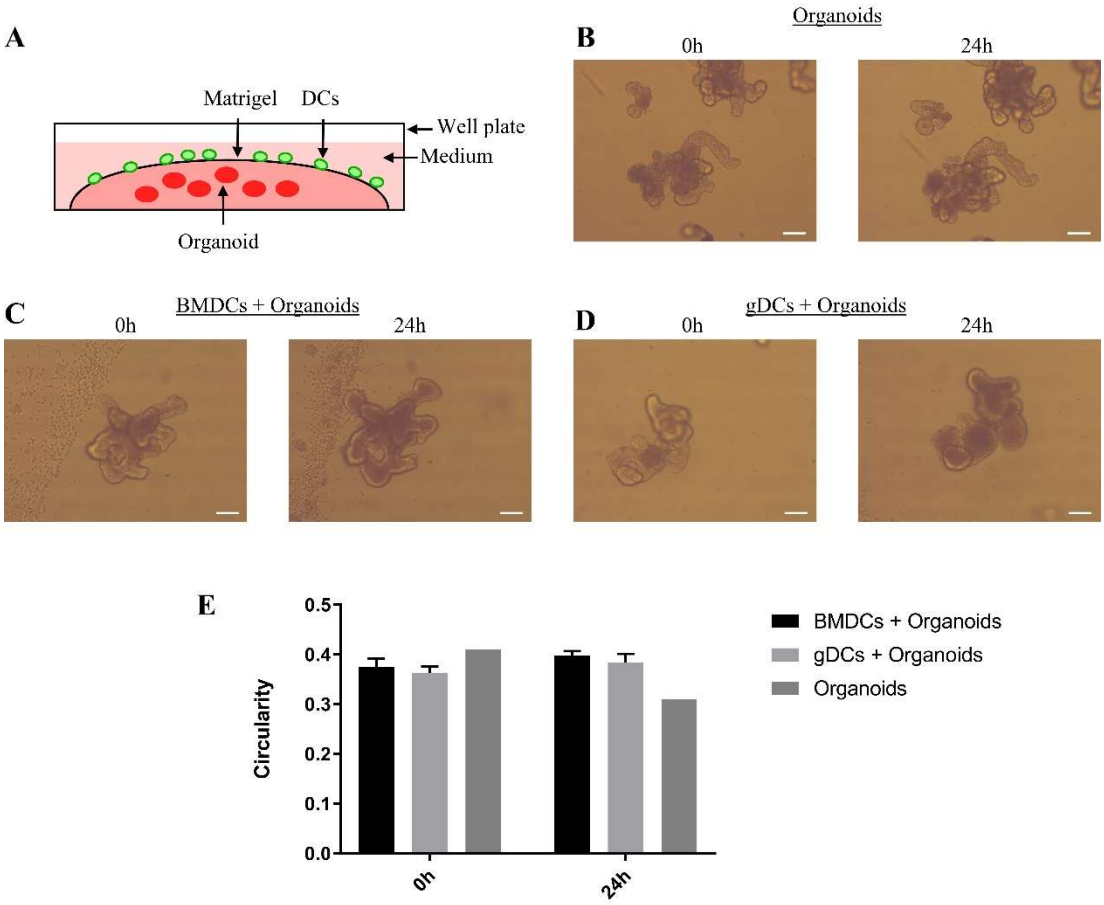

Figure 42. BM-derived gut-like DCs do not increase cell shedding of organoids.
BMDCs and gDCs were harvested after 8 days in culture and enriched for CD11c by MACS. **A**, $2x10^6$/ml of cells were added to organoid wells and (**B**) brightfield images of organoids were taken at 0h and 24h of organoids without DCs, (**C**) organoids with BMDCs, (**D**) and organoids with gDCs. **E**, Circularity of organoids in the three cultures were calculated using ImageJ software. Data from a single preliminary experiment. Graph shows mean +/- SEM. Duplicate samples of cocultures per condition, two replicate images per sample, except for the organoid control sample where single images were obtained. Scale bar: 200µm

To assess the densities and culture period whereby circularity of organoids is affected, increasing quantities of BMDCs and gDCs were added to organoids over a 72h time-period. Brightfield images and circularity of organoids were obtained as previously described. After 24h of coculture, organoid circularities were similar to those not cultured with DCs (Figure 43). After 48h, organoids became more circular in both BMDCs and gDCs with greatest organoid circularity reached after 72h of coculture (Figure 43). However, after 24h organoid circularity does not increase, verifying the use of DC/organoid cocultures for this period of time. Cell shedding was evident in live imaging of cocultures whereby shedding occurred in conjunction with DC contacts and may suggest a reason for the increased circularity (Movie S4).

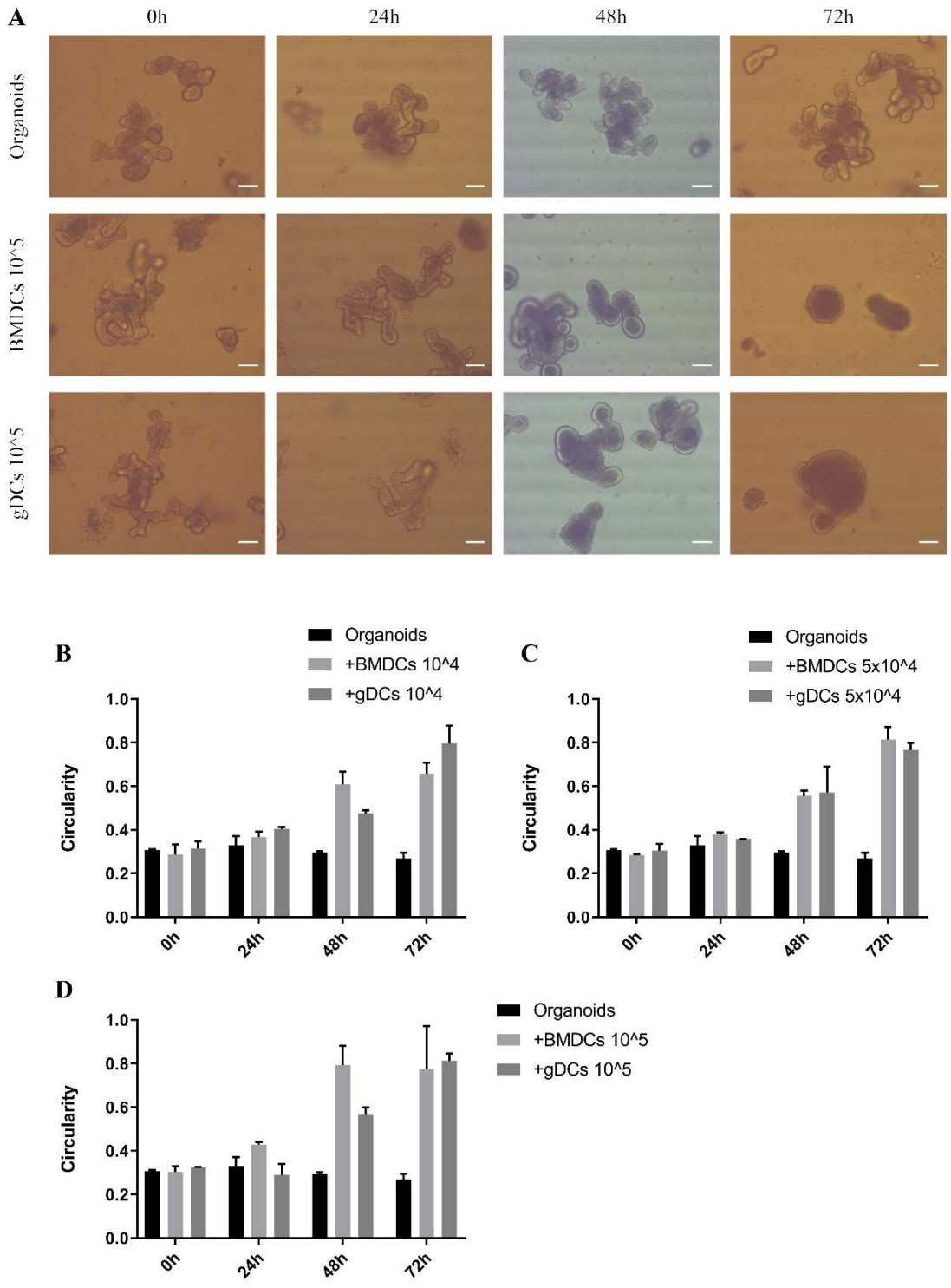

Figure 43. BM-derived gut-like DCs increase organoid circularity over an extended culture period.
BMDCs and gDCs were harvested after 8 days and enriched for CD11c by MACS. Different densities were added to organoid cultures and brightfield images of organoids were obtained every 24h over a 72h period. Circularity was calculated using ImageJ software. BMDCs and gDCs were added to organoid cultures at (**A**) $1x10^4$ cells per well ($1x10^5$/ml), (**B**) $5x10^4$ cell per well ($2.5x10^5$/ml), and (**C**) $1x10^5$ cells per well ($5x10^5$/ml). Data from a single preliminary experiment. Graphs show mean+/- SEM. Duplicate coculture samples per condition, two replicate images per sample. Scale bar: 200µm

5.3.5 BMDCs and gDCs show similar characteristics to SI LP DCs in culture with organoids

With the generation of gut-like DC cultures and isolation of DCs from the SI LP, the next step was to characterise all sets of DCs when in culture with the small intestinal epithelium in the form of organoids. These cocultures would determine the morphology of BM-derived DCs and their interactions with organoids compared to intestinal DCs. Organoid and DC coculture methods were optimised using BMDCs and gDCs due to their ease of production and high cell yields. DCs were CD11c-enriched and labelled with CFSE as described above (chapter 2.10.2, page 110). The cells were suspended in Matrigel, added to $ROSA^{mT/mG}$ organoids, and plated onto culture dishes. After polymerisation of the Matrigel phenol red-free medium was added and the samples imaged using 2-photon microscopy. Z-stack images were obtained over a 50-minute period at 2-minute intervals. These provided 3D time-lapse images of the cocultures. Imaris software (Bitplane) was used for analysis as described above (chapter 2.10.3, page 111). Optimum cell density of DCs added to organoid cultures was established as $4.4x10^5$/ml to provide at least 10 DCs per z-stack image, assessed by live imaging. With the optimised protocol, LP DCs were also labelled with CFSE, added to the Matrigel of $ROSA^{mT/mG}$ organoids and imaged using 2-photon microscopy. The 'surfaces' function in Imaris software (Bitplane) was also used for assessing motility and morphology of DCs with corresponding movies (Movie S5-6).

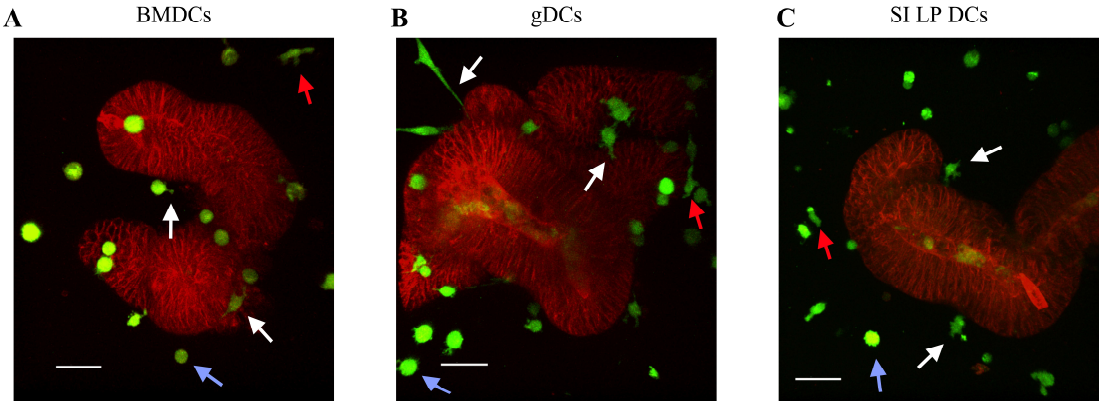

Figure 44. Morphology of DCs in culture with organoids reveal heterogeneity in cell morphology
BMDCs and gDCs were generated by culture of BM cells and SI LP DCs were isolated as described above. DCs were labelled with CFSE and added to the Matrigel of ROSA$^{mT/mG}$ organoids for live imaging by 2-photon microscopy. Z-stack time-lapse images were obtained and analysed using Imaris software. (**A**) Single timepoint from a two-photon movie showing CFSE-labelled BMDCs (green) co-cultured with Rosa-mT/mG organoids (red). White arrow indicates a DC extending a process, while blue arrow indicates a DC with rounded morphology and red arrows indicate BMDCs with amoeboid morphology. Whole images can be viewed in Movie S5 (**B**) Single timepoint from a two-photon movie showing CFSE-labelled gDCs (green) co-cultured with Rosa-mT/mG organoids (red). White arrow indicates a DC extending a process, while blue arrow indicates a DC with rounded morphology and red arrows indicate gDCs with amoeboid morphology. Whole images can be viewed in Movie S6 (**C**) Single timepoint from a two-photon movie showing CFSE-labelled SI LP DCs (green) co-cultured with Rosa-mT/mG organoids (red). White arrow indicates a DC extending a process, while blue arrow indicates a DC with rounded morphology and red arrows indicate SI LP DCs with amoeboid morphology. Whole images can be viewed in Movie S7. Figure representative of 3 independent experiments, one sample per coculture, duplicate replicates per sample.

DC morphology was quantified by performing sphericity and volume measurements in Imaris. In all cultures, a mixture of cells that extended cytoplasmic projections (dendrites) and those that remained more rounded were observed with some cells taking on amoeboid or stellate morphologies (Figure 44, Movie S5, Movie S6, Movie S7). The gDC population were less spherical than BMDCs and SI LP DCs indicating a greater amount of dendritic processes (Figure 45C), with SI LP DCs exhibiting smaller volumes than gDCs and BMDCs (Figure 45F).

SI LP DCs possessed a higher mean speed over the duration of culture ($P < 0.0001$, one-way ANOVA with Tukey's mean comparison test) with longer track lengths than either BMDCs or gDCs ($P < 0.005$ and $P < 0.05$, respectively) (Figure 45A and D). However, analysis of maximum displacement from the point of origin showed that

gDCs travelled smaller distances than BMDCs and SI LP DCs (P <0.0005 and P <0.0001, respectively) (Figure 45B). SI LP DCs are therefore more motile and travel further distances than gDCs and BMDCs. However, the track straightness is greater in BMDCs suggesting a confinement in the migration in SI LP DCs and gDCs (P <0.0001) (Figure 45E). The motility analysis of SI LP DCs may suggest the presence of a sub-population with higher speeds, greater displacement, and longer track lengths (Figure 45A, B, and D). This population may be due to the composition of subsets in the SI LP and may constitute cDC1 cells. However, these may also represent contaminating macrophages since these were not eliminated during isolation. The sphericity of gDCs was less than both BMDCs and SI LP DCs (P <0.0005) (Figure 45C), with SI LP DCs also significantly smaller in volume than both BMDCs and gDCs (Figure 45F) (P<0.0001, One-way ANOVA with Tukey's mean comparison test).

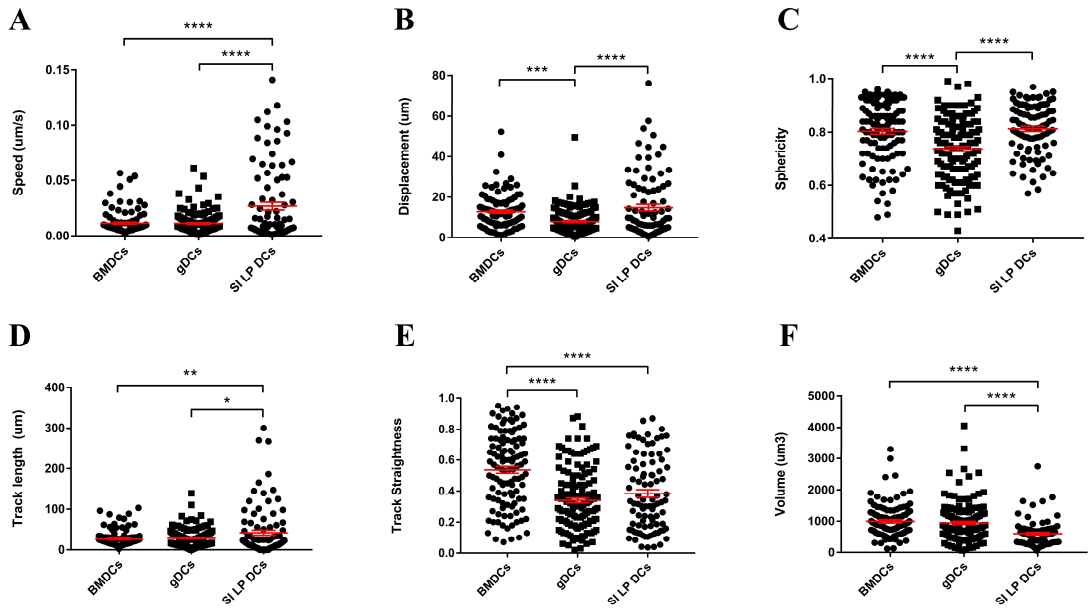

Figure 45. SI LP DCs exhibit greater speed and motility and smaller volume than gDCs and BMDCs
BMDCs, gDCs and LP DCs were cultured with organoids and imaged over a 50-minute period at 2-minute intervals by 2-photon microscopy. Z-stack time-lapse images were assessed using Imaris software to calculate motility and morphology of DCs. The 'surfaces' function in Imaris was used to calculate (**A**) mean speed (μm/s). (**B**) track displacement (μm), (**C**) sphericity, (**D**) track length (μm), (**E**) track straightness, (**F**) volume (μm^3) of DCs.

BMDCs and gDCs are representative of 4 independent experiments, SI LP DCs representative of 3 independent experiments. Graphs plotted as means with +/- SEM. Duplicate samples per condition. *P <0.05, **P <0.005, ***P <0.0005, ****P <0.0001 (one-way ANOVA with Tukey's mean comparison test)

5.3.6 DCs interact with the organoid surface

Imaging the interactions of DCs with the small intestinal epithelium have been carried out using live mice and demonstrated $CD103^+$ DCs crawling along the surface of the epithelium (Farache *et al.*, 2013). These close interactions are important for antigen transfer from the lumen to initiate pathogen clearance or tolerance towards infections or commensal bacteria, respectively. Antigen is transferred to DCs through transepithelial dendrites that extend between epithelial cells to reach the lumen, or through antigen transfer by Goblet cells (McDole *et al.*, 2012; Farache *et al.*, 2013). The close association of DCs with the epithelium is also thought to expose DCs to RA and TGF-β that conditions DCs to express CD103 and Aldh1a2 (Bain *et al.*, 2017). In our study BMDCs, gDCs, and SI LP DCs were observed interacting with the surface of organoids, with a portion of cells remaining attached throughout the time lapse period of 50 minutes. Some were immotile and extended processes along the surface of organoids, mainly seen in BMDC cocultures (Figure 46A, Movie S8). BMDCs remained fixed to a point of attachment whereas gDCs were seen to crawl further distances along the organoid surface (Figure 46B, Movie S9), with SI LP DCs observed to crawl much further than both BMDCs and gDCs (Figure 46C, Movie S10). The proportion of DCs in contact with organoids to those that were not in contact was similar between BMDCs, gDCs and SI LP DCs (Figure 47). Those cells in contact with organoids were analysed for their duration in contact and their speed (Figure 47). The duration of the contacts between organoids and

DCs was calculated manually by inspecting movies frame-by-frame. SI LP DCs were in contact with organoids for a shorter period of time compared to BMDCs and gDCs ($P < 0.005$ and $P < 0.05$, respectively, one-way ANOVA with Tukey's means comparison test) with greater motility as determined by their mean speed ($P < 0.0001$). SI LP DCs displayed a higher mean speed while in contact with the epithelium, which may allow for more efficient scanning of the epithelial surface for invasive pathogens or sites of epithelial infection. Overall, BMDCs, gDCs and SI LP DCs interact with the surface of organoids, with SI LP DCs showing a greater crawling ability. This is possibly owing to a more conditioned phenotype since they were derived from the LP of the small intestine where they are exposed to factors required for their full development.

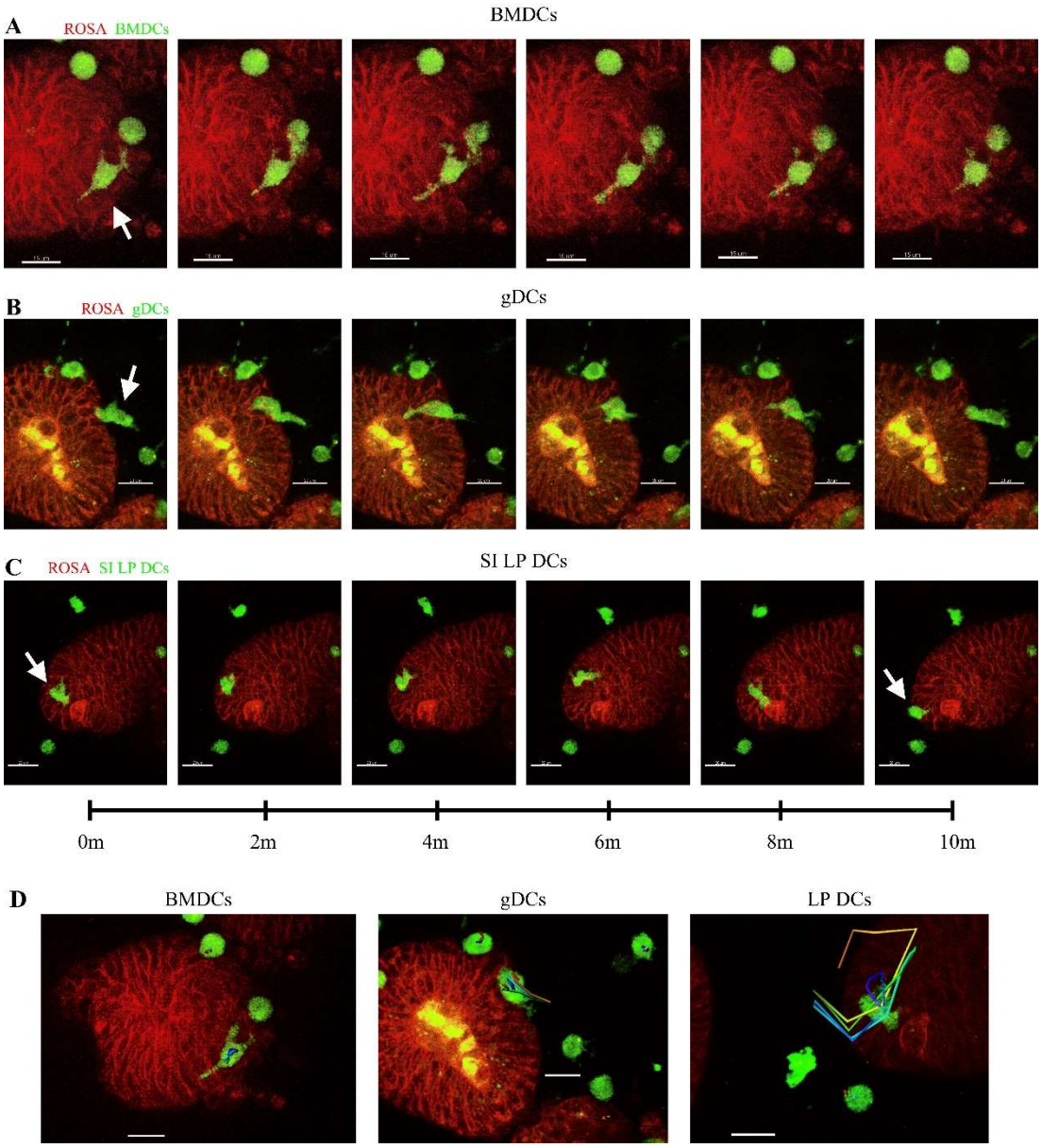

Figure 46. DCs isolated from the SI LP and gDCs crawl along the organoid surface
DCs cultured from bone marrow and those isolated from the SI LP were cultured with organoids and time-lapse images were acquired by 2-photon microscopy. Images show 10 minutes of each DC coculture. **A**. BMDCs attached to organoids extended processes along the surface but were less motile. Whole images can be viewed in Movie S8. **B**. Organoid cocultures with gDCs displayed greater crawling ability. Whole images can be viewed in Movie S9. **C**. SI LP DCs were more motile than cultured DCs and possessed higher crawling abilities. White arrows mark the DCs of interest. Whole images can be viewed in Movie S10. **D**, tracks of DCs are represented as multicoloured cylindrical tracks. Figures representative of 3 independent experiments.

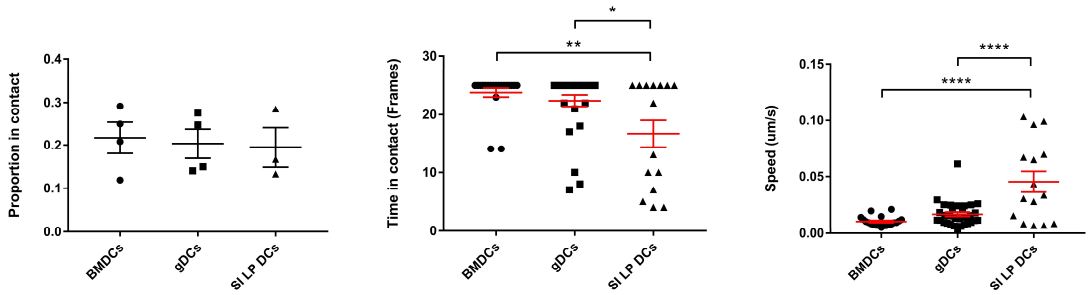

Figure 47. DCs from the SI LP are in direct contact with organoids for a shorter time and at greater speeds than those cultured from BM.
DCs cultured from bone marrow and those isolated from the SI LP were cultured with organoids and time-lapse images were acquired by 2-photon microscopy. Images were analysed by Imaris software to obtain measurements of DC motility and morphology. The proportions of DCs in each sample that were in contact with organoids were determined, the amount of time the interactions occurred as measured by frames, and the mean speed while interacting. Data representative of 4 independent experiments for BMDCs and gDCs, and 3 independent experiments for SI LP DCs. Graphs plotted as mean and SEM. *P <0.05, **P <0.005, ****P <0.0001, one-way ANOVA with Tukey's means comparison test.

5.3.7 Gut-like dendritic cells enter the lumen of organoids, or extend processes to sample the luminal space

A characteristic of SI LP DCs is their ability to extend processes between epithelial cells into the luminal space for sampling. Luminal sampling was evident in cocultures of gDCs and ROSA$^{mT/mG}$ organoids (Figure 48, Movie S11A-C). The gDCs attached to the outer surface of the organoids and extended dendritic processes between epithelial cells into the luminal space. Over time, the extended dendrite actively changed shape and direction (Figure 48A, Movie S11A). Although this occurrence was rare (observed in two of eight experiments), it was only seen in gDCs and not BMDCs or SI LP DCs.

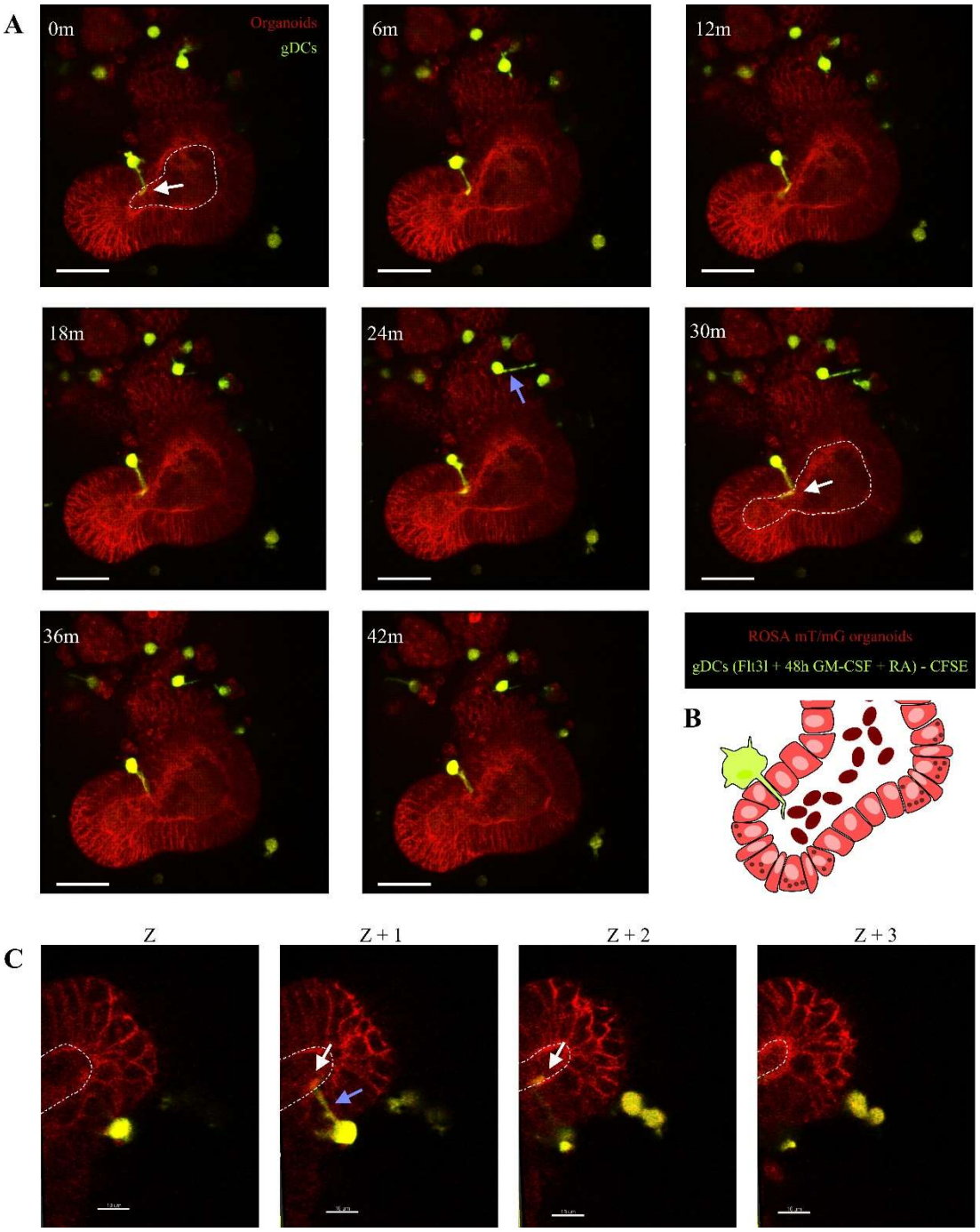

Figure 48. BM-derived gDCs interact with the surface of organoids with evidence of luminal sampling. 2-photon z-stack time-lapse imaging of gDCs cocultured with ROSA$^{mT/mG}$ organoids for 50 minutes at 2-minute intervals. DCs were cultured from bone marrow in Flt3L for 8 days, with the last 48h of culture with added GM-CSF and RA to produce a gut-like phenotype. Cells were labelled with CFSE and added to organoids cultured from ROSA mice with z-stack, time-lapse images obtained using 2-photon microscopy. **A**, single pane of time-lapse imaging of a gDCs interacting with the surface of organoids and extending dendrites (arrows) into the luminal space (white arrow) (dotted line represents luminal surface). Scale bar 40µm. **B**, schematic of gDC interaction with organoids and dendrite projection into lumen. **C**, Sections of z-stack image showing dendritic process extending between epithelial cells into the luminal space of the organoid. Scale bar: 10µm. Whole images can be viewed as Movie S11.

$CD11c^{+}CX3CR1^{+}CD11b^{-}$ cells enter the luminal space of the small intestine to internalise *Salmonella* but do not return to the tissue (Arques *et al.*, 2009). These were termed DCs, however since cDC2s express CX3CR1 and CD11b, these markers suggest that the intraluminal population were likely macrophages, and this was verified by flow cytometry analysis of intraluminal $CX3CR1^{+}$ cells after *Salmonella* infection that expressed F4/80 and not CD103 (Man *et al.*, 2017). Therefore, it remains uncertain whether DCs migrate into the lumen to protect the intestinal epithelium against pathogen invasion. In our study, gDCs were observed within the lumen of organoids (Figure 49, Movie S12). Organoids become disrupted during the coculture process, breaking them open to expose their luminal surface, therefore intraluminal gDCs may be because of this. However, at the start this live imaging sample the gDC is partly within the organoid epithelium that may suggest it entered the lumen via an intraepithelial pathway (Figure 49, blue arrow). Further experiments need to be carried out for longer time periods to verify this characteristic.

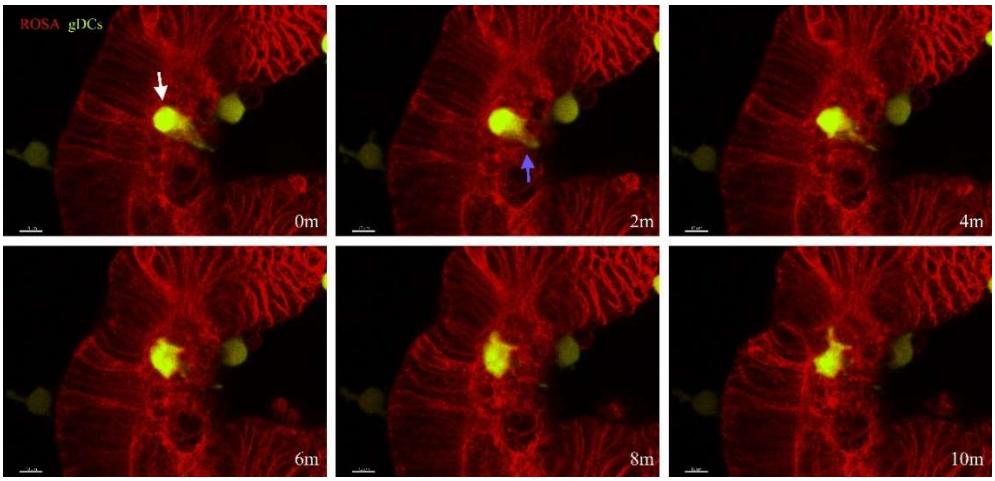

Figure 49. Organoids contained intraluminal gDCs
gDCs were labelled with CFSE and added to organoids cultured from ROSA$^{mT/mG}$ mice with z-stack, time-lapse images obtained using 2-photon microscopy. An intraluminal gDC (white arrow) was observed with part of the cell coming from within the organoid epithelium (blue arrow). Corresponding live image Movie S12 .Scale bar 10µm. Whole images can be viewed in Movie S12.

5.3.8 Co-culture with organoids results in downregulation of ALDH in DCs

The intestinal epithelium is thought to condition DCs towards a gut-like phenotype by increasing ALDH and CD103 cell populations. To determine if organoids could induce ALDH and CD103 expression in BMDCs and gDCs, cells were added to the Matrigel of organoid cultures for 24h and analysed by flow cytometry. Purity was analysed on the day of coculture to assure addition of phenotypically consistent DCs based on CD45^{+}, CD11c^{+}, and F4/80^{-} expression (Figure 50A). The proportion of DCs expressing CD103 remained unchanged after 24h in coculture with organoids (Figure 50Bi). However, the proportion of cells expressing ALDH declined in both BMDCs and gDCs to almost zero (mean 0.5% and 3.9%, respectively) with this drop being significant in gDC cocultures (Figure 50Bii) ($P < 0.05$). This decrease was dependent on the presence of organoids, since DCs cultured in Matrigel alone with organoid medium maintained ALDH expression.

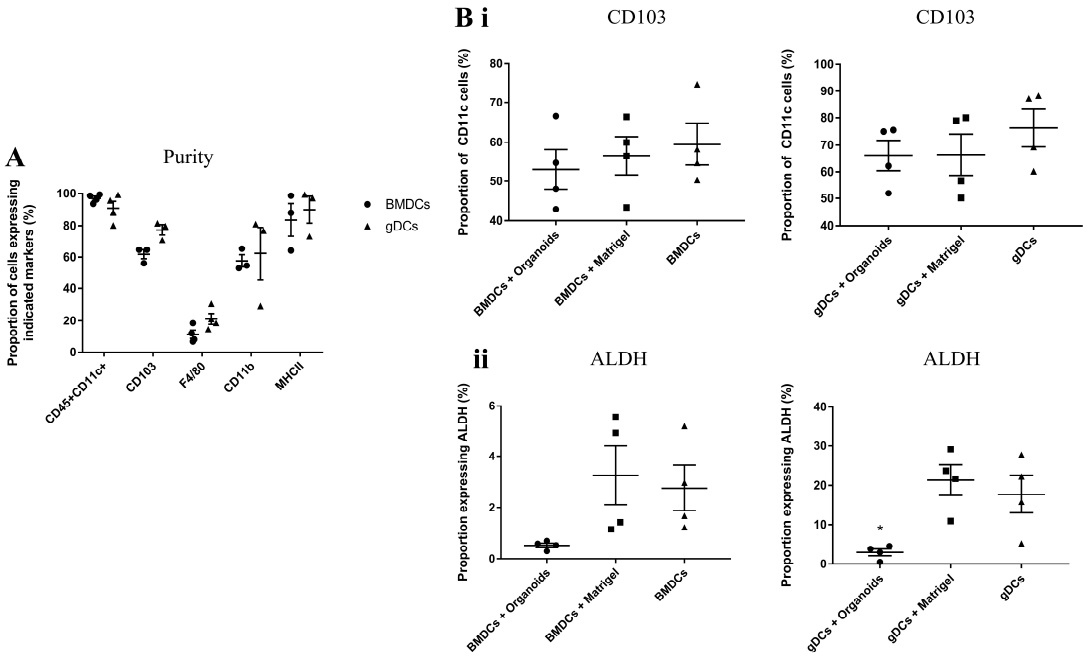

Figure 50. Coculture of DCs with organoids downregulates ALDH expression in DCs.
BMDCs and gDCs were cultured in Matrigel with B57Bl/6 organoids for 24h before analysing by flow cytometry. **A**, BMDCs and gDCs were analysed by flow cytometry and cultured with organoids. **B**, After 24h, cocultures were analysed by flow cytometry for changes in **i)** CD103 and **ii)** ALDH. Data pooled from 4 independent experiments. For purity data, 3 results were obtained for CD103, CD11b, and MHCII staining. Duplicate samples per condition. Graphs plotted as means +/- SEM. *P<0.05 One-way ANOVA with Tukey's comparison test.

5.3.9 Retinol does not increase ALDH expression in DCs in culture with organoids

The downregulation in ALDH expression in DCs may be due to a lack of dietary vitamin A for the epithelial cells to metabolise into RA that would induce DCs to express ALDH. The small intestinal epithelium is known as a major source of RA in the SI LP, and DCs in the SI LP are conditioned by the presence of RA. Therefore, providing organoids with a metabolite of vitamin A to increase production of RA may induce DC conditioning in cocultures. Retinol (ROL), a precursor to RA, was added to organoid samples cocultured with BMDCs or gDCs in Matrigel as described above. DCs were analysed after 24h of culture by flow cytometry (Figure 51). The proportion of DCs expressing CD103 remained unchanged (Figure 51Bi) whereas

ALDH expression declined in both BMDC and gDC cocultures supplied with ROL, although only significantly in gDCs ($P < 0.05$) (Figure 51Bii). Therefore, provision of retinol was not sufficient to maintain or induce expression of ALDH in DC.

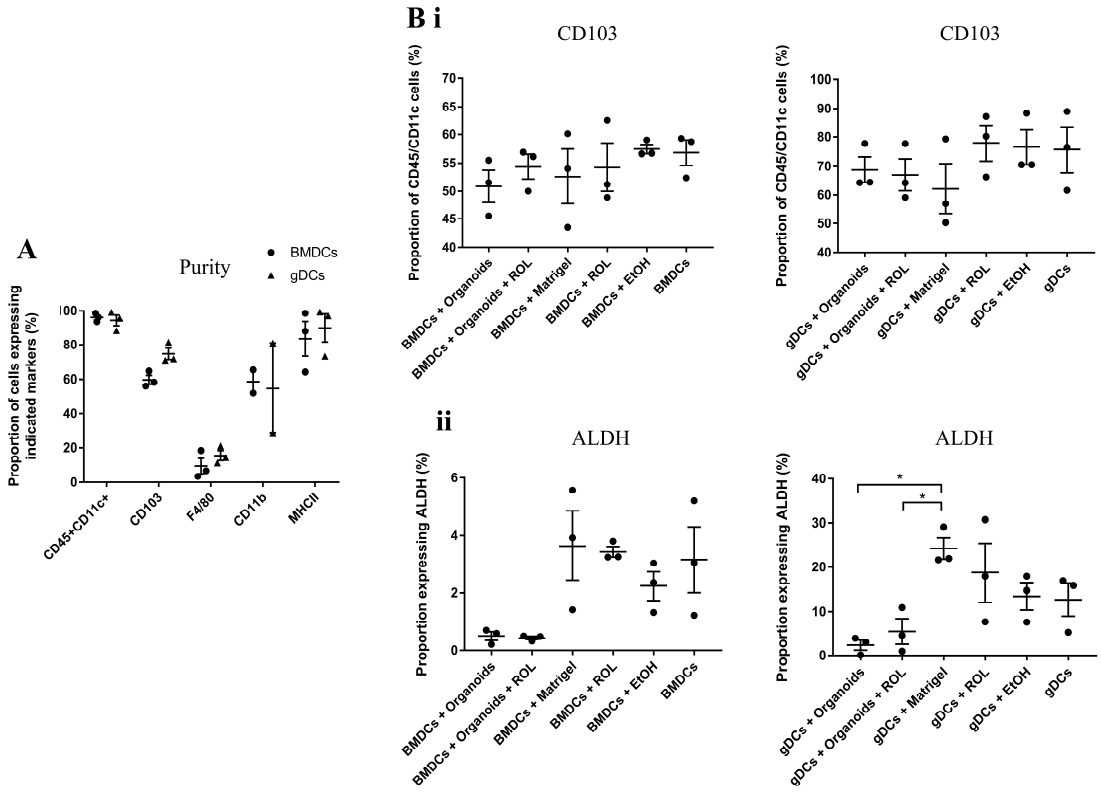

Figure 51. Addition of retinol to organoid cocultures does not increase ALDH expression in DCs.
BMDCs and gDCs were added to the Matrigel of organoid samples and cultured for 24h in the presence of Retinol or vehicle control. Cocultures were removed from Matrigel and assessed by flow cytometry. (**A**) Flow cytometric analysis of purity and subset composition of BMDCs and gDCs prior to culture. (**B**) Flow cytometric analysis of CD103 expression on BMDCs (left) and gDCs (right) following organoid co-culture under the indicated conditions. (**C**) Flow cytometric analysis of ALDH expression on BMDCs (left) and gDCs (right) following organoid co-culture under the indicated conditions. Data are pooled results from 3 independent experiments. Duplicate samples per condition were analysed. Graphs depict mean +/- SEM. *P <0.05, one-way ANOVA with Tukey's means comparison test.

5.3.10 Dendritic cell subset composition is not altered by co-culture with organoids

Studies suggest that the SP cDC2 subset can be conditioned to become CD103$^+$ by exposure to TGF-β, RA from IECs or by direct contact with the small intestinal

epithelium (McDonald *et al.*, 2012; Bain *et al.*, 2017). Therefore, addition of DCs to organoid cultures may induce an increase in the DP cDC2 subset. However, following co-culture with organoids for 24h, the subset composition of BMDCs and gDCs (as defined by CD11b and CD103 expression) remained unchanged (Figure 52).

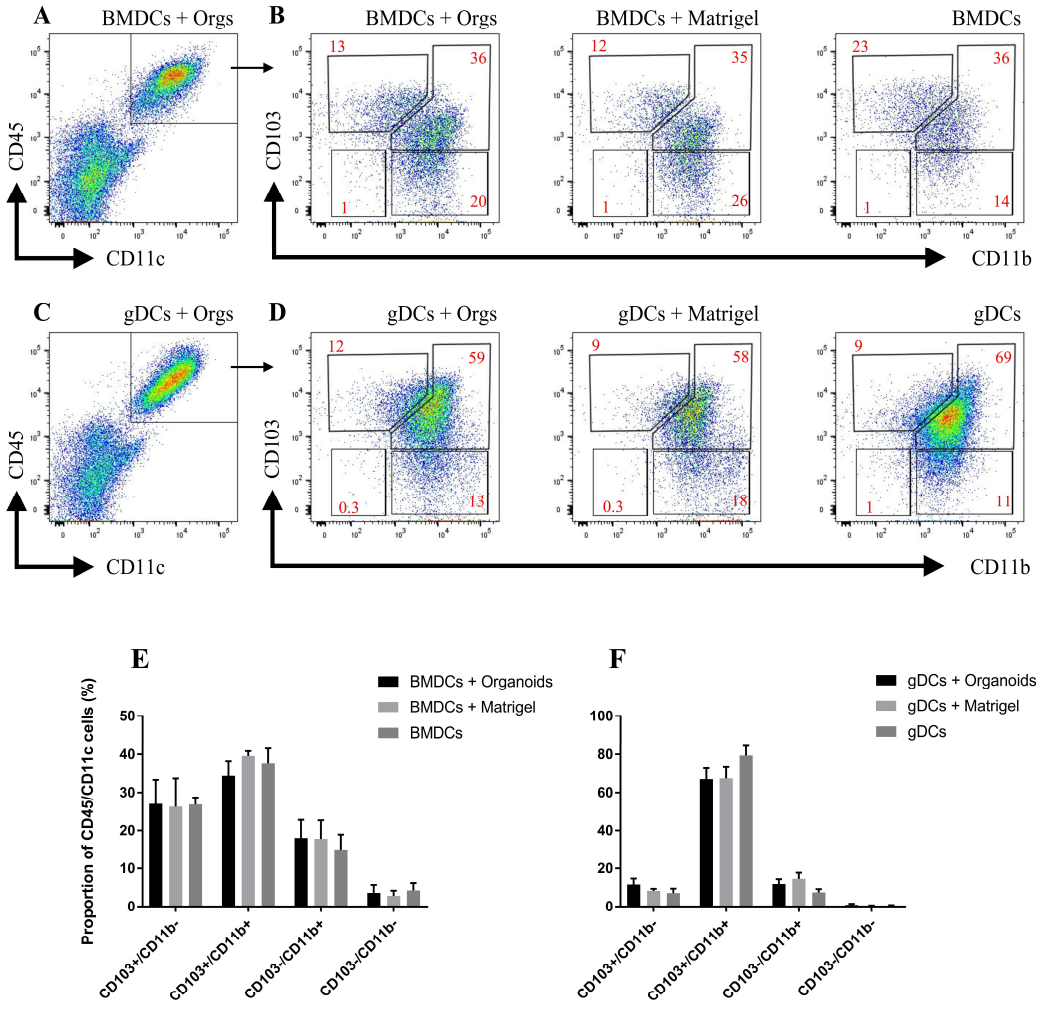

Figure 52. Cocultures of DCs with organoids do not affect subset proportions
BMDCs and gDCs were cultured in Matrigel with organoids for 24h and analysed by flow cytometry. **A**, BMDC cocultures were gated for CD45+CD11c+ cells as represented here. **B**, CD45+/CD11c+ BMDCs were analysed for CD103 and CD11b expression. **C**, gDC cocultures were gated for CD45+CD11c+ cells as represented here. **D**, CD45+/CD11c+ gDCs were analysed for CD103 and CD11b expression Data representative of 3 independent experiments. **E**, the differing expression profiles were quantified for BMDC cocultured with organoids for 24h. **F**, the differing expression profiles were quantified for BMDC cocultured with organoids for 24h. Results show pooled data from 3 independent experiments. Graphs plotted as means +/- SEM. No significant differences, one-way ANOVA with Tukey's means comparison test.

5.3.11 Injections of CpG into organoids does not maintain ALDH expression in DCs

Exposure of organoids to ROL alone may not be sufficient to induce ALDH expression in DCs and may depend on other stimulatory factors such as TLR signalling that induce IECs to express factors known to condition DCs. For example, TLR9 is responsible for detecting unmethylated CpG sequences in pathogen-derived DNA in host cell endosomes. TLR9 signalling in IECs stimulates the production of galectin-9, a factor that drives ALDH expression in DCs (De Kivit *et al.*, 2017; Hayen *et al.*, 2018). Therefore, subjecting organoids to TLR9 stimulation may support ALDH expression in BMDCs and gDCs. To restrict TLR9 stimulation largely to IECs, 5µM CpG ODN was microinjected into the lumen of organoids. At least 10 organoids per sample were injected and PBS was microinjected as a vehicle control. An additional control for physical damage to the organoids was also performed, with organoids being pierced with the microneedle but not injected. 24h later, BMDCs and gDCs were added to the cultures for a further 24h before being analysed by flow cytometry (Figure 53 and Figure 54).

CD11c expression was used to distinguish DCs from epithelial cells, which were then analysed for CD103, CD11b, ALDH, and CCR7 expression. Firstly, BMDC cultures were analysed and those in culture with organoids injected with CpG only slightly increased ALDH expression in BMDCs compared to PBS and piercing controls (Figure 53). However, ALDH expression was still lower than in BMDCs cultured alone (Figure 53 and Figure 55A). This reduction in ADLH expression may be due to the lack of a costimulatory factor in organoids to induce ALDH expression in BMDCs or through

the presence of inhibitory factors expressed by organoids. CCR7 is a chemokine receptor in cDCs that is upregulated upon acquisition of antigen for migration to MLNs and was assessed in these microinjection cocultures. There were greater proportions of BMDCs expressing CCR7 when in culture with organoids (Figure 55B).

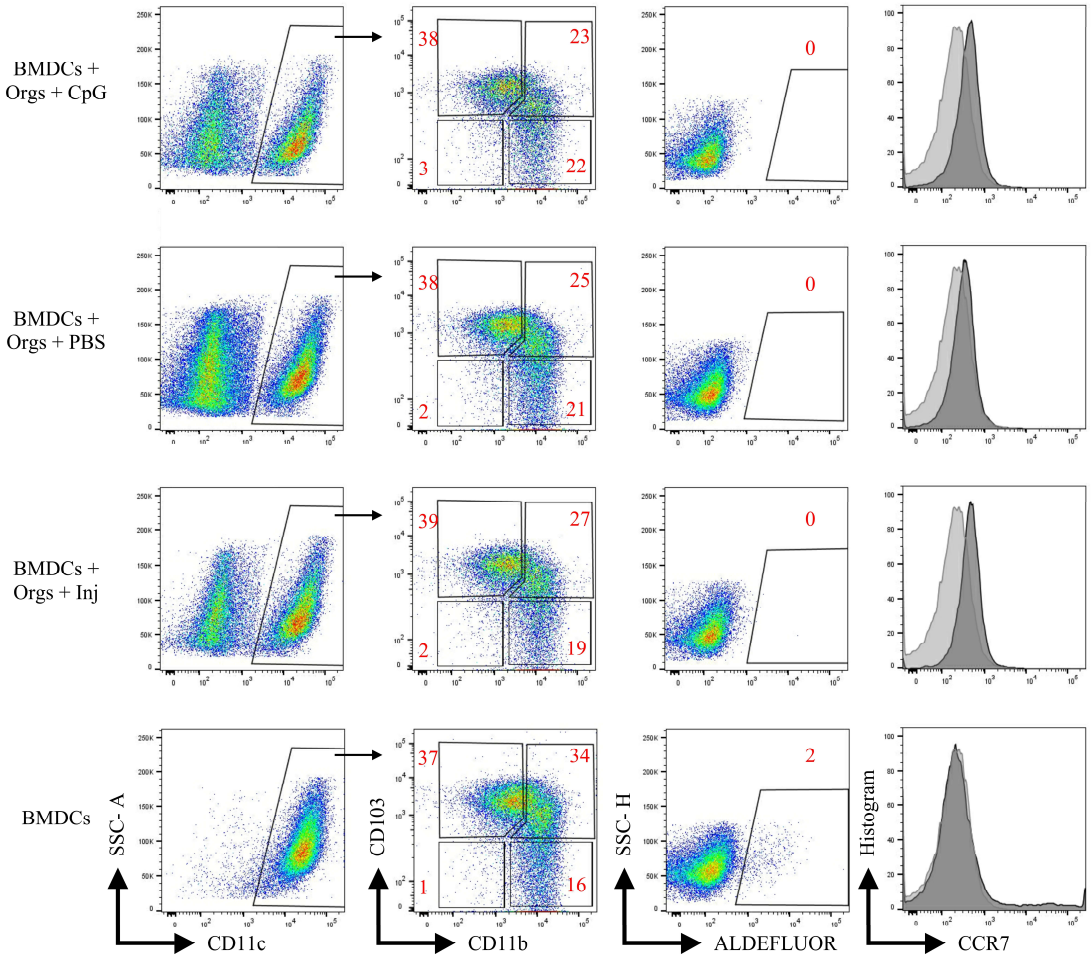

Figure 53. Microinjections of CpG into the lumen of organoids does not increase ALDH expression in cocultured BMDCs.
Organoids were microinjected with 5μM CpG ODN into the luminal space and incubated for 24h. As controls, organoids were microinjected with PBS and others pierced with a microneedle (BMDCs + Orgs + Inj). BMDCs were added to the Matrigel of organoid samples and assessed by flow cytometry after 24h. Cells were analysed for CD103, CD11b, ALDH and CCR7 after gating for CD11c+ cells. Light grey overlay in CCR7 histograms represent CCR7 isotype control. Data representative of one independent experiment. Duplicate samples for BMDCs + Orgs + CpG and BMDCs + Orgs + PBS. Single samples for BMDCs + Orgs + Inj and BMDCs.

The gDC cocultures were also assessed for ALDH and CCR7 expression. The gDCs co-cultured with CpG-stimulated organoids still showed a reduction in ALDH expression compared to gDCs cultured alone, but this reduction was less than in the presence of PBS-injected, or microneedle pierced organoids (Figure 54 and Figure 55A). Since gDCs and BMDCs cultured in Matrigel alone with organoid medium did not affect ALDH expression, it is likely that the organoids are producing inhibitory factors that prevent ALDH expression. As with BMDC coculture samples, CpG may be acting to counteract these inhibitory effects in gDC cocultures. Repeated experiments are required to verify this, with possible improvements by increasing CpG concentration and the number of injected organoids. These preliminary results also indicate an increase in CCR7 expression in gDCs in culture with injected CpG, PBS, or microneedle pierced organoids (Figure 55B).

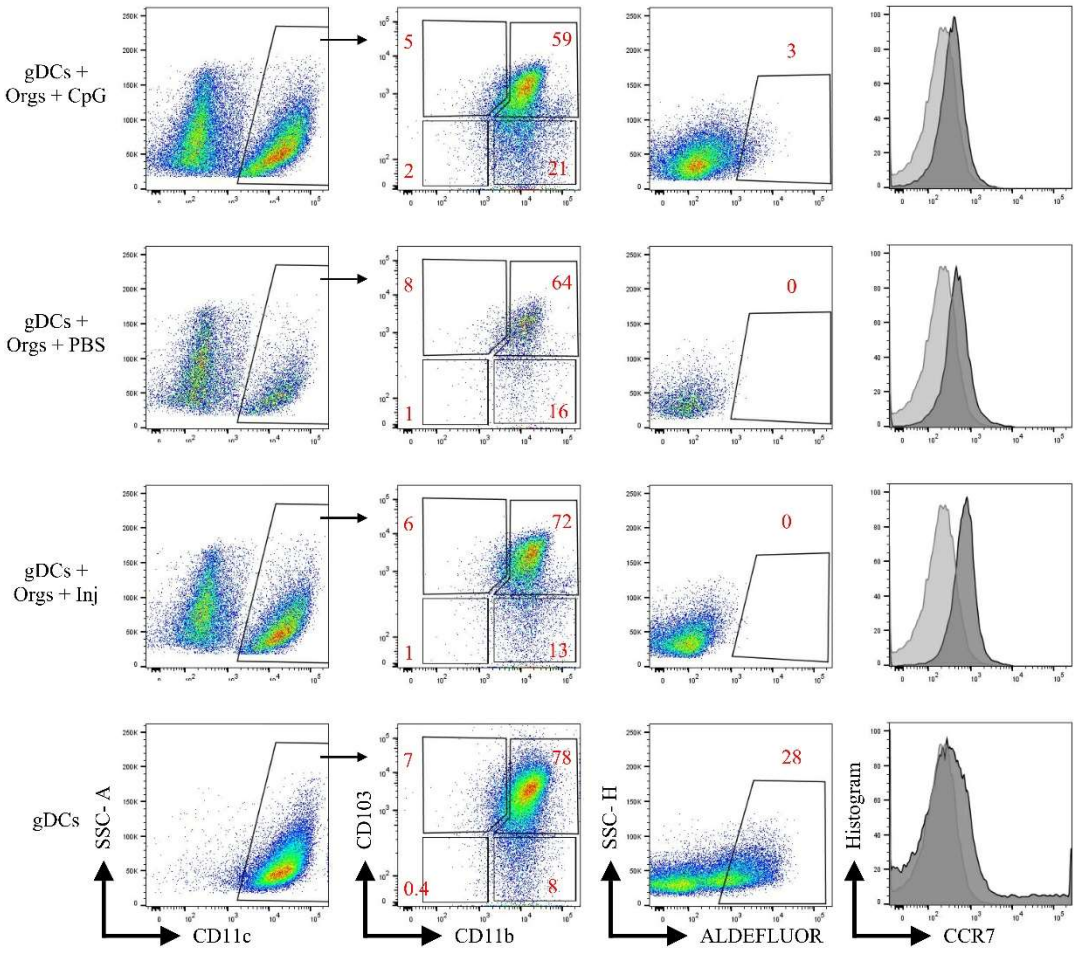

Figure 54. Microinjections of CpG into the lumen of organoids does not increase ALDH expression in cocultured gDCs.

Organoids were microinjected with 5µM CpG ODN into the luminal space and incubated for 24h. As controls, organoids were microinjected with PBS and others pierced with a microneedle (gDCs + Orgs + Inj). The gDCs were added to the Matrigel of organoid samples and assessed by flow cytometry after 24h. Cells were analysed for CD103, CD11b, ALDH and CCR7 after gating for CD11c+ cells. Light grey overlay in CCR7 histograms represent CCR7 isotype control. Data representative of one independent experiment. Duplicate samples for gDCs + Orgs + CpG and gDCs + Orgs + PBS. Single samples for gDCs + Orgs + Inj and gDCs.

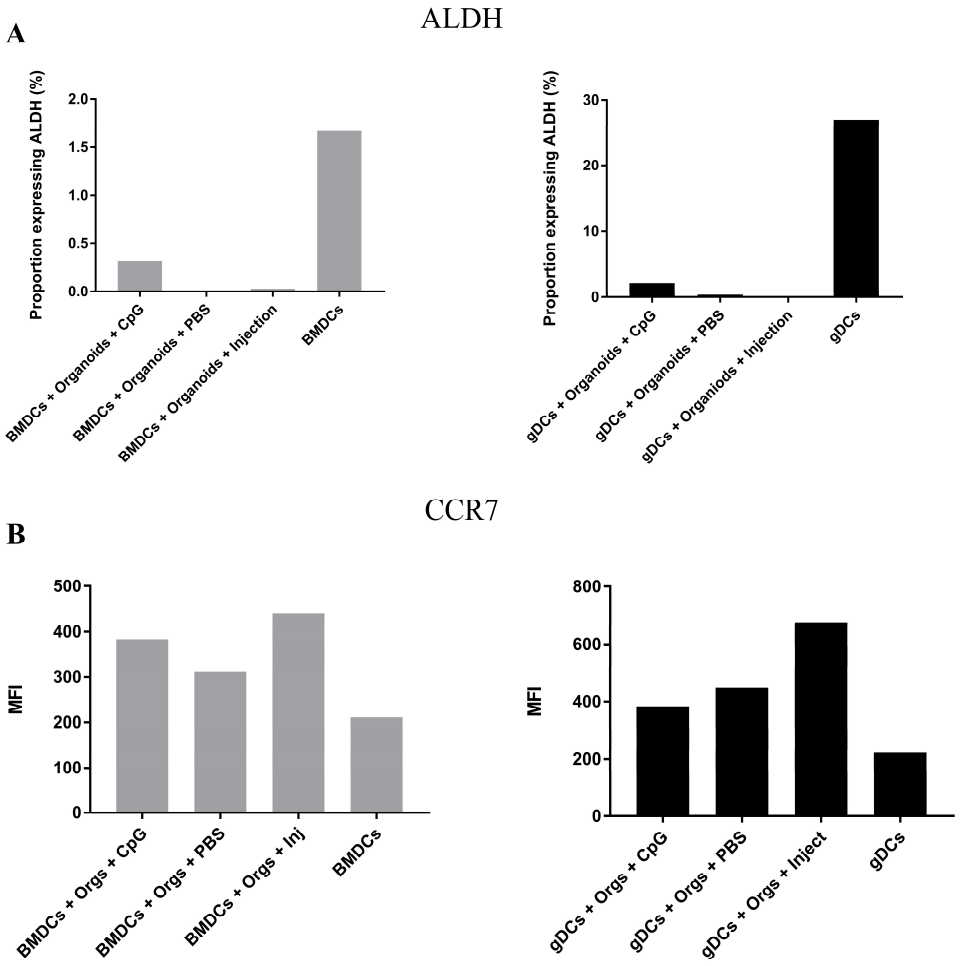

Figure 55. Organoids microinjected with CpG limited the reduction in ALDH expression in BMDCs and gDCs
Organoids were microinjected with 5μM CpG ODN into the luminal space and incubated for 24h. As controls, organoids were microinjected with PBS and others pierced with a microneedle (DCs + Orgs + Inj). DCs were added to the Matrigel of organoid samples and assessed by flow cytometry after 24h. Cells were gated for CD11c and quantified for expressing ALDH in (**A**) BMDCs and (**B**) gDCs. Data representative of one experiment. Duplicate samples for cocultures with CpG and PBS. Single samples for pierced organoids and DCs.

5.3.12 Organoids infected with *T. gondii* causes a change in DC morphology

Intestinal DCs play a dual role in *T. gondii* infection: they produce IL-12 to drive protective IFN-γ responses, and their migratory pathways are co-opted by the parasite to aid its spread throughout the body. At present, it is uncertain how *T. gondii* migrates across the small intestinal epithelium to infect DCs, how the infected epithelium communicates with DCs to initiate protective responses, and

how DCs influence IECs during infection. Cocultures of infected organoids and intestinal DCs would provide a valuable tool in evaluating these questions.

ROSA$^{mT/mG}$ organoids were infected with the Cre-expressing line of *T. gondii* Pru-tdTomato as described above (chapter 2.5, page 100). Infected samples were incubated for 24h to allow epithelial cells to mount an inflammatory response to infection, as well as allowing for any remaining extracellular parasites to perish. It was hoped that this approach would limit direct infection of DCs by tachyzoites that had not first come into contact with the small intestinal epithelium. As a further control, *T. gondii* was incubated in Matrigel in the absence of organoids. After 24h, gDCs were labelled with CFSE and added to infected and uninfected organoids in Matrigel, and to Matrigel containing *T. gondii* alone. Live imaging was performed by two-photon microscopy. Z-stack images were obtained from samples over a 1h period at 2-minute 40 second intervals. The increased time intervals in comparison to previous DC/organoid coculture imaging experiments allowed for deeper z-stacks to be acquired, anticipating potential increased motility in gDCs. Time-lapse images were analysed by Imaris software using the 'surfaces' function to quantify gDC motility as before (Figure 56).

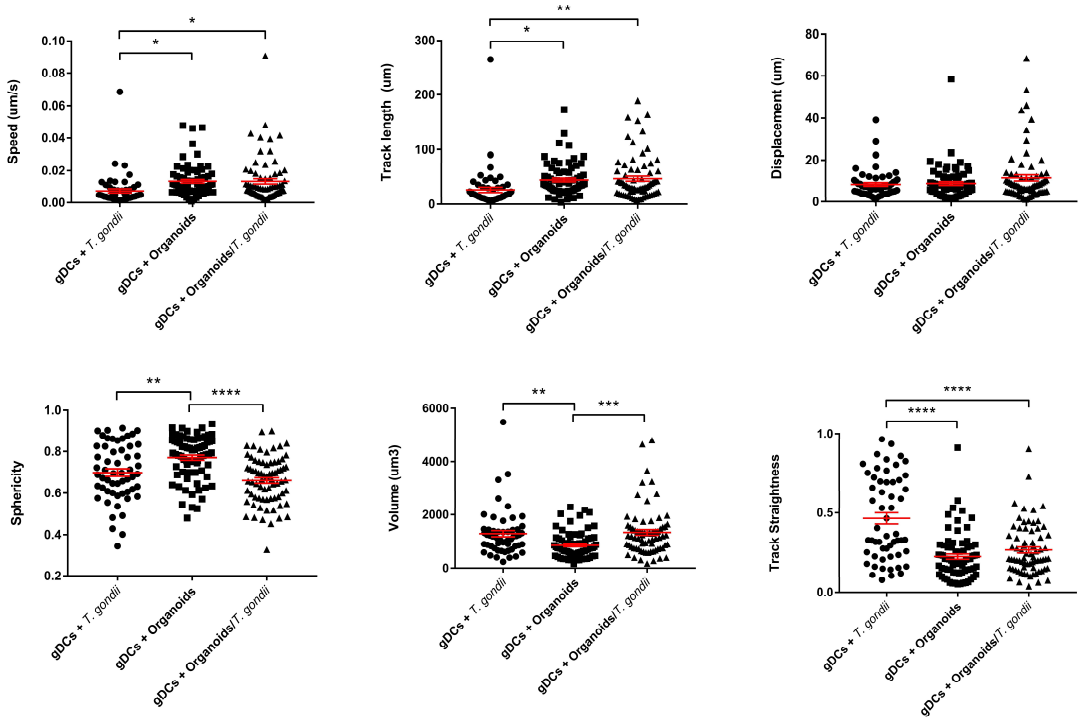

Figure 56. Organoids infected with *T. gondii* do not affect gDC motility but affects gDC morphology
Organoids from ROSA$^{mT/mG}$ mice were infected with *T. gondii* Pru-tdTom-Cre as described previously. Cocultures of infected organoids with gDCs and gDCs with *T. gondii* in Matrigel were imaged over a 1h period at 2:40min intervals to generate a 3D time-lapse image. Motility of gDCs was quantified to obtain measurements for mean speed, track length and displacement and straightness, sphericity, and volume. Data representative of 3 independent experiments. Duplicate images obtained per sample, one sample per condition. *P <0.05, **P <0.005, ***P <0.0005, ****P <0.0001, one-way ANOVA with Tukey's means comparisons test.

Organoids infected with *T. gondii* did not have any significant effects on gDC motility when compared to uninfected organoids (Figure 56). However, gDCs in culture with organoids regardless of infection affected gDC motility compared to gDCs in culture with *T. gondii* alone. The gDCs in culture with organoids had a higher mean speed and longer track length but had a reduced track straightness indicating confinement of their increased motility (Figure 57B, Movie S14). The gDCs cultured with *T. gondii*-infected organoids were larger and had more cytoplasmic projections (indicated by volume and reduced sphericity, respectively)(Figure 57C, Movie S15) than gDCs cultured with uninfected organoids. However, these alterations in gDC

morphology were also observed when gDCs were cultured with *T. gondii* alone, suggesting that communication with the epithelium played no significant role (Figure 57, Movie S13). No differences were observed in the proportion of gDCs contacting the organoid surface in the presence or absence of infection. In some instances, gDCs extended and retracted processes that connected to infected organoids, although this was never observed at sites of infection (Figure 58).

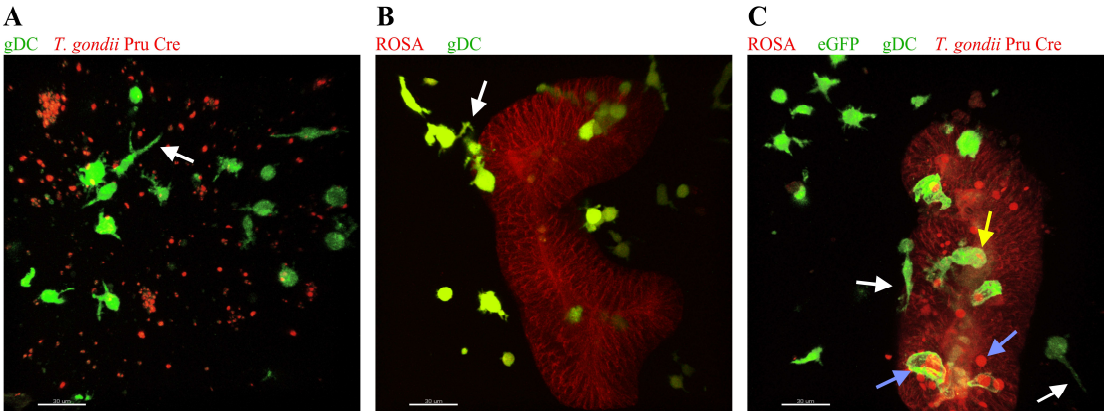

Figure 57. Cultures of gDCs with *T. gondii* appear to contain more projections than in uninfected organoid cultures
Infected and uninfected ROSA$^{mT/mG}$ organoids were cultured with gDCs labelled with CFSE, and gDCs were cultured with *T. gondii* Pru-tdTom-Cre as a control. Time-lapse images were acquired over a 1h period at 2:40min intervals using 2-photon microscopy. **A**, Single timepoint from a two-photon movie showing gDCs (green) cultured with *T. gondii* (red) in Matrigel. White arrow indicates extended dendrite. Whole images can be viewed in Movie S13. **B**, Single timepoint from a two-photon movie showing gDCs (green) cultured with organoids (red) in Matrigel. White arrow indicates extended dendrite. Whole images can be viewed in Movie S14. **C**, Single timepoint from a two-photon movie showing gDCs (green) cultured with organoids (red) infected with *T. gondii* (red) in Matrigel. White arrow indicates extended dendrite. Blue arrows indicate examples of infected eGFP^{+} cells and infected eGFP^{-} cells. Whole images can be viewed in Movie S15. Figures representative of 3 independent experiments.

Although gDCs were not directed toward infected cells, there were some indications that infections affected gDC behaviour. On one occasion, a gDC attached to an organoid extended a projection along the surface towards a newly infected cell (Figure 59A, Movie S16). Due to the *T. gondii* parasite being singular and therefore having not replicated, and its closeness to the surface of the organoid, it is possible that this is an early stage of infection (Figure 59B).

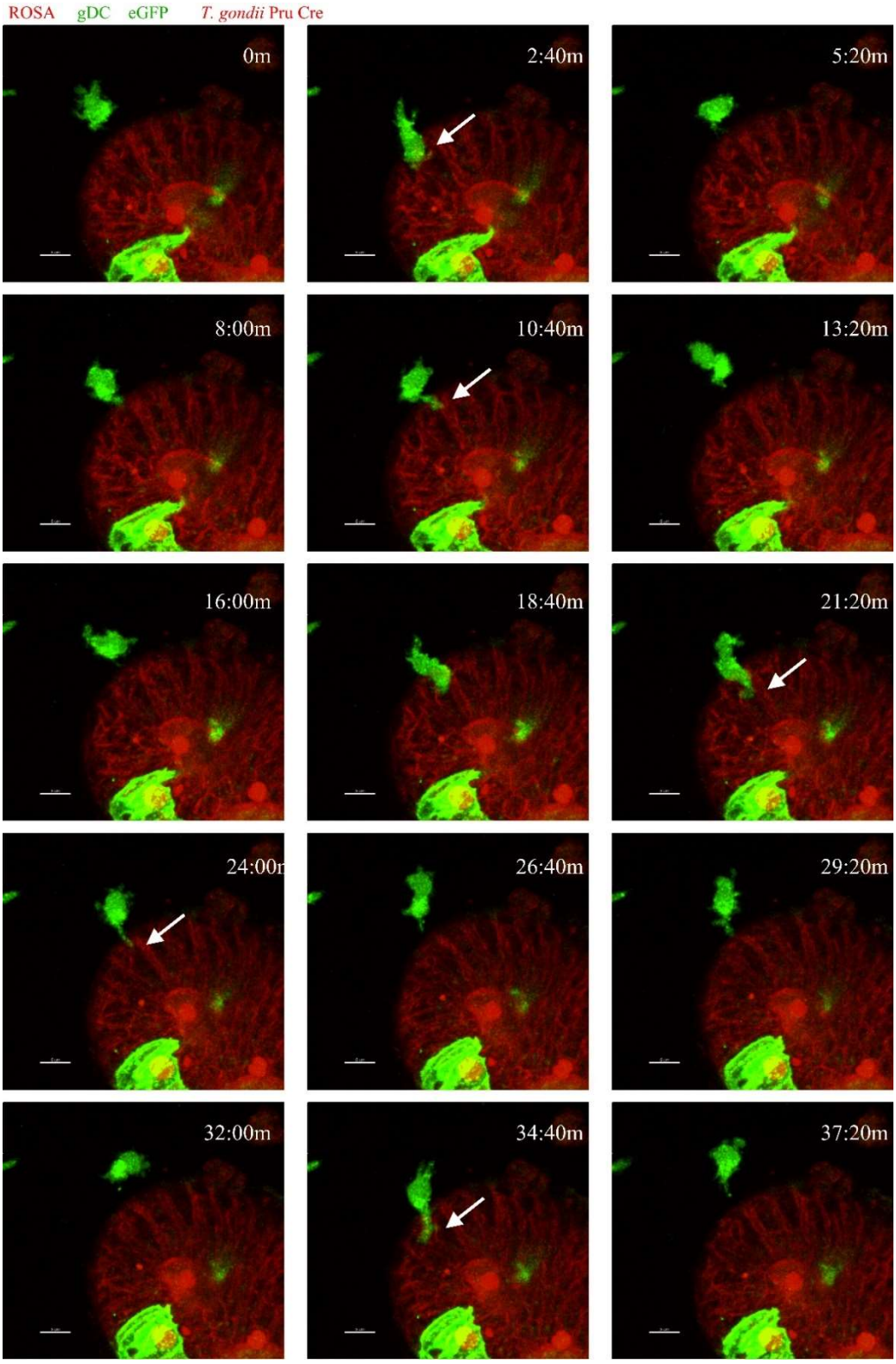

Figure 58. Gut-like DCs establish connections with the surface of organoids through the extension of processes.

Organoids from ROSA$^{mT/mG}$ mice were infected with *T. gondii* Pru-tdTom-Cre as described previously. Cocultures of infected organoids with gDCs labelled with CFSE were imaged over a 1h period at 2:40min intervals to generate a 3D time-lapse image. Some gDCs extended processes that attached to the organoid surface (white arrows). Scale bar: 5µm

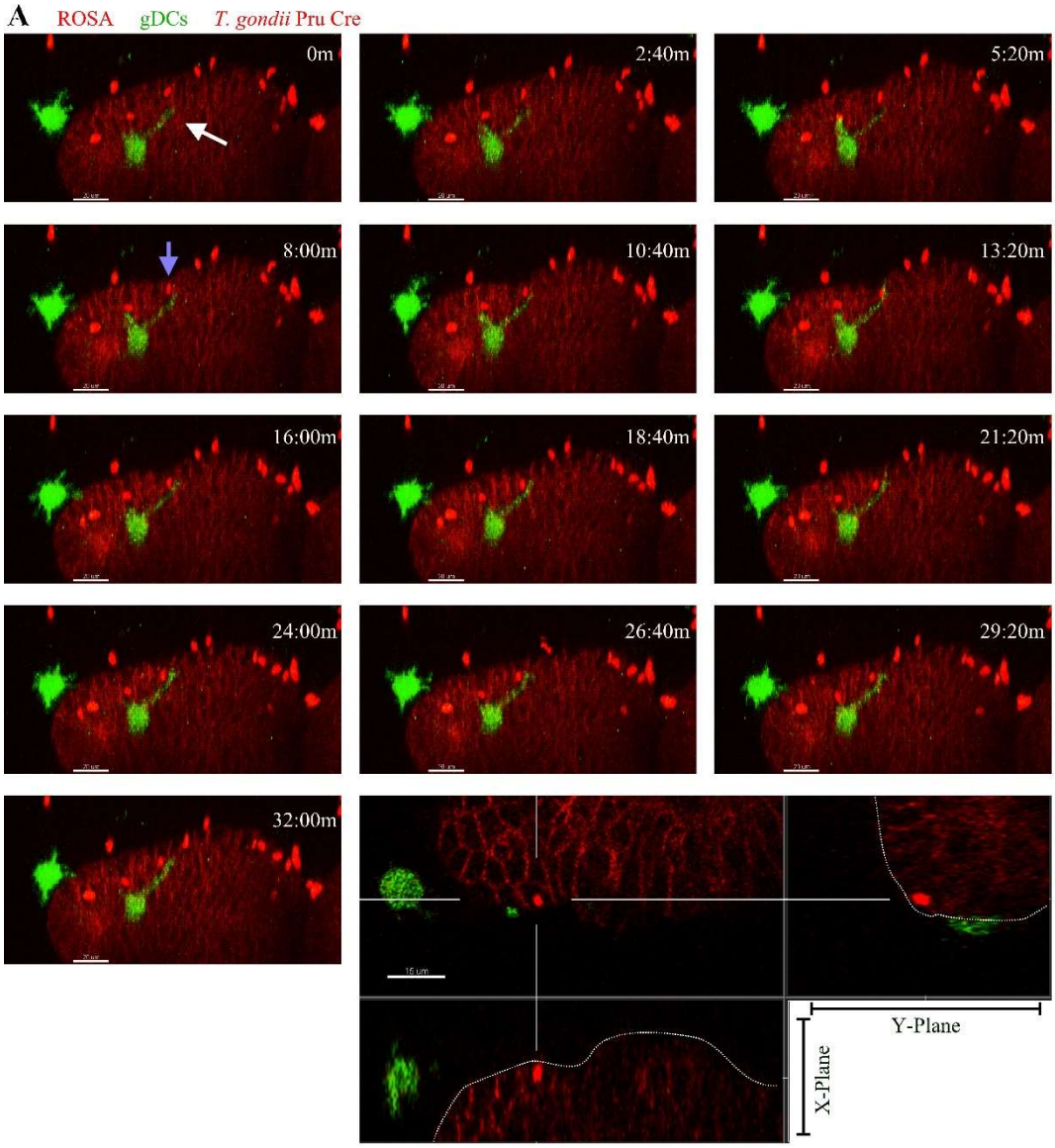

Figure 59.Gut-like DCs attached to the surface of organoids extend processes towards sites of infections. Organoids infected with *T. gondii* for 24h were cocultured with gDCs and time-lapse images were obtained as previously described. **A**. Attached gDCs to the surface of organoids extended processes (white arrow) towards sites of infection (blue arrow). **B**. Cross-section of infected organoids shows the parasite (blue arrow in **A**) within organoid cells (organoid surface marked with dotted line). Whole images can be viewed in Movie S16

5.3.13 Phagocytosed *T. gondii* are destroyed by gDCs

Intestinal DCs infected with *T. gondii* exhibit a hypermotile phenotype that aids in the dissemination of the parasite throughout the body (Fuks *et al.*, 2012; Weidner *et al.*, 2013; Kanatani *et al.*, 2017). However, *T. gondii* can also be phagocytosed and

destroyed by DCs. Cocultures of gDCs with organoids infected for 24h with *T. gondii* displayed gDCs with internalised parasites that lost fluorescence over a relatively short period of time indicating parasite death (Figure 60). Extracellular parasites were not seen to lose fluorescence intensity over the time-lapse periods. This gDC presented here did not undergo a hypermotile phenotype that only occurs after active invasion of a live parasite (Weidner and Barragan, 2014), suggesting this *T. gondii* was phagocytosed.

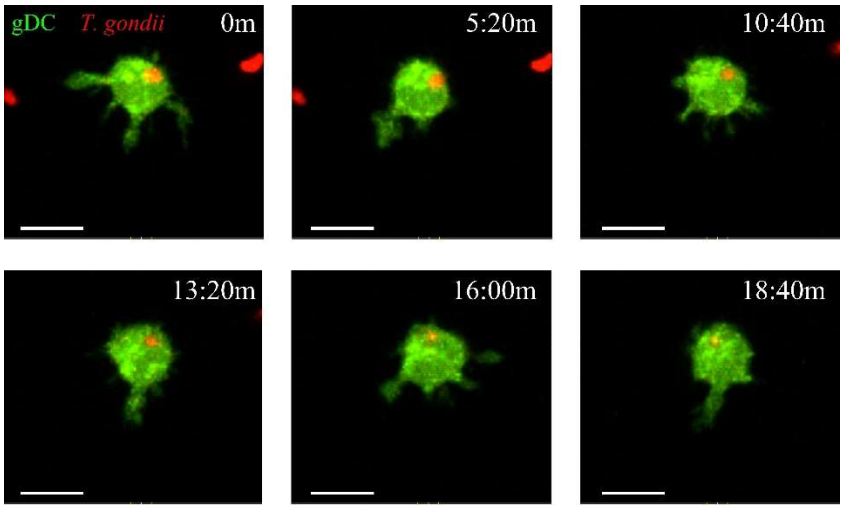

Figure 60. Phagocytosed *T. gondii* are destroyed by gDCs
Organoids from ROSA$^{mT/mG}$ mice were infected with *T. gondii* Pru-tdTom-Cre as described previously. Cocultures of infected organoids with gDCs labelled with CFSE were imaged over a 1h period at 2:40min intervals to generate a 3D time-lapse image. The gDC shown here contains a *T. gondii* that loses fluorescence indicating the death of the parasite. Scale bar 10µm

5.3.14 *Toxoplasma gondii*-invaded gDCs display a change in morphology

DCs infected with *T. gondii* increase in motility, a function that aids in parasite dissemination throughout the body (Fuks *et al.*, 2012; Weidner *et al.*, 2013; Weidner and Barragan, 2014; Kanatani *et al.*, 2017). Although the overall mean speeds of all gDCs in culture with infected organoids were similar to those in uninfected cultures, hypermotile gDCs that had been directly invaded by *T. gondii*

were present (Figure 61). These appeared during time-lapse imaging and moved through the Matrigel in elongated forms at a high speed.

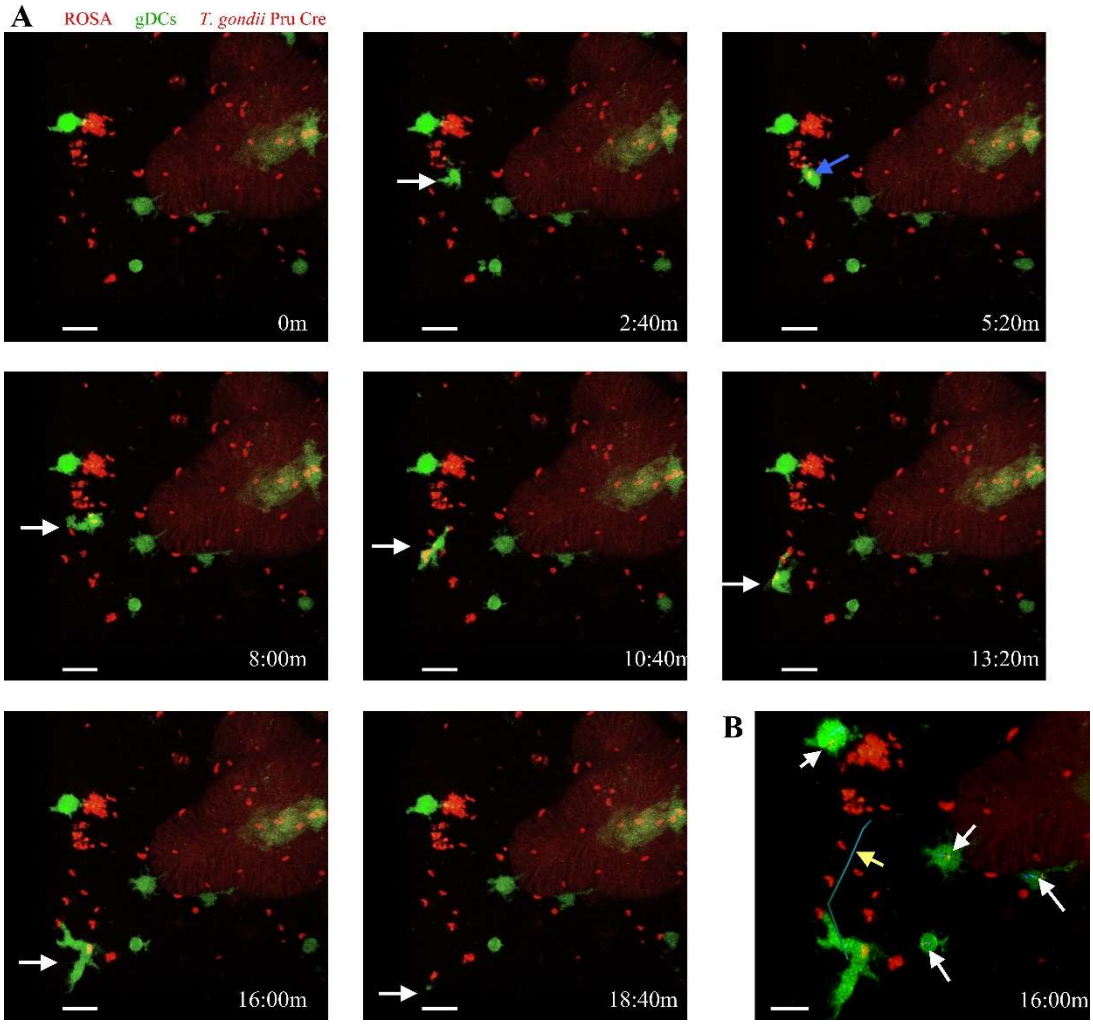

Figure 61. Infected gDCs exhibit a hypermigratory phenotype
Organoids infected with T. gondii were cultured with gDCs and time-lapse images were obtained using 2-photon microscopy (**A**)Individual timepoints from a two-photon movie showing T. gondii (red) invaded DCs (green) migrating in Matrigel. **B**. Individual timepoints from a two-photon movie showing the tracks of T. gondii invaded (yellow) and bystander (white) DCs across the whole imaging period. Scale bar: 20µm.

Only a subset of gDCs infected with *T. gondii* exhibited increased speed coupled with elongated morphology. Other infected gDCs remained immotile yet acquired an elongated morphology (Figure 63A). Others remained attached to the organoid surface and extended processes (Figure 63B). However, the majority of infected

gDCs did not increase in motility compared to uninfected gDCs (Figure 62). The observed changes in morphology in infected gDCs were quantified through measurements of sphericity and volume using Imaris software. Infected gDCs were similar in volume but significantly less spherical than non-infected gDCs in cocultures with infected organoids (Figure 62). This is indicative of the increased dendritic extensions of infected gDCs.

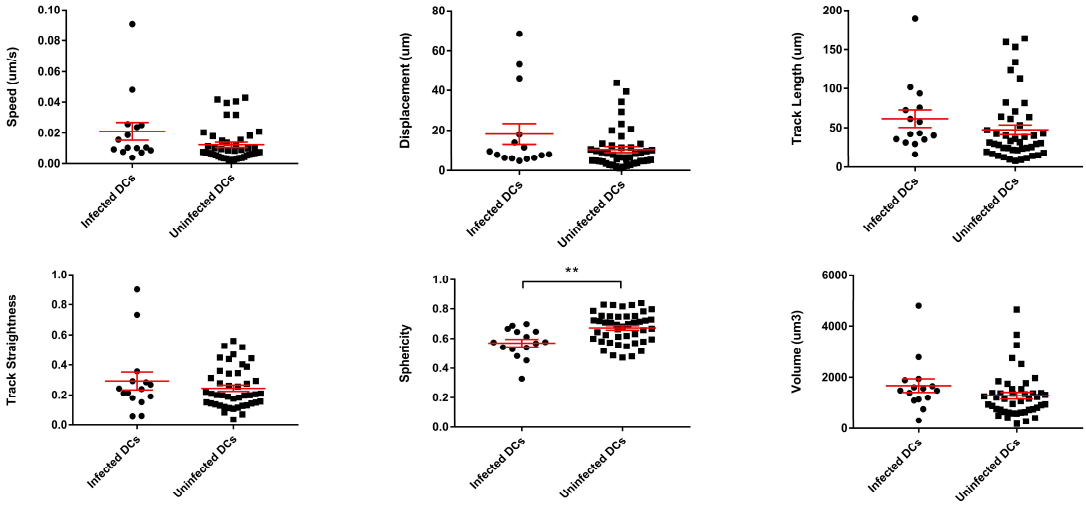

Figure 62. Infected gDCs exhibit reduced sphericity
Organoids infected with *T. gondii* were cultured with gDCs and imaged over a period of 1h at 2:40min intervals by 2-photon microscopy. Motility was assessed as speed (µm/s), displacement (µm), track length (µm), and track straightness, with morphology assessed as sphericity and volume (μm^3) of infected and non-infected gDCs. These parameters were quantified using Imaris software. **P <0.005. Unpaired sample t test with two-tailed P-value. Results show 3 independent experiments, 1 sample per condition with duplicate images obtained. Graphs show mean +/- SEM.

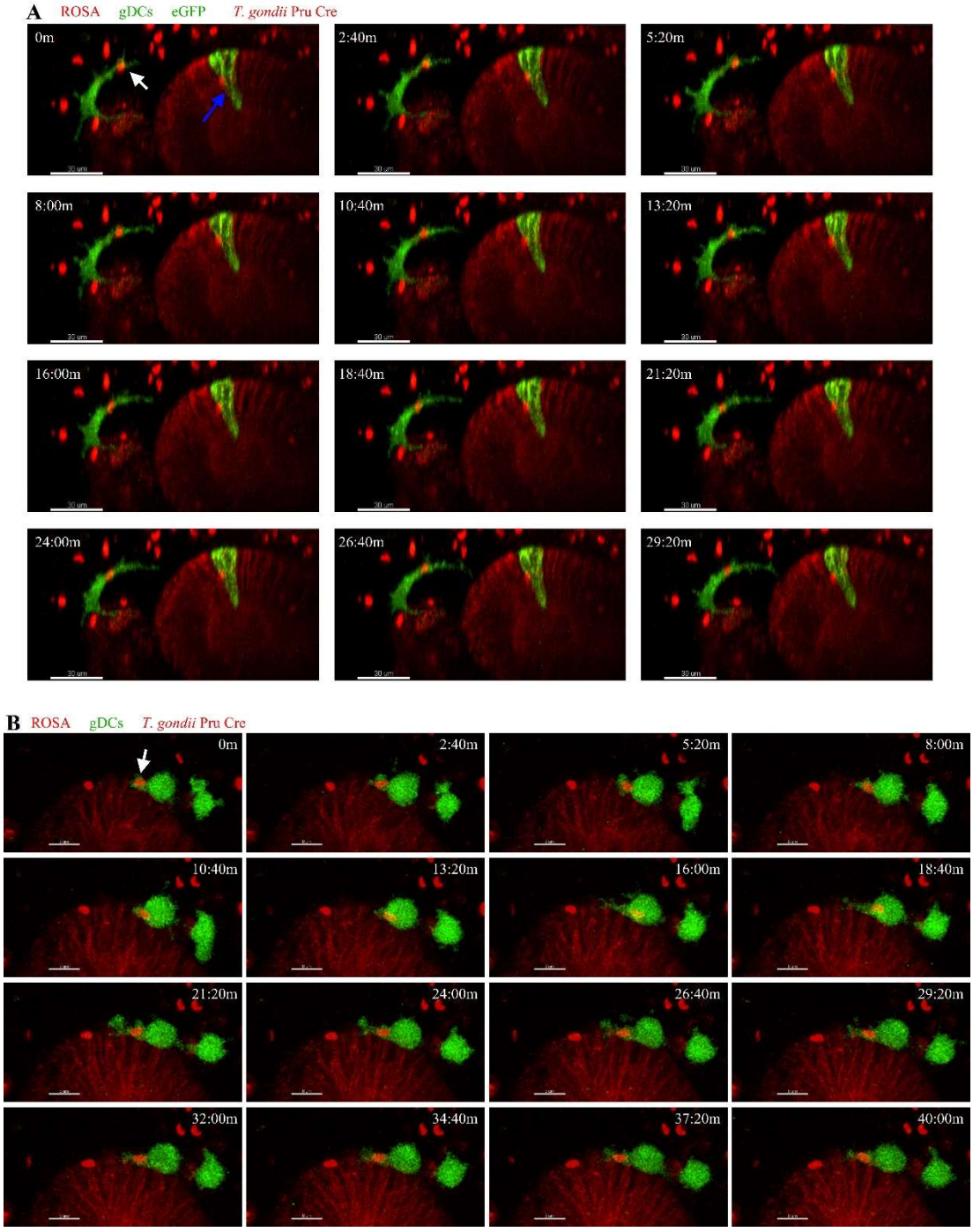

Figure 63. Infected gDCs exhibit elongated morphologies or remain attached to organoid surfaces and extend process.

Infected organoids were cultured with gDCs and time-lapse images obtained. **A**. Infected gDCs were observed to extend processes but remained immotile, with an elongated morphology. Scale bar 30um. **B**. Infected gDCs attached to organoids remained at the organoid surface with certain gDCs extending processes. In this instance, an infected gDCs possessed a parasite within its projection (white arrow) where it moved in both directions. Scale bar: 8µm

5.4 Discussion

DCs of the small intestinal lamina propria are key regulators of intestinal homeostasis, playing important roles in bridging innate and adaptive immune responses. Tolerance towards commensal microbiota is driven by DCs that impart a tolerogenic phenotype on certain immune cells, such as FoxP3 induction in T cells and IgA production in B cells. SI DCs derive from a common progenitor in the BM, with their development into pre-cDCs dependent on Flt3L. Upon their arrival to the SI LP pre-cDCs are exposed to GM-CSF from ILCs and stromal cells and high levels of RA derived from dietary vitamin A that are considered to condition them into intestinal DCs. The relatively recent improvements in defining markers for DCs and macrophages has meant that earlier studies into the functions on intestinal DCs are difficult to interpret. Intestinal DCs are now defined by expression of CD11c and the absence of F4/80 and/or CD64. Within this, they are further divided into four subsets based on expression of CD103 and CD11b. The cDC1 subset consist of $CD103^{+}CD11b^{-}$ cells that are most prominent in the colon LP. The cDC2 subset consists of $CD103^{+}CD11b^{+}$ (DP) and $CD103^{-}CD11b^{+}$ (SP) cells containing low to intermediate expression of CX3CR1, with DP cDC2s the most prominent in the SI LP. Recent studies in developing $CD103^{+}$ cells from BM have been inconsistent in their use of growth factors, with Flt3L, GM-CSF, RA, and IL-4 used. Many of these studies generated heterogenous populations of cDCs and macrophages with those cDCs lacking in subset specific transcriptional factors and surface markers of intestinal-like DCs. In our study, BM cells from untreated mice were cultured in Flt3L for 8 days with GM-CSF and RA added for the last 48h of culture to provide cells mostly

consisting of the DP cDC2 subset and, to a lesser extent, the SP cDC2 subset. This sequential exposure to growth factors mimics the signals in the BM and then the small intestine. The culture method provides a source of cells that are most prominent in the SI LP that is less technically demanding than other methods that require treatment of mice with Flt3L and sorting for pre-cDCs (Zeng *et al.*, 2016).

Very little is known about the earliest events following infection with *T. gondii* in the small intestinal epithelium, and the interactions between the parasite, the intestinal epithelium, and lamina propria cDCs (Courret *et al.*, 2006; Lambert *et al.*, 2006; Coombes *et al.*, 2013). It is thought that DCs are preferentially invaded by *T. gondii* in the small intestine, and migration of the invaded DCs contributes to parasite dissemination. However, the precise timing and molecular mechanisms underpinning this pathway remain unclear. Infection of all cDC subsets by *T. gondii* are overrepresented compared to other immune populations, with SP cDC2s suggested to be the preferentially invaded cDC subset in the SI LP (Cohen and Denkers, 2015). However, the DP cDC2 subset is the main migratory subset within the SI LP to MLNs in the steady state, and upon *Salmonella* infection of the small intestine is the first subset delivering pathogenic antigen to the MLNs (Bogunovic *et al.*, 2009). *T. gondii* experiments using animal models were analysed 7 days after infection, therefore DP cDC2s may have migrated from the intestinal epithelium within that time. In fact, DCs from foci of *T. gondii* infections in the epithelium were absent after 7 days infection, indicating that by this time DCs may have migrated away (Coombes *et al.*, 2013). Therefore, assessing *T. gondii* infections of the small intestinal epithelium with DP cDC2s during early infection, as in the model

presented here, may reveal interactions that have not previously been addressed. Protection against *T. gondii* infections relies on a Th1 response through IL-12 production by the cDC1 subset ($CD103^+CD11b^-$) (Cohen and Denkers, 2015), therefore the development of a culture system to develop these cells may also be useful for studying host pathogen interactions in *T. gondii* infections. Generation of bona fide cDC1 has recently been achieved through the exposure of BM progenitor cells to Flt3L and Notch signalling and could be adapted by the provision of RA to generate cDC1s with a gut-like phenotype (Kirkling *et al.*, 2018).

To develop bona fide cDCs in culture they would need to express characteristic transcription factors such as *Batf3* and *Irf8* in cDC1s and *Irf4* and *Notch2* in cDC2s. Previous studies that aimed to increase $CD103^+$ cells in BM cultures did not resemble *in vivo* populations. For instance, the addition of GM-CSF to Flt3L BM cultures produced $CD103^+CD11b^-$ cells that were $Id2^+$ but $Batf3^-$, therefore cannot be termed bona fide cDC1s since this subset requires the expression of both transcription factors (Jackson *et al.*, 2011). The expression of *Batf3* is induced in prolonged cultures with Flt3L and GM-CSF, however these cells are also $CD103^+CD11b^+$ whereas *Batf3* is expressed in cDC1s only (Mayer *et al.*, 2014). Cell surface expression profiles are also important in defining cDC subsets, such that pre-cDCs cultured in Flt3L and GM-CSF lack TLR3 and Clec9a on cDC1s, and TLR11 and CD101 on cDC2s (Zeng *et al.*, 2016). RA is a key component in generating cDCs from Flt3L and GM-CSF cultures to improve the similarities in transcription factors and cell surface markers of cDC1s and cDC2s to their *in vivo* counterparts, however this technique involves the pre-treatment of mice with Flt3L and subsequent sorting

of BM cells for pre-cDCs (Zeng *et al.*, 2016). Nonetheless, the addition of RA to pre-cDC BM cultures downregulates *Irf4* expression in cDC1 populations, and increases *Irf4* and *Notch2* in cDC2s, thereby also increasing the generation of cDC2 populations (Zeng *et al.*, 2016). RA also increases cell surface markers TLR3 and Clec9a in cDC1s, and TLR11 and CD101 in cDC2s providing a culture with cDCs that more closely resembles the cDC subsets *in vivo*. In our study we have developed a culture method to generate a large population of cDC2s most prominent in $CD103^{+}CD11b^{+}$ cells that resemble the phenotype of gut-like cDCs. Further characterisation of this newly developed culture by qPCR or RNA-Seq would be necessary to assess transcriptomic profiling that will determine the conditioning levels of cDC subsets and their relevance to bona fide intestinal cDCs.

To further evaluate the relevance of these cultured gut-like DCs, comparisons were made to DCs isolated from the SI LP. A protocol was optimised to purify SI LP DCs from mice and assess their phenotype by flow cytometry. Using MACS enrichment for CD11c provided a heterogenous population of DCs and macrophages based on F4/80 expression. However, a proportion of $F4/80^{+}$ cells also expressed CD103. It has been suggested that DCs can have low levels of F4/80 expression (Sichien *et al.*, 2017), although this is controversial and is generally considered that DCs of the SI LP are $F4/80^{-}$. The addition of CD64 macrophage marker may add further clarification to this discrepancy in the literature. Within our study, it was considered that any level of F4/80 expression renders the cell a macrophage. DP cDC2s were the dominant subset of DCs isolated from the LP, which reflects previous studies of the conformation of cDC subsets in the small intestine (Denning *et al.*, 2011; Scott *et al.*,

2015). The BM cultures in our study produce cDCs with a subset composition representative of those found in the SI LP and is therefore a relevant culture method. DCs from the LP contain similar, low proportions of $ALDH^+$ cells in all subsets bar the DN cDC2 subset that contain almost no ALDH expression (Cohen and Denkers, 2015). In our BM cultures all the cDC subsets bar the DN cDC2s have a greater proportion of ALDH expression than those found in the SI LP. The higher proportion of $ALDH^+$ cells may also indicate a greater quantity of tolerogenic cDCs since RA suppresses pro-inflammatory NF-κB target genes, particularly in the cDC1 subset (Zeng *et al.*, 2016).

CD103 attaches to E-cadherin on the epithelial cell surface and allows close contact to the small intestinal epithelium for conditioning during resting and infective states. The close association also allows for the transfer of antigens from the lumen for subsequent migration to MLNs and T cell induction. However, the importance of CD103 itself in this close association is uncertain since DCs from *CD103*$^{-/-}$ mice had the same ability to induce gut-homing receptors on T cells, suggesting conditioning was intact (Jaensson *et al.*, 2008). However, the contact between $CD103^+$ cDCs and the small intestinal epithelium may improve reaction time to infections. Interactions between organoids and BM-derived DCs or those isolated from the SI LP were assessed and compared using time-lapse imaging by 2-photon microscopy, with SI LP DCs displaying a greater motility than those cultured from BM. Other studies have imaged DCs in the small intestine and have shown that $CD103^+$ DCs exhibit a relatively slow motility in the LP, although this was not quantified (Farache *et al.*, 2013). DCs within the epithelium itself and those crawling along the small intestinal

epithelium possess much greater motilities (Farache *et al.*, 2013). This was observed in our study with DCs isolated from the LP and cultured with organoids whereby the DCs attached to the organoid and crawled along its surface, however these DCs were not seen between organoid cells. This was also evident to some degree with gDCs at a slower average speed, and to a lesser extent in BMDCs whereby they remained fixed to organoid surfaces and extended processes along the surface. However, it has been suggested that the processing of small intestinal tissue through collagenase digestion to isolate DCs may elicit their activation which may suggest a possible reason why isolated SI LP DCs exhibit greater speeds and smaller volumes (Geem *et al.*, 2012). Another possibility is that since SI LP DCs are fully conditioned, DCs derived from BM cultures are likely less developmentally similar as they have not been exposed to the same factors. Also, the isolated SI LP DCs had a minor population of contaminating macrophages that may account for the small fraction of cells that exhibited greater speeds.

Studies have displayed the ability of DCs to sample the luminal space of the small intestine from the LP through transepithelial dendrites (Niess *et al.*, 2005; Chieppa *et al.*, 2006; McDole *et al.*, 2012; Farache *et al.*, 2013). These utilised intravital imaging in dual reporter mice expressing fluorescence proteins under the CD11c and CX3CR1 promoters. Although cDC2 cells express low to intermediate levels of CX3CR1, this marker was used to distinguish macrophages. Transepithelial sampling was only seen during *Salmonella* infections and occurred at a very low rate only by $CD11c^{+}CX3CR1^{-}$ cells, likely representing the cDC1 subset. Another study showed sampling by $CX3CR1^{+}$ cells that were defined as DCs, but now can't be distinguished

from macrophages due to the selection of inappropriate surface markers (Niess *et al.*, 2005; Chieppa *et al.*, 2006). In our study, only cultured gDCs that were conditioned with RA were observed sampling the lumen of organoids through transepithelial dendrites, seen twice in eight samples obtained. The gDC culture mostly consisted of DP cDC2s, that supposedly express low levels of CX3CR1 (Scott *et al.*, 2015; Joeris *et al.*, 2017). Therefore, transepithelial sampling may not be restricted to cDC1s as previously thought and does not require infection for this behaviour to be observed. Although differences in motility and volume were present between DCs in this study, gDCs exhibited similar characteristics to intestinal DCs in sampling behaviour and crawling along organoid surfaces. Further conditioning may improve their gut-like phenotype and since the final developmental stage is suggested to be within the SI LP, organoids may provide the necessary factors to achieve this.

The small intestinal epithelium is suggested to condition cDCs into a mucosal phenotype through expression of TSLP, TGF-β, and RA, and direct contact with E-cadherin through CD103 signalling (Rimoldi *et al.*, 2005; McDonald *et al.*, 2012; Yokota-Nakatsuma *et al.*, 2016; Bain *et al.*, 2017). RA plays a vital role in intestinal homeostasis and cDC development by increasing CD103 and ALDH expression (McDonald *et al.*, 2012; Zeng *et al.*, 2016). Epithelial cells are an important source of RA in the small intestine, therefore we assessed if organoids can condition BMDCs and gDCs towards gut like phenotypes. Unexpectedly, BMDCs and gDCs cocultured for 24h with organoids did not increase expression of either ALDH or CD103. On the contrary, ALDH production was repressed to only a tiny fraction of gDCs and BMDCs

which contrasts studies using a murine epithelial cell line for IEC-conditioned medium with DCs that resulted in their expression of ALDH (Iliev, Spadoni, *et al.*, 2009). Intestinal epithelial cells express ALDH1a1 for metabolising dietary vitamin A into RA that conditions DCs to produce RA themselves, therefore a possible reason for not increasing ALDH expression may be due to the lack of vitamin A (or retinol) for organoids to metabolise. However, retinol added to organoid cultures did not increase ALDH expression in either gDCs or BMDCs, resulting in the same level of suppression. Another source of RA in the intestine derives from stromal cells that also condition DCs to express RA. Stromal cells also express GM-CSF that is required to maintain RA expression in DCs (Vicente-Suarez *et al.*, 2015). The absence of a GM-CSF source in these coculture models may contribute to the reduction in ALDH in DCs, however, no reduction in ALDH expression was observed in gDCs and BMDCs cultured in Matrigel alone, where GM-CSF was also not present. This suggests the production of an inhibitory factor by the epithelium against ALDH expression. CCR7 is expressed on DCs during inflammation and infection of the small intestine, and the proportion of DCs expressing CCR7 in culture with organoids was greater than those DCs cultured alone. Inflammatory signals such as TNF have been implicated in the suppression of ALDH expression in DCs (Sato *et al.*, 2013). The suppression of ALDH along with the increase in $CCR7^{+}$ cells may suggest a possible inflammatory state of the organoids, however evaluating the cytokine expression in organoid cultures is necessary to confirm this. The microbiota influences intestinal homeostasis by inducing tolerogenic cytokine expression in immune cells derived by TLR signalling and metabolism of dietary products such as vitamin D and butyrate.

Without the presence of microbiota or dietary products to reverse the possible inflammatory signals expressed by organoids, DCs may be driven to an inflammatory phenotype.

Intestinal DCs bridge the innate and adaptive immune responses, driving tolerance to commensal bacteria and clearance of pathogens through inflammation. Infections of intestinal epithelial cells induce expression of cytokines and chemokines that attract DCs to the sites of infection (Cruickshank *et al.*, 2009). Infections of IEC monolayer cultures with *T. gondii* results in the production of varying cytokines including IL-8, TNF-α, CCL5, and IL-6, and antimicrobial peptides such as β-defensins (Ju, Chockalingam and Leifer, 2009; Morampudi, Braun and D'Souza, 2011; Guiton *et al.*, 2017; S.-W. Huang *et al.*, 2017). Low dose *T. gondii* infections result in a Th1 response, driven by the cDC1 subset through IL-12 expression. Direct invasion of intestinal DCs, preferential in the SP cDC2 subset, decreases IL-12 and ALDH expression, whereas uninfected DCs increase expression of these factors (Cohen and Denkers, 2015). Due to lack of relevant models, early DC responses following infection of the small intestinal epithelium with *T. gondii* have not been studied. Current models rely on live animals inoculated with the parasite and intestinal DCs assessed days after infection due to difficulties in locating foci of infection early on. Organoids allow for the study of early infection events and are also more relevant than monolayer cultures due to their increased cellular diversity and similar architecture to the small intestinal epithelium. Cocultures of BMDCs or gDCs with organoids infected with *T. gondii* did not stimulate increased recruitment of DCs to the organoid surface. This coculture

infection model was assessed after 24h of infection, therefore *T. gondii* invasion had already been established. Intestinal DCs have been proposed to play a role in the early dissemination of parasites since DP cDC2s transport pathogens such as *Salmonella* at early stages of infection and DCs are not seen at sites of *T.* gondii infections in the intestine after 7 days (Courret *et al.*, 2006; Coombes *et al.*, 2013). Therefore, the established *T. gondii* infections within organoids may not be sufficient to drive DC recruitment. Microinjections of *T. gondii* into the lumen of organoids already in culture with gDCs will allow for the study of the very earliest infection events and should be considered for future research.

The dissemination of *T. gondii* from the small intestine to other locations throughout the body is reliant on immune cells. There are variabilities between *T. gondii* strains in the ability to disseminate, whereby type I parasites do not use immune cells and likely migrate through the blood, and types II and III hijack the migratory characteristics of immune cells such as DCs (Lambert *et al.*, 2009). DCs take on a hypermotile phenotype and amoeboid morphology upon infection with *T. gondii* type II Pru strain (Fuks *et al.*, 2012; Weidner *et al.*, 2013; Kanatani, Uhlén and Barragan, 2015; Kanatani *et al.*, 2017). Upon infection, DCs increase their surface expression of CCR7 and lose podosomes that otherwise interact with the ECM that consequently increases their migration potential (Weidner *et al.*, 2013). This increased migration also occurs in 3D cultures of collagen (Kanatani, Uhlén and Barragan, 2015). However, in our study gDCs infected with *T. gondii* did not increase in motility determined by speed, track length and track displacement. A possible explanation may lie with the viability of the parasites in the coculture systems

whereby infected organoids were incubated for 24h before the addition of gDCs, allowing for extracellular *T. gondii* to perish. Increased DC motility occurs only after active invasion of live parasites (Weidner *et al.*, 2013), therefore the *T. gondii* seen in gDCs within our experiment may not have been viable in order to induce a hypermotile phenotype and may have been phagocytosed by the gDCs rather than through active invasion. Although DCs display a more rounded morphology when infected with *T. gondii* (Kanatani, Uhlén and Barragan, 2015), our study showed that intracellular parasites decreased sphericity in gDCs. Once again, this may be due to the viability of *T. gondii* in our study since heat-inactivated *T. gondii* only caused discrete morphological changes in DCs (Weidner *et al.*, 2013). However, the studies just mentioned utilised DCs that derived from human monocytes or from mouse BM cultured in GM-CSF. Monocyte-derived DCs (moDCs) and cDCs derive from different precursors in the BM and with the newly defined phenotypic markers for DCs, early studies into the functions of moDCs are difficult to interpret since they contained many overlapping markers with macrophages. Although moDCs express the cDC transcription factor *Zbtb46*, they are thought to impose an inflammatory role and are recruited to sites of inflammation (Zigmond *et al.*, 2012; Segura and Amigorena, 2013). Due to the poorly defined characteristics of moDCs, their use as *T. gondii* infection models for DCs may not be relevant. The BM-derived DCs used in previous infection studies utilised GM-CSF as the growth factor, which has now been determined to generate a heterogenous population of DCs and macrophages (Helft *et al.*, 2015). Therefore, these studies may not fully represent host-pathogen

interactions and the use of gDCs developed in our study may be a more suitable alternative.

In this study a novel and straightforward method for the generation of gut-like DCs has been established that does not require procedures in mice or isolation of pre-cDCs, providing a predominantly DP cDC2 population that is most prominent within the SI LP. The coculture of intestinal organoids with these DCs provides a novel model of the intestinal epithelium with gut-like DCs that could be used to answer key questions relating to immune homeostasis of the intestine, chronic inflammatory diseases, and enteric infections.

Chapter 6: General discussion

The development of organoid cultures provides an *in vitro* model of the small intestinal epithelium that recapitulates the cellular diversity and structure to its *in vivo* counterpart. However, technical challenges associated with the 3D conformation of organoids means they have not been fully exploited to study enteric parasitic infections. The work set out in this thesis dissertation established novel infection models of organoids with *T. gondii*, and live imaging revealed potential novel behaviours of parasite-invaded cells. Organoid models were further developed to incorporate gut-like DCs, allowing the analysis of epithelial-DC interactions and the effects of DCs on epithelial response to infection. Collectively these models will allow us to explore the mechanisms of host defence against enteric parasitic infection and to test novel therapeutics and vaccines.

In Chapter 3, partly dissociated organoids were infected with *T. gondii* in suspension before culture in Matrigel. The dissociation of organoids during this process allowed the parasite to access and invade the luminal surface of the epithelium but did not restrict infections to this route. Nonetheless, the parasite successfully invaded and replicated in organoids. Organoids generated from a Cre-reporter mouse model allowed for the visual verification of successful invasion as determined by the expression of membrane GFP in response to secretion of *T. gondii* toxofilin-Cre into the host cell cytosol. Membrane GFP fluorescence was also detected in host cells that did not contain parasites, either as a result of infected cells dividing, or through the aborted invasion of host cells by the parasite, or through the host cell clearance

of the parasite by autophagy. This uninfected-injected phenotype has been described in the brains of mice where these uninfected-injected cells greatly outnumber infected cells, and in human foreskin fibroblasts but never before in the intestinal epithelium, thereby supporting to the relevance of this organoid model (Koshy *et al.*, 2012). Extending the live imaging period of infected organoids would allow for the observation of the sequence of events leading to eGFP expression, discriminating between the division of $eGFP^+$ cells, aborted invasion events, and autophagy. Membrane GFP is expressed upon exposure to a Cre-fusion protein with toxofilin, a rhoptry protein. The release of rhoptry proteins into the cytoplasm of host cells affects cell function. For example, ROP16 activates host STAT3, leading to reduced IL-12p40 production (Saeij *et al.*, 2007). IL-12p40 is important in driving T and NK cell production of IFN-γ which is critical to protect the host from infection. Since *T. gondii* infects a small proportion of cells, the reduction in IL-12 may not be significant compared to uninfected cells that are responding to infection. Therefore, the ability to reduce IL-12 in more than just the cell it invades may be an advantage. This wider reaching effect can be achieved through injection of effector proteins into cells that the parasite does not invade. However, STAT3 activation is not seen in type II strains of *T. gondii*. Rather, type II strains induce a greater NF-κB activation than types I and III through the expression of GRA15, however this is only expressed after invasion since this is a protein associated with the PV (Rosowski *et al.*, 2011). Nonetheless, our model can be used to identify other parasite effectors that may act in a similar way to ROP16 in affecting host cell response within the small intestinal epithelium.

The aborted invasion events may be due to a preferential invasion of a certain IEC type. Cell tropism in the intestine occurs in infections with norovirus that select for the invasion of tuft cells (Wilen *et al.*, 2018), and *Mycobacterium avium paratuberculosis* in goblet cells (Golan *et al.*, 2009). However, it remains uncertain whether *T. gondii* exhibit cell tropism within the small intestinal epithelium. Staining for specific intestinal cell types in infected organoid samples will determine whether *T. gondii* displays any preference, and if the uninfected-injected cells are part of a cell selection process by *T. gondii.* If so, the organoid model could be further employed to dissect the parasite factors responsible for driving this specificity and the molecular pathways that might mediate this specificity.

Live imaging also provided evidence of interesting host cell behaviour whereby infected cells were expelled into the lumen. This could explain the spread of infection within the small intestine observed *in vivo*. A low number of infection sites are present in the small intestine early after oral infection with *T. gondii*, but the number of infection sites increases after 7 days, with viable tachyzoites present within the lumen (Coombes *et al.*, 2013; Gregg *et al.*, 2013). The release of viable tachyzoites into the lumen may allow for autoinfection of other epithelial cells, explaining the increase in infection sites. However, it is uncertain whether this is the case or whether expulsion of infected epithelial cells is a host defence mechanism. Increasing the time-lapse imaging period of infected organoids may aid is elucidating whether released tachyzoites are able to form new foci of infection.

The advantage of using the organoid dissociation method for *T. gondii* infection is that it allows for high throughput analyses, such as drug screenings for compounds that inhibit parasite invasion and replication. This could include the Pathogen Box that has been used to identify possible compounds to prevent *T. gondii* growth in Vero cells (Spalenka *et al.*, 2018). The Pathogen Box is a freely available collection of 400 compounds with confirmed activity against pathogens initially designed for developing drugs against malaria. Applying the Pathogen Box to infected organoids may reveal more relevant compounds as potential drug targets. This would also allow for studying any undesirable off-target effects on a more relevant model of the intestinal epithelium. However, this method of infection does not restrict infection to the apical surface. This is important since IECs are polarised, containing different receptors at different densities between the apical and basal sides, meaning responses to infection may differ depending on which surface of the epithelium that this occurs. This also makes it difficult to image the transmigration of the parasite from the luminal to basal surface.

An issue with employing organoids as a disease model is that the luminal surface is enclosed and difficult to access. Microinjection techniques have been used to insert viral and bacterial pathogens into the lumen, but at the beginning of this project this technique had not been used for relatively larger parasites. Only in July of this year was this achieved for *Cryptosporidium parvum* (Heo *et al.*, 2018). Microinjection of *T. gondii* was a challenging technique to optimise, requiring the generation of microneedles of suitable bore size to prevent blockages, and development of injection proficiency. Successful microinjection of *T. gondii* took 2

years to optimise and was not completed until near the end of this thesis dissertation. Therefore, this model could not be fully exploited. Nonetheless, this technique allowed for the successful invasion of *T. gondii* from the luminal surface, albeit at a very low rate. This is comparable to the scarcity of infectious foci seen *in* vivo and in the organoid model described in chapter 3, suggesting it may reflect robust host defence mechanisms (Coombes *et al.*, 2013; Gregg *et al.*, 2013). As with the dissociation infection model, microinjections can help determine whether *T. gondii* displays tropism for particular epithelial cell populations. Paracellular migration of *T. gondii* was observed during live imaging of the infection models using dissociation of organoids. However, this infection pathway was not limited to the luminal to basal route. Therefore, microinjections of *T. gondii* would provide a means to study the relevant transmigration pathway.

This microinjection model can also be applied to better understand how different clonal lineages of *T. gondii* differ in their virulence and capacity for paracellular migration (Lambert *et al.*, 2009). *T. gondii* strains differ in their ability to transmigrate across the intestinal epithelium whereby type I strains have long-distance migration and transmigrate at much faster speeds than type II and type III strains (Barragan and Sibley, 2002). This model would help elucidate the significance of the route of infection for dissemination between strains and elucidate common factors involved in their infection and transmigration that could be used to develop vaccines. Each strain also differ in their activation of host cell response, such as NF-κB signalling (Rosowski *et al.*, 2011), therefore this infection

model can be used to discover the properties that influence difference host cell responses between strain types.

Work performed in the lab in parallel to this project led to the development of novel bovine organoid cultures, which we were also able to successfully microinject (Derricott *et al.*, 2018; Hamilton *et al.*, 2018). This opens up the opportunity to study the host epithelial response to major enteric pathogens of livestock, such as *Cryptosporidium parvum* and bovine viral diarrhoea. Our current knowledge on the small intestinal epithelial response to *C. parvum* within cattle is extremely limited due to the difficulties in ascertaining suitable models. Current *in vitro* models of *C. parvum* infections rely on monolayer cultures derived from kidney or colonic cell lines that are not representative of the intestinal epithelium in which this parasite preferentially invades. Microinjections of *C. parvum* in organoids derived from the human small intestine have be shown to support parasite infection and generation of infectious oocysts (Heo *et al.*, 2018). However, these organoids were generated from monogastrics, so may not be representative of bovine infections. Therefore, the use of bovine organoids and the microinjection technique will provide a species-relevant infection model that may help in establishing new insights into developing therapeutics against zoonotic enteric infections.

With the establishment of a microinjection protocol for *T. gondii*, the bradyzoite or sporozoite forms can be injected into organoids. However, due to the difficulties in culturing bradyzoites and sporozoites, tachyzoites were used in this study due to their ease of culture. Using bradyzoites or sporozoites would be more suitable since

these are the forms ingested that infect the epithelium. Host cell response differ between the developmental stages of *T. gondii*, for example, sporozoites induce a TNF-α response via NF-κB in host cells that is not seen in tachyzoite infections (Guiton *et al.*, 2017). Sporozoites also have 85 genes not present in tachyzoites that encode secretory proteins that have not been characterised (Guiton *et al.*, 2017). Also, the differentially expressed proteins in each developmental stage may incur different host cell responses to infection (Wang *et al.*, 2017). Bradyzoite infection induces a reduced host cell response in HFFs compared to tachyzoites, such as the dampened expression of the chemokine CCL2 (Fouts and Boothroyd, 2007). Therefore, using bradyzoites and sporozoites may be a more relevant model for early infection of the small intestine. The *in vitro* development of bradyzoites is achievable through the reduction in pH and ambient CO_2 conditions in infected cell lines (Weilhammer *et al.*, 2012), or through isolation of cysts from the brains of infected mice. Injections of bradyzoites into organoids may reveal novel mechanisms in *T. gondii* infections.

In chapter 5, DCs with an intestinal-like phenotype were generated from BM, referred to as gDCs. This is a method that can be easily replicated in other research laboratories, unlike methods already published that require treatment of mice and sorting for pre-cDCs (Zeng *et al.*, 2016), necessitating the need for a home office license and a specialised flow cytometry facility. Adding gDCs to organoids provides a novel *in vitro* model allowing for the analysis of interactions between intestinal DCs and an appropriate model of the small intestinal epithelium. Interactions were observed in preliminary studies of the coculture model whereby contact points

between gDCs and organoids sometimes led to the expulsion of an organoid cell. This could be a cause for the increased circularity of organoids, indicative of increased cell shedding, in coculture samples. The most interesting observation was the luminal sampling behaviour exhibited by gDCs, likely to be cDC2s, in the absence of any overt stimuli. This contrasted with *in vivo* models, where cDC1 performed sampling behaviour only in response to infection. TLR signalling in the intestinal epithelium recruits $CD103^{+}$ cDCs that subsequently sample the lumen (Farache *et al.*, 2013). Therefore, the mechanisms involved in initiating sampling behaviour can be studied using the novel coculture model developed in our study. For example, CD103 integrin binds to E-cadherin on epithelial cell surfaces, therefore using $CD103^{-/-}$ mice to generate gDCs may reveal the importance of CD103 expression in sampling behaviour. This mouse model may also reveal the importance of CD103 in the cellular shedding seen in organoid cocultures. These provide a suitable model for studying intestinal DC characteristics, and for infections with *T. gondii* since current models use BM cultures that contain contaminating macrophages, or moDCs that are generated through a different developmental pathway to cDCs and therefore may not be functionally similar.

Utilising the microinjection technique, microbial components can be inserted into the lumen of organoids in coculture with gDCs to assess the conditioning effects on gDCs. The microbiota is thought to play a key role in the initiation of tolerance by driving the generation of tolerogenic DCs. Understanding the molecular mechanisms involved in driving this tolerogenic phenotype may also improve our understanding into the development of inflammatory diseases such as Crohn's

disease. The pathogenesis of Crohn's disease is largely unknown but is suggested that the impaired sensing and killing of commensal bacteria contribute to the onset of disease. Additionally, since very little is known about the interactions between DCs and the intestinal epithelium, the use of transgenic or knockout mouse models to generate organoids and gDCs would help establish the particular molecular pathways involved in their communication during intestinal homeostasis and inflammation. The downregulation of ALDH together with increased CCR7 expression in gDCs cocultured with organoids suggests a possible inflammatory state of organoids, which may have wider implications for the current use of organoids in research studies. Further analysis may reveal the inhibitory factors involved, with possible associations to inflammatory bowel diseases. The observations of luminal sampling may also be an indication of organoid inflammation, since it is suggested that only through TLR signalling does luminal sampling occur. The development of culture methods to maintain organoids in a reduced inflammatory state may involve the application of IL-22. This cytokine is produced by immune cells and is involved in intestinal epithelial repair and reduces colonic inflammation (Monteleone *et al.*, 2011; Lindemans *et al.*, 2015).

The establishment of protocols for infecting organoids with *T. gondii* have provided models that can be utilised to answer many outstanding questions of early infection events. The straightforward method for the generation of relevant intestinal-like DCs from BM makes this technique accessible to many research laboratories. The addition of gDCs to organoids provides a novel *in vitro* coculture model that can be

applied to a wide range of intestinal diseases and infections to identify vaccine targets or molecular pathways for the development of therapeutics.

Supplementary Movies

Movie S1: Infected cells are expelled into the lumen of organoids
Organoids from ROSA $^{mT/mG}$ mice were infected with *T. gondii* Pru-tdTom-Cre for 24h and time-lapse imaging by 2-photon microscopy. Infected cells that are also eGFP^{+} were observed being expelled into the lumen of organoids.

Movie S2: Organoid cells infected with *T. gondii* are expelled into the lumen, with the parasite remaining within the epithelium
Organoids from ROSA $^{mT/mG}$ mice were infected with *T. gondii* Pru-tdTom-Cre for 24h and time-lapse imaging by 2-photon microscopy. Time-lapse image shows a section of an infected organoid. The eGFP^{+} cell is expelled into the lumen, with the parasite remaining within the organoid epithelium. Scale bar 15µm

Movie S3: *T. gondii* microinjected into organoid lumen exhibits helical movement and attachment to cell
ROSA$^{mG/mT}$ organoids (red) were microinjected with *T. gondii* Pru-GFP (green) and time-lapse, z-stack images obtained by 2-photon microscopy over a 2h period. Motile *T. gondii* was observed within the organoid lumen and attachment to a cell that is likely dead as determined by its lack of fluorescence.

Movie S4: Cell shedding in organoids occur at sites of gDC attachment
gDCs were generated by culture of BM cells as described above. gDCs were labelled with CFSE and added to the Matrigel of ROSA$^{mT/mG}$ organoids for live imaging by 2-photon microscopy. Z-stack time-lapse images were obtained. Cell shedding can be observed at points of gDC contact with the organoid epithelium.

Movie S5: BMDCs in coculture with organoids
BMDCs were generated by culture of BM cells with Flt3L and the last 48h with GM-CSF. BMDCs were labelled with CFSE and added to the Matrigel of ROSA$^{mT/mG}$ organoids for live imaging by 2-photon microscopy. Z-stack time-lapse images were obtained. Two-photon movie showing CFSE-labelled BMDCs (green) co-cultured with Rosa-mT/mG organoids (red).

Movie S6: gDCs in coculture with organoids
gDCs were generated by culture of BM cells in Flt3L and the last 48h with GM-CSF and RA. The gDCs were labelled with CFSE and added to the Matrigel of ROSA$^{mT/mG}$ organoids for live imaging by 2-photon microscopy. Z-stack time-lapse images were obtained. Two-photon movie showing CFSE-labelled gDCs (green) co-cultured with Rosa-mT/mG organoids (red).

Movie S7: SI LP DCs in coculture with organoids
SI LP DCs were isolated as described above. DCs were labelled with CFSE and added to the Matrigel of ROSA$^{mT/mG}$ organoids for live imaging by 2-photon microscopy. Z-stack time-lapse images were obtained. Two-photon movie showing CFSE-labelled SI LP DCs (green) co-cultured with Rosa-mT/mG organoids (red).

Movie S8: BMDCs interact with organoid surface
BMDCs were cultured with organoids and time-lapse images were acquired by 2-photon microscopy. BMDCs attached to organoids extended processes along the surface but were less motile than gDCs and SI LP DCs.

Movie S9: gDCs crawl along the organoid surface
gDCs were cultured with organoids and time-lapse images were acquired by 2-photon microscopy. gDCs displayed greater crawling ability along the organoid surface than BMDCs.

Movie S10: SI LP DCs crawl along the organoid surface
SI LP DCs were cultured with organoids and time-lapse images were acquired by 2-photon microscopy. SI LP DCs displayed greater crawling ability along the organoid surface than BMDCs and gDCs.

Movie S11: gDCs extend dendrites into the luminal space of organoids for sampling
gDCs were labelled with CFSE and added to the Matrigel of ROSA$^{mT/mG}$ organoids for live imaging by 2-photon microscopy. Z-stack time-lapse images were obtained. **A**, gDC extends a dendritic process into the lumen of an organoid for sampling. **B**, another culture of gDC can be seen extending a dendrite into the lumen of the organoid for sampling, **C** just the CSFE channel of **B** to show the extended dendrite.

Movie S12: Organoids contained intraluminal gDCs
gDCs were labelled with CFSE and added to organoids cultured from ROSA$^{mT/mG}$ mice with z-stack, time-lapse images obtained using 2-photon microscopy. Intraluminal gDCs were observed.

Movie S13: C**ultures of gDCs with *T. gondii***
gDCs were cultured with T. gondii Pru-tdTom-Cre as a control. Time-lapse images were acquired over a 1h period at 2:40min intervals using 2-photon microscopy. Two-photon movie showing gDCs (green) cultured with T. gondii (red) in Matrigel.

Movie S14: Cultures of gDCs with organoids
ROSA$^{mT/mG}$ organoids were cultured with gDCs labelled with CFSE and time-lapse images were acquired over a 1h period at 2:40min intervals using 2-photon microscopy. Two-photon movie showing gDCs (green) cultured with organoids (red) infected with T. gondii (red) in Matrigel.

Movie S15: Cultures of gDCs with *T. gondii*-infected organoids
Infected ROSA$^{mT/mG}$ organoids were cultured with gDCs labelled with CFSE and time-lapse images were acquired over a 1h period at 2:40min intervals using 2-photon microscopy. Two-photon movie showing gDCs (green) cultured with organoids (red) in Matrigel.

Movie S16: Gut-like DCs attached to the surface of organoids extend processes towards sites of infections.
Organoids infected with *T. gondii* for 24h were cocultured with gDCs and time-lapse images were obtained as preciously described. Attached gDCs to the surface of organoids extended processes towards sites of infection.

References

Alexander, D. L. *et al.* (2005) 'Identification of the moving junction complex of Toxoplasma gondii: A collaboration between distinct secretory organelles', *PLoS Pathogens*, 1(2), pp. 0137–0149. doi: 10.1371/journal.ppat.0010017.

Arques, J. L. *et al.* (2009) 'Salmonella Induces Flagellin- and MyD88-Dependent Migration of Bacteria-Capturing Dendritic Cells Into the Gut Lumen', *Gastroenterology*, 137(2), p. 579–587.e2. doi: 10.1053/j.gastro.2009.04.010.

Atarashi, K. *et al.* (2011) 'Induction of Colonic Regulatory T Cells by Indigenous Clostridium Species', *Science*, 331(6015), pp. 337–341. doi: 10.1126/science.1198469.

Aychek, T. *et al.* (2015) 'IL-23-mediated mononuclear phagocyte crosstalk protects mice from Citrobacter rodentium-induced colon immunopathology', *Nature Communications*, 6. doi: 10.1038/ncomms7525.

Bachem, A. *et al.* (2012) 'Expression of XCR1 characterizes the Batf3-dependent lineage of dendritic cells capable of antigen cross-presentation', *Frontiers in Immunology*, 3(JUL). doi: 10.3389/fimmu.2012.00214.

Bain, C. C. *et al.* (2017) 'TGFβR signalling controls CD103+CD11b+dendritic cell development in the intestine', *Nature Communications*. Springer US, 8(1). doi: 10.1038/s41467-017-00658-6.

Bakdash, G. *et al.* (2015) 'Retinoic acid primes human dendritic cells to induce gut-homing, IL-10-producing regulatory T cells', *Mucosal Immunology*, 8(2), pp. 265–278. doi: 10.1038/mi.2014.64.

Barker, N. *et al.* (2007) 'Identification of stem cells in small intestine and colon by marker gene Lgr5.', *Nature*, 449(7165), pp. 1003–1007. doi: 10.1038/nature06196.

Barragan, A., Brossier, F. and Sibley, L. D. (2005) 'Transepithelial migration of Toxoplasma gondii involves an interaction of intercellular adhesion molecule 1 (ICAM-1) with the parasite adhesin MIC2', *Cellular Microbiology*, 7, pp. 561–568. doi: 10.1111/j.1462-5822.2005.00486.x.

Barragan, A. and Sibley, L. D. (2002) 'Transepithelial migration of Toxoplasma gondii is linked to parasite motility and virulence.', *The Journal of experimental medicine*, 195(12), pp. 1625–1633. doi: 10.1084/jem.20020258.

Basu, R. *et al.* (2015) 'IL-1 signaling modulates activation of STAT transcription factors to antagonize retinoic acid signaling and control the TH17 cell–iTreg cell balance', *Nature Immunology*, 16(3), pp. 286–295. doi: 10.1038/ni.3099.

Becker, M. *et al.* (2014) 'Ontogenic, phenotypic, and functional characterization of

XCR1+ dendritic cells leads to a consistent classification of intestinal dendritic cells based on the expression of XCR1 and SIRPα', *Frontiers in Immunology*, 5(JUL), p. 326. doi: 10.3389/fimmu.2014.00326.

Béduneau, A. *et al.* (2014) 'A tunable Caco-2/HT29-MTX co-culture model mimicking variable permeabilities of the human intestine obtained by an original seeding procedure', *European Journal of Pharmaceutics and Biopharmaceutics*, 87(2), pp. 290–298. doi: 10.1016/j.ejpb.2014.03.017.

Benson, A. *et al.* (2009) 'Gut Commensal Bacteria Direct a Protective Immune Response against Toxoplasma gondii', *Cell Host and Microbe*. Elsevier Ltd, 6(2), pp. 187–196. doi: 10.1016/j.chom.2009.06.005.

Bereswill, S. *et al.* (2011) 'Novel murine infection models provide deep insights into the "Ménage à trois" of campylobacter jejuni, microbiota and host innate immunity', *PLoS ONE*. Edited by D. W. Metzger. Public Library of Science, 6(6), p. e20953. doi: 10.1371/journal.pone.0020953.

Bhattacharya, N. *et al.* (2016) 'Normalizing Microbiota-Induced Retinoic Acid Deficiency Stimulates Protective CD8+T Cell-Mediated Immunity in Colorectal Cancer', *Immunity*. Elsevier, 45(3), pp. 641–655. doi: 10.1016/j.immuni.2016.08.008.

Bierly, A. L. *et al.* (2008) 'Dendritic Cells Expressing Plasmacytoid Marker PDCA-1 Are Trojan Horses during Toxoplasma gondii Infection', *Journal of immunological methods*, 181, pp. 8485–8491. doi: 10.4049/jimmunol.181.12.8485.

Black, M. W. and Boothroyd, J. C. (2000) 'Lytic cycle of Toxoplasma gondii.', *Microbiology and molecular biology reviews : MMBR*, 64(3), pp. 607–623. doi: 10.1128/MMBR.64.3.607-623.2000.

Bogunovic, M. *et al.* (2009) 'Origin of the Lamina Propria Dendritic Cell Network', *Immunity*. Cell Press, 31(3), pp. 513–525. doi: 10.1016/j.immuni.2009.08.010.

Bonnardel, J. *et al.* (2017) 'Distribution, location, and transcriptional profile of Peyer's patch conventional DC subsets at steady state and under TLR7 ligand stimulation', *Mucosal Immunology*, 10(6), pp. 1412–1430. doi: 10.1038/mi.2017.30.

Bonnefoy, F. *et al.* (2011) 'TGF-beta-exposed plasmacytoid dendritic cells participate in Th17 commitment.', *Journal of immunology (Baltimore, Md. : 1950)*, 186(11), pp. 6157–64. doi: 10.4049/jimmunol.1002497.

Boucard-Jourdin, M. *et al.* (2016) 'β8 Integrin Expression and Activation of TGF-β by Intestinal Dendritic Cells Are Determined by Both Tissue Microenvironment and Cell Lineage', *The Journal of Immunology*, 197(5), pp. 1968–1978. doi: 10.4049/jimmunol.1600244.

Bowie, W. R. *et al.* (1997) 'Outbreak of toxoplasmosis associated with municipal drinking water', *Lancet*, 350(9072), pp. 173–177. doi: 10.1016/S0140-6736(96)11105-3.

Brasel, K. *et al.* (2000) 'Generation of murine dendritic cells from flt3-ligand-supplemented bone marrow cultures.', *Blood*, 96(9), pp. 3029–39. Available at: http://www.ncbi.nlm.nih.gov/pubmed/11049981 (Accessed: 12 December 2017).

Briceno, M. P. *et al.* (2016) 'Toxoplasma gondii Infection Promotes Epithelial Barrier Dysfunction of Caco-2 Cells', *Journal of Histochemistry & Cytochemistry*, 64(8). doi: 10.1369/0022155416656349.

Briske-Anderson, M. J., Finley, J. W. and Newman, S. M. (1997) 'The Influence of Culture Time and Passage Number on the Morphological and Physiological Development of Caco-2 Cells', *Experimental Biology and Medicine*, 214(3), pp. 248–257. doi: 10.3181/00379727-214-44093.

Burger, E. *et al.* (2018) 'Loss of Paneth Cell Autophagy Causes Acute Susceptibility to Toxoplasma gondii-Mediated Inflammation', *Cell Host and Microbe*. doi: 10.1016/j.chom.2018.01.001.

Buxton, D. and Innes, E. A. (1995) 'A commercial vaccine for ovine toxoplasmosis', *Parasitology*, 110(Supplement S1), pp. S11--S16. doi: 10.1017/S003118200000144X.

Cadwell, K. *et al.* (2008) 'A key role for autophagy and the autophagy gene Atg16l1 in mouse and human intestinal Paneth cells', *Nature*. Nature Publishing Group, 456(7219), pp. 259–263. doi: 10.1038/nature07416.

Carruthers, V. B., Giddings, O. K. and Sibley, L. D. (1999) 'Secretion of micronemal proteins is associated with toxoplasma invasion of host cells.', *Cellular microbiology*. Wiley/Blackwell (10.1111), 1(3), pp. 225–235. doi: 10.1046/j.1462-5822.1999.00023.x.

Centers for Disease Control and Prevention (2016) *Parasites - Neglected Parasitic Infections (NPIs)*.

Cérède, O. *et al.* (2005) 'Synergistic role of micronemal proteins in Toxoplasma gondii virulence', *The Journal of Experimental Medicine*, 201(3), pp. 453–463. doi: 10.1084/jem.20041672.

Cerovic, V. *et al.* (2012) 'Intestinal CD103(-) dendritic cells migrate in lymph and prime effector T cells', *Mucosal Immunology*, 6(1), pp. 104–113. doi: 10.1038/mi.2012.53.

Cerovic, V. *et al.* (2015) 'Lymph-borne CD8α+ dendritic cells are uniquely able to cross-prime CD8+ T cells with antigen acquired from intestinal epithelial cells', *Mucosal Immunology*, 8(1), pp. 38–48. doi: 10.1038/mi.2014.40.

Charron, A. J. and Sibley, L. D. (2004) 'Molecular partitioning during host cell penetration by Toxoplasma gondii', *Traffic*, 5(11), pp. 855–867. doi: 10.1111/j.1600-0854.2004.00228.x.

Chieppa, M. *et al.* (2006) 'Dynamic imaging of dendritic cell extension into the small bowel lumen in response to epithelial cell TLR engagement', *The Journal of Experimental Medicine*. Rockefeller University Press, 203(13), pp. 2841–2852. doi: 10.1084/jem.20061884.

Chng, S. H. *et al.* (2016) 'Ablating the aryl hydrocarbon receptor (AhR) in CD11c+ cells perturbs intestinal epithelium development and intestinal immunity', *Scientific Reports*. Nature Publishing Group, 6(1), p. 23820. doi: 10.1038/srep23820.

Cliffe, L. J. *et al.* (2005) 'Immunology - Accelerated intestinal epithelial cell turnover: A new mechanism of parasite expulsion', *Science*, 308(5727), pp. 1463–1465. doi: 10.1126/science.1108661.

Cohen, S. B. and Denkers, E. Y. (2015) 'Impact of Toxoplasma gondii on Dendritic Cell Subset Function in the Intestinal Mucosa', *Journal of immunology*, 195, pp. 2754–2762. doi: 10.4049/jimmunol.1501137.

Cong, Y. *et al.* (2009) 'A dominant, coordinated T regulatory cell-IgA response to the intestinal microbiota', *Proceedings of the National Academy of Sciences* , 106(46), pp. 19256–19261. Available at: http://www.pnas.org/content/106/46/19256.abstract.

Coombes, J. L. *et al.* (2007) 'A functionally specialized population of mucosal CD103+ DCs induces Foxp3+ regulatory T cells via a TGF-β– and retinoic acid–dependent mechanism', *The Journal of Experimental Medicine* , 204(8), pp. 1757–1764. Available at: http://jem.rupress.org/content/204/8/1757.abstract.

Coombes, J. L. *et al.* (2013) 'Motile invaded neutrophils in the small intestine of Toxoplasma gondii -infected mice reveal a potential mechanism for parasite spread', *Proceedings of the National Academy of Sciences*, 110(21), pp. E1913–E1922. doi: 10.1073/pnas.1220272110.

Cooney, R. *et al.* (2010) 'NOD2 stimulation induces autophagy in dendritic cells influencing bacterial handling and antigen presentation', *Nature Medicine*. Nature Publishing Group, 16(1), pp. 90–97. doi: 10.1038/nm.2069.

Cortez, V. S. *et al.* (2014) 'CRTAM controls residency of gut CD4 + CD8 + T cells in the steady state and maintenance of gut CD4 + Th17 during parasitic infection', *The Journal of Experimental Medicine*, 211(4), pp. 623–633. doi: 10.1084/jem.20130904.

Costello, C. M. *et al.* (2014) 'Synthetic small intestinal scaffolds for improved studies of intestinal differentiation', *Biotechnology and Bioengineering*, 111(6), pp. 1222–1232. doi: 10.1002/bit.25180.

Courret, N. *et al.* (2006) 'CD11c- and CD11b-expressing mouse leukocytes transport single Toxoplasma gondii tachyzoites to the brain', *Blood*, 107(1), pp. 309–316. doi: 10.1182/blood-2005-02-0666.

Cruickshank, S. M. *et al.* (2009) 'Rapid Dendritic Cell Mobilization to the Large Intestinal Epithelium Is Associated with Resistance to Trichuris muris Infection', *The Journal of Immunology*. Europe PMC Funders, 182(5), pp. 3055–3062. doi: 10.4049/jimmunol.0802749.

D'Amico, A. and Wu, L. (2003) 'The early progenitors of mouse dendritic cells and plasmacytoid predendritic cells are within the bone marrow hemopoietic precursors expressing Flt3.', *The Journal of experimental medicine*. Rockefeller University Press, 198(2), pp. 293–303. doi: 10.1084/jem.20030107.

Dardé, M. L. (2008) 'Toxoplasma gondii , "new" genotypes and virulence', *Parasite*, 15(3), pp. 366–371. doi: 10.1051/parasite/2008153366.

de-la-Torre, A. *et al.* (2013) 'Severe South American Ocular Toxoplasmosis Is Associated with Decreased Ifn-γ/Il-17a and Increased Il-6/Il-13 Intraocular Levels', *PLoS Neglected Tropical Diseases*. Edited by A. Jardim, 7(11), p. e2541. doi: 10.1371/journal.pntd.0002541.

Demar, M. *et al.* (2007) 'Fatal outbreak of human toxoplasmosis along the Maroni River: epidemiological, clinical, and parasitological aspects.', *Clinical infectious diseases : an official publication of the Infectious Diseases Society of America*, 45(7), pp. e88–e95. doi: 10.1086/521246.

Demiri, M. *et al.* (2017) 'Distinct DC subsets regulate adaptive Th1 and 2 responses during Trichuris muris infection', *Parasite Immunology*, 39(10), p. e12458. doi: 10.1111/pim.12458.

Denning, T. L. *et al.* (2007) 'Lamina propria macrophages and dendritic cells differentially induce regulatory and interleukin 17-producing T cell responses', *Nat Immunol*, 8(10), pp. 1086–1094. Available at: http://dx.doi.org/10.1038/ni1511.

Denning, T. L. *et al.* (2011) 'Functional specializations of intestinal dendritic cell and macrophage subsets that control Th17 and regulatory T cell responses are dependent on the T cell/APC ratio, source of mouse strain, and regional localization.', *Journal of immunology (Baltimore, Md. : 1950)*, 187(2), pp. 733–747. doi: 10.4049/jimmunol.1002701.

DePaolo, R. W. *et al.* (2011) 'Co-adjuvant effects of retinoic acid and IL-15 induce inflammatory immunity to dietary antigens', *Nature*, 471(7337), pp. 220–224. doi: 10.1038/nature09849.

Derricott, H. *et al.* (2018) 'Developing a 3D intestinal epithelium model for livestock species', *Cell and Tissue Research*. doi: 10.1007/s00441-018-2924-9.

Dubey, J. P. (1997) 'Bradyzoite-Induced Murine Toxoplasmosis: Stage Conversion, Pathogenesis, and Tissue Cyst Formation in Mice Fed Bradvzoites of - Different Strains of Toxoplasma gondii', *Journal of Eukaryotic Microbiology*. Blackwell Publishing Ltd, 44(6), pp. 592–602. doi: 10.1111/j.1550-7408.1997.tb05965.x.

Dubey, J. P. (1998) 'Advances in the life cycle of Toxoplasma gondii', *International Journal for Parasitology*, 28(7), pp. 1019–1024. doi: http://dx.doi.org/10.1016/S0020-7519(98)00023-X.

Dubey, J. P. *et al.* (2005) 'Prevalence of viable Toxoplasma gondii in beef, chicken, and pork from retail meat stores in the United States: risk assessment to consumers.', *The Journal of parasitology*, 91(5), pp. 1082–93. doi: 10.1645/GE-683.1.

Dubey, J. P. and Frenkel, J. K. (1972) 'Cyst-Induced Toxoplasmosis in Cats*', *The Journal of Protozoology*. Blackwell Publishing Ltd, 19(1), pp. 155–177. doi: 10.1111/j.1550-7408.1972.tb03431.x.

Dupont, C. D. *et al.* (2015) 'Flt3 Ligand Is Essential for Survival and Protective Immune Responses during Toxoplasmosis', *The Journal of Immunology*, 195(9), pp. 4369–4377. doi: 10.4049/jimmunol.1500690.

Edelson, B. T. *et al.* (2010) 'Peripheral CD103 + dendritic cells form a unified subset developmentally related to CD8α + conventional dendritic cells', *The Journal of Experimental Medicine*. The Rockefeller University Press, 207(4), pp. 823–836. doi: 10.1084/jem.20091627.

Everts, B. *et al.* (2016) 'Migratory CD103 + dendritic cells suppress helminth-driven type 2 immunity through constitutive expression of IL-12', *The Journal of Experimental Medicine*, 213(1), pp. 35–51. doi: 10.1084/jem.20150235.

Farache, J. *et al.* (2013) 'Luminal Bacteria Recruit CD103+ Dendritic Cells into the Intestinal Epithelium to Sample Bacterial Antigens for Presentation', *Immunity*. Elsevier Inc., 38(3), pp. 581–595. doi: 10.1016/j.immuni.2013.01.009.

Feng, T. *et al.* (2010) 'Generation of mucosal dendritic cells from bone marrow reveals a critical role of retinoic acid.', *Journal of immunology (Baltimore, Md. : 1950)*, 185(10), pp. 5915–25. doi: 10.4049/jimmunol.1001233.

Food Standards Agency (2012) *Risk profile in relation to toxoplasma in the food chain*, *Advisory Committee on the Microbiological Safety of Food*. Available at: http://www.food.gov.uk/sites/default/files/multimedia/pdfs/committee/acmsfrtaxopasm.pdf.

Forbester, J. L. *et al.* (2015) 'Interaction of Salmonella enterica Serovar Typhimurium with Intestinal Organoids Derived from Human Induced Pluripotent Stem', *Infection and Immunity*, 83(7), pp. 2926–2934. doi: 10.1128/IAI.00161-15.

Foureau, D. M. *et al.* (2010) 'TLR9-Dependent Induction of Intestinal -Defensins by Toxoplasma gondii', *The Journal of Immunology*. American Association of Immunologists, 184(12), pp. 7022–7029. doi: 10.4049/jimmunol.0901642.

Fouts, A. E. and Boothroyd, J. C. (2007) 'Infection with Toxoplasma gondii Bradyzoites Has a Diminished Impact on Host Transcript Levels Relative to Tachyzoite Infection', *Infection and Immunity*. American Society for Microbiology Journals, 75(2), pp. 634–642. doi: 10.1128/IAI.01228-06.

Fransen, K. *et al.* (2013) 'Polymorphism in the retinoic acid metabolizing enzyme CYP26B1 and the development of Crohn's disease', *PLoS ONE*. Public Library of Science, 8(8), p. e72739. doi: 10.1371/journal.pone.0072739.

Fuks, J. M. *et al.* (2012) 'GABAergic Signaling Is Linked to a Hypermigratory Phenotype in Dendritic Cells Infected by Toxoplasma gondii', *PLoS Pathogens*. Edited by C. A. Hunter, 8(12), p. e1003051. doi: 10.1371/journal.ppat.1003051.

Gao, Y. *et al.* (2013) 'Control of T Helper 2 Responses by Transcription Factor IRF4-Dependent Dendritic Cells', *Immunity*, 39(4), pp. 722–732. doi: 10.1016/j.immuni.2013.08.028.

Geem, D. *et al.* (2012) 'Isolation and Characterization of Dendritic Cells and Macrophages from the Mouse Intestine 3 . Antibody Staining for Multi-Color Flow Cytometric Analysis of DCs and Macrophages', *JOVE*, (May), pp. 2–7. doi: 10.3791/4040.

Gersemann, M. *et al.* (2009) 'Differences in goblet cell differentiation between Crohn's disease and ulcerative colitis', *Differentiation*. Elsevier, 77(1), pp. 84–94. doi: 10.1016/J.DIFF.2008.09.008.

Golan, L. *et al.* (2009) 'Mycobacterium avium paratuberculosis Invades Human Small-Intestinal Goblet Cells and Elicits Inflammation', *The Journal of Infectious Diseases*. Oxford University Press, 199(3), pp. 350–354. doi: 10.1086/596033.

Gold, D. A. *et al.* (2015) 'The Toxoplasma dense granule proteins GRA17 and GRA23 mediate the movement of small molecules between the host and the parasitophorous vacuole', *Cell Host and Microbe*. doi: 10.1016/j.chom.2015.04.003.

Gopal, R., Birdsell, D. and Monroy, F. P. (2011) 'Regulation of chemokine responses in intestinal epithelial cells by stress and Toxoplasma gondii infection', *Parasite Immunology*, 33(1), pp. 12–24. doi: 10.1111/j.1365-3024.2010.01248.x.

Graumann, K. *et al.* (2015) 'Toxoplasma gondii inhibits cytochrome c-induced caspase activation in its host cell by interference with holo-apoptosome assembly', *Microbial Cell*. Shared Science Publishers, 2(5), pp. 150–162. doi: 10.15698/mic2015.05.201.

Gregg, B. *et al.* (2013) 'Replication and distribution of toxoplasma gondii in the small intestine after oral infection with tissue cysts', *Infection and Immunity*, 81(5), pp. 1635–1643. doi: 10.1128/IAI.01126-12.

Grigg, M. E. *et al.* (2001) 'Success and virulence in Toxoplasma as the result of sexual recombination between two distinct ancestries.', *Science (New York, N.Y.)*, 294(OCTOBER), pp. 161–165. doi: 10.1126/science.1061888.

Guilliams, M. *et al.* (2016) 'Unsupervised High-Dimensional Analysis Aligns Dendritic Cells across Tissues and Species', *Immunity*. Cell Press, 45(3), pp. 669–684. doi: 10.1016/j.immuni.2016.08.015.

Guiton, P. S. *et al.* (2017) 'An in vitro model of intestinal infection reveals a developmentally regulated transcriptome of Toxoplasma sporozoites and a NF-κB-like signature in infected host cells', *PLOS ONE*. Edited by S. N. Moreno, 12(3), p. e0173018. doi: 10.1371/journal.pone.0173018.

Guo, M. *et al.* (2015) 'Prevalence and risk factors for Toxoplasma gondii infection in meat animals and meat products destined for human consumption', *Journal of Food Protection*, 78(2), pp. 457–476. doi: 10.4315/0362-028X.JFP-14-328.

Guttman, J. A. and Finlay, B. B. (2009) 'Tight junctions as targets of infectious agents', *Biochimica et Biophysica Acta (BBA) - Biomembranes*, 1788(4), pp. 832–841. doi: 10.1016/j.bbamem.2008.10.028.

Haag, L. M. *et al.* (2012) 'Campylobacter jejuni induces acute enterocolitis in gnotobiotic IL-10-/- mice via toll-like-receptor-2 and -4 signaling', *PLoS ONE*. Edited by M. A. Deli. Public Library of Science, 7(7), p. e40761. doi: 10.1371/journal.pone.0040761.

Hakim, M. S. *et al.* (2018) 'Basal interferon signaling and therapeutic use of interferons in controlling rotavirus infection in human intestinal cells and organoids', *Scientific Reports*. Nature Publishing Group, 8(1), p. 8341. doi: 10.1038/s41598-018-26784-9.

Hakimi, M. A. and Bougdour, A. (2015) 'Toxoplasma's ways of manipulating the host transcriptome via secreted effectors', *Current Opinion in Microbiology*. Elsevier Current Trends, pp. 24–31. doi: 10.1016/j.mib.2015.04.003.

Hamilton, C. A. *et al.* (2018) 'Development of in vitro enteroids derived from bovine small intestinal crypts', *Veterinary Research*, 49(1), p. 54. doi: 10.1186/s13567-018-0547-5.

Hammerschmidt, S. I. *et al.* (2008) 'Stromal mesenteric lymph node cells are essential for the generation of gut-homing T cells in vivo.', *The Journal of experimental medicine*. Rockefeller University Press, 205(11), pp. 2483–90. doi: 10.1084/jem.20080039.

Hansen, I. S. *et al.* (2018) 'FcαRI co-stimulation converts human intestinal CD103+ dendritic cells into pro-inflammatory cells through glycolytic reprogramming', *Nature Communications*, 9(1), p. 863. doi: 10.1038/s41467-018-03318-5.

Haramis, A. P. G. *et al.* (2004) 'De Novo Crypt Formation and Juvenile Polyposis on BMP Inhibition in Mouse Intestine', *Science*, 303(5664), pp. 1684–1686. doi: 10.1126/science.1093587.

Hart, A. L. *et al.* (2005) 'Characteristics of intestinal dendritic cells in inflammatory bowel diseases', *Gastroenterology*, 129(1), pp. 50–65. doi: 10.1053/j.gastro.2005.05.013.

Hayen, S. M. *et al.* (2018) 'Exposure of intestinal epithelial cells to short- and long-chain fructo-oligosaccharides and CpG oligodeoxynucleotides enhances peanut-specific T Helper 1 polarization', *Frontiers in Immunology*, 9(MAY). doi: 10.3389/fimmu.2018.00923.

Helft, J. *et al.* (2015) 'GM-CSF Mouse Bone Marrow Cultures Comprise a Heterogeneous Population of CD11c+MHCII+ Macrophages and Dendritic Cells', *Immunity*, 42(6), pp. 1197–1211. doi: 10.1016/j.immuni.2015.05.018.

Heo, I. *et al.* (2018) 'Modelling Cryptosporidum infection in human small intestinal and lung organoids', *Nature Microbiology*. Nature Publishing Group, 3(July), pp. 814–823. doi: 10.1038/s41564-018-0177-8.

Houston, S. A. *et al.* (2016) 'The lymph nodes draining the small intestine and colon are anatomically separate and immunologically distinct', *Mucosal Immunology*. Nature Publishing Group, 9(2), pp. 468–478. doi: 10.1038/mi.2015.77.

Howe, D. K. and Sibley, L. D. (1995) 'Toxoplasma gondii comprises three clonal lineages: Correlation of parasite genotype with human disease', *Journal of Infectious Diseases*, 172(6), pp. 1561–1566. doi: 10.1093/infdis/172.6.1561.

Howitt, M. R. *et al.* (2016) 'Tuft cells, taste-chemosensory cells, orchestrate parasite type 2 immunity in the gut', *Science*, 351(6279), pp. 1329–1333. doi: 10.1126/science.aaf1648.

Huang, L. *et al.* (2017) 'Crosstalk between H9N2 avian influenza virus and crypt-derived intestinal organoids', *Veterinary Research*. BioMed Central, 48(1), p. 71. doi: 10.1186/s13567-017-0478-6.

Huang, S.-W. *et al.* (2017) 'P2X7 Receptor-Dependent Tuning of Gut Epithelial Responses to Infection', *Immunology and Cell Biology Biology*. Nature Publishing Group, 95(2), pp. 178–188. doi: 10.1038/icb.2016.75.

Hugot, J. P. *et al.* (2001) 'Association of NOD2 leucine-rich repeat variants with susceptibility to Crohn's disease', *Nature*, 411(6837), pp. 599–603. doi:

10.1038/35079107.

Hurst, R. J. M. and Else, K. J. (2013) 'The retinoic acid-producing capacity of gut dendritic cells and macrophages is reduced during persistent T. muris infection', *Parasite Immunology*, 35(7–8), pp. 229–233. doi: 10.1111/pim.12032.

Ihara, S. *et al.* (2018) 'Adhesive interactions between Mononuclear Phagocytes and Intestinal Epithelium Perturb Normal Epithelial Differentiation and Serve as a Therapeutic Target in Inflammatory Bowel Disease.', *Journal of Crohn's & colitis*. doi: 10.1093/ecco-jcc/jjy088.

Iliev, I. D., Spadoni, I., *et al.* (2009) 'Human intestinal epithelial cells promote the differentiation of tolerogenic dendritic cells', *Gut*, 58(11), pp. 1481–1489. doi: 10.1136/gut.2008.175166.

Iliev, I. D., Mileti, E., *et al.* (2009) 'Intestinal epithelial cells promote colitis-protective regulatory T-cell differentiation through dendritic cell conditioning', *Mucosal Immunology*. Nature Publishing Group, 2(4), pp. 340–350. doi: 10.1038/mi.2009.13.

Ingram, W. M. *et al.* (2013) 'Mice Infected with Low-Virulence Strains of Toxoplasma gondii Lose Their Innate Aversion to Cat Urine, Even after Extensive Parasite Clearance', *PLoS ONE*. Edited by E. H. Wilson. Public Library of Science, 8(9), pp. 1–6. doi: 10.1371/journal.pone.0075246.

Iwasaki, a and Kelsall, B. L. (2001) 'Unique functions of CD11b+, CD8 alpha+, and double-negative Peyer's patch dendritic cells.', *Journal of immunology (Baltimore, Md. : 1950)*, 166(8), pp. 4884–4890. doi: 10.4049/jimmunol.166.8.4884.

Iwata, M. *et al.* (2004) 'Retinoic acid imprints gut-homing specificity on T cells', *Immunity*, 21(4), pp. 527–538. doi: 10.1016/j.immuni.2004.08.011.

Iwata, M., Eshima, Y. and Kagechika, H. (2003) 'Retinoic acids exert direct effects on T cells to suppress Th1 development and enhance Th2 development via retinoic acid receptors.', *International immunology*, 15(8), pp. 1017–25. doi: 10.1093/intimm/dxg101.

Jackson, J. T. *et al.* (2011) 'Id2 expression delineates differential checkpoints in the genetic program of CD8α+ and CD103+ dendritic cell lineages.', *The EMBO journal*, 30(13), pp. 2690–704. doi: 10.1038/emboj.2011.163.

Jaensson-Gyllenbäck, E. *et al.* (2011) 'Bile retinoids imprint intestinal CD103+ dendritic cells with the ability to generate gut-tropic T cells.', *Mucosal immunology*, 4(4), pp. 438–47. doi: 10.1038/mi.2010.91.

Jaensson, E. *et al.* (2008) 'Small intestinal CD103+ dendritic cells display unique functional properties that are conserved between mice and humans.', *The Journal*

of experimental medicine, 205(9), pp. 2139–49. doi: 10.1084/jem.20080414.

Jang, M. H. *et al.* (2004) 'Intestinal villous M cells: An antigen entry site in the mucosal epithelium', *Proceedings of the National Academy of Sciences*, 101(16), pp. 6110–6115. doi: 10.1073/pnas.0400969101.

Jang, M. H. *et al.* (2006) 'CCR7 is critically important for migration of dendritic cells in intestinal lamina propria to mesenteric lymph nodes.', *Journal of immunology (Baltimore, Md. : 1950)*, 176(2), pp. 803–10. Available at: http://www.ncbi.nlm.nih.gov/pubmed/16393963 (Accessed: 14 November 2017).

Jijon, H. B. *et al.* (2018) 'Intestinal epithelial cell-specific RARα depletion results in aberrant epithelial cell homeostasis and underdeveloped immune system', *Mucosal Immunology*. Nature Publishing Group, 11(3), pp. 703–715. doi: 10.1038/mi.2017.91.

Joeris, T. *et al.* (2017) 'Diversity and functions of intestinal mononuclear phagocytes', *Mucosal Immunology*, 10(4), pp. 845–864. doi: 10.1038/mi.2017.22.

Johansson, M. E. V *et al.* (2015) 'Normalization of Host Intestinal Mucus Layers Requires Long-Term Microbial Colonization.', *Cell host & microbe*. NIH Public Access, 18(5), pp. 582–92. doi: 10.1016/j.chom.2015.10.007.

Jones, E. J., Korcsmaros, T. and Carding, S. R. (2017) 'Mechanisms and pathways of Toxoplasma gondii transepithelial migration', *Tissue Barriers*. Taylor & Francis, 5(1), pp. 1–11. doi: 10.1080/21688370.2016.1273865.

Jones, J. L. and Dubey, J. P. (2010) 'Waterborne toxoplasmosis - Recent developments', *Experimental Parasitology*, pp. 10–25. doi: 10.1016/j.exppara.2009.03.013.

Jones, J. L. and Dubey, J. P. (2012) 'Foodborne toxoplasmosis', *Clinical Infectious Diseases*, 55(6), pp. 845–851. doi: 10.1093/cid/cis508.

Ju, C.-H., Chockalingam, A. and Leifer, C. a (2009) 'Early response of mucosal epithelial cells during Toxoplasma gondii infection.', *Journal of immunology (Baltimore, Md. : 1950)*, 183(11), pp. 7420–7427. doi: 10.4049/jimmunol.0900640.

Van Kaer, L. and Olivares-Villagómez, D. (2018) 'Development, Homeostasis, and Functions of Intestinal Intraepithelial Lymphocytes.', *Journal of immunology (Baltimore, Md. : 1950)*, 200(7), pp. 2235–2244. doi: 10.4049/jimmunol.1701704.

Kanatani, S. *et al.* (2017) 'Voltage-dependent calcium channel signaling mediates GABAA receptor-induced migratory activation of dendritic cells infected by Toxoplasma gondii.', *PLoS pathogens*, 13(12), p. e1006739. doi: 10.1371/journal.ppat.1006739.

Kanatani, S., Uhlén, P. and Barragan, A. (2015) 'Infection by Toxoplasma gondii

Induces Amoeboid-Like Migration of Dendritic Cells in a Three-Dimensional Collagen Matrix', *PLOS ONE*. Edited by M. A. Hakimi, 10(9), p. e0139104. doi: 10.1371/journal.pone.0139104.

Karve, S. S. *et al.* (2017) 'Intestinal organoids model human responses to infection by commensal and Shiga toxin producing Escherichia coli', *PLoS ONE*. Edited by N. J. Mantis. Public Library of Science, 12(6), p. e0178966. doi: 10.1371/journal.pone.0178966.

Kaufman, H. E. and Maloney, E. D. (1962) 'Multiplication of Three Strains of Toxoplasma gondii in Tissue Culture', *The Journal of Parasitology*, 48(3), p. 358. doi: 10.2307/3275195.

Kelly, D. *et al.* (2004) 'Commensal anaerobic gut bacteria attenuate inflammation by regulating nuclear-cytoplasmic shuttling of PPAR-[gamma] and RelA', *Nat Immunol*, 5(1), pp. 104–112. Available at: http://dx.doi.org/10.1038/ni1018.

Kiesslich, R. *et al.* (2012) 'Local barrier dysfunction identified by confocal laser endomicroscopy predicts relapse in inflammatory bowel disease', *Gut*, 61, pp. 1146–1153. doi: 10.1136/gutjnl-2011-300695.

Kim, H. J. *et al.* (2016) 'Contributions of microbiome and mechanical deformation to intestinal bacterial overgrowth and inflammation in a human gut-on-a-chip', *Proceedings of the National Academy of Sciences*. National Academy of Sciences, 113(1), pp. E7–E15. doi: 10.1073/pnas.1522193112.

King, D. A. *et al.* (2006) 'Epidemiology. Infectious diseases: preparing for the future.', *Science (New York, N.Y.)*, 313(5792), pp. 1392–3. doi: 10.1126/science.1129134.

Kinnebrew, M. A. *et al.* (2012) 'Interleukin 23 Production by Intestinal CD103+CD11b+ Dendritic Cells in Response to Bacterial Flagellin Enhances Mucosal Innate Immune Defense', *Immunity*, 36(2), pp. 276–287. doi: 10.1016/j.immuni.2011.12.011.

Kirkling, M. E. *et al.* (2018) 'Notch Signaling Facilitates In Vitro Generation of Cross-Presenting Classical Dendritic Cells', *Cell Reports*. NIH Public Access, 23(12), p. 3658–3672.e6. doi: 10.1016/j.celrep.2018.05.068.

De Kivit, S. *et al.* (2017) 'Galectin-9 Produced by Intestinal Epithelial Cells Enhances Aldehyde Dehydrogenase Activity in Dendritic Cells in a PI3K- and p38-Dependent Manner', *Journal of Innate Immunity*, 9(6), pp. 609–620. doi: 10.1159/000479817.

Klebanoff, C. A. *et al.* (2013) 'Retinoic acid controls the homeostasis of pre-cDC–derived splenic and intestinal dendritic cells', *The Journal of Experimental Medicine*, 210(10), pp. 1961–1976. doi: 10.1084/jem.20122508.

Klotz, C., Aebischer, T. and Seeber, F. (2012) 'Stem cell-derived cell cultures and organoids for protozoan parasite propagation and studying host–parasite interaction', *International journal of medical microbiology : IJMM*. Elsevier GmbH., 302(4–5), pp. 203–209.

Korinek, V. *et al.* (1998) 'Depletion of epithelial stem-cell compartments in the small intestine of mice lacking Tcf-4', *Nature Genetics*, 19(4), pp. 379–383. doi: 10.1038/1270.

Koshy, A. A. *et al.* (2010) 'Toxoplasma secreting Cre recombinase for analysis of host-parasite interactions', *Nature Methods*, 7(4), pp. 307–309. doi: 10.1038/nmeth.1438.

Koshy, A. A. *et al.* (2012) 'Toxoplasma co-opts host cells it does not invade', *PLoS Pathogens*. Edited by G. S. Yap. Public Library of Science, 8(7), p. 18. doi: 10.1371/journal.ppat.1002825.

Kulkarni, D. H. *et al.* (2018) 'Goblet cell associated antigen passages are inhibited during Salmonella typhimur/cium infection to prevent pathogen dissemination and limit responses to dietary antigens', *Mucosal Immunology*. doi: 10.1038/s41385-018-0007-6.

Laffont, S., Siddiqui, K. R. R. and Powrie, F. (2010) 'Intestinal inflammation abrogates the tolerogenic properties of MLN CD103+ dendritic cells', *European Journal of Immunology*, 40(7), pp. 1877–1883. doi: 10.1002/eji.200939957.

Lakhrif, Z. *et al.* (2018) 'Targeted Delivery of Toxoplasma gondii Antigens to Dendritic Cells Promote Immunogenicity and Protective Efficiency against Toxoplasmosis', *Frontiers in Immunology*, 9(FEB). doi: 10.3389/fimmu.2018.00317.

Lambert, H. *et al.* (2006) 'Induction of dendritic cell migration upon Toxoplasma gondii infection potentiates parasite dissemination', *Cellular Microbiology*. doi: 10.1111/j.1462-5822.2006.00735.x.

Lambert, H. *et al.* (2009) 'The Toxoplasma gondii-Shuttling Function of Dendritic Cells Is Linked to the Parasite Genotype', *Infection and Immunity*, 77(4), pp. 1679–1688. doi: 10.1128/IAI.01289-08.

De Lau, W. *et al.* (2011) 'Lgr5 homologues associate with Wnt receptors and mediate R-spondin signalling', *Nature*, 476(7360), pp. 293–297. doi: 10.1038/nature10337.

Lavine, M. D. and Arrizabalaga, G. (2009) 'Induction of mitotic S-phase of host and neighboring cells by Toxoplasma gondii enhances parasite invasion', *Molecular and Biochemical Parasitology*. NIH Public Access, 164(1), pp. 95–99. doi: 10.1016/j.molbiopara.2008.11.014.

Leslie, J. L. *et al.* (2015) 'Persistence and Toxin Production by Clostridium difficile within Human Intestinal Organoids Result in Disruption of Epithelial Paracellular Barrier Function', *Infection and Immunity*, 83(1), pp. 138–145. doi: 10.1128/IAI.02561-14.

Lewis, K. L. *et al.* (2011) 'Notch2 Receptor Signaling Controls Functional Differentiation of Dendritic Cells in the Spleen and Intestine', *Immunity*, 35(5), pp. 780–791. doi: 10.1016/j.immuni.2011.08.013.

Lindemans, C. A. *et al.* (2015) 'Interleukin-22 promotes intestinal-stem-cell-mediated epithelial regeneration', *Nature*, 528(7583), pp. 560–564. doi: 10.1038/nature16460.

Lingelbach, K. and Joiner, K. a (1998) 'The parasitophorous vacuole membrane surrounding Plasmodium and Toxoplasma: an unusual compartment in infected cells.', *Journal of cell science*, 111 (Pt 1, pp. 1467–1475.

Liu, Y. *et al.* (2018) 'Monolayer culture of intestinal epithelium sustains Lgr5 + intestinal stem cells', *Cell Discovery*. Nature Publishing Group, 4(1), pp. 4–6. doi: 10.1038/s41421-018-0036-z.

Lu, S. *et al.* (1996) 'Transport properties are not altered across Caco-2 cells with heightened TEER despite underlying physiological and ultrastructural changes', *Journal of Pharmaceutical Sciences*, 85(3), pp. 270–273. doi: 10.1021/js950269u.

Luda, K. M. *et al.* (2016) 'IRF8 Transcription-Factor-Dependent Classical Dendritic Cells Are Essential for Intestinal T Cell Homeostasis', *Immunity*. Elsevier Inc, 44(4), pp. 860–874. doi: 10.1016/j.immuni.2016.02.008.

Macpherson, A. J. and Uhr, T. (2004) 'Induction of Protective IgA by Dendritic Cells Carrying Commensal Bacteria', *Science*, 1662, pp. 1–8. doi: 10.1126/science.1091334.

Magnusson, M. K. *et al.* (2016) 'Macrophage and dendritic cell subsets in IBD: ALDH+cells are reduced in colon tissue of patients with ulcerative colitis regardless of inflammation', *Mucosal Immunology*. Nature Publishing Group, 9(1), pp. 171–182. doi: 10.1038/mi.2015.48.

Man, A. L. *et al.* (2017) 'CX3CR1+ Cell–Mediated Salmonella Exclusion Protects the Intestinal Mucosa during the Initial Stage of Infection', *The Journal of Immunology*, 198(1), pp. 335–343. doi: 10.4049/jimmunol.1502559.

Maraskovsky, E. *et al.* (1996) 'Dramatic increase in the numbers of functionally mature dendritic cells in Flt3 ligand-treated mice: multiple dendritic cell subpopulations identified.', *The Journal of experimental medicine*. Rockefeller University Press, 184(5), pp. 1953–62. doi: 10.1084/JEM.184.5.1953.

Martínez-López, M. *et al.* (2015) 'Batf3-dependent CD103+ dendritic cells are major producers of IL-12 that drive local Th1 immunity against Leishmania major infection in mice', *European Journal of Immunology*, 45(1), pp. 119–129. doi: 10.1002/eji.201444651.

Mashayekhi, M. *et al.* (2011) 'CD8α+ Dendritic Cells Are the Critical Source of Interleukin-12 that Controls Acute Infection by Toxoplasma gondii Tachyzoites', *Immunity*. Cell Press, 35(2), pp. 249–259. doi: 10.1016/j.immuni.2011.08.008.

Mayer, C. T. *et al.* (2014) 'Selective and efficient generation of functional Batf3-dependent CD103+ dendritic cells from mouse bone marrow.', *Blood*, 124(20), pp. 3081–91. doi: 10.1182/blood-2013-12-545772.

Mayer, J. U. *et al.* (2017) 'Different populations of CD11b+ dendritic cells drive Th2 responses in the small intestine and colon', *Nature Communications*. Nature Publishing Group, 8(May), p. 15820. doi: 10.1038/ncomms15820.

Mazzini, E. *et al.* (2014) 'Oral Tolerance Can Be Established via Gap Junction Transfer of Fed Antigens from CX3CR1+ Macrophages to CD103+ Dendritic Cells', *Immunity*. Elsevier Inc., 40(2), pp. 248–261. doi: 10.1016/j.immuni.2013.12.012.

McDole, J. R. *et al.* (2012) 'Goblet cells deliver luminal antigen to CD103+ dendritic cells in the small intestine', *Nature*. Nature Publishing Group, 483(7389), pp. 345–349. doi: 10.1038/nature10863.

McDonald, K. G. *et al.* (2012) 'Epithelial expression of the cytosolic retinoid chaperone cellular retinol binding protein II is essential for in vivo imprinting of local gut dendritic cells by lumenal retinoids', *American Journal of Pathology*, 180(3), pp. 984–997. doi: 10.1016/j.ajpath.2011.11.009.

McKenna, H. J. *et al.* (2000) 'Mice lacking flt3 ligand have deficient hematopoiesis affecting hematopoietic progenitor cells, dendritic cells, and natural killer cells.', *Blood*, 95(11), pp. 3489–3497. doi: https://doi.org/.

Mercier, C. and Cesbron-Delauw, M.-F. (2015) 'Toxoplasma secretory granules: one population or more?', *Trends in Parasitology*. Elsevier Ltd, 31(2), pp. 60–71. doi: 10.1016/j.pt.2014.12.002.

Molenaar, R. *et al.* (2011) 'Expression of retinaldehyde dehydrogenase enzymes in mucosal dendritic cells and gut-draining lymph node stromal cells is controlled by dietary vitamin A.', *Journal of immunology (Baltimore, Md. : 1950)*, 186(4), pp. 1934–42. doi: 10.4049/jimmunol.1001672.

Monteleone, I. *et al.* (2011) 'Aryl Hydrocarbon Receptor-Induced Signals Up-regulate IL-22 Production and Inhibit Inflammation in the Gastrointestinal Tract', *Gastroenterology*. W.B. Saunders, 141(1), p. 237–248.e1. doi: 10.1053/j.gastro.2011.04.007.

Montoya, J. G. and Liesenfeld, O. (2004) 'Toxoplasmosis', *Lancet*, 363(9425), pp. 1965–1976. doi: 10.1016/S0140-6736(04)16412-X.

Mora, J. R. *et al.* (2006) 'Generation of Gut-Homing IgA-Secreting B Cells by Intestinal Dendritic Cells', *Science*. American Association for the Advancement of Science, 314(5802), pp. 1157–1160. doi: 10.1126/science.1132742.

Morampudi, V., Braun, M. Y. and D'Souza, S. (2011) 'Modulation of Early β-Defensin-2 Production as a Mechanism Developed by Type I Toxoplasma gondii To Evade Human Intestinal Immunity', *Infection and Immunity*. Edited by J. H. Adams, 79(5), pp. 2043–2050. doi: 10.1128/IAI.01086-10.

Morrissette, N. S. and Sibley, L. D. (2002) 'Cytoskeleton of Apicomplexan Parasites', *Microbiology and Molecular Biology Reviews*, 66(1), pp. 21–38. doi: 10.1128/MMBR.66.1.21-38.2002.

Mortha, A. *et al.* (2014) 'Microbiota-Dependent Crosstalk Between Macrophages and ILC3 Promotes Intestinal Homeostasis', *Science*, 343(6178), pp. 1249288–1249288. doi: 10.1126/science.1249288.

Mowat, A. M. (2018) 'To respond or not to respond — a personal perspective of intestinal tolerance', *Nature Reviews Immunology*. Springer US. doi: 10.1038/s41577-018-0002-x.

Muniz-Feliciano, L. *et al.* (2013) 'Toxoplasma gondii-Induced Activation of EGFR Prevents Autophagy Protein-Mediated Killing of the Parasite', *PLoS Pathogens*. Edited by E. Y. Denkers. Public Library of Science, 9(12), pp. 1–15. doi: 10.1371/journal.ppat.1003809.

Muzaki, A. R. B. M. *et al.* (2016) 'Intestinal CD103+CD11b− dendritic cells restrain colitis via IFN-γ-induced anti-inflammatory response in epithelial cells', *Mucosal Immunology*, 9(2), pp. 336–351. doi: 10.1038/mi.2015.64.

Muzumdar, M. D. *et al.* (2007) 'A global double-fluorescent cre reporter mouse', *Genesis*, 45(9), pp. 593–605. doi: 10.1002/dvg.20335.

Naik, S. H. *et al.* (2007) 'Development of plasmacytoid and conventional dendritic cell subtypes from single precursor cells derived in vitro and in vivo', *Nature Immunology*. Nature Publishing Group, 8(11), pp. 1217–1226. doi: 10.1038/ni1522.

Neish, A. S. *et al.* (2000) 'Prokaryotic regulation of epithelial responses by inhibition of IkappaB- alpha ubiquitination [see comments]', *Science*, 289(5484), pp. 1560–1563. Available at: http://www.ncbi.nlm.nih.gov/cgi-bin/Entrez/referer?http://www.ncbi.nlm.nih.gov/htbin-post/Omim/getmim?field=medline_uid&search=10968793.

Niess, J. H. *et al.* (2005) 'CX3CR1-mediated dendritic cell access to the intestinal

lumen and bacterial clearance.', *Science (New York, N.Y.)*, 307(5707), pp. 254–8. doi: 10.1126/science.1102901.

Noel, G. *et al.* (2017) 'A primary human macrophage- enteroid co-culture model to investigate mucosal gut physiology and host-pathogen interactions'. doi: 10.1038/srep45270.

Nozaki, K. *et al.* (2016) 'Co-culture with intestinal epithelial organoids allows efficient expansion and motility analysis of intraepithelial lymphocytes', *Journal of Gastroenterology*. Springer Japan, pp. 1–5. doi: 10.1007/s00535-016-1170-8.

Ohta, T. *et al.* (2016) 'Crucial roles of XCR1-expressing dendritic cells and the XCR1-XCL1 chemokine axis in intestinal immune homeostasis', *Scientific Reports*. Nature Publishing Group, 6(March), pp. 1–11. doi: 10.1038/srep23505.

Olias, P. *et al.* (2016) 'Toxoplasma Effector Recruits the Mi-2/NuRD Complex to Repress STAT1 Transcription and Block IFN-γ-Dependent Gene Expression', *Cell Host and Microbe*, 20(1), pp. 72–82. doi: 10.1016/j.chom.2016.06.006.

Pappas, G., Roussos, N. and Falagas, M. E. (2009) 'Toxoplasmosis snapshots: Global status of Toxoplasma gondii seroprevalence and implications for pregnancy and congenital toxoplasmosis', *International Journal for Parasitology*. Australian Society for Parasitology Inc., 39(12), pp. 1385–1394. doi: 10.1016/j.ijpara.2009.04.003.

Parthasarathy, S. *et al.* (2013) 'Protective immune response in BALB/c mice induced by DNA vaccine of the ROP8 gene of Toxoplasma gondii.', *The American journal of tropical medicine and hygiene*. doi: 10.4269/ajtmh.12-0727.

Persson, E., Scott, C., *et al.* (2013) 'Dendritic cell subsets in the intestinal lamina propria: Ontogeny and function', *European Journal of Immunology*, 43(12), pp. 3098–3107. doi: 10.1002/eji.201343740.

Persson, E., Uronen-Hansson, H., *et al.* (2013) 'IRF4 Transcription-Factor-Dependent CD103+CD11b+ Dendritic Cells Drive Mucosal T Helper 17 Cell Differentiation', *Immunity*, 38(5), pp. 958–969. doi: 10.1016/j.immuni.2013.03.009.

Pifer, R. *et al.* (2011) 'UNC93B1 Is Essential for TLR11 Activation and IL-12-dependent Host Resistance to Toxoplasma gondii', *Journal of Biological Chemistry*. American Society for Biochemistry and Molecular Biology, 286(5), pp. 3307–3314. doi: 10.1074/jbc.M110.171025.

Powell, R. H. and Behnke, M. S. (2017) 'WRN conditioned media is sufficient for in vitro propagation of intestinal organoids from large farm and small companion animals', *Biology Open*. The Company of Biologists Ltd, 6(5), pp. 698–705. doi: 10.1242/bio.021717.

Prescott, M. J. and Lidster, K. (2017) 'Improving quality of science through better

animal welfare: The NC3Rs strategy', *Lab Animal*, pp. 152–156. doi: 10.1038/laban.1217.

Quan, J. H. *et al.* (2018) 'P2X7 receptor mediates NLRP3-dependent IL-1β secretion and parasite proliferation in Toxoplasma gondii-infected human small intestinal epithelial cells', *Parasites and Vectors*. Parasites & Vectors, 11(1), pp. 1–10. doi: 10.1186/s13071-017-2573-y.

Redpath, S. A. *et al.* (2018) 'Functional specialization of intestinal dendritic cell subsets during Th2 helminth infection in mice', *European Journal of Immunology*, 48(1), pp. 87–98. doi: 10.1002/eji.201747073.

Rimoldi, M. *et al.* (2005) 'Intestinal immune homeostasis is regulated by the crosstalk between epithelial cells and dendritic cells', *Nature Immunology*, 6(5), pp. 507–514. doi: 10.1038/ni1192.

Robert-Gangneux, F. and Dardé, M. L. (2012) 'Epidemiology of and diagnostic strategies for toxoplasmosis', *Clinical Microbiology Reviews*, 25(2), pp. 264–296. doi: 10.1128/CMR.05013-11.

Rogoz, A. *et al.* (2015) 'A 3-D enteroid-based model to study T-cell and epithelial cell interaction', *Journal of Immunological Methods*. Elsevier B.V., 421, pp. 89–95. doi: 10.1016/j.jim.2015.03.014.

Rosowski, E. E. *et al.* (2011) 'Strain-specific activation of the NF-κB pathway by GRA15, a novel Toxoplasma gondii dense granule protein', *The Journal of Experimental Medicine*. Rockefeller University Press, 208(1), pp. 195–212. doi: 10.1084/jem.20100717.

Roxas, J. L. *et al.* (2010) 'Enterohemorrhagic E. coli alters murine intestinal epithelial tight junction protein expression and barrier function in a Shiga toxin independent manner', *Laboratory Investigation*. Nature Publishing Group, 90(8), pp. 1152–1168. doi: 10.1038/labinvest.2010.91.

Sack, D. a *et al.* (2001) 'Antimicrobial resistance in shigellosis, cholera and campylobacteriosis', *World Health*, (17), pp. 1–56. Available at: http://www.who.int/drugresistance/Antimicrobial_resistance_in_shigellosis_cholera_and_cam.pdf (Accessed: 25 September 2018).

Saeij, J. P. J. *et al.* (2007) 'Toxoplasma co-opts host gene expression by injection of a polymorphic kinase homologue', *Nature*, 445(7125), pp. 324–327. doi: 10.1038/nature05395.

Salzman, N. H. *et al.* (2003) 'Protection against enteric salmonellosis in transgenic mice expressing a human intestinal defensin', *Nature*, 422(6931), pp. 522–526. doi: 10.1038/nature01520.

Santamaria, M. H., Perez Cabarello, E. and Corral, R. S. (2016) 'Unmethylated CpG motifs in Toxoplasma gondii DNA induce TLR9- and IFN-β-dependent expression of α-defensin-5 in intestinal epithelial cells', *Parasitology*, 143(01), pp. 60–68. doi: 10.1017/S0031182015001456.

Sathe, P. *et al.* (2011) 'The Acquisition of Antigen Cross-Presentation Function by Newly Formed Dendritic Cells', *The Journal of Immunology*. American Association of Immunologists, 186(9), pp. 5184–5192. doi: 10.4049/jimmunol.1002683.

Sato, T. *et al.* (2009) 'Single Lgr5 stem cells build crypt-villus structures in vitro without a mesenchymal niche.', *Nature*. Nature Publishing Group, 459(7244), pp. 262–265. doi: 10.1038/nature07935.

Sato, T. *et al.* (2011) 'Long-term expansion of epithelial organoids from human colon, adenoma, adenocarcinoma, and Barrett's epithelium', *Gastroenterology*, 141(5), pp. 1762–1772. doi: 10.1053/j.gastro.2011.07.050.

Sato, T. *et al.* (2013) 'Human CD1c+ Myeloid Dendritic Cells Acquire a High Level of Retinoic Acid-Producing Capacity in Response to Vitamin D3', *The Journal of Immunology*, 191(6), pp. 3152–3160. doi: 10.4049/jimmunol.1203517.

Sato, T. and Clevers, H. (2013a) 'Growing self-organizing mini-guts from a single intestinal stem cell: mechanism and applications.', *Science (New York, N.Y.)*, 340(June), pp. 1190–4. doi: 10.1126/science.1234852.

Sato, T. and Clevers, H. (2013b) 'Primary Mouse Small Intestinal Epithelial Cell Cultures', in Randell, S. H. and Fulcher, M. L. (eds) *Epithelial Cell Culture Protocols SE - 19*. Humana Press (Methods in Molecular Biology), pp. 319–328. doi: 10.1007/978-1-62703-125-7_19.

Satpathy, A. T. *et al.* (2013) 'Notch2-dependent classical dendritic cells orchestrate intestinal immunity to attaching-and-effacing bacterial pathogens', *Nature Immunology*. Nature Publishing Group, 14(9), pp. 937–948. doi: 10.1038/ni.2679.

Saxena, K. *et al.* (2016) 'Human Intestinal Enteroids : a New Model To Study Human Rotavirus Infection , Host Restriction , and Pathophysiology', *Journal of Virology*, 90(1), pp. 43–56. doi: 10.1128/JVI.01930-15.Editor.

Scanga, C. A. *et al.* (2002) 'Cutting Edge: MyD88 Is Required for Resistance to Toxoplasma gondii Infection and Regulates Parasite-Induced IL-12 Production by Dendritic Cells', *The Journal of Immunology*, 168(12), pp. 5997–6001. doi: 10.4049/jimmunol.168.12.5997.

Scott, C. L. *et al.* (2015) 'CCR2+CD103− intestinal dendritic cells develop from DC-committed precursors and induce interleukin-17 production by T cells', *Mucosal Immunology*. Nature Publishing Group, 8(2), pp. 327–339. doi: 10.1038/mi.2014.70.

Scott, C. L. *et al.* (2016) 'The transcription factor Zeb2 regulates development of conventional and plasmacytoid DCs by repressing Id2', *The Journal of Experimental Medicine*, 213(6), pp. 897–911. doi: 10.1084/jem.20151715.

Segura, E. and Amigorena, S. (2013) 'Inflammatory dendritic cells in mice and humans', *Trends in Immunology*, 34(9), pp. 440–445. doi: 10.1016/j.it.2013.06.001.

Shah, P. *et al.* (2016) 'A microfluidics-based in vitro model of the gastrointestinal human-microbe interface', *Nature Communications*. Nature Publishing Group, 7, p. 11535. doi: 10.1038/ncomms11535.

Shan, M. *et al.* (2013) 'Mucus Enhances Gut Homeostasis and Oral Tolerance by Delivering Immunoregulatory Signals', *Science*, 342(6157), pp. 447–453. doi: 10.1126/science.1237910.

Sichien, D. *et al.* (2017) 'Development of conventional dendritic cells: from common bone marrow progenitors to multiple subsets in peripheral tissues', *Mucosal Immunology*. Nature Publishing Group, (January). doi: 10.1038/mi.2017.8.

Singh, N. *et al.* (2014) 'Activation of Gpr109a, Receptor for Niacin and the Commensal Metabolite Butyrate, Suppresses Colonic Inflammation and Carcinogenesis', *Immunity*. Elsevier Inc., 40(1), pp. 128–139. doi: 10.1016/j.immuni.2013.12.007.

Snippert, H. J. *et al.* (2010) 'Intestinal crypt homeostasis results from neutral competition between symmetrically dividing Lgr5 stem cells', *Cell*, 143(1), pp. 134–144. doi: 10.1016/j.cell.2010.09.016.

Spalenka, J. *et al.* (2018) 'Discovery of New Inhibitors of Toxoplasma gondii via the Pathogen Box.', *Antimicrobial agents and chemotherapy*. American Society for Microbiology Journals, 62(2), pp. e01640-17. doi: 10.1128/AAC.01640-17.

Sun, T. *et al.* (2017) 'Intestinal Batf3-dependent dendritic cells are required for optimal antiviral T-cell responses in adult and neonatal mice', *Mucosal Immunology*, 10(3), pp. 775–788. doi: 10.1038/mi.2016.79.

Takemura, N. and Uematsu, S. (2016) 'Isolation and Functional Analysis of Lamina Propria Dendritic Cells from the Mouse Small Intestine', *Methods in Molecular Biology*, 1422, pp. 181–188. doi: 10.1007/978-1-4939-3603-8.

Tanaka, T. *et al.* (2010) 'Parasiticidal activity of human alpha-defensin-5 against Toxoplasma gondii.', *In vitro cellular & developmental biology. Animal*, 46(6), pp. 560–5. doi: 10.1007/s11626-009-9271-9.

Thorne, C. A. *et al.* (2018) 'Enteroid Monolayers Reveal an Autonomous WNT and BMP Circuit Controlling Intestinal Epithelial Growth and Organization', *Developmental Cell*. Cell Press, 44(5), p. 624–633.e4. doi:

10.1016/j.devcel.2018.01.024.

Vaishnava, S. *et al.* (2011) 'The Antibacterial Lectin RegIII Promotes the Spatial Segregation of Microbiota and Host in the Intestine', *Science*, 334(6053), pp. 255–258. doi: 10.1126/science.1209791.

Valentini, P. *et al.* (2014) 'Spiramycin/cotrimoxazole versus pyrimethamine/sulfonamide and spiramycin alone for the treatment of toxoplasmosis in pregnancy', *Journal of Perinatology*. Nature Publishing Group, 35(2), pp. 90–94. doi: 10.1038/jp.2014.161.

VanDussen, K. L. *et al.* (2012) 'Notch signaling modulates proliferation and differentiation of intestinal crypt base columnar stem cells', *Development*. Oxford University Press for The Company of Biologists Limited, 139(3), pp. 488–497. doi: 10.1242/dev.070763.

Vicente-Suarez, I. *et al.* (2015) 'Unique lamina propria stromal cells imprint the functional phenotype of mucosal dendritic cells', *Mucosal Immunology*. Nature Publishing Group, 8(1), pp. 141–151. doi: 10.1038/mi.2014.51.

Villablanca, E. J. *et al.* (2011) 'MyD88 and Retinoic Acid Signaling Pathways Interact to Modulate Gastrointestinal Activities of Dendritic Cells', *Gastroenterology*. Elsevier Inc., 141(1), pp. 176–185. doi: 10.1053/j.gastro.2011.04.010.

Vremec, D. *et al.* (1997) 'The influence of granulocyte/macrophage colony-stimulating factor on dendritic cell levels in mouse lymphoid organs', *European Journal of Immunology*. WILEY-VCH Verlag GmbH, 27(1), pp. 40–44. doi: 10.1002/eji.1830270107.

Wang, G. and Gao, M. (2016) 'Influence of Toxoplasma gondii on in vitro proliferation and apoptosis of hepatoma carcinoma H7402 cell', *Asian Pacific Journal of Tropical Medicine*. No longer published by Elsevier, 9(1), pp. 63–66. doi: 10.1016/j.apjtm.2015.12.013.

Wang, S. *et al.* (2015) 'Protective immunity against acute toxoplasmosis in BALB/c mice induced by a DNA vaccine encoding Toxoplasma gondii 10kDa excretory–secretory antigen (TgESA10)', *Veterinary Parasitology*, 214(1–2), pp. 40–48. doi: 10.1016/j.vetpar.2015.09.016.

Wang, Z.-X. *et al.* (2017) 'Proteomic Differences between Developmental Stages of Toxoplasma gondii Revealed by iTRAQ-Based Quantitative Proteomics', *Frontiers in Microbiology*, 8(JUN), p. 985. doi: 10.3389/fmicb.2017.00985.

Watchmaker, P. B. *et al.* (2014) 'Comparative transcriptional and functional profiling defines conserved programs of intestinal DC differentiation in humans and mice', *Nature Immunology*, 15(1), pp. 98–108. doi: 10.1038/ni.2768.

Wehkamp, J. *et al.* (2004) 'NOD2 (CARD15) mutations in Crohn's disease are associated with diminished mucosal α-defensin expression', *Gut*, 53(11), pp. 1658–1664. doi: 10.1136/gut.2003.032805.

Weidner, J. M. *et al.* (2013) 'Rapid cytoskeleton remodelling in dendritic cells following invasion by Toxoplasma gondii coincides with the onset of a hypermigratory phenotype', *Cellular Microbiology*, 15(10), pp. 1735–1752. doi: 10.1111/cmi.12145.

Weidner, J. M. and Barragan, A. (2014) 'Tightly regulated migratory subversion of immune cells promotes the dissemination of Toxoplasma gondii', *International Journal for Parasitology*. Australian Society for Parasitology Inc., 44(2), pp. 85–90. doi: 10.1016/j.ijpara.2013.09.006.

Weight, C. M. *et al.* (2015) 'Elucidating pathways of Toxoplasma gondii invasion in the gastrointestinal tract: Involvement of the tight junction protein occludin', *Microbes and Infection*. Elsevier Masson SAS, 17(10), pp. 698–709. doi: 10.1016/j.micinf.2015.07.001.

Weight, C. M. and Carding, S. R. (2012) 'The protozoan pathogen Toxoplasma gondii targets the paracellular pathway to invade the intestinal epithelium', *Annals of the New York Academy of Sciences*, 1258(1), pp. 135–142. doi: 10.1111/j.1749-6632.2012.06534.x.

Weilhammer, D. R. *et al.* (2012) 'Host metabolism regulates growth and differentiation of Toxoplasma gondii', *International Journal for Parasitology*. doi: 10.1016/j.ijpara.2012.07.011.

Wilen, C. B. *et al.* (2018) 'Tropism for tuft cells determines immune promotion of norovirus pathogenesis', *Science*. American Association for the Advancement of Science, 360(6385), pp. 204–208. doi: 10.1126/science.aar3799.

Williamson, I. A. *et al.* (2018) 'A High-Throughput Organoid Microinjection Platform to Study Gastrointestinal Microbiota and Luminal Physiology', *Cellular and Molecular Gastroenterology and Hepatology*, 6(3), pp. 301–319. doi: 10.1016/j.jcmgh.2018.05.004.

Wilson, C. L. *et al.* (1999) 'Regulation of intestinal alpha-defensin activation by the metalloproteinase matrilysin in innate host defense.', *Science (New York, N.Y.)*, 286(5437), pp. 113–117. doi: 10.1126/science.286.5437.113.

Wilson, S. S. *et al.* (2014) 'A small intestinal organoid model of non-invasive enteric pathogen-epithelial cell interactions.', *Mucosal immunology*. Nature Publishing Group, (August), pp. 1–10. doi: 10.1038/mi.2014.72.

Wong, V. W. Y. *et al.* (2012) 'Lrig1 controls intestinal stem-cell homeostasis by negative regulation of ErbB signalling', *Nature Cell Biology*, 14(4), pp. 401–408. doi:

10.1038/ncb2464.

World Health Organization (2015) 'WHO estimates of the global burden of foodborne diseases', p. 254. Available at: https://extranet.who.int/sree/Reports?op=vs&path=/WHO_HQ_Reports/G36/PROD/EXT/FoodborneDiseaseBurden (Accessed: 21 July 2018).

Worthington, J. J. *et al.* (2011) 'Intestinal dendritic cells specialize to activate transforming growth factor-β and induce Foxp3 + regulatory T cells via integrin αvβ8', *Gastroenterology*. Elsevier Inc., 141(5), pp. 1802–1812. doi: 10.1053/j.gastro.2011.06.057.

Xiao, J. *et al.* (2018) 'Toxoplasma gondii: Biological Parameters of the Connection to Schizophrenia.', *Schizophrenia bulletin*. doi: 10.1093/schbul/sby082.

Xiao, S. *et al.* (2008) 'Retinoic Acid Increases Foxp3+ Regulatory T Cells and Inhibits Development of Th17 Cells by Enhancing TGF- -Driven Smad3 Signaling and Inhibiting IL-6 and IL-23 Receptor Expression', *The Journal of Immunology*, 181(4), pp. 2277–2284. doi: 10.4049/jimmunol.181.4.2277.

Xu, M. M. *et al.* (2017) 'Dendritic Cells but Not Macrophages Sense Tumor Mitochondrial DNA for Cross-priming through Signal Regulatory Protein α Signaling', *Immunity*, 47(2), p. 363–373.e5. doi: 10.1016/j.immuni.2017.07.016.

Yan, K. S. *et al.* (2012) 'The intestinal stem cell markers Bmi1 and Lgr5 identify two functionally distinct populations', *Proceedings of the National Academy of Sciences*, 109(2), pp. 466–471. doi: 10.1073/pnas.1118857109.

Yin, Y. *et al.* (2015) 'Modeling rotavirus infection and antiviral therapy using primary intestinal organoids', *Antiviral Research*. Elsevier, 123, pp. 120–131. doi: 10.1016/j.antiviral.2015.09.010.

Yokota-Nakatsuma, A. *et al.* (2016) 'Beta 1-integrin ligation and TLR ligation enhance GM-CSF-induced ALDH1A2 expression in dendritic cells, but differentially regulate their anti-inflammatory properties', *Scientific Reports*. Nature Publishing Group, 6(1), p. 37914. doi: 10.1038/srep37914.

Yokota, A. *et al.* (2009) 'GM-CSF and IL-4 synergistically trigger dendritic cells to acquire retinoic acid-producing capacity', *International Immunology*, 21(4), pp. 361–377. doi: 10.1093/intimm/dxp003.

Yoshida, M. *et al.* (2004) 'Human Neonatal Fc Receptor Mediates Transport of IgG into Luminal Secretions for Delivery of Antigens to Mucosal Dendritic Cells', *Immunity*, 20, pp. 769–783. Available at: https://www.cell.com/immunity/pdf/S1074-7613(04)00142-6.pdf (Accessed: 23 June 2018).

Zelante, T. *et al.* (2013) 'Tryptophan Catabolites from Microbiota Engage Aryl Hydrocarbon Receptor and Balance Mucosal Reactivity via Interleukin-22', *Immunity*, 39, pp. 372–385. doi: 10.1016/j.immuni.2013.08.003.

Zeng, R. *et al.* (2013) 'Retinoic acid regulates the development of a gut-homing precursor for intestinal dendritic cells.', *Mucosal immunology*. Nature Publishing Group, 6(4), pp. 847–56. doi: 10.1038/mi.2012.123.

Zeng, R. *et al.* (2016) 'Generation and transcriptional programming of intestinal dendritic cells: essential role of retinoic acid', *Mucosal Immunology*. Nature Publishing Group, 9(1), pp. 183–193. doi: 10.1038/mi.2015.50.

Zhang, D. *et al.* (2017) 'Human intestinal organoids express histo-blood group antigens, bind norovirus VLPs, and support limited norovirus replication', *Scientific Reports*. Nature Publishing Group, 7(1), p. 12621. doi: 10.1038/s41598-017-12736-2.

Zhang, X. *et al.* (2016) '*Cryptosporidium parvum* infection attenuates the ex vivo propagation of murine intestinal enteroids', *Physiological Reports*, 4(24), p. e13060. doi: 10.14814/phy2.13060.

Zhang, Y.-G. *et al.* (2014) 'Salmonella-infected crypt-derived intestinal organoid culture system for host-bacterial interactions', *Physiological Reports*, 2(9), pp. e12147–e12147. doi: 10.14814/phy2.12147.

Zhu, B. *et al.* (2013) 'IL-4 and Retinoic Acid Synergistically Induce Regulatory Dendritic Cells Expressing Aldh1a2', *The Journal of Immunology*, 191(6), pp. 3139–3151. doi: 10.4049/jimmunol.1300329.

Zhu, W. N. *et al.* (2017) 'Evaluation of protective immunity induced by DNA vaccination with genes encoding Toxoplasma gondii GRA17 and GRA23 against acute toxoplasmosis in mice', *Experimental Parasitology*. doi: 10.1016/j.exppara.2017.06.002.

Zigmond, E. *et al.* (2012) 'Ly6Chi Monocytes in the Inflamed Colon Give Rise to Proinflammatory Effector Cells and Migratory Antigen-Presenting Cells', *Immunity*, 37(6), pp. 1076–1090. doi: 10.1016/j.immuni.2012.08.026.